A Numerical Study of the Suitability of Rigid Inclusion Ground Reinforcement Beneath Caisson Quay Walls

Andrew Graham Holmwood

Supervisor: Dr Denis Kalumba

Department of Civil Engineering

University of Cape Town

March 2017

This dissertation is submitted in partial fulfilment for the degree of

Master of Science in Engineering

Preface

This dissertation was submitted in partial fulfilment of the requirements for the degree of Master of Science in Engineering.

I, Andrew Graham Holmwood, know the meaning of plagiarism and declare that all the work in this dissertation, save for that which is properly acknowledged, is my own. I have used the Harvard referencing style to cite information sources.

Mr Andrew Graham Holmwood

MSc candidate and author

Signed by candidate

Signed

13 March 2017

Date

For the Lord

Acknowledgements

Firstly, my sincere thanks to my supervisor Dr Denis Kalumba for his ideas, discussions, remarks, and reviews of the various chapters; in particular for identifying the “rambling” and recommending a more concise scientific approach.

I am extremely grateful to ZAA Engineering Projects and Naval Architecture Pty (Ltd) for funding my postgraduate study and, without exception, providing all the resources I required to complete this study. Without their insights into the problem and support I could not have completed this research.

I would also like to thank Plaxis bv for sponsoring their PLAXIS 3D Suite for two years. The objectives of this study could not have been achieved without the capabilities of advanced numerical modelling software.

I would like to thank TERRASOL for sponsoring their deep and shallow foundation design software FOXTA V3 for two years. To the author’s knowledge this is the only software package that deals specifically with the design of ground reinforced with rigid inclusions, within the framework of accepted industry guidelines, in this case ASIRI (2012).

Thanks to all those friends and family who have shared in the pain of a part-time masters.

Lastly, thanks to my wife who has lived this master’s and only ever been my greatest supporter. What can I say! It’s time to have fun again.

Abstract

The objective of this study was to determine whether rigid inclusions are suitable for reinforcement of the foundation of a caisson quay wall functioning as a container terminal. Apart from their brittle behaviour under lateral loading, rigid inclusions are well suited to the large uniform loads and stringent post-construction deflection tolerances associated with container terminal structures. Their inherent strength and stiffness means they have certain advantages over other stiffening columns commonly used for ground reinforcement in port expansion projects. Their mechanical properties allow construction to unrestricted heights at any construction rate and, in theory, RIs can be applied to all soil types. Additionally the locations of many ports coincide with rivers, deltas and estuaries which are associated with poor soil conditions often requiring ground improvement. Their suitability is of practical significance to port planners and engineers who are faced with the challenge of providing satisfactory foundation performance that is cost effective. The addition of RI ground reinforcement for this structural application would allow for greater flexibility in meeting these challenges.

The literature review for this study was broad in its scope with emphasis placed on describing the mechanics of the problem, analysis methods and suitable installation methods for execution in the marine environment. One of the key outcomes of the literature review was identifying the problem of lateral loading due to “free-field” lateral ground movements. In light of this, suitable strategies for limiting and accommodating lateral loading of the RIs were proposed. A numerical study of the proposed ground improvement scheme was undertaken using the 3D finite element method. The key model outputs were caisson deflections and RI forces, moments and stresses, for the various simulated construction phases up to operational conditions. The model results were assessed in terms of the key foundation performance criteria which were related to STS crane rail tolerances and limiting tensile stresses in the RIs. This study found that for a firm clay subsoil condition the proposed RI ground reinforcement scheme met the foundation performance criteria for this structural application provided (i) strategies to limit lateral loading were implemented and (ii) the RIs were reinforced over the length where they were not fully compressed. While this study provided insights into the behaviour of RIs

for this structural application, ultimately suitability is a function of range of factors, in addition to the limited technical performance criteria derived for this study.

Contents

List of Figures

List of Tables

Nomenclature

CMCs	Controlled modulus columns	2D	Two-dimensional
CPT	Cone penetration test	3D	Three-dimensional
DR	Dynamic replacement	A_c	Cross sectional area of column
DEM	Discrete element method	A_s	Area of unit cell (support surface)
ESP	Effective stress path	C_v	Coefficient of consolidation
FEM	Finite element method	E	Load transfer efficiency
FDM	Finite difference method	$E'_{s\,50}$	Reference tangent stiffness from CIDC test
GCCs	Geotextile confined columns	E_{lat}	Lateral deflection efficiency
GR	Geosynthetic reinforcement	E_{sett}	Settlement efficiency
HS	Hardening soil model	V	Shear force
HSsmall	HS with small strain stiffness	Q_0	Load acting on head of a single inclusion
LTP	Load transfer platform	V	Shear force
LNG	Liquefied natural gas	F_s	Factor of safety
LE	Linear elastic	G	Overload efficiency
MC	Mohr-Coulomb	H	Fill height above the inclusion head
NC	Normally consolidated	I_D	Soil's density index
OCR	Over consolidation ratio	K_s	Earth pressure coefficient against the pile shaft
OC	Over consolidated	K_0	In situ stress ratio
POP	Pre-overburden pressure	M	Bending moment
RIs	Rigid inclusions	E_i	Inclusion modulus
SCs	Stone columns	M_s	Constrained modulus
SCPs	Sand compaction piles	N	Axial force
VR	Vibro replacement	N_q	Bearing pressure coefficient
VCC	Vibro-concrete column	Q_{-hr}	Vertical load acting on the LTP
YSR	Yield stress ratio	R_b	Resistance of the pile base

R_s	Resistance along inclusion shaft
R_t	Total bearing resistance of inclusion
W	Weight of the LTP
a	Width of square piles caps
a_s	Area replacement ratio
c'	Effective cohesion
d	Diameter of the rigid inclusion or pile
$h_r \ or \ h_m$	Fill height above the inclusion heads
$k_{x,y}$	Permeability in horizontal or vertical
p'	Normal mean stress
q	Surcharge load acting on the LTP
q	Deviatoric stress
q_{s0}	Stress on the soil between inclusions
$q_{s,}$	Shaft resistance
$q_{s;neg}$	Unit negative shaft friction
q_b	Unit base resistance
q_c	Cone resistance
q_{i0}	Stress at the inclusion head
s	Spacing between rigid inclusions or piles
u	Pore pressure in subsoil
α_{disp}	Empirical coefficient for displacement
δ	Interface friction angle
δ_{vi}	Settlement of the inclusion
δ_{li}	Lateral deflection of the inclusion
n	Stress concentration ratio
q_{inc}	Stress in the inclusion
σ_h'	Horizontal effective stress
σ_p	Pre-consolidation stress
σ_{rf}'	Local radial effective stress at failure
σ_s	Stress on soil between inclusions
σ_i	Vertical stress in the inclusion
δ_{vs}	Soil settlement
σ_v'	Vertical effective stress
τ	Shear stress
φ'	Effective angle of internal friction
φ_{cv}'	Constant volume angle of shearing
φ_{pk}'	Peak angle of shearing resistance

Chapter 1 Introduction

1.1 Background Information

The term Rigid Inclusions (RIs) refers to a type of ground improvement technique where pile-like rigid columns are used to reinforce the ground with the aim of decreasing settlement and increasing bearing capacity (Chu et al., 2009). RIs fall into the broad category of ground improvement techniques which use stiffening columns to reinforce the ground. Although in the same category as stone columns and sand compaction piles, RIs are composed of a material with a strong permanent cohesion such as concrete. They are "rigid" as opposed to granular such as sand or stone (ASIRI, 2012). Their inherent strength and stiffness means they are well suited to heavy loads and stringent deflection tolerances. This gives RIs certain advantages over other stiffening columns. Their mechanical properties potentially allow construction to unrestricted heights at any construction rate with subsequent, controlled post-construction settlements (BS 8006, 2010). Additionally RIs can in theory be applied to all soil types including highly variable soil conditions. Despite these advantages, concrete RIs are largely absent from the ground improvement records for recent port expansion projects (Hamidi et al., 2013). For example, the most common columnar techniques used to support gravity quay walls include stone columns, sand compaction piles or overlapping soil-cement columns (Kitazume, 2005; Leung & Shen, 2008; Kitazume & Terashi, 2013a). The selection of these alternative techniques is likely due to a combination of factors; however it is suggested that one of the primary reasons is their performance under lateral loading. Stone columns and sand compaction piles behave in a ductile manner and the deep mixing methodology allows continuous shear walls to be constructed from overlapping soil cement columns. Both of these types of reinforcement are suited to lateral loading, albeit for different reasons.

By comparison concrete RIs are typically unreinforced and therefore behave in a brittle manner with low tensile strength. This behaviour has been mitigated in other fields of application, such as piled bridge abutments and piled embankments, by implementing strategies to limit and accommodate

lateral loading and the effects of lateral loading. It is proposed that these strategies could be applied to the case of a gravity container quay supported by ground reinforced with rigid inclusions (Figure 1.1). Apart from their behaviour under lateral loading, RIs are well suited to the large uniform loads and stringent post construction deflection tolerances associated with port container terminals. Additionally the locations of many ports coincide with rivers, deltas and estuaries which are associated with poor soil conditions often requiring ground improvement. Their suitability is of practical significance to port planners and engineers who are faced with the challenge of providing satisfactory foundation performance that is cost effective. The addition of Rigid Inclusion ground improvement for this structural application would allow for greater flexibility in meeting these challenges.

1.2 Objectives

The main objective of this study was to determine whether rigid inclusions are suitable for the reinforcement of the foundation of a caisson container quay wall. Their suitability for this purpose was assessed by reviewing relevant literature and by numerical analysis. The following sub-objectives were developed:

- Describe the mechanics of the problem
- Identify suitable strategies to limit lateral loading and the effects of lateral loading
- Develop foundation performance criteria in terms of RI behaviour and caisson behaviour
- Validate the three-dimensional finite element model for simulating the problem
- Assess the numerical results in relation to the performance criteria, providing insight into the suitability of RIs for this application

1.3 Scope

The scope of this research was limited to concrete rigid inclusions formed by displacement methods. In theory RIs may be used to reinforce all soil types. In practice however, their use is generally limited to reinforcing fine grained soils and therefore in this study only reinforcement of firm clays is considered.

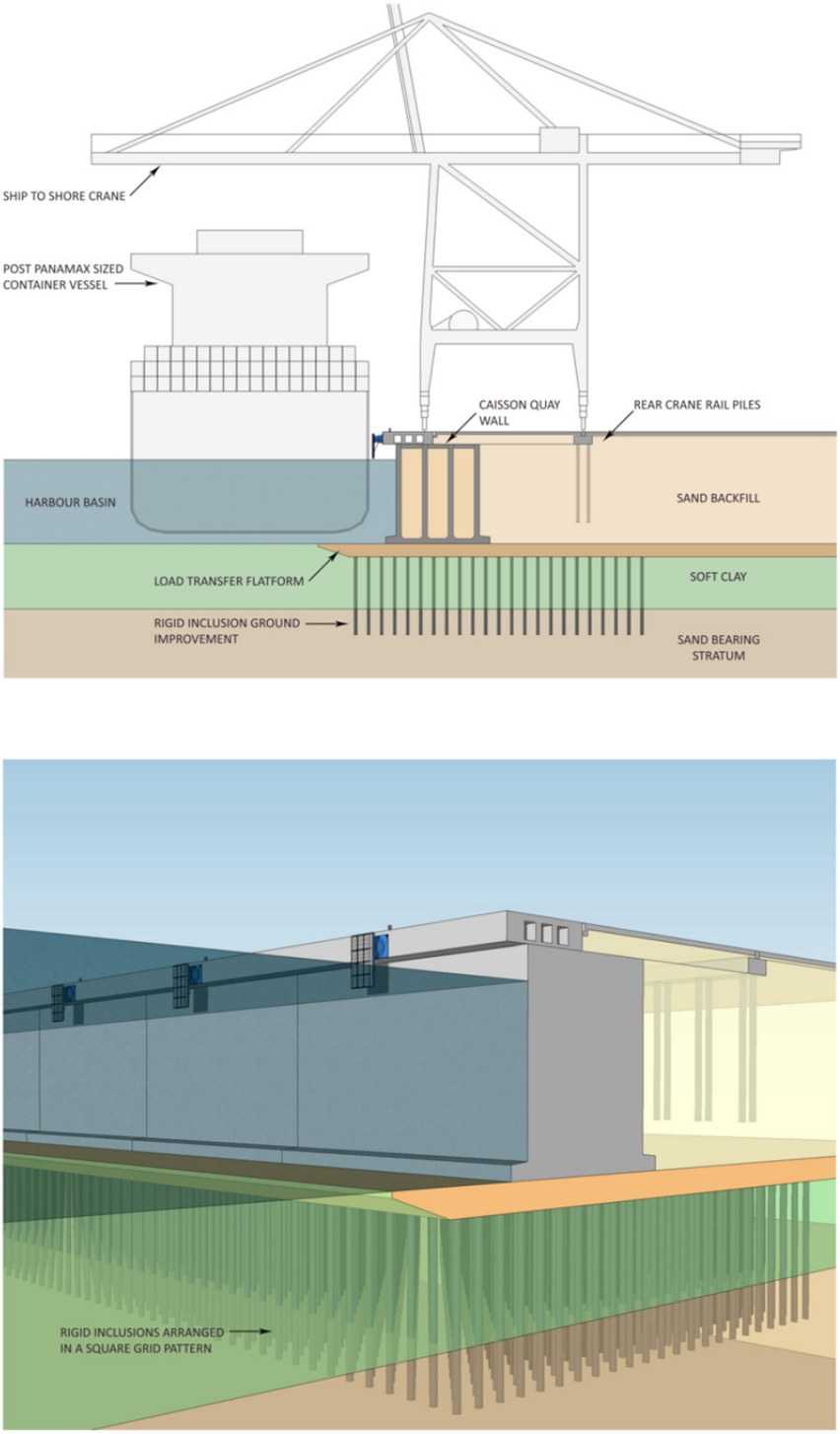

Figure 1.1– Caisson quay wall supported on clay reinforced with rigid inclusions

The overlying structure is a gravity-caisson functioning as a quay front structure of a modern day container terminal. In this regard the geometry of the caisson and the imposed environmental and operational loading are related to Post Panamax sized vessels and ship-to-shore cranes. Dynamic loading due to a seismic situation was not considered in this study.

This is a numerical study using the 3D finite element method. Numerical models require validation to determine the accuracy to which they represent reality (Brinkgreve, 2013). The scope of the model validation for this study was limited because of the absence of published information on physical model tests, full scale model tests, or projects where RIs have been used for this purpose. Instead the validation process for this study has focused on some of the soil-structure interaction phenomena for which there are known approximate solutions.

1.4 Thesis Overview

In the first part of chapter 2 RI ground reinforcement is defined, classified and the load transfer mechanisms relevant to the problem are described. In the second part, the various strategies to reduce lateral loading and the effects of lateral loading are presented. Importantly, this chapter highlights the load transfer mechanisms which need to be validated in the numerical model. In chapter 3, the development of the ground improvement strategy is explained and justified. In chapter 4 the numerical model is described and the numerical analysis methodology explained. This chapter outlines the modelling strategy used to achieve the objectives of this research. The results of the numerical simulations are described in chapter 5. Finally, chapter 6 summarises the main conclusions, as well as providing recommendations for further research.

Chapter 2 Literature Review

2.1 Introduction

In line with the objectives of this research the first part of this literature review provides an overview of rigid inclusion ground improvement. It is broad in its scope which enables a technical appraisal of the method for the case of a caisson container quay wall. In this regard emphasis is placed on the scientific understanding of the mechanics of the problem, analysis methods and suitable installation methods for marine execution. One of the key outcomes of this section was identifying the problem of lateral loading of the inclusions due to "free-field" lateral ground movements. Unreinforced rigid inclusions are vulnerable to lateral loading due to their brittle behaviour. The second part of this review addresses this problem by presenting strategies for limiting and accommodating lateral loading of piles due to ground movements. A wide range of literature sources have been used, including published research, case histories, state of the art reports and design guidelines and codes.

2.2 Rigid Inclusion Ground Improvement

2.2.1 General concept, classification and definitions

The following sections firstly place the RI foundation system within the general framework of the major foundation types. Secondly rigid inclusions are classified and distinguished from the other categories of ground improvement and reinforcement. Finally the various components of the rigid inclusion system are described in detail.

2.2.1.1 The rigid inclusion system and other foundation types

In civil engineering, foundations can be classified as either shallow, deep / piled or mixed (Figure 2.1). In a general sense shallow foundations are those foundations for which the depth of embedment is less than the minimum lateral dimension of the foundation element; for example spread footings, strip footings and mat or raft foundations (API, 2005). By comparison deep foundations such as drilled shafts or piled foundations generally have a much longer depth dimension.

Shallow foundations are preferable if the foundation soil, under load, undergoes limited shear failure and yields associated settlements acceptable for the structure. If either of these two requirements are not met then deep or piled foundations are typically used. Piles are designed to carry the entire load from the structure via a rigid connection at their head. The majority of the load is often transferred to a deeper better quality bearing stratum. However there are many intermediate situations where shallow foundations, such as a raft, have adequate bearing capacity but the settlement or differential settlement exceeds acceptable values for the structure. Applying a deep foundation system may lead to an "overdesigned" solution.

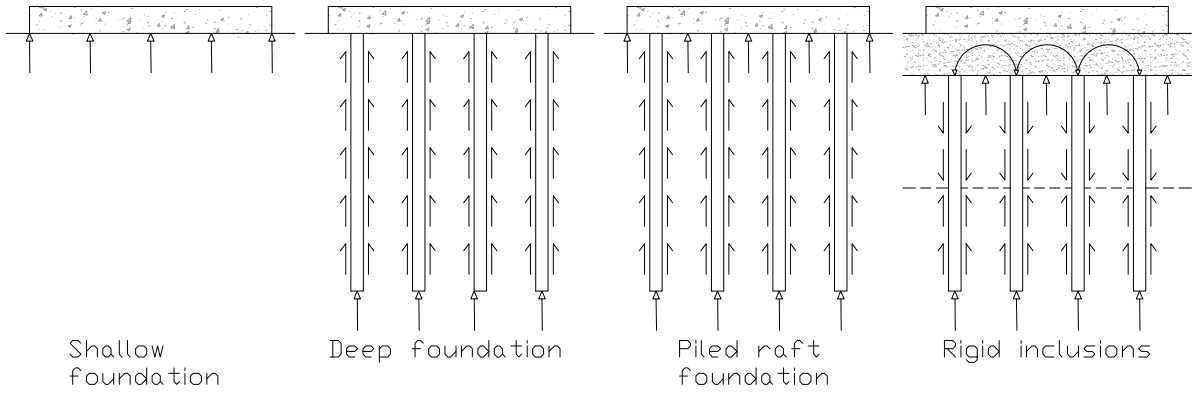

Figure 2.1– Various types of foundations (ASIRI, 2012)

An alternative intermediate solution between shallow and deep foundations, known as a piled raft foundation, was first proposed by Davis and Poulos in 1972 and in recent decades has been described by many authors (Cooke 1986, Horikoshi & Randolph 1996, Chow et al. 2001, Poulos 2001). The concept of a piled raft foundation is relevant where the load sharing between the piles and the raft, via a rigid connection, is taken into account. The benefit of this system is immediately apparent as the load shared with the raft means a decreased design load transferred to the pile head and a potential reduction in the required pile length or diameter. A common design approach is to use the piles as purely settlement reducing elements. In this case the piles are not required to insure stability because

the raft in this system has adequate bearing capacity. Therefore, the piled raft foundation can be very economical compared to traditional foundation concepts.

A foundation reinforced with RIs is similar to a piled raft foundation. Both are characterized by vertical rigid columns overlain by the general foundation; in this case a raft. From a purely theoretical standpoint the RI concept becomes valid once the conventional rigid linkage between the piles and the overlying structure disappears (ASIRI, 2012). This is achieved by introducing a load transfer platform between the inclusions and the overlying structure. Similar to the piled raft concept, a foundation reinforced with RIs involves load sharing between structure, inclusions and in situ soil. The RI foundation system is classed a composite foundation, comprising various modes of interaction between the various components making up the system.

Figure 2.2 shows the various components of a foundation reinforced with RIs. (1) The in situ soil, usually soft to firm, is reinforced with (2) rigid inclusion's which may or may not have a cap; (3) a granular layer overlies the rigid inclusions which sometimes includes (4) geotextile/geogrid type reinforcements, both of which serve to transfer the load from the (5) structure to the soil and RIs.

2.2.1.2 Classification of rigid inclusions

In the TC17 State of the Art Report (Chu et al., 2009) covering geotechnical construction processes, Rigid Inclusions are defined as a type of ground reinforcement, and are described as semi-rigid or rigid integrated columns, or bodies, installed in soft ground to improve the ground performance globally, so as to decrease settlement and increase the bearing capacity of the ground. The same report classifies RIs in category C, for ground improvement with admixtures or inclusions, in the same category as vibro-replacement (VR), stone columns (SCs), dynamic replacement (DR), sand compaction piles (SCPs) and geotextile confined columns (GCCs). In a broad sense SCs and SCPs are similar to RIs. They all involve the introduction of vertical columnar elements significantly stiffer than the surrounding soil. However they are treated separately in the TC17 report because the materials used for those columns such as sand and stone (granular) would collapse without the lateral confining support of the surrounding soil.

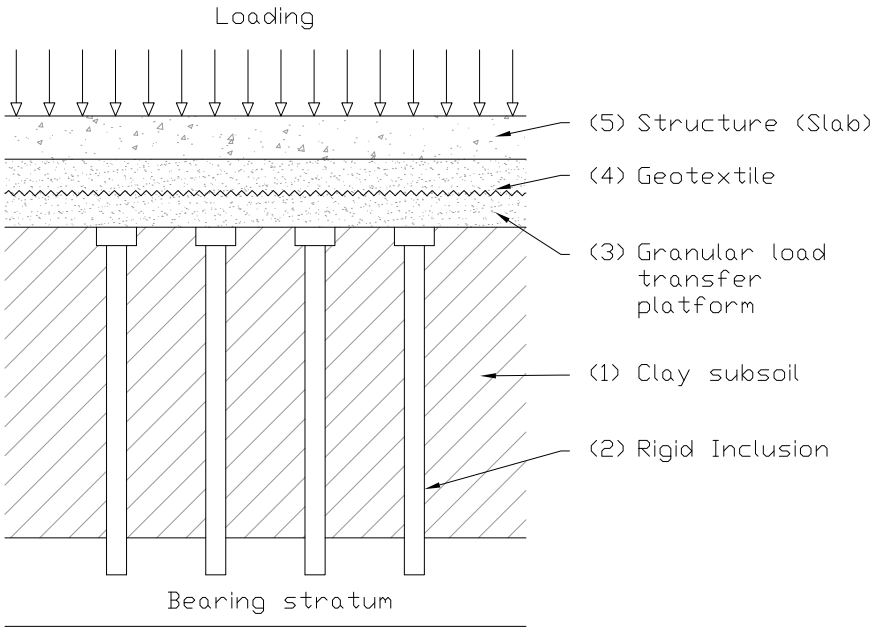

Figure 2.2 – Components of the rigid inclusion system (ASIRI, 2012)

It is helpful at this stage to make a distinction in terminology between a rigid inclusion "system" and the rigid inclusion elements themselves. The pile-like point bearing elements are referred to as rigid inclusions, and the load transfer platform together with the in situ soil reinforced with rigid inclusions is referred to as the overall "system".

2.2.1.3 Rigid inclusions

Rigid inclusions are similar to piles in geometry with predominately round or square cross sections. They are typically long, slender and orientated vertically (Figure 2.2). They are generally arranged in a regular rectangular or triangular grid pattern as shown in Figure 2.3 (Han, 2015). The term "group" is employed in describing these regular patterns of RIs (ASIRI, 2012). The diameter and layout of a group of inclusions is a function of the applied load, in situ soil conditions and structural performance criteria.

RIs are defined by their significant stiffness in relation to the surrounding soil and the term "rigid" is thus employed to describe their rigidity (ASIRI, 2012). Their stiffness varies widely depending on the material used to construct the RIs, such as lime, concrete, steel or a soil binder mix. Typical RI stiffness varies from 250 MPa to 30000 MPa (ASIRI, 2012). Although a range of materials are used,

they all exhibit a strong permanent cohesion, meaning column stability is provided without any lateral confinement from the surrounding soil (Simon, 2012).

Figure 2.3– Rigid Inclusions (Vibro Concrete Columns) in a rectangular grid pattern (Balfour Beatty, 2016)

There are many different types of RIs which are differentiated on the basis of their installation technique and mechanical properties such as stiffness and strength. Table 2.9 in section 2.2.10 identifies large families of RIs. The four main installation techniques are driven/hammered, displacement, bored and treated. Driven or hammered RIs usually require some form of dynamic action such as vibration for installation. Displacement methods involve pushing the in situ soil aside during installation. Bored inclusions involve excavation of the in situ soil where the inclusion is to be formed. When a binding agent such as grout or lime is jetted or mixed into the soil the term treated soil columns is used. The stiffness and strength of the various types of inclusions varies according to the type of concrete, grout or binder and soil; broad families of RIs can be further subdivided on this basis.

RIs are generally designed to carry a large share of the applied load. For this reason they are generally extended through any unfavourable material to a stronger, stiffer load bearing stratum. In most applications loading is predominately vertical and RIs are designed to withstand these loads, typically without the need for reinforcement.

In comparison to piles RIs are only broadly similar. Typically RIs have much lower strengths and stiffness's, mainly for economic reasons (Chu et al., 2009). The mechanism by which they transfer load is different. RIs are designed reduce the load on the in situ soil rather than transmit the entire

load to a deeper load bearing stratum. Finally, as will be discussed in the following section, load transfer between structure and inclusion takes place through a flexible layer as opposed to a rigid connection to the structure.

2.2.1.4 Load transfer platform

The rigid inclusion concept by definition implies that there is no rigid connection to the overlying structure. The load from the structure is transferred and distributed by an interposed layer between the structure and RIs (Figure 2.2). This layer is called the “load transfer platform”, but has been variously described in literature as a “granular mattress”, “thin-fill platform” and a “granular mat”.

The load transfer platform (LTP) is typically thin in relation to its lateral extent. However its thickness is a significant variable in controlling load transfer efficiency and vertical settlement. Typical LTP thicknesses are in the order of 40 cm to 80 cm which allows for efficient load transfer between inclusions and soil and a uniform stress distribution at the interface with the overlying structure (ASIRI, 2012).

The materials used to construct the LTP vary depending on the type of overlying structure as well as the installation conditions. Load transfer platforms are typically composed of a well compacted granular material such as sand or stone (ASIRI, 2012). Geotextile sheets can be used to reinforce the granular material to create a composite LTP. Hydraulic binders such as lime or cement are sometimes incorporated in the LTP. The strength and stiffness of these component materials influence the load transfer efficiency of the LTP.

2.2.2 Applicability: soils and structures

2.2.2.1 Applicable soils

In theory the rigid inclusion system may be applied to all soil types (Figure 2.4). In practice however, the most efficient and cost effective use of this method is in saturated, very soft to firm, fine grained soils i.e. clays, silts, peat (ASIRI, 2012). Due to their low strength, high compressibility and low permeability these soils generally have inadequate bearing capacity and undergo excessive long term deformation.

The RI system is not uniquely suited to improving the foundation performance of very soft to firm cohesive soils. Other methodologies include preloading with vertical drains, vibro replacement or

stone columns, sand compaction piles, and deep mixing methods. The most widespread application of rigid inclusions relates mainly to the limits of these conventional soil improvement techniques in terms of degree and depth of improvement (ASIRI, 2012).

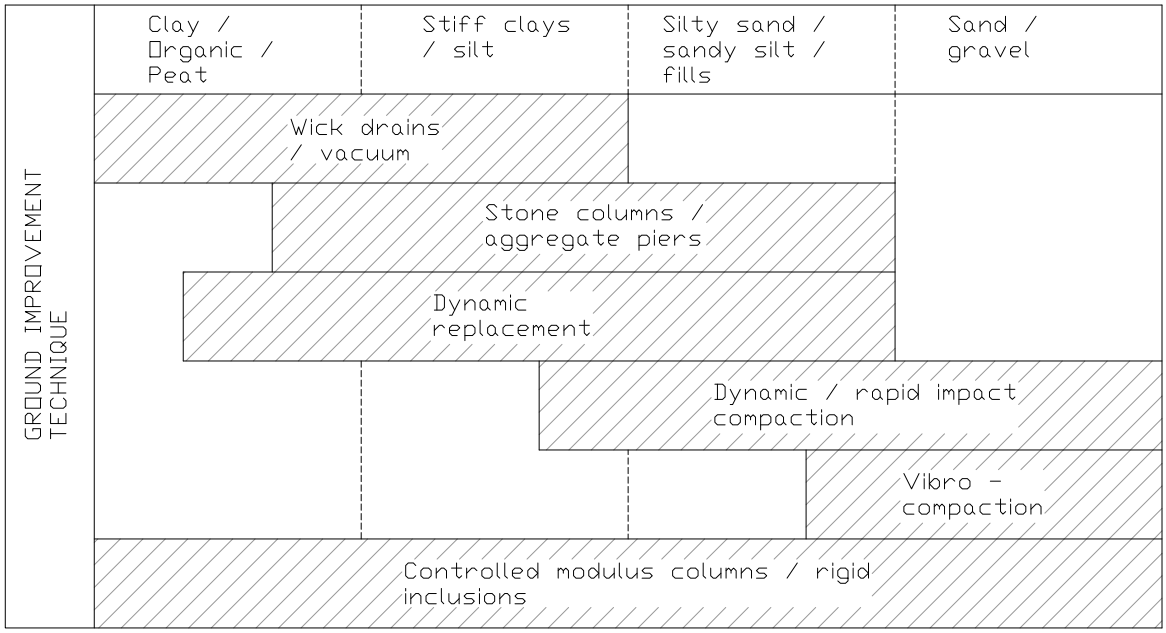

Figure 2.4 – Applicable soils for various ground improvement techniques (Menard, 2016a)

2.2.2.2 Applicable structures

RI ground reinforcement has been implemented in the foundation works for a diverse range of structures. Examples include piled earth embankments, piled bridge abutments with piled embankment approaches, slabs and foundations for industrial buildings, tanks and basins (Figure 2.5 to Figure 2.7). These structures can be divided into flexible structures such as earth embankments and rigid structures such as slabs and rafts. They all have large foundation footprints with relatively large loads which are uniformly distributed. Generally speaking under these conditions RI ground reinforcement is well suited to improving ground performance. In contrast very large locally concentrated loads will typically remain in the domain of more conventional deep foundations with piles (ASIRI, 2012).

The RI system allows for quickly raising the structure and immediately mobilising the design ground resistance (ASIRI, 2012). This is advantageous for slab or raft type structures where there is little allowance for settlement during construction; and for embankment type structures where there may be

little or no construction time available for a phase by phase embankment lift operation, which may be required to ensure stability.

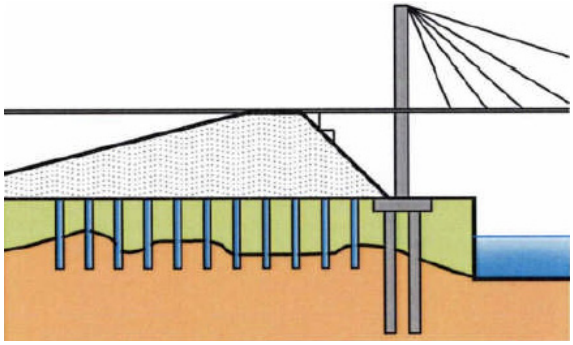

Figure 2.5 – Piled bridge abutment with piled embankment approach (ASIRI, 2012)

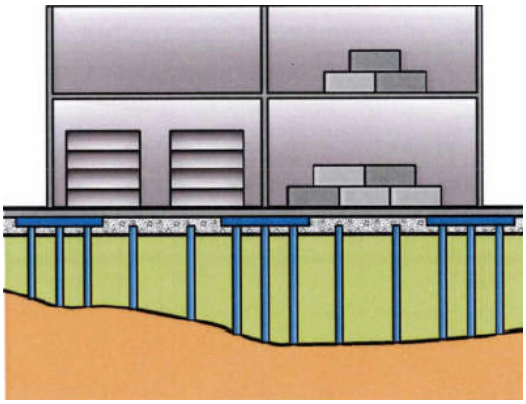

Figure 2.6 – Slabs and foundations of industrial buildings (ASIRI, 2012)

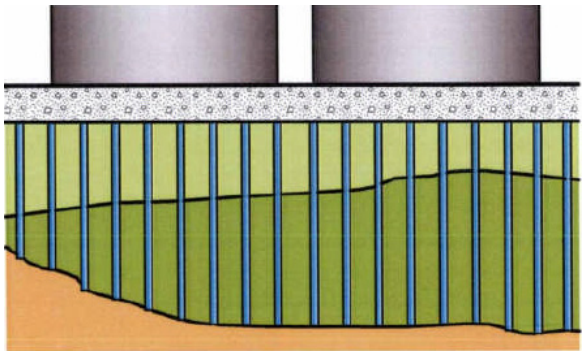

Figure 2.7 – Tanks and basins (ASIRI, 2012)

2.2.3 Research initiatives and implementation in major civil projects

2.2.3.1 Research initiatives

In the TC211 general report covering recent developments in the field of rigid inclusion ground improvement, Simon (2012) pointed out that construction practice has developed ahead of the design methods adapted for this new foundation concept. The application of RI ground reinforcement varies between countries but most commonly relates to piled embankments. More recently as the methodology has become more accepted in the marketplace their use has been extended to support structural elements such as rafts, slabs and spread footings.

In recent years several national funded research programmes have been undertaken to close the gap between research and construction practice. These institutions and programmes include the Research Centre for Soft Soils in Malaysia (NO RECESS), the Marie Curie Research Training Network "Advanced modelling of Ground Improvement on Soft Soils (AMGISS), the ASIRI National Project funded by the French Government and the Institute for Applied Research and Experimentation in Civil Engineering (IREX). The Dutch initiated a research programme on piled embankments with the aim of further optimising the Dutch CUR 226 design guidelines for piled embankments. A German research project undertaken by the Institute of Geotechnics at the University of Kassel was aimed at developing new design procedures for introduction into EBGEO, chapter 6.9 "Reinforced earth structures on point or line shaped bearing elements" (German Geotechnical Society, 2012).

As a result of these research initiatives, amongst others, several key publications have been issued in recent years covering recommendations for the design, construction and monitoring of rigid inclusion ground improvements. Germany, Britain and the Netherlands published revised guidelines for the design of piled embankments (EBGEO, 2010, BS8006, 2010, CUR 226, 2010). Importantly, France is the only country to publish guidelines that cover both piled embankments and slab or raft foundations (ASIRI, 2012).

2.2.3.2 Implementation in major civil projects

Table 2.1 and Figure 2.8 to Figure 2.13 provide examples of major projects where RI ground improvement has been implemented in the foundation design.

Table 2.1 – Examples of RI implementation in major civil projects

Brief description of project and structure	Application	Country / year	Reference
Large diameter oil storage tanks - Foundations include soil reinforcement using CMCs	Ring beam	USA / 2012	(Buschmeier et al., 2012)
Large embankment and bridge approach for the West Coast Highway B5 - Foundations include soil reinforcement using CMCs	Embankment	Germany / 2012	(Kirstein, Wittorf & Wittorf, 2012)
Large embankment and bridge approach for the relocation of highway B176 - Foundations include soil reinforcement using CMCs	Embankment	Germany / 2012	(Kirstein et al., 2013)
Large embankment and bridge approach for Breakwater Road Bridge - Foundations include soil reinforcement using CMCs	Embankment	Australia / 2011	(Fok et al., 2012)
Storage facility for active nuclear waste (ICEDA Project) – Foundations include soil reinforcement using concrete inclusions. See Figure 2.11.	Raft	France / 2010	(ASIRI, 2012)
Rion-Antirion Bridge - Soil reinforcement using steel tubes for three bridge supports. See Figure 2.12 and Figure 2.13.	Gravity caisson	Greece / 2004	(Dobry et al., 2003)
Transition between deck-on-piles and embankment for a container dock (Saint-Nazaire Port authority) - Foundations include soil reinforcement using fiber-reinforced concrete inclusions. See Figure 2.10.	Embankment & pavement	France / 1999	(ASIRI, 2012)
Access embankments and shallow foundations for the A43 motorway - Foundations include soil reinforcement using deep mixed columns. See Figure 2.9.	Embankment & raft	France / 1991	(ASIRI, 2012)
Reinforced earth protection walls (Indonesian LNG retention reservoirs) - Foundations include soil reinforcement using open tell tubular piles.	Reinforced earth wall	Indonesia / 1982	(Simon & Schlosser, 2006)

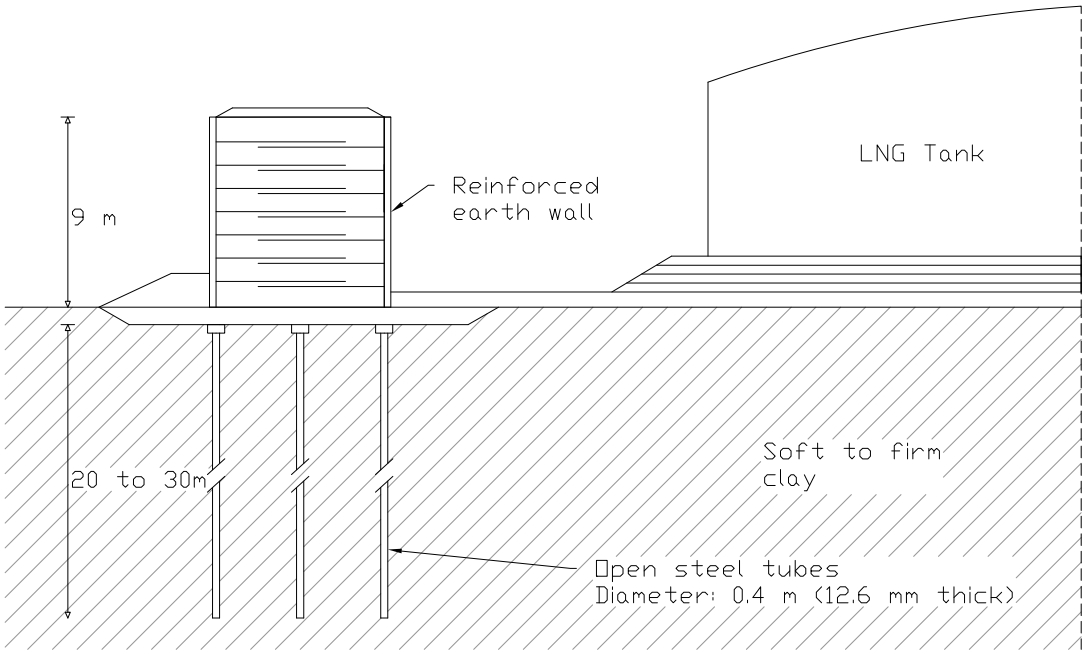

Figure 2.8 – Schematic diagram of a reservoir foundation supported on RIs in Indonesia (ASIRI, 2012)

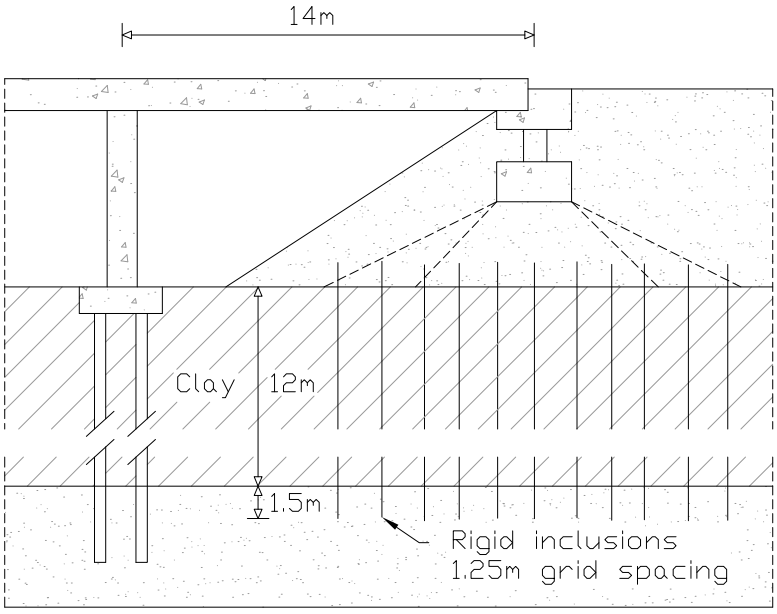

Figure 2.9 – Schematic diagram of a bridge abutment and embankment supported on RIs for the A43 motorway in France (ASIRI, 2012)

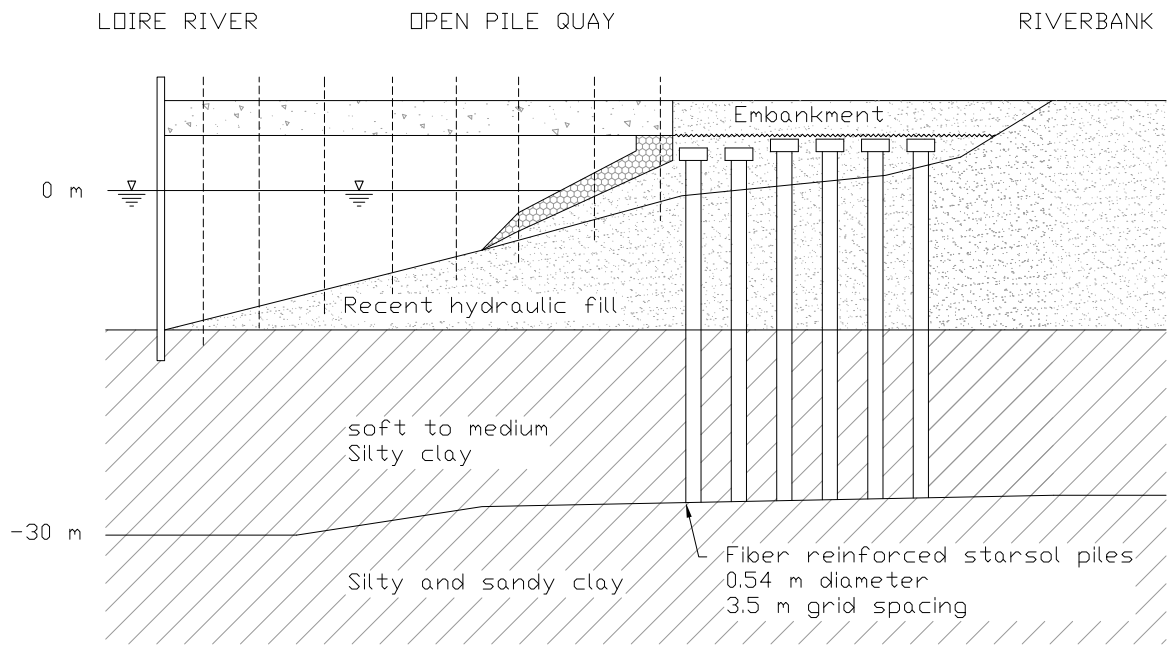

Figure 2.10 – RIs between deck on piles and riverbank in France (adapted from ASIRI, 2012)

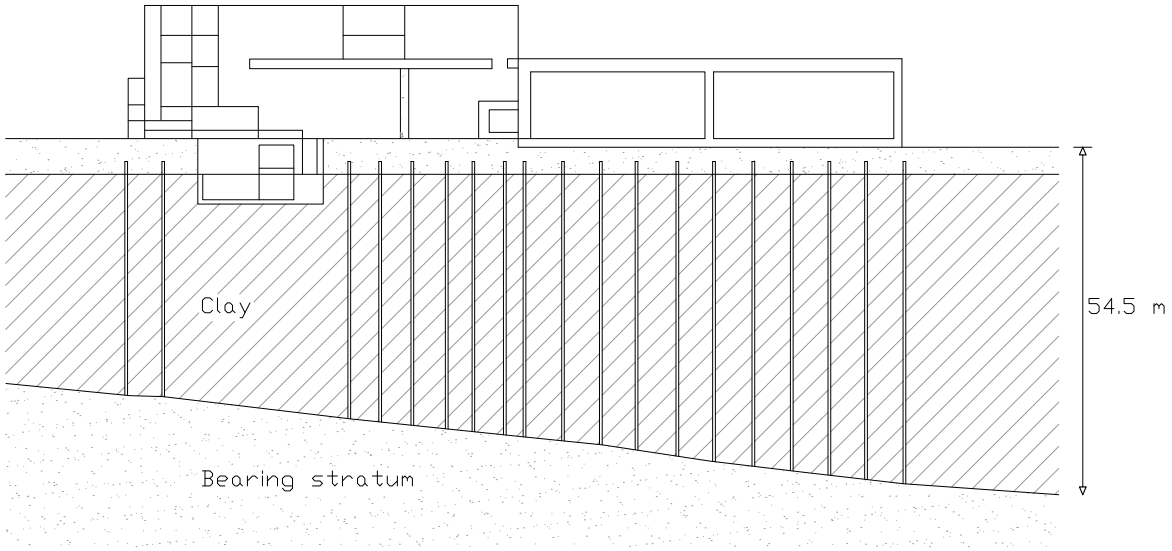

Figure 2.11 – RIs under an active waste facility (ICEDA) in France (adapted from ASIRI, 2012)

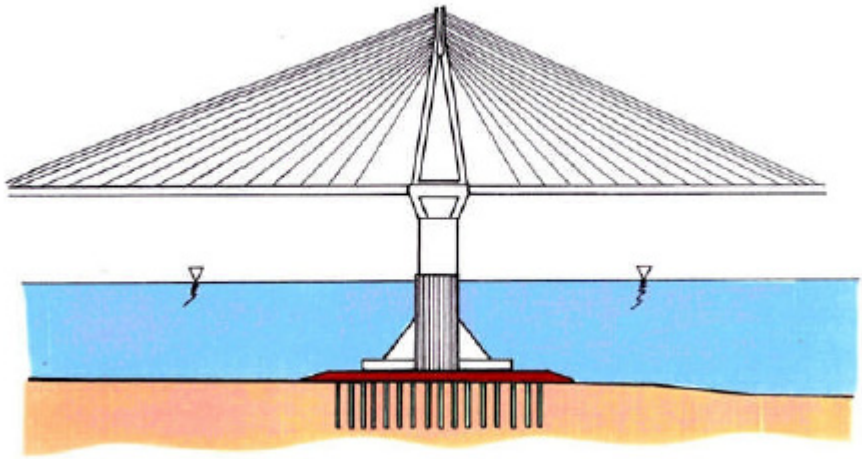

Figure 2.12 – The Rion-Antirion Bridge in Greece (ASIRI, 2012)

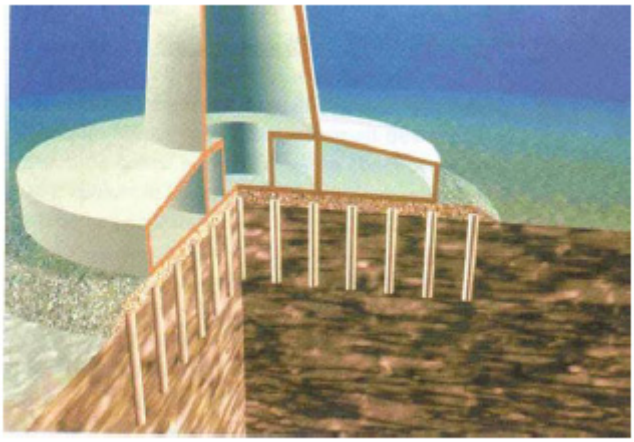

Figure 2.13 –Rion Antirion Bridge pier showing caisson, gravel layer, natural clay and RIs (Dobry et al., 2003)

2.2.4 Vertical load transfer mechanisms above the inclusion head

2.2.4.1 Introduction

This section describes the mechanisms by which vertical load is transferred from the structure to the inclusion head through a granular load transfer platform (Figure 2.14). The primary mechanism is known as arching (Figure 2.15). When geosynthetic reinforcement (GR) is included in the system, additional load transfer occurs due to membrane action. The boundary condition imposed at the base of flexible structures is different from a rigid structure. This affects the way load is transferred to the reinforced soil and therefore the load transfer mechanisms for rigid and flexible loading are presented separately in in section 2.2.4.5 and section 2.2.4.6.

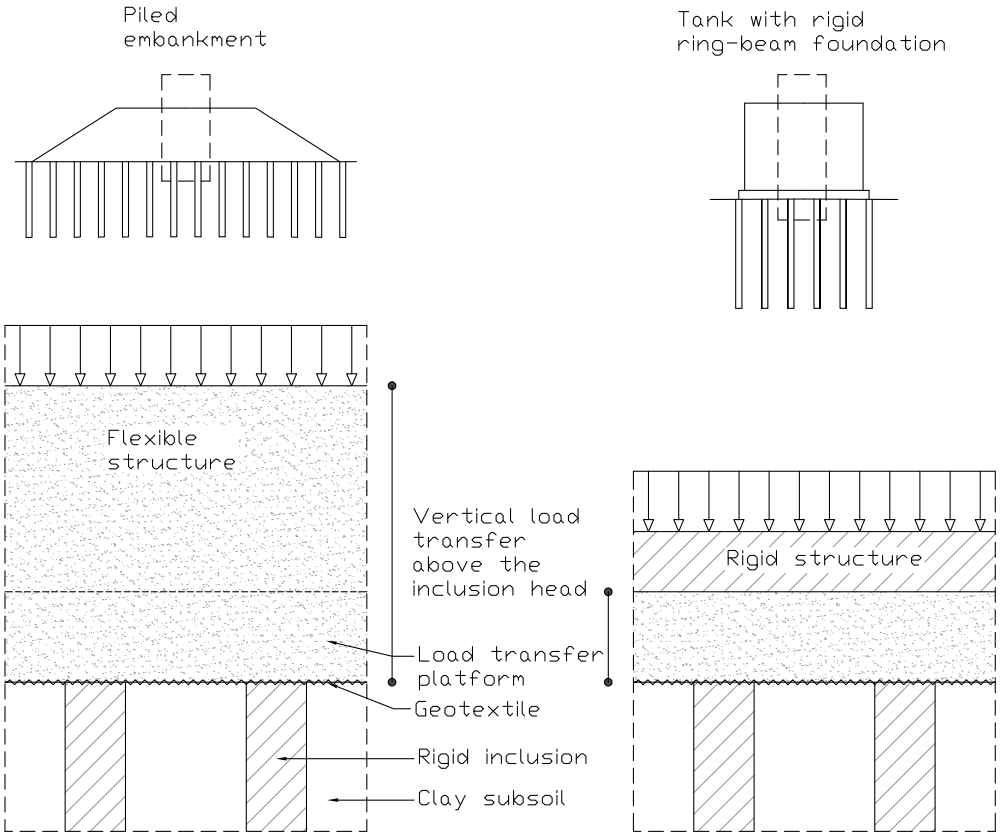

Figure 2.14 – Vertical load transfer above the inclusion head

2.2.4.2 Boundary conditions imposed by a rigid or flexible structure

The boundary conditions imposed at the base of a structure affects the way load is transferred to the underlying foundation. For the case of an earth embankment this boundary may not be distinct from the embankment in terms of state and composition (Figure 2.14). There are two ideal loading and displacement conditions at this boundary, namely equal strain and equal stress (Han, 2015). The equal strain condition exists under rigid loading (slabs, rafts or footings). The equal stress condition exists under flexible loading (earth embankment).

Figure 2.16(b) shows rigid loading from a slab imposing a plane of equal settlement at its base. For the case of flexible loading from an embankment, a plane of equal stress is located at some height above the inclusions, in this case at the surface (Figure 2.16a). Both types of loading result in the columns carrying a higher stress than the surrounding soil due to the difference in stiffness between the soil and the columns. In both situations the reinforced soil between the columns settles more than the columns, resulting in differential settlement at the level of the columns. It is apparent that the particle displacement patterns are different for the two types of loading. While both result from an arching mechanism the arching patterns are different. The significance of these features is discussed in more detail in the following sections.

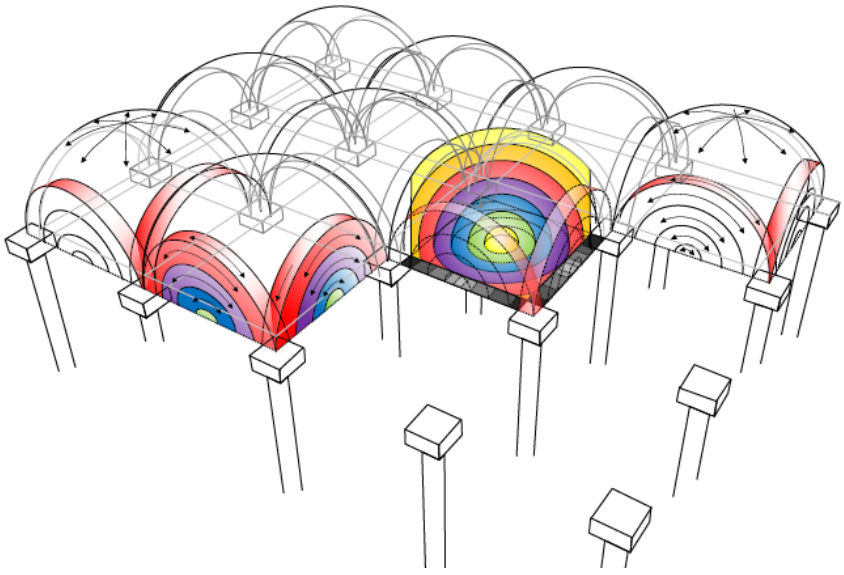

Figure 2.15 – The analytical concentric arch model (van Eekelen, Bezuijen & van Tol, 2013)

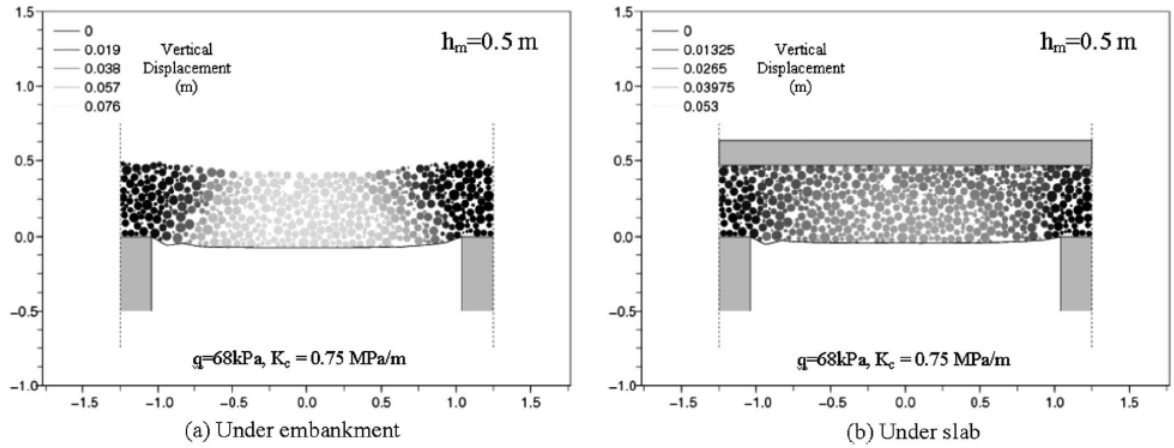

Figure 2.16 – Particle displacements in the LTP (a) under an embankment and (b) under a slab (Girout et al., 2014)

2.2.4.3 Unit cells, area replacement ratio and other terminology

Along with idealised assumptions of the boundary conditions, researchers often use a simplified "unit cell" approach to analyse and describe columnar reinforced foundations. The term "unit cell" describes the support offered by a single column, A_c and its zone of influence in the surrounding soil A_s (Figure 2.17).The dimensions of a unit cell are influenced by the columns cross sectional area, column spacing and column layout pattern. To compare the effects of these parameters in terms of the area of soil replaced by the column, an area replacement ratio is defined as the ratio of the sectional area of a column to the ground occupied by a single column:

$$a_s = \frac{A_c}{A_s} = C\left(\frac{d_c}{s}\right)^2; \tag{2.1}$$

$$C = 0.785\ for\ square\ pattern\ \&\ 0.907\ for\ equilateral\ triangular\ pattern$$

The area replacement ratio varies widely depending on the structural application and type of inclusion. In Sweden and Finland a_s values are typically between 10 % and 25 % (Broms, 2004). In Japan values generally larger than 30% and often exceeding 50% are used (Kitazume & Terashi, 2013). In Dutch practice values between 4.5 % and 12 % are commonly used (van Eekelen, Bezuijen & van Tol, 2013). Codes of practice often specify a minimum spacing of three to four diameters between displacement piles to limit their interaction, which can place a practical limit on the area replacement ratio (ASIRI, 2012).

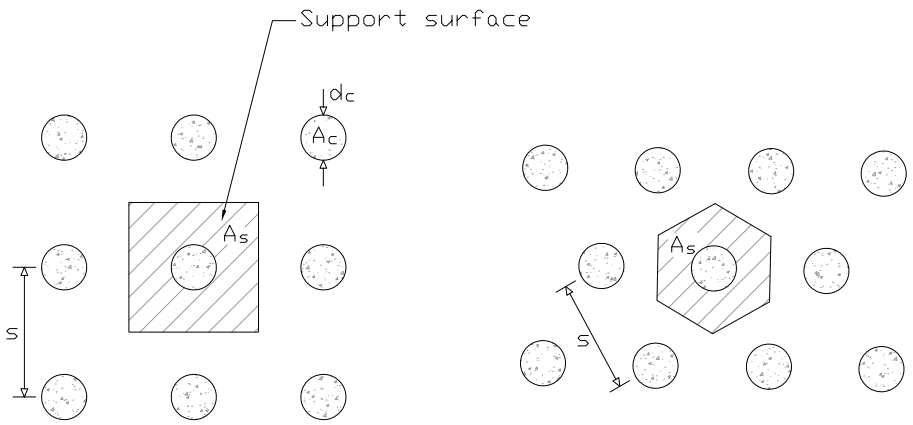

Figure 2.17 – Spacing of bearing elements, zone of influence and support surface

As described in the previous section RIs attract a higher stress than the surrounding soil due to the difference in stiffness between inclusion (E_i) and soil (E_s). The stress concentration ratio (n) is often used to describe this load transfer above the inclusion head and is defined as the ratio of the stress on the inclusion (σ_i) to that on the soil between inclusions (σ_s):

$$n = \frac{\Delta\sigma_i}{\Delta\sigma_s} = \frac{E_i}{E_s} \tag{2.2}$$

The stress concentration ratio is not constant and depends on the stress-strain relationship between inclusion and soil. Concrete columns with their high stiffness have n values of more than 10 whereas granular columns typically have values from 1.0 to 5.0 (Han, 2015).

Another important aspect of columnar reinforced foundations is the degree to which they reduce foundation settlement. It is common practice to consider the settlement efficiency (E_{sett}) of the reinforcement system, which is given by:

$$E_{sett} = 1 - (\delta_v/\delta_0)$$

Where, δ_0 is the settlement of the virgin soil without reinforcement and δ_v is the settlement of the reinforced soil. Lateral deflection efficiency (E_{lat}) can be evaluated in the same way. Both are a measure of the effectiveness of the reinforcement in reducing settlement or lateral deflection.

2.2.4.4 Arching and membrane action

Arching is the load transfer mechanism that results in stress concentration at the inclusion heads. It occurs in soils when there is an "inclusion" within the soil mass with significantly different material properties and/or structure (Iglesia, Einstein & Whitman, 2014). Handy (1987) stated that "arching" is defined in civil engineering as the transfer of stress from a yielding part of a soil mass to adjoining less-yielding or restrained parts of the mass. Considering the case of an embankment supported on ground reinforced with RIs (Figure 2.18), the inclusions are significantly stiffer and stronger than the surrounding soil mass. During loading, stress redistribution brings about an increase in loading (passive arching) over the less deformable areas above the inclusions, as well as a decrease in load over the adjoining deflecting or yielding areas between inclusions.

The remaining portion of the embankment load that is not redistributed towards the inclusions through arching is carried by the soil between the inclusions. When the load transfer platform includes a geotextile at its base, this load is applied to the geotextile causing the soil to deform and the geotextile to deform in a similar manner. The geotextile is supported at the inclusion positions which results in differential deformation. Stretching occurs along its longitudinal axis with the result being the development of tension in the geotextile layer. This is known as membrane action. Espinoza & Bray (1995) state that the purpose of adding a geotextile is to increase the bearing capacity of the system due to three soil-structure interaction effects:

- Membrane support contribution due to the deformed geotextile sustaining normal stresses that result in membrane tension forces.
- Membrane support contribution due to the deformed geotextile sustaining shear stresses that result in a membrane tension forces.
- A subgrade bearing capacity improvement due to the geotextile reducing outward shear stresses transmitted from the overlying structure to the top of the subgrade.

The load transfer mechanisms described above have been the focus of much research in recent years. A diverse range of research methodologies have been used including small scale laboratory model tests, centrifuge model tests, full scale tests, field tests and numerical modelling. The findings from this research have led to a better understanding of the fundamental load transfer mechanisms, and importantly the factors affecting the transfer of load. The following two sections describe the major findings with respect to two common structural applications.

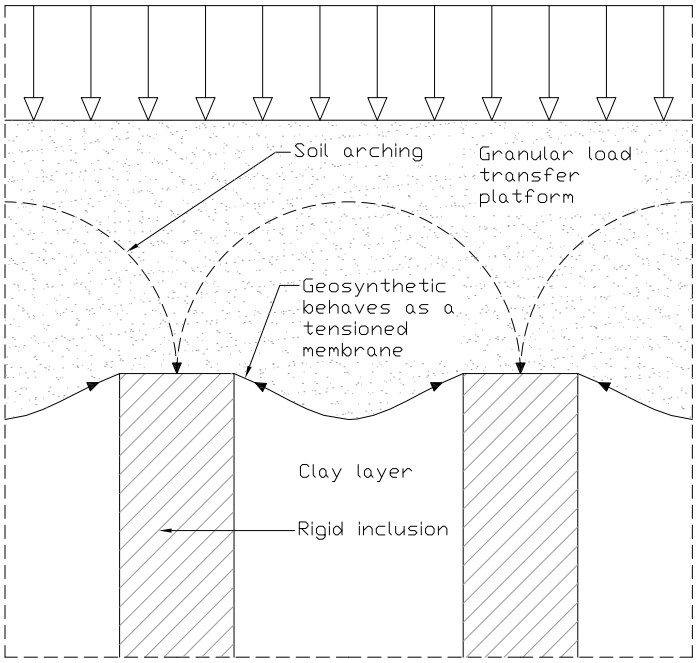

Figure 2.18 – Mechanisms of load transfer and interaction at the inclusion head (adapted from Kempfert & Raithel, 2005)

2.2.4.5 Case of an earth embankment

Several researchers have carried out experimental investigations on piled embankments. Most researchers have used simplified 3D small scale laboratory models (van Eekelen et al., 2012) or 3D centrifuge models (Ellis & Aslam, 2009; Okyay et al. 2010; Blanc et al. 2012; Girout et al. 2014). Jenck et al. (2009) used a number of stacked steel rods (soil analogue) to model the embankment (Figure 2.19), and Chen et al. (2008) modelled the inclusion head with a wall (beam). Both of these simplifications result in 2D symmetry which will simulate plane soil arching. Le Hello and Villard (2009) carried out four full scale instrumented experiments.

All researchers modelled the earth embankment with a granular sand material, except for Jenck et al. (2009) who used a soil analogue. Most researchers included geosynthetic reinforcement (GR).

A variety of methods were used to simulate the consolidation of the foundation soil and subsequent settlement of the load transfer platform. Le Hello and Villard (2009) simply took the foundation soil away, whereas other researchers used rubber foam or rubber foam chips to simulate compression of the subsoil (Ellis & Aslam, 2009; van Eekelen et al., 2012). Chen et al. (2008) simulated

consolidation by discharging water from two water bags. In their centrifuge models Okyay et al. (2010), Blanc et al. (2013) and Girout et al. (2014) simulated settlement by vertical displacement of a mobile tray.

Most researchers measured the stresses at the inclusion tops or bottoms, as well as the differential displacement of the embankment and load transfer platform (Chen, Cao & Chen, 2008; Le Hello & Villard, 2009; Blanc et al., 2012; van Eekelen et al., 2012; Girout et al., 2014; Okyay et al., 2014). Importantly, Van Eekelen et al. (2012) and Le Hello & Villard (2009) were the only researchers to measure separately the distribution of load over the foundation soil, the geosynthetic reinforcement and the inclusions. This makes it possible to compare the measurement results with the separate parts of the existing analytical models (van Eekelen et al., 2012).

Some researchers carried out numerical modelling. Both the finite element method (Le Hello & Villard, 2009; Girout et al., 2014), and discrete element method (Jenck, Dias & Kastner, 2009; Le Hello & Villard, 2009; Chevalier, Villard & Combe, 2010) were used.

The research results were used to discuss the mechanism of arching as well as the effect of several influencing factors such as the height of the load transfer platform, the properties of the load transfer platform, the properties of foundation soil, the effect of geotextile reinforcement, the effect of the area replacement ratio, and the effect of different types of loading.

Arching:

All researchers confirmed that load transfer to the inclusion heads occurred by arching. Many researchers visually observed arching, either through a transparent window on the model or by model photography during testing (Figure 2.19).

The arching mechanism is typically quantified by the load transfer efficiency (E), defined as the load acting on a single rigid inclusion head Q_{i0} to the total load applied on an unit cell Q_t (ASIRI, 2012):

$$E = \frac{Q_{i0}}{Q_t} \tag{2.3}$$

Chevalier et al. (2010) described an additional ratio G which quantifies the ability of the load transfer layer to redistribute any additional surcharge load ΔQ to the inclusion:

$$G = \frac{\Delta Q_t}{Q_t} \tag{2.4}$$

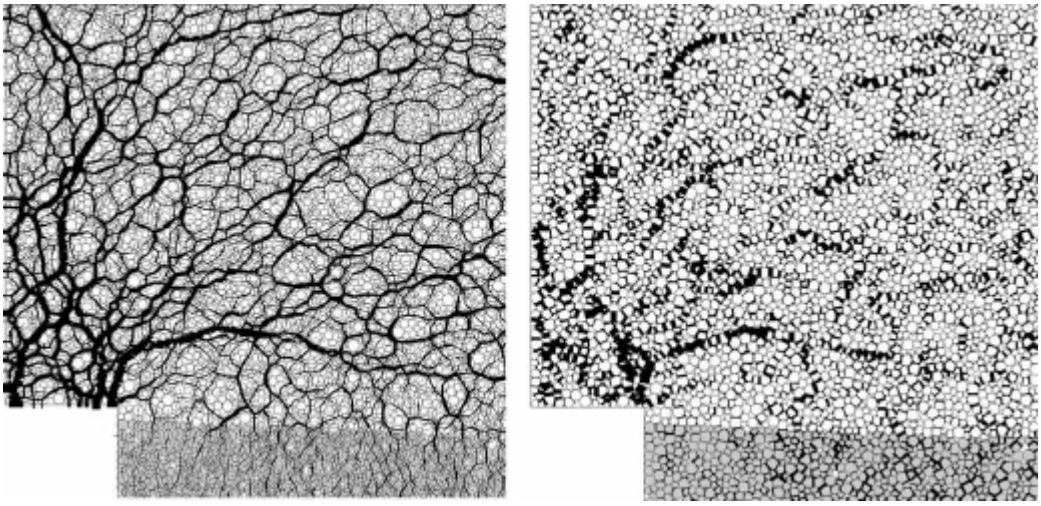

Figure 2.19 – Normal forces (left) and shear forces (right) highlighting arching in LTP (Jenck, Dias & Kastner, 2009)

Soil arching is strongly dependent on the relative displacement between the inclusion head and foundation subsoil, and there exists a critical relative displacement where the soil arching is most efficient in transferring load to the inclusion head (Chen, Cao & Chen, 2008; Chevalier, Villard & Combe, 2010). Chen et al. (2008) reported that the magnitude of this relative displacement is 8-13 mm. This point corresponds to the gradual mobilisation of shear strength within the granular material of the load transfer platform (ASIRI, 2012). A characteristic displacement pattern forms within the load transfer platform. A conical zone of relatively low displacement forms above the inclusion head. Shear stress concentrates along the boundary of the cone and the zone of higher settlement between inclusions. With reference to this characteristic pattern Carlsson (1987) suggested a cone angle, or angle of arching (Figure 2.20) equal to 15°, regardless of the LTP material characteristics (Chevalier, Villard & Combe, 2010). This is in agreement with Van Eekelen et al. (2003, 2012) who reported angle of arching values between 13.7° and 16.9°. Contrary to these findings, for a numerical study, Chevalier et al. (2010) reported an angle between 30° and 45° (Figure 2.21), which was correlated to the residual friction angle and peak friction angle of the LTP material respectively.

Influence of the height of fill:

Several researchers have reported that the load efficiency (E) increases with increasing fill height (H) above the rigid inclusion heads (Chen et al. 2008; Le Hello & Villard 2009; Jenck et al. 2009; Ellis & Aslam 2009; Chevalier et al. 2010; Okyay et al. 2010).

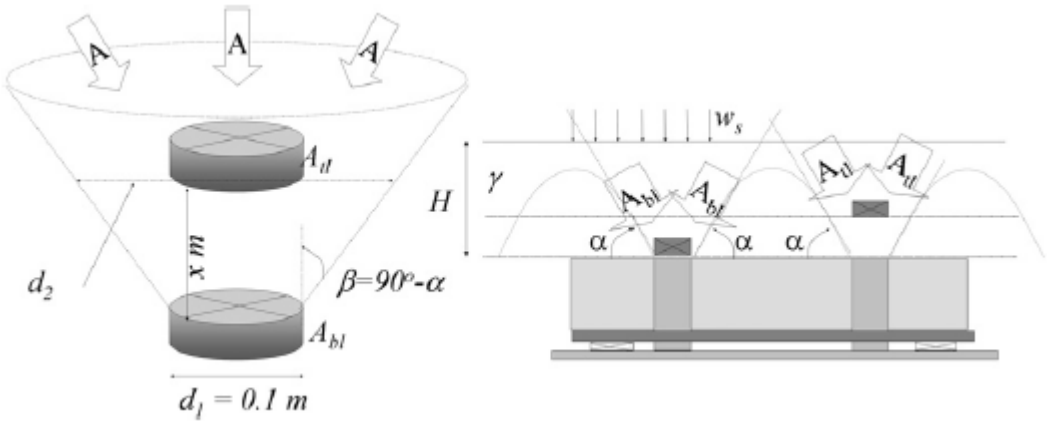

Figure 2.20 – Measuring the angle of arching (van Eekelen et al., 2012)

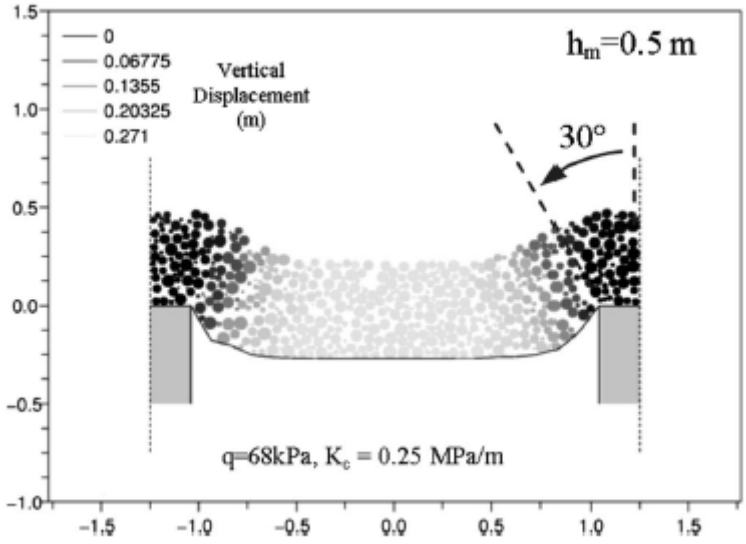

Figure 2.21 – Angle of arching measured from particle displacements (DEM) in vertical cross-section (Chevalier, Villard & Combe, 2010)

This increase in efficiency reaches a limiting value that defines what is called the critical height (Figure 2.22). This height corresponds to a plane of equal settlement in the arched embankment fill, where the shear forces have reduced to zero (Naughton, 2007). The critical height decreases with increasing fill height (van Eekelen, Bezuijen & van Tol, 2013). The critical height is a function of the diameter or width of the inclusions (d or a), spacing between inclusions (s) and the properties of the load transfer platform (ASIRI, 2012). In this regard the critical height is often expressed as a

proportionality factor multiplied by the clear span between adjacent columns (McGuire et al., 2012). To ensure full arching action and a plane of equal settlement at the LTP surface, various recommendations have been made with respect to the appropriate proportionality factor (Table 2.2 and Figure 2.22).

Table 2.2 – Summary of existing recommendations for minimum embankment height (McGuire et al., 2012)

Reference	Minimum embankment height*
BS8006 (1995)	$0.7(s-a)$
Carlsson (1987)	$1.0(s-a)$
Nordic Handbook (2002)	$1.2(s-a)$
Chen et al. (2008)	$1.6(s-a)$
Demerdash (1996)	$1.7(s-a)$
Hewlett & Randolph (1988)	$2.0(s-a)$
$*\ s = center\ to\ center\ spacing\ of\ columns\ or\ pile\ caps\ \ *a = width\ of\ square\ pile\ caps$	

Influence of the properties of the load transfer platform:

It has been shown (Figure 2.19) that shearing mechanisms result in arching in the load transfer platform. Shearing is related to the angle of internal friction of the LTP. Several researchers have confirmed this relationship (Jenck et al., 2009; Chevalier et al., 2010; Van Eekelen et al., 2012, 2013; Iglesia et al., 2014). Based on laboratory experiments Van Eekelen et al. (2012) concluded that the lower the friction angle of the LTP material, the less arching occurs during consolidation of the foundation soil.

Influence of geotextile reinforcement:

When the GR is stiff enough it works in membrane action by attracting load and distributing it to the inclusion head, resulting in larger loads at or near the inclusion head. It has been shown by Van Eekelen et al. (2012, 2013) that when GR is used in the LTP, the result is more efficient arching, a concentration of load on the GR, an inverse triangular load distribution on the GR, and a larger fall in stress with depth in the embankment, between the RIs, above the GR.

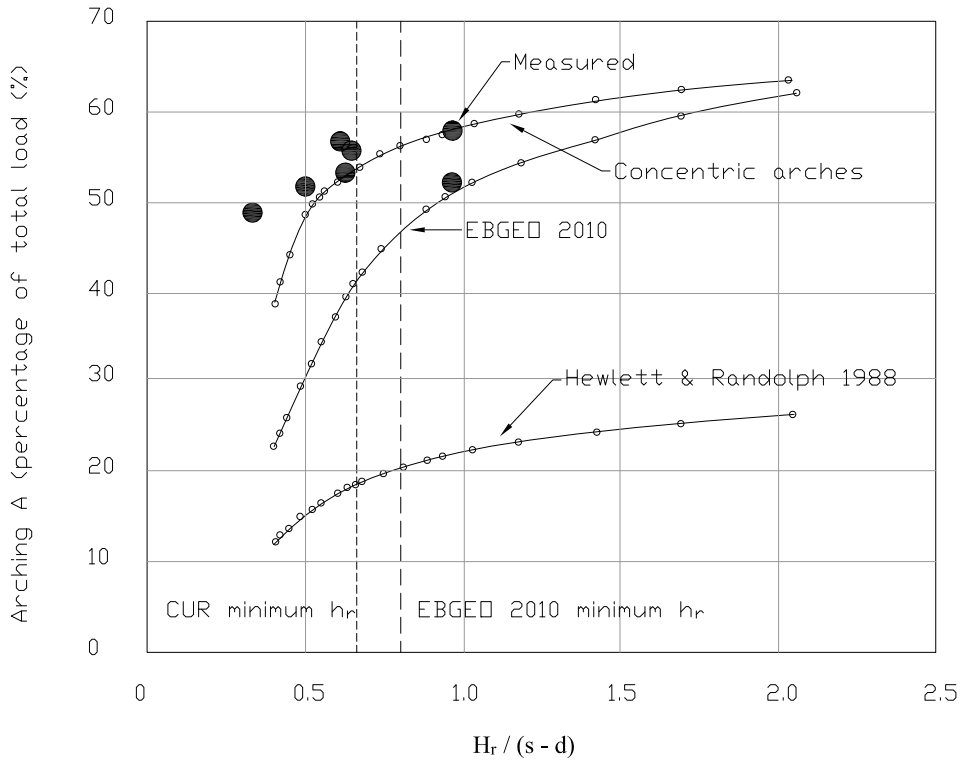

Figure 2.22 – Load efficiency (arching A) with fill height (van Eekelen, Bezuijen & van Tol, 2013)

Influence of the area replacement ratio:

The area replacement ratio describes the density of reinforcement. Various researchers have shown that the area replacement ratio has a strong influence on the load transfer efficiency (Jenck, Dias & Kastner, 2009; Okyay et al., 2014). Jenck et al. (2009) showed that the larger the area replacement ratio the greater the load transfer efficiency, with good correlation between experimental and numerical results.

Influence of the foundation subsoil conditions:

Van Eekelen et al. (2012) showed that consolidation or compaction of the subsoil results in an increase in arching. This agrees with Chen et al. (2008) who showed that soil arching is strongly dependent on the relative displacement between the inclusion head and foundation subsoil.

Influence of the type of loading:

In a centrifuge experiment with loading and unloading cycles applied by successive displacements of a mobile tray, Okyay et al. (2010) showed that loading-unloading cycles do not influence the maximum load at the inclusion head. However, they did report additional settlement of the foundation subsoil due to cyclic loading.

Analytical models:

Various analytical models have been developed which attempt to describe load transfer by arching and membrane action in piled embankments. Section 2.2.8 presents an overview of the available analytical models.

2.2.4.6 Case of a rigid slab, raft or footing

Rigid structures supported on ground reinforced by rigid inclusions, such as a slab on grade (Chevalier, Villard & Combe, 2010; ASIRI, 2012), the so called non-contact piled raft foundation (Fioravante & Giretti, 2010), or disconnected piled raft foundation (Cao, Wong & Chang, 2004) and footings (Dias & Simon, 2012), have received less research attention when compared to piled embankments.

Fioravante & Giretti (2010) performed a series of multi-g centrifuge test on piled raft models to understand the influence of a granular layer disconnecting the piles from structure. The load transfer platform as well as the subsoil was modelled using sand. Some of the model piles were instrumented with miniaturised load cells. Load was applied by a servo-controlled hydraulic actuator. Their focus was on the overall load-settlement behaviour of the system.

Cao et al. (2004) used a small scale laboratory model which simulated two dimensional plane-strain conditions. Both the foundation subsoil and load transfer platform were modelled using sand. The piles were instrumented with strain gauges and loads applied with hydraulic jacks. Various patterns of foundation reinforcement were investigated and their influence on foundation stiffness, differential settlement, pile forces and skin friction, load sharing between pile and raft and the effect of pile arrangement and number of piles.

Chevalier et al. (2010) carried out a numerical study by coupling the discrete element method (DEM) and the finite element method (FEM). These methods were used to model the granular load transfer layer and geosynthetic reinforcement respectively. Importantly this method was validated by Villard

et al. (2009) who carried out full scale field experiments. This study focused on the load transfer mechanisms in the load transfer platform. The results helped draw conclusions regarding the importance of the LTP thickness in relation to load transfer efficiency and magnitude of vertical settlement.

Load transfer mechanisms:

The stiffness of a rigid structure imposes a boundary condition of equal settlement at the base of the structure (Figure 2.16). When the LTP is less than the critical height, the resulting load transfer mechanisms are fundamentally different to those for a flexible structure. When a rigid structure is involved, a zone of relatively low displacement is restricted to a column between the inclusion head and the base of the rigid structure (Chevalier, Villard & Combe, 2010). Figure 2.16 clearly shows that this zone is less conical and more columnar than the displacement field of a flexible structure. Chevalier et al. (2010) commented that under rigid loading the total vertical settlement is a function of the deformation of the zone of relatively low displacement.

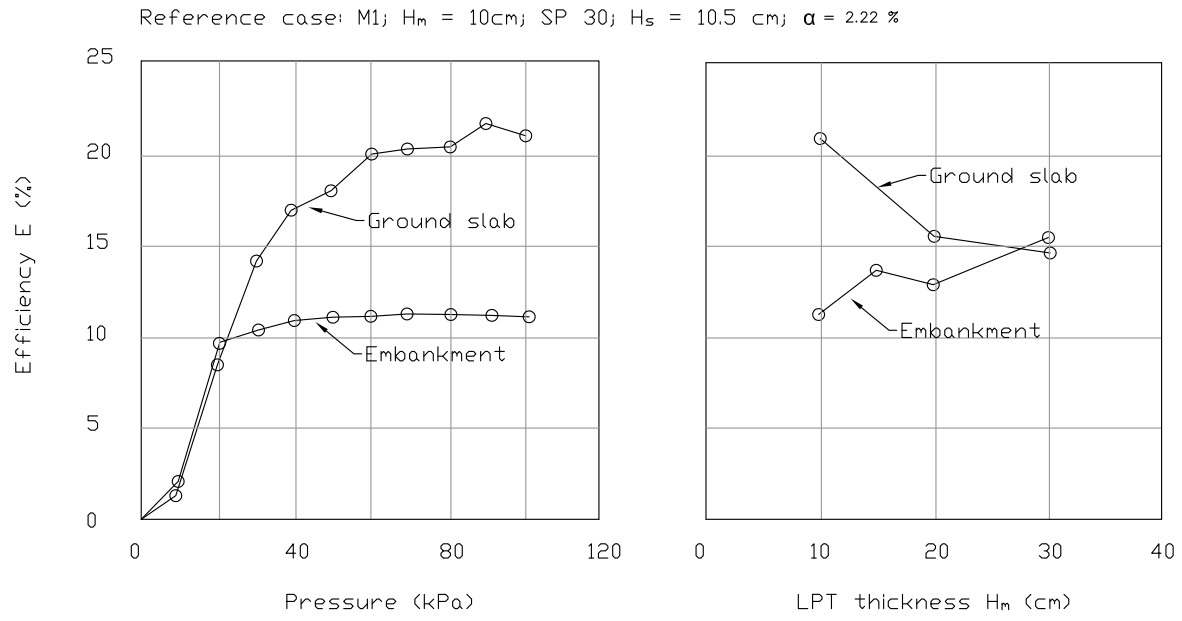

Figure 2.23 – Evolution of load efficiency versus transfer platform thickness for the case of an embankment and rigid structure (ASIRI, 2012)

Influence of the rigid structure

A rigid structure has a significant influence when the LTP thickness is less than the critical height. In this case the effect of the rigid structure is to increase both the load transfer efficiency (E) and transfer of surcharge (G) towards the inclusion heads (Chevalier, Villard & Combe, 2010).

Thickness of the LTP:

The thickness of the LTP has a controlling effect on both load transfer efficiency and the stresses developed in the base of the rigid structure. As the load transfer platform thickness increases the load efficiency decreases with a corresponding reduction in the bending stresses within the rigid base of a structure (ASIRI, 2012). Figure 2.23 shows that as the thickness of the transfer platform increases the efficiencies converge on a single vale.

Edge effect:

The conditions within the LTP at the edge of a structure may be significantly different to those under the central area of the structure. This is due to changes in geometrical conditions at the edge of a structure such as a limited lateral extent of the LTP. Additionally there may be a change in the effective stress conditions acting to confine the LTP in the vertical and horizontal directions. These factors may lead to significant stress variations at the edge of the structure which may result in a reduction in load transferred to the inclusion head, as well as inclined loading (ASIRI, 2012).

2.2.4.7 Summary

Fundamental concepts:

- The boundary conditions imposed at the base of a structure affect the way load is transferred to the underlying foundation.
- An equal strain condition exists under rigid loading such as slabs, rafts or footings.
- An equal stress condition exists under flexible loading from earth embankments.
- Both types of loading result in the columns carrying a higher stress than the surrounding soil due to the difference in stiffness between the soil and the columns.
- Arching is the load transfer mechanism that results in a stress concentration at the inclusion heads.
- When the load transfer platform includes a geotextile at its base additional load transfer occurs due to membrane action.

- The Area replacement ratio (a_s) is a measure of the density of reinforcement.
- The stress concentration ratio (n) is a measure of stress concentration at inclusion head.
- Load transfer efficiency (E and G) are a measures of load transfer efficiency to inclusion head.
- Settlement efficiency (E_{sett}) is a measure of the efficiency of the ground improvement system to reduce settlement.

Flexible structures – Embankments:

- Increasing embankment fill height increases the load transfer efficiency.
- There is a critical height where full arching action is achieved.
- An increase in the LTP strength (φ') increase the load transfer efficiency or arching efficiency.
- The additional of basal reinforcement in the LTP increases arching efficiency and results in additional load transfer by of membrane action.
- An increase in a_s results in increased load transfer efficiency.
- An increase in differential displacement due to subsoil deformation results in an increase in load transfer efficiency.
- Load transfer efficiency is unaffected by cyclic loading.

Rigid structures – Rafts, slabs footings:

- When the LTP is less than the critical a rigid boundary condition results in an increase in load transfer efficiency.
- An increase in LTP thickness reduces the load transfer efficiency.
- The geometrical conditions and stress conditions at the edge of structures can result in a reduction in load transfer efficiency and may cause eccentric or inclined loading.

2.2.5 Vertical load transfer mechanisms between inclusion and surrounding soil

2.2.5.1 Introduction

This section describes the load transfer mechanisms between the inclusion and the surrounding soil (Figure 2.24). Load transfer occurs along the inclusion shaft and at its base. When a pile settles more than the surrounding soil, shear stresses develop along the length of the pile resulting in positive shaft friction. Alternatively when the soil settles more than the pile, negative skin friction develops along a portion of the pile shaft resulting in an increase in axial load (Kempfert, Dieter & Smoltczyk, 2003). The forces acting to push the pile down or pull the pile up, together with any additional load due to negative skin friction, are balanced by any mobilised bearing resistance at the pile toe and positive shaft resistance.

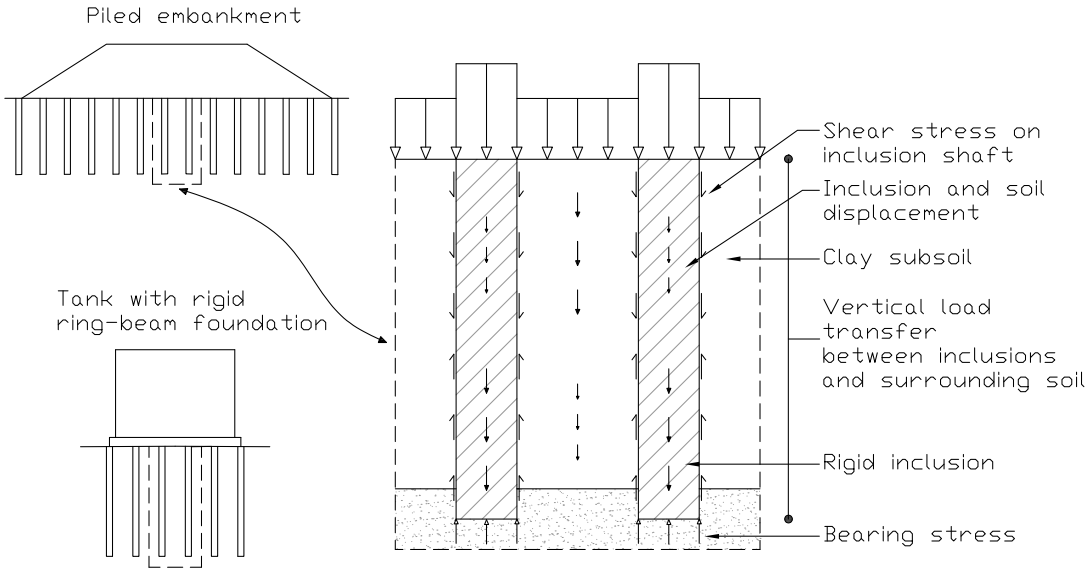

Figure 2.24 –Vertical load transfer between inclusion and the surrounding soil.

These basic mechanisms of axial load transfer are influenced by changes that occur during the main phases of the history of a displacement pile (Randolph, 2003). These phases are installation, equilibration of excess pore pressures and loading (Figure 2.25). The following sections describe the basic mechanisms of load transfer for displacement piles in sand and clay; consideration is given to the changes that occur during installation through to loading. For the purposes of this study only end-bearing in sand is considered.

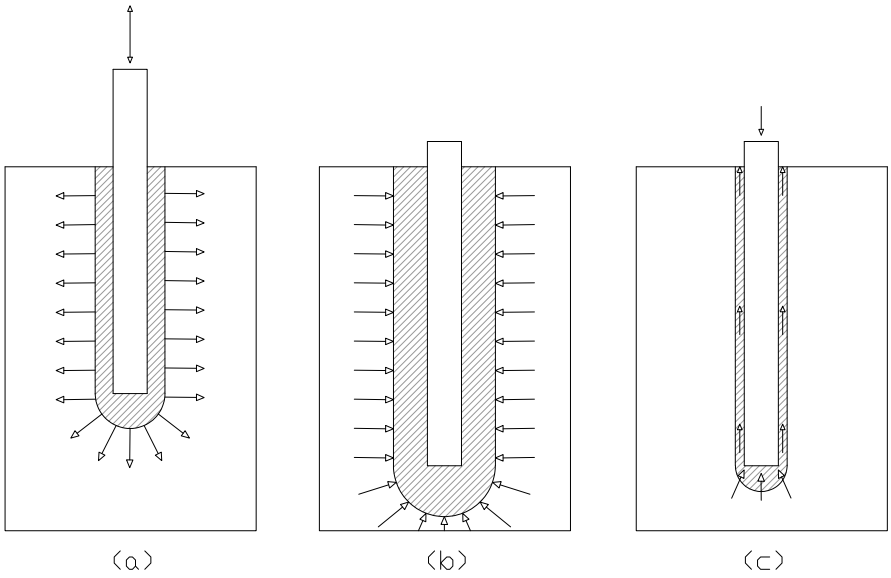

Figure 2.25 – The three main phases during the history of a driven pile (a) installation (b) equilibration (c) loading (Randolph, 2003).

2.2.5.2 Basic mechanisms for displacement piles in clay

The driving of a displacement pile changes the soil in the vicinity of the pile. Randolph (2003) describes these changes to the soil immediately adjacent to the pile as severe distortion, alteration of the soil fabric, remoulding and the possible formation of residual shear bands. The soil outside this shear zone is displaced outwards resulting in an excess pore pressure field around the pile. As time passes the induced pore pressures gradually dissipate to the hydrostatic pressure as pore water flows away from the pile. This process results in consolidation of the soil adjacent to the pile with a decrease in water content and an increase in effective stress. When the pile is finally loaded and moves relative to the soil, shear stresses develop along the shaft at the pile-soil interface and end-bearing pressure at the pile tip. In this way the pile offers resistance to the applied load by shaft friction and end-bearing.

The magnitude of shaft friction in clays as well as sands has been shown to be governed by the local radial effective stress at failure σ'_{rf} and the interface friction angle δ (Randolph, 2003; Jardine et al., 2005; Fellenius, 2006). This relationship is expressed by the effective stress interface friction law:

$$\tau = \sigma'_{rf} \tan \delta \tag{2.5}$$

The magnitudes of δ and σ'_{rf} are strongly influenced by the complex installation processes. The radial effective stress on a pile shaft has been shown to depend on the clays local yield stress ratio (YSR or apparent OCR), its sensitivity, plasticity index and the relative pile tip depth (Randolph, 2003; Jardine et al., 2005). Randolph (2003) comments that the interface friction angle will reduce to a residual value as high rates of shearing occur between pile and soil. The appropriate value of δ can be measured using a ring shear test which simulates the changes that occur during installation and loading.

Simple correlations for shaft friction have typically been expressed as empirical constants of proportionality α (τ_s/s_u) and β (τ_s/σ'_{v0}). The undrained shear strength ratio S_u/σ'_{v0} is a function of the YSR and alternative correlations were introduced incorporating both shear strength and vertical effective stress. New more rigorous approaches such as the ICP method (Jardine et al., 2005) have been developed through a combination of field, laboratory and theoretical research which account for the various soil parameters described above.

2.2.5.3 Basic mechanisms for displacement piles in sand

The installation of a displacement pile in sand changes the stress state and soil fabric around the pile. These changes influence the behaviour of the pile during loading. During installation the sand close to the tip of the pile undergoes large displacement and failure. The mean effective stress at the tip rises from the in situ value to a limiting value at failure. This value can be approximated by the CPT cone resistance q_c (White, 2005). During driving, the soil is displaced radially away from the pile and shear stresses develop along the pile shaft. The soil immediately adjacent to the shaft undergoes a gradual densification under the cyclic shearing action of installation (Randolph, 2003). This mechanism results in a reduction in horizontal stress acting on the shaft as the pile is installed. This phenomenon is termed friction degradation (Randolph, 2003). The installation process leaves the far-field soil in a heavily over consolidated state, having been highly stressed at the tip during installation and then unloaded as the tip is driven deeper.

The pile installation phase is then followed by a period of equalisation in which steady state conditions are reached. Jardine et al. (2005) has reported that the shaft resistance of piles driven in sand may grow with time, possibly due to relaxation through creep which results in increased radial effective stresses. During loading the radial effective stress increases by a relatively small amount due to interface dilation (Randolph, 2003).

The magnitude of shaft friction can be expressed by the simple interface friction law given by equation (2.5). For reasons already discussed the effective radial stress at failure σ'_{rf} is the equalised value acting a few days after installation combined with any changes developed during loading (Jardine et al., 2005). The local effective radial stress may be estimated from CPT cone resistance q_c which shows that the values of σ'_{rf} varies strongly with sand relatively density (Jardine et al., 2005). The appropriate interface friction angle δ is the constant volume value operating after dilation during shearing.

The end-bearing pressure is typically correlated with CPT cone resistance. Bearing pressure is strongly dependent on the relative density and critical state friction angle of the soil. Research has shown that there will be a gradually decreasing gradient of end-bearing pressure with depth (Fleming et al., 2009). This is due to the influence of a decreasing friction angle with increasing confining pressure, and the non-linear relationship between stiffness and stress (Randolph, 2003). The implication of this for practical pile lengths is a gradually decreasing rate of bearing pressure with depth that asymptotes towards values in the range of 10 to 20 MPa (Fleming et al., 2009). The movement required to mobilise the ultimate end-bearing pressure is typically taken as 10% of the pile diameter (Randolph, 2003).

2.2.5.4 Negative skin friction

During the application of load from the overlying structure the soil between the inclusions settles relative to the inclusions. This results in the soil moving down relative to the piles and the development of interface shear stress and load transfer from soil to pile. This shear stress is called negative skin friction. Negative skin friction results in the development of additional axial forces and additional settlement of the rigid inclusion. Fellenius (1984; 2006) called this accumulation of load due to a settling soil drag load. The resulting additional settlement caused by negative skin friction is termed down drag (Fellenius, 2006) or to avoid connotations with other terms drag settlement (Poulos, 2009).

It is recognised by many authors that the magnitude of the drag load can be very large for long piles (Bjerrum, Johannessen & Eide, 1969; Bozozuk, 1972; Fellenius, 1984). Historically the effect of negative skin friction has been discussed with respect to the drag load reducing the piles bearing capacity. In contrast Fellenius (1984; 2006) and Poulos (1997; 2009) suggest that this is incorrect, and that the problem of negative skin friction is one of pile settlement and not bearing capacity. They argue that for bearing failure to occur, the pile must move past the soil. In this case negative skin

friction cannot be present and therefore bearing capacity cannot be reduced by negative skin friction (Poulos, 2009). In light of this the main concerns for design are, the effect of the additional down drag loads on the structural integrity of the pile, and the additional settlement of the pile (Poulos, 1997).

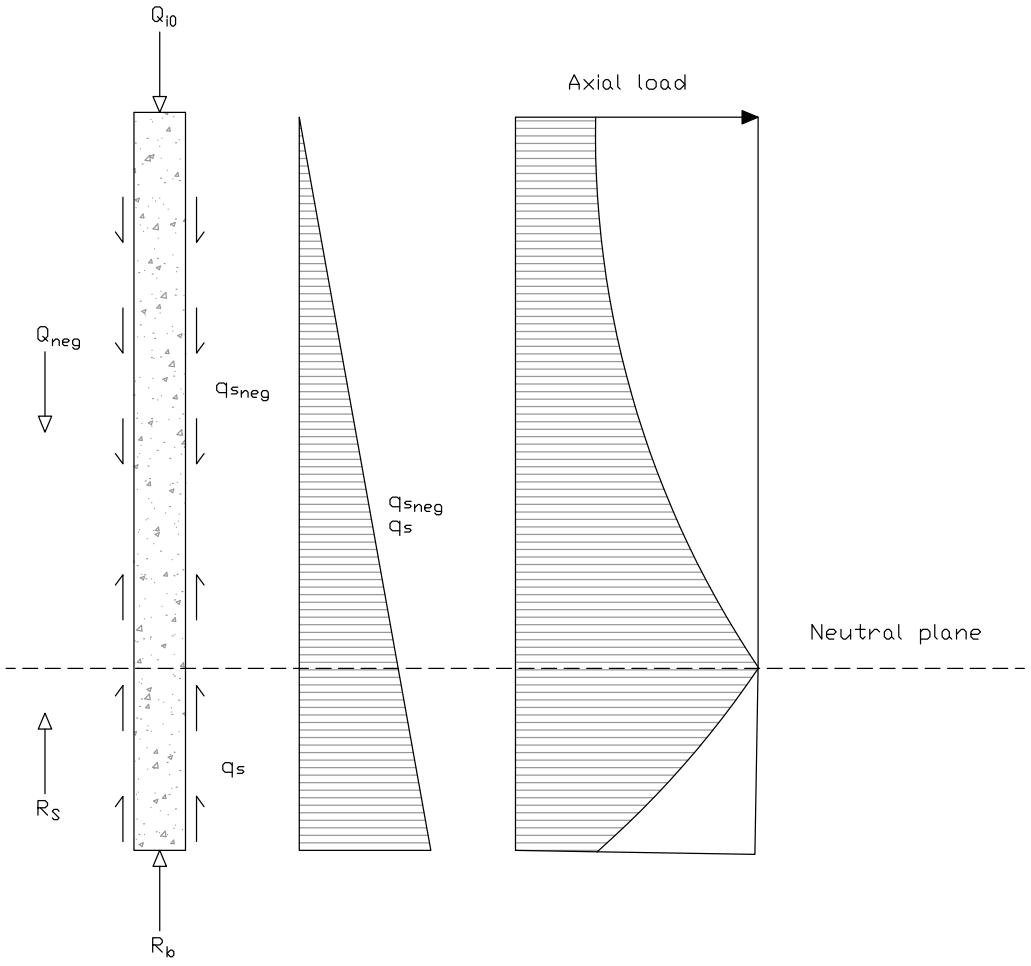

Figure 2.26 – Definition of the neutral plane

The forces acting on the inclusion include the load acting on the inclusion head, the drag load acting on the inclusion shaft, positive shaft resistance and toe resistance (Figure 2.26). These forces are in equilibrium when there is no accelerating movement in the inclusion. This means that negative skin friction along the upper portion of the inclusion results in an increase in axial force from the inclusion head to a maximum value at the depth of equilibrium (Fellenius, 2013). Below this point of equilibrium, known as the neutral plane, the axial load decreases as load is transferred to the soil by positive shaft resistance and toe resistance. The neutral plane is thus defined as the depth at which the shear stress along the shaft changes from negative skin friction to positive shaft resistance (Fellenius,

2013). This reversal of shear stress corresponds with zero relative displacement between inclusion and the surrounding soil. Fleming et al. (2009) suggests that the location of the neutral plane varies depending on the nature of the bearing stratum, or whether the pile is predominantly shaft-bearing "floating". The neutral plane typically lies below the mid-point of a pile, the extreme case being a pile bearing on rock where the neutral plane can be as deep as the bedrock level itself (Fleming et al., 2009).

2.2.5.5 Summary

Fundamental concepts:

- Relative inclusion-soil movement due to loading at the head results in load transfer from soil to inclusion and inclusion to soil. The applied loading at the inclusion head has been discussed in the previous section.
- Negative shaft friction results from the soil settling more than the inclusion. Load is transferred from soil to inclusion. This results in an increase in the axial load in the inclusion.
- Positive shaft resistance results from the inclusion settling more than the soil. Load is transferred from inclusion to soil. This results in a decrease in the axial load in the inclusion.
- The neutral plane is defined as the depth along the inclusion shaft where the shear stress changes from negative shaft friction to positive shaft resistance (Fellenius, 2013).
- The installation of a displacement pile changes the stress state and soil fabric adjacent to the pile which affects inclusion-soil load transfer.
- The magnitude of shaft friction in clays and sands is governed by the radial effective stress at failure σ'_{rf} and the effective interface angle δ and can be described by the effective stress interface friction law, $\tau_s = \sigma'_{rf} \tan \delta$.

Displacement piles in clay:

- The installation process results in shearing along the shaft, consolidation of the "far-field" soil and a change in the magnitude of σ'_{rf} and δ.
- Radial effective stress at failure σ'_{rf} is dependent on the clays YSR (Apparent OCR), PI and the relative inclusion tip depth.
- The interface friction angle δ reduces to a residual value during shearing.

Displacement piles in sand:

- The installation process results in an heavily OC "far-field" soil, friction degradation along shaft and a change in the magnitude of σ'_{rf} and δ.
- Radial effective stress σ'_{rf} varies strongly with relatively density and can estimated by CPT q_c.
- The appropriate interface friction angle δ is the constant volume value operating after dilation during shearing.
- The bearing resistance is influenced by RD and φ' of the soil and can be correlated with CPT q_c.The rate of endearing pressure gradually deceases with depth towards values in the range of 10 to 20 MPa.

2.2.6 Lateral load transfer mechanisms between inclusion and surrounding soil

2.2.6.1 Introduction

When rigid inclusions are used to support an embankment on clay, or when an embankment on clay forms an approach to a piled bridge abutment, ground movements due to embankment construction may produce significant lateral loading of the RIs and piles (Figure 2.27 and Figure 2.28). This "free-field" ground movement in addition to any lateral loading applied at the inclusion head, will induce deflections and bending moments in the inclusions. In extreme cases this may cause structural distress or failure of the rigid inclusions or piles or damage to the overlying structure (Stewart et al. 1994).

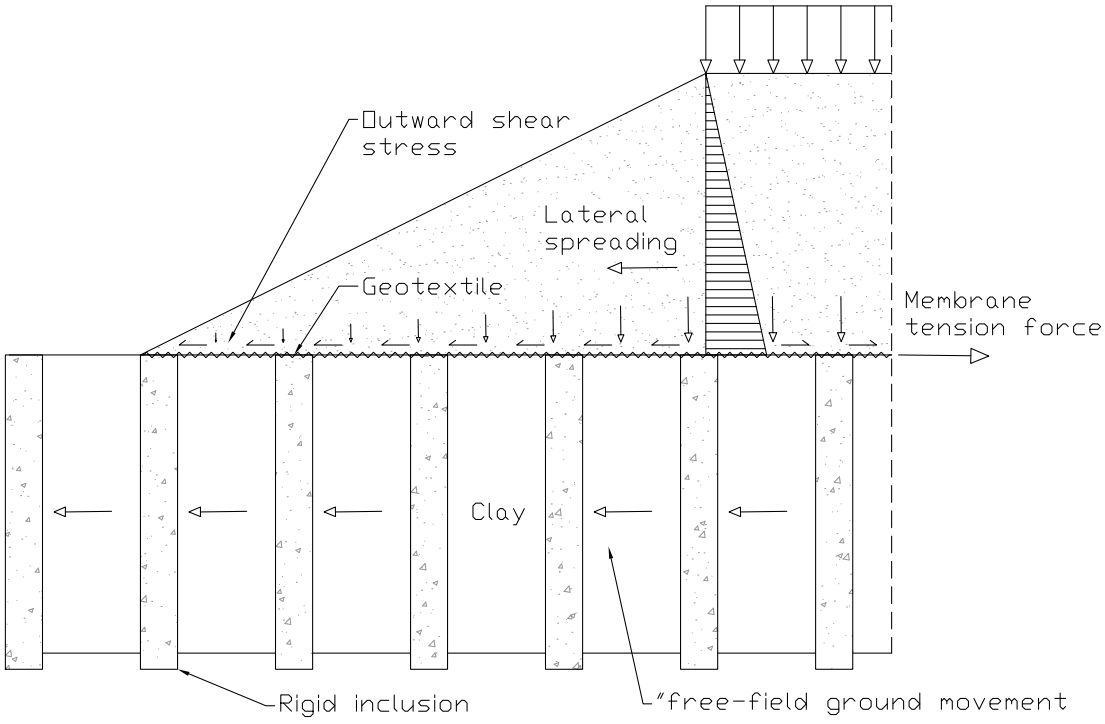

Figure 2.27 – Lateral spreading of a reinforced embankment (adapted from Farag, 2008)

The follow sections describe the various sources and mechanisms of lateral loading and their effects on RIs and piles. Although there are other loading conditions which result in lateral ground movement only embankment loading is considered. The reader is referred to Poulos (2007) where some of the other types of loading are considered.

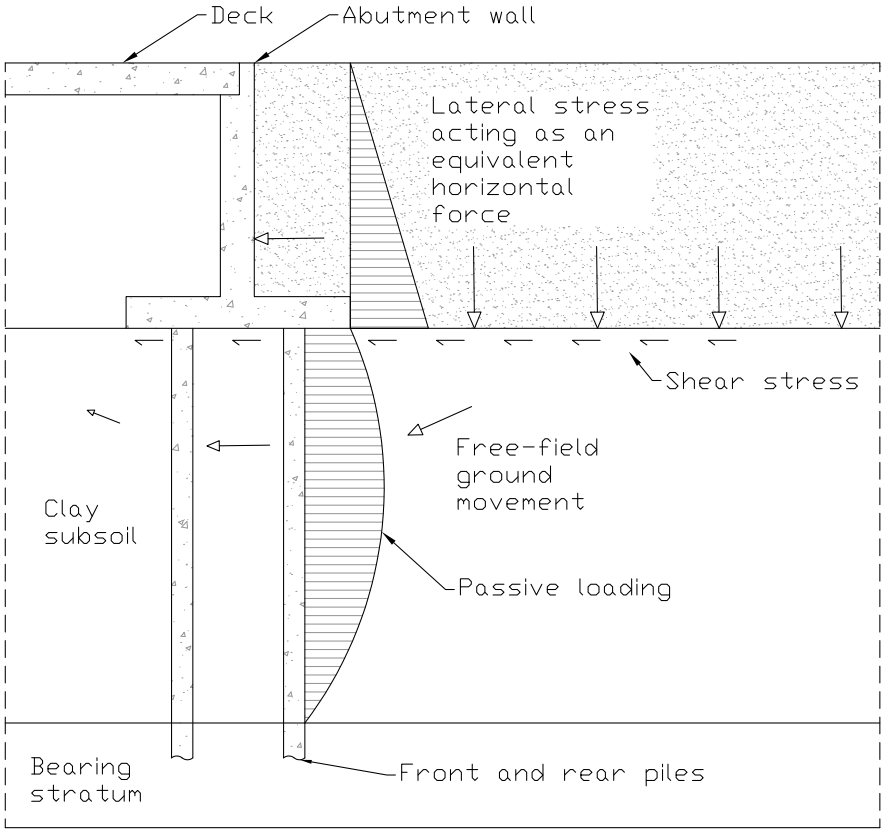

Figure 2.28 – Loads on piled bridge abutment originating from approach embankment (adapted from Kelesoglu & Springman, 2011)

2.2.6.2 Clay behaviour during embankment loading

Consider a soft to firm clay stratum under an embankment (Figure 2.27). During construction the weight from the embankment results in undrained loading of the clay and the generation of positive excess pore pressures in the region of the loading. With increasing embankment height there is a corresponding increase in undrained loading and excess pore pressure. A hydraulic gradient is created between the region of excess pore pressure and any region where steady state pore pressures exist. Seepage flows occur with time which results in the expulsion of water from the clay pores. The clay reduces in volume with an associated increase in effective stress as the pore pressures dissipate. This process is known as consolidation and results in deformation as well as an increase in strength and stiffness of the clay stratum. With time the rate of volume change decreases and eventually stops when the pore pressures fully dissipate. Provided no additional loading takes place, a state of constant

effective stress is reached and generally any deformation from this point on is related to secondary compression (creep).

During embankment construction to full height, the magnitude of the loading increases and depending on the rate and duration of the loading, the clay may yield. In idealised terms the yield point (or yield loci) of soft to firm clay separates broadly recoverable (elastic) and irrecoverable (plastic) straining (Graham, 2006). As the clay is loaded close to the yield stress its stress-strain behaviour becomes nonlinear before yielding is fully developed resulting in larger plastic straining. Figure 2.29 shows the effective stress path (ESP) in $p' - q$ stress space, for various undrained triaxle tests (CIU) on clay. The ESP corresponding to contractant clays bend to the left due to an increase in pore pressure during loading. As the ESP approaches its yield point on the critical state line (CSL), large shear strains develop as a result of undrained failure. A clay's ability to sustain shear stress before failure is a function of its strength. The ultimate strength is the maximum shear stress that can be sustained before yield.

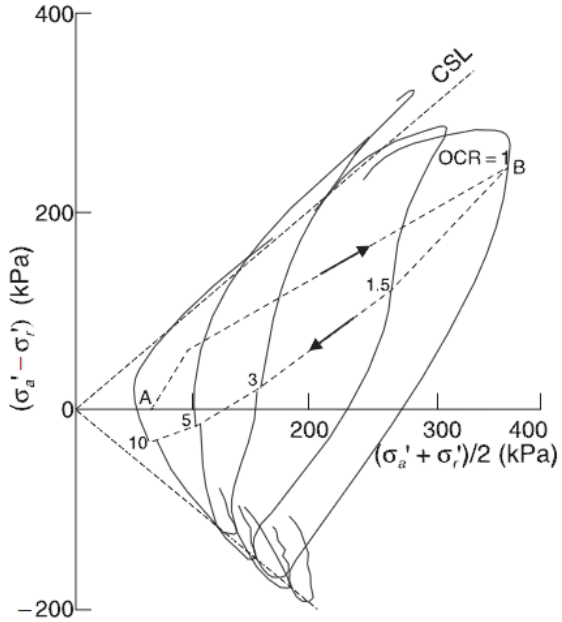

Figure 2.29 – Undrained shearing of clay during triaxial (CIU) testing (Potts, 2002)

2.2.6.3 Mechanisms of lateral loading

Disturbing and resisting forces:

Considering an embankment overlying clay subsoil without reinforcement, the main disturbing force is the vertical self-weight loading of the embankment fill (Figure 2.27). The other significant disturbing force is the outward lateral thrust in the embankment slope caused by the equilibrium shear stress in the fill required to maintain slope stability under self-weight (Jewell, 1988). This outward lateral thrust is analogous to the equilibrium shear stress along the base of a retaining structure for the case of a bridge abutment (Figure 2.28). The main resisting force is the shear resistance of the clay subsoil. The shearing resistance of the embankment fill also offers resistance as it affects the magnitude of the outward shear stress.

In simplified terms the foundation is subjected to combined vertical and horizontal loading. The effect of the outward shear stress at the base of the structure is to reduce the capacity of the foundation to carry the vertical load from the overlying structure (Jewell, 1988). Jewell (1988) demonstrated for the case of a footing overlying clay, that the bearing capacity of the clay subsoil is reduced by half when the foundation is subjected to an outward shear stress (Figure 2.30).

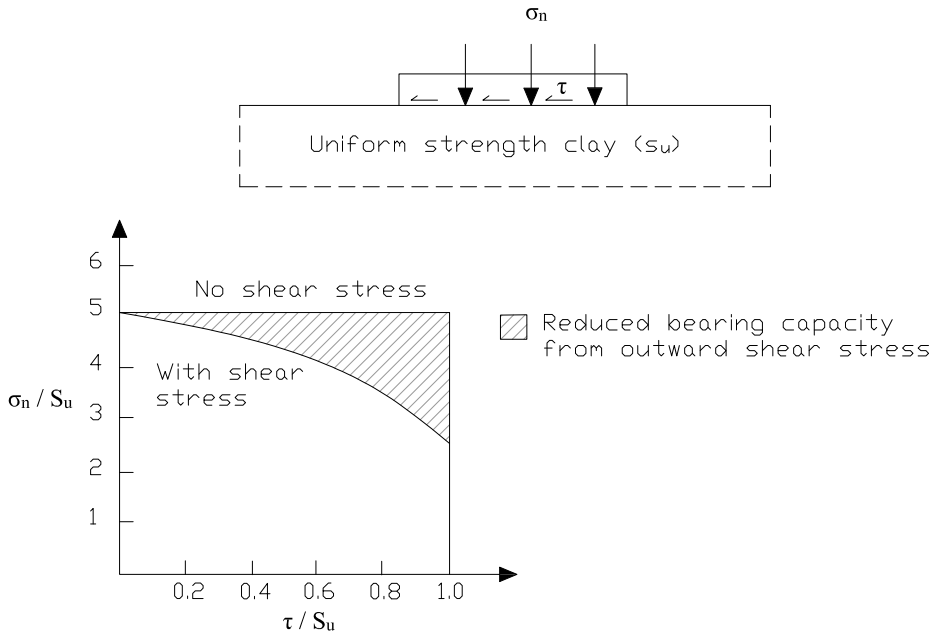

Figure 2.30 – The influence of outward shear stress in reducing the bearing capacity for a surface footing (Jewell, 1988)

Yielding of clay and failure modes:

When the disturbing forces exceed the resisting forces in an unreinforced foundation there is insufficient soil shearing resistance to maintain equilibrium. The clay subsoil will yield leading to progressive failure which will manifest as excessive settlement and lateral deformations. The various modes of failure are local bearing failure (soil squeeze), general bearing failure and global slope failure. The various modes of failure are discussed further in section 2.2.7.

Rate of loading:

Reducing the rate of construction loading can minimise the development of excess pore water pressures by allowing seepage to occur. A controlled construction rate can limit the magnitude of undrained loading and allow the clay shear strength to increase during consolidation. This construction technique allows the foundation to increase in strength and stiffness resulting in the resisting forces with the imposed loading.

Observed yielding of clay and lateral loading of piles:

Stewart et al. (1994) conducted a series of centrifuge model tests to clarify the effect of these processes on the lateral loading of pile groups adjacent to embankments constructed on soft clay. The response of a pile group with increasing embankment height is shown in Figure 2.31 and Figure 2.32 . Stewart et al. (1994) concludes the following regarding the observed behaviour:

- Two generally linear sections are observed in the data relating pile bending moment and deflection to embankments loading.
- The first section shows relatively small bending moments and deflections before reaching a threshold point.
- Beyond this threshold point there is a substantial increase in the rate of bending moments and deflections with load.
- This threshold was observed to occur at three times the undrained shear strength of the soft clay stratum.
- The increase in load applied to the piles is caused by an increase in soil displacement due to the initiation of significant plastic deformation in the soft clay stratum.
- The threshold loading could be considered a limit to elastic behaviour.
- The threshold loading is not sharp but occurs gradually.

– This behaviour compares well with the field data as detailed in Stewart et al. (1991) and Stewart (1992).

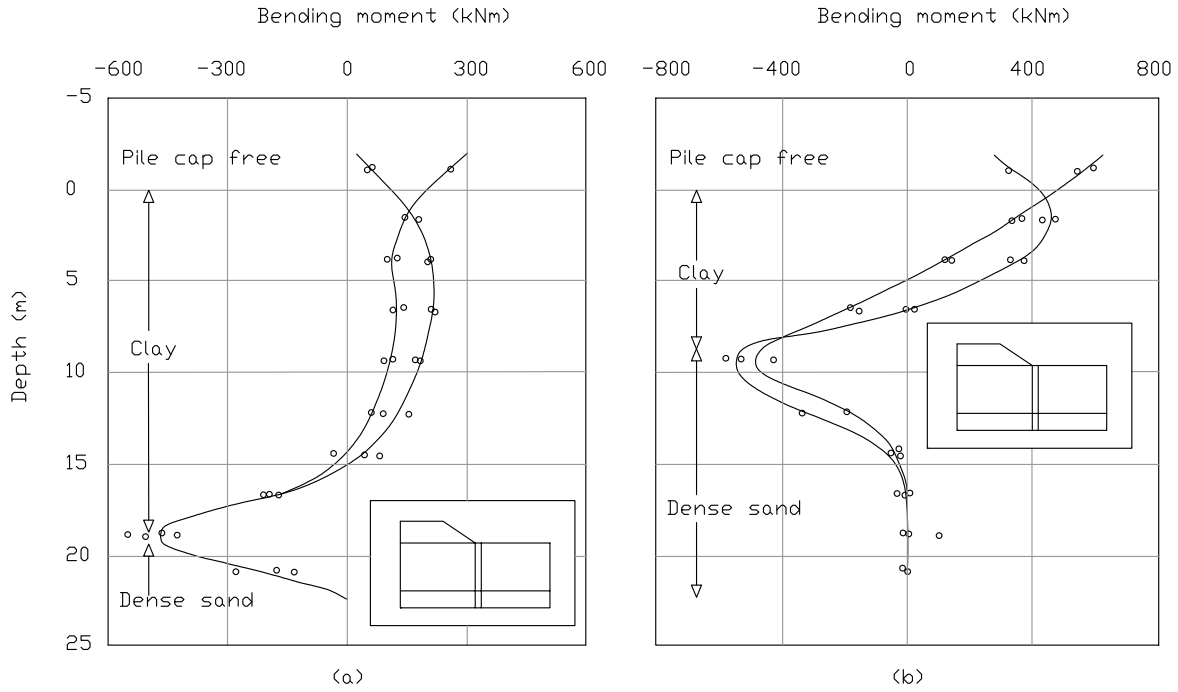

Figure 2.31 – Typical pile bending moment distribution from centrifuge tests (after Stewart 1992): (a) test 9, 18 m thick soft clay layer; (b) test 11, 8 m thick soft clay layer (Stewart, Jewell & Randolph, 1994)

Figure 2.32(b) shows the corresponding development of lateral pile cap deflection with embankment settlement. Stewart et al. (1994) concludes the following regarding the observed behaviour:

– The initial loading behaviour shows lateral displacement of a similar magnitude to embankment settlement.
– This initial behaviour is consistent with initial undrained conditions where large displacements are generated.
– A gradual change then occurs as pore pressures dissipate leading to smaller lateral movements as vertical displacements become more prevalent.
– Approximately 70% of the pile cap deflection occurred during the undrained phase and the remaining 30% during the ongoing consolidation.
– Correspondingly about 25 – 30 % of embankment settlement occurred during the undrained phase.
– This behaviour compares well with the field trials described by Oteo (1977).

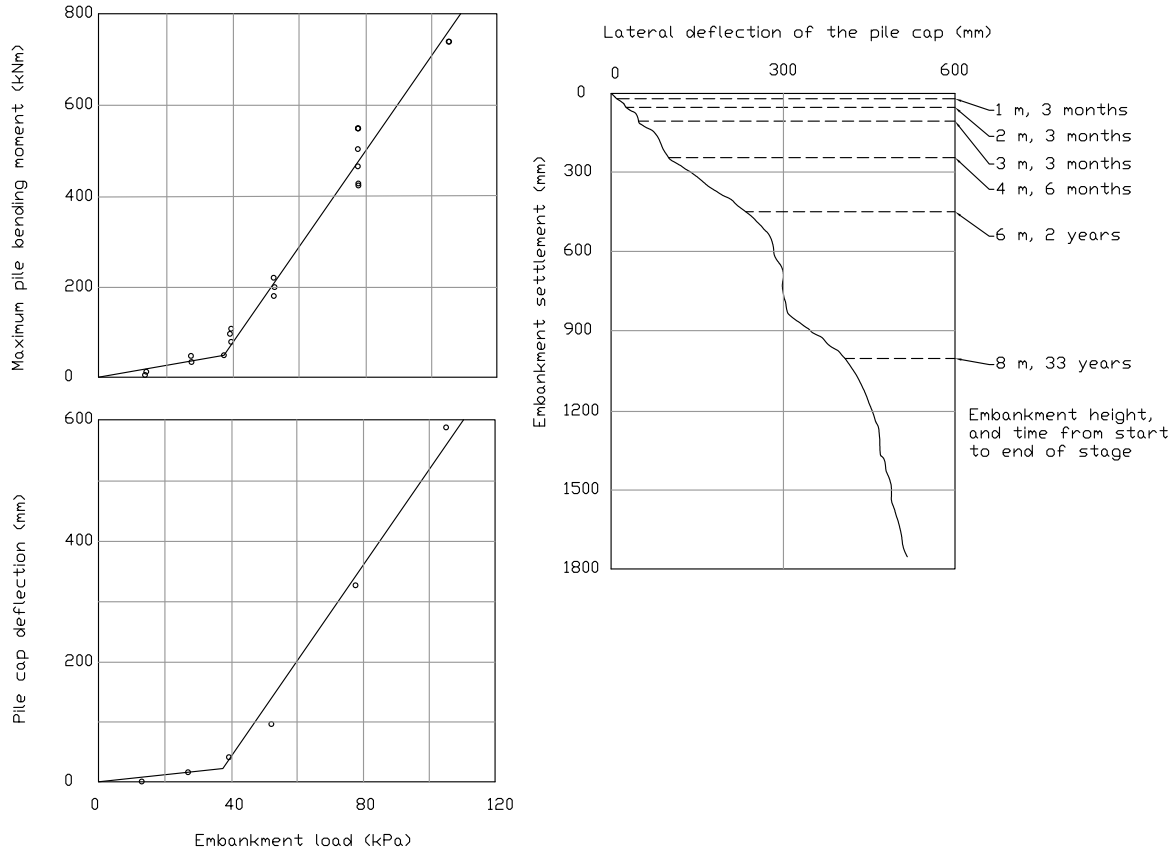

Figure 2.32 – Centrifuge test 9 results (after Stewart 1992) showing (a) pile group response; (b) development of pile cap deflection (Stewart, Jewell & Randolph, 1994)

2.2.6.4 Mechanics of reinforcement

Two common methods of providing structural support will be considered in this section. Firstly reinforcement placed across the base of the embankment in the LTP and secondly embankment support using a group of rigid inclusions.

Only the reinforcement mechanisms will be discussed in this section. Emphasis is placed on identifying the mechanics of how the reinforcement acts to improve the foundation bearing capacity and the embankment stability. The implementation of the reinforcement into the overall strategy for limiting lateral ground movements is discussed in section 2.3.

Reinforcement of the embankment fill:

There are two separate ways that reinforcement may be used in embankments. Firstly, reinforcement can be placed across the base of the embankment. Secondly reinforcement can be incorporated in the embankment slope. Only the first method will be considered. Reinforcement placed across the base of the structure improves the shearing resistance of the soil in two separate ways; firstly by reducing the forces causing failure and secondly by increasing the forces resisting failure (Jewell, 1988).

The basal reinforcement firstly sustains the outward shear stresses from the structure resulting in the development of membrane tension forces. When the outward thrust is in equilibrium with the tensile force there is no relative movement between the reinforcement and the foundation surface (Jewell, 1988). Due to the extension of the reinforcement during loading the geotextile may only reduce the outward shear stress transmitted from the overlying structure to the top of the foundation. The reinforcement in this instance is acting to reduce the forces causing failure (Jewell, 1988).

The basal reinforcement also acts to restrain the surface of the foundation soil against lateral movement; an unreinforced embankment cannot restrain the foundation soil from displacing laterally due to embankment loading (Jewell, 1988). The basal reinforcement provides restraint at the foundation surface by the same mechanism described above. The reinforcement in this instance is acting to increase the forces resisting failure (Jewell, 1988).. Both reinforcement mechanisms improve the bearing capacity of the foundation and hence the stability of the overlying structure (Jewell, 1988).

Embankment support piles / rigid inclusions:

Embankment support piles also act to reduce the forces causing failure and increasing the forces resisting failure. As discussed in section 0 the main disturbing force for an embankment on soft clay is the vertical self-weight loading of the embankment fill on the foundation surface. Support piles attract a large portion of this load due to arching mechanism in the LTP and transfer it to a deeper bearing stratum. The residual load is transferred to the clay between the piles. In this instance the piles are acting to reduce the forces causing failure.

When piles are situated in a soft soil layer displacing laterally they limit the lateral movement of the soil in the vicinity of the pile. Horizontal stresses develop between the pile and soil which generally results in pile movement and bending moment. This pile-soil interaction is the lateral-load analogue of the phenomenon of “negative skin friction” developed in piles when the surrounding soil settles more than the pile (Poulos & Davis, 1980). If the piles are closely spaced aching may occur between the piles and soil. The presence of a group of piles in a deforming soil layer will reduce the overall

magnitude of the movement and in this instance the rigid inclusions are acting to increase the forces resisting failure. The behaviour of the piles and the degree to which they offer resistance is influenced by a number of factors which are discussed in the following section.

2.2.6.5 The effects of lateral ground movements on piles

The problem of a pile subjected to a laterally displacing soil has been analysed on a theoretical basis by Poulos & Davis (1980) and is described below. The behaviour of the pile was shown to be influenced by the relative pile-soil flexibility, restraint conditions at the pile head and tip, pile spacing and diameter and distribution of soil movement. Additionally the behaviour of piles in moving ground is dependant of the mode of ground failure.

Pile-soil interaction is dependant the relative pile-soil flexibility. Very flexible piles will deform with the soil almost exactly and develop small lateral earth pressures and moments. A stiffer pile resists the soil movement resulting in an increase in earth pressure and moment. A possible exception to this behaviour is a very stiff pile undergoing rigid body tilt rather than bending about a point along its length. When a pile deflects due to moving soil, the horizontal earth pressure on the pile is partially relieved. The nonlinear stress-strain behaviour of soil undergoing large displacements results in a reduction in soil stiffness and as a consequence a reduction in the applied lateral earth pressure on the pile. The applied stress reaches a limiting value as the soil begins to yield and flow around the pile.

The effect of the boundary conditions at the pile head and tip are shown in Figure 2.33. The provision of head restraint reduces the pile movement near the tip, but also increases the bending moment (Poulos & Davis, 1980). For a piles of equivalent flexibility, subjected to the same soil movement distribution, the free head condition results in greater movement near tip and a lower moment.

The effect of the soil movement distribution has a large effect on the pressures and moments developed in the pile. Three typical movement distributions were considered; a uniform soil-movement profile, a triangular distribution and a uniform-triangular distribution. Figure 2.34 presents movement and moment distributions for an unrestrained free head and pinned tip. The uniform soil-movement profile produces the greatest moment in the pile. The lowest moment results from a triangular distribution with zero movement at the base of the layer and the maximum movement at the top of the layer (Poulos & Davis, 1980). For relatively flexible piles, the head movement is largely dependent on the soil surface movement (Poulos & Davis, 1980).

The principal effect of changing the pile diameter is to change the pile flexibility. Increasing the pile diameter, reduces the pile flexibility, increases the lateral earth pressures and moments and changes the pile-movement distribution. The effect of reducing the spacing of the piles is to maximise the soil arching between the piles which minimises the flow of soil between them.

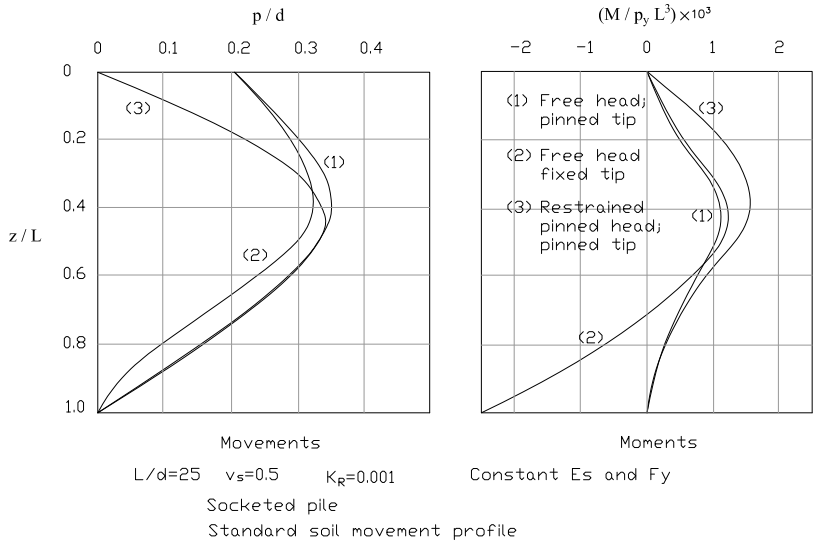

Figure 2.33 – Effect of boundary conditions on pile movements and moment

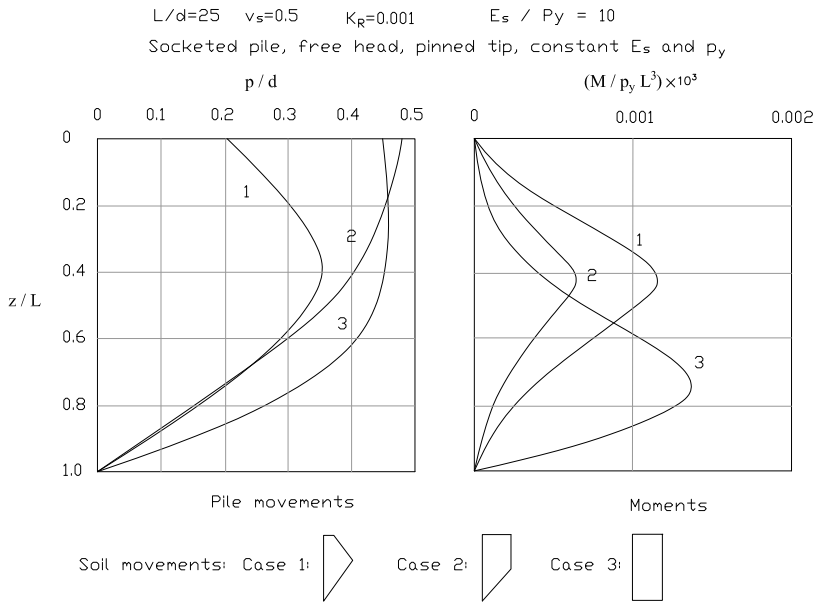

Figure 2.34 – Effect of distribution of soil movement on pile movements and moment

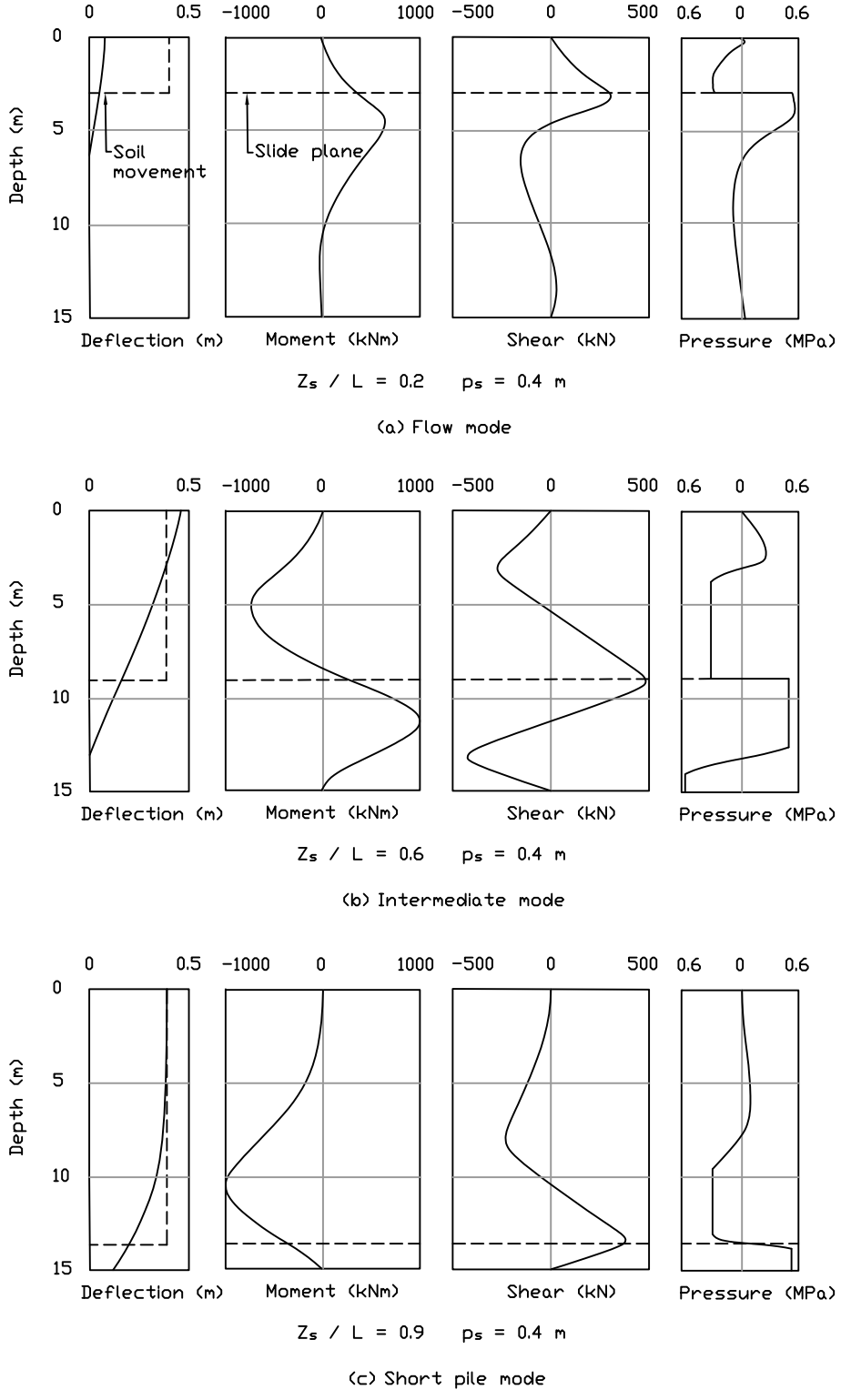

Figure 2.35 – Pile behaviour for various modes of ground failure (Poulos, 1995)

Poulos (1995) related the behaviour of piles in moving ground to three modes of ground failure (Figure 2.35) and a structural failure mode. The first is the flow mode when a shallow slide results in the unstable zone deforming plastically and flowing around the pile. The short pile mode is characterised by a deep slide relative to the pile toe; the unstable zone drags the pile through the stable zone and full mobilization of soil strength in the stable layer occurs. The intermediate mode occurs when the soil strength in both the unstable and stable soil is fully mobilised along the pile length (Poulos, 1995). The long pile failure mode occurs when the pile yields due to structural failure in bending or shear; this mode can be associated with any of the three modes of ground failure, although Poulos (1995) comments it is most likely to occur with the intermediate mode. Two important practical applications may be drawn from Figure 2.35. Firstly the flow mode results in the smallest structural forces and moments in the pile. Secondly the intermediate mode develops the largest structural forces and moments in the pile. The soil failure modes are dependent on a number of factors including, geometrical properties of the pile, relative pile-soil strength and stiffness and the relative lengths of the pile in the stable and unstable zone.

2.2.6.6 Summary

Clay behaviour during embankment loading:

- The construction of an embankment or rigid structure over clay subsoil results in undrained loading.
- The magnitude and rate of loading may cause the clay to yield resulting in plastic deformation manifesting as excessive settlement and lateral ground movement.
- The onset of yield is a function of the clays undrained shear strength
- If the rate of loading is slow enough the clay consolidates resulting in an increase in shear strength and stiffness. Slow construction can avoid yielding in the clay subsoil and limit settlement and lateral ground movement.

Mechanics of "free-field" lateral loading due to ground movement:

- When a foundation is subjected to both vertical and lateral loading the effect of any outward shear force is to reduce the ability of foundation to carry the vertical load (Jewell, 1988).
- The main disturbing force is the vertical self-weight of the embankment or structure (Jewell, 1988).

- The secondary disturbing force is the outward lateral thrust in the embankment slope or rigid structure (Jewell, 1988).
- The main resisting force is the shear resistance of clay.
- A secondary resisting force is the shear resistance of fill.
- When disturbing forces exceed resisting forces the clay yields signalling the onset of plastic deformation and results in lateral "free-field" ground movement.
- Stewart et al. (1994b) observed this transition from elastic to plastic behaviour at an embankment load of three times the clay's undrained shear strength.
- The majority of lateral ground movement occurs during undrained loading and results in lateral loading of piles.
- Stewart et al. (1994b) observed that 70% of the pile cap deflection occurred during the undrained phase.

Mechanics of reinforcement:

- Two methods of reinforcement were considered, namely, basal reinforcement and embankment support with a group of rigid inclusions.
- Reinforcement acts to reduce the forces causing failure and increase the forces resisting failure (Jewell, 1988).
- Basal reinforcement sustains the outward shear stress and restrains the surface of the foundation soil against lateral movement (Jewell, 1988).

Factors affecting the behaviour of a pile subjected to laterally displacing soil:

- Relative pile-soil flexibility: The stiffer the pile the more it resists the soil movement resulting in an increase in bending moment and earth pressure against the pile.
- Boundary conditions at head of inclusion: Head restraint reduces the pile movement near the tip, but also increases the moment (Poulos & Davis, 1980).
- Soil movement distribution: affects the pressures and moments developed; three typical movement profiles, (1) uniform soil-movement profile, a (2) triangular distribution and a (3) uniform-triangular distribution. The uniform soil-movement profile produces the greatest moment in the pile.
- Pile diameter: Affects pile-soil flexibility (See above).
- Failure mode of soil: flow mode; short pile mode; intermediate mode; long pile mode. Intermediate mode develops the largest structural forces and moments in the pile.

2.2.7 Failure modes of a group of individual inclusions

2.2.7.1 Introduction

Research since the 1980s has revealed that individual columns under embankment type loading have various modes of failure which are dependent on their location relative to the superstructure and the active, transitional and passive zones in the foundation. Historically embankment stability has been evaluated for a single failure mode based on a slip circle shear failure mechanism.

In the late 1980s and the middle of the 1990s a series of centrifuge model tests were carried out in Japan to identify the modes of failure of group column improved ground (Kitazume & Terashi, 2013a). The centrifuge model tests were carried out for rigid structures such as concrete caissons (Kitazume et al., 1996; Kitazume, Okano & Miyajima, 2000), as well as flexible structures such as earth embankments (Kitazume, 2008). In the 1990s following several failures of column supported embankments, Nordic engineers reconsidered the mode of failure of a group of individual columns (Kivelö, 1998; Broms, 1999). More recently numerical simulations have been carried out to investigate the various proposed modes of failure (Han et al., 2004; Navin, 2005; Filz & Navin, 2006).

The following sections describe the failure modes of a group of columns under rigid and flexible loading based on centrifuge model testing, theoretical considerations and numerical analysis.

2.2.7.2 Observed failure modes from centrifuge model testing

Bearing capacity of a caisson supported by a group of individual columns:

A series of centrifuge model tests were carried out at the Port and Airport Research Institute to study the bearing capacity problem of a rigid caisson breakwater resting on a group of individual columns (Kitazume et al., 1996; Kitazume, Okano & Miyajima, 2000). The strength of the columns in terms of unconfined compressive strength, varied from 0.2 to 27 MPa and the area replacement ratio was 79%. The foundation comprised normally consolidated soft clay. The caisson was subjected to both vertical loading as well as combined vertical and lateral loading.

Under combined loading the caisson was observed to collapse due to foundation bearing failure. The columns sustaining relatively large vertical loads failed during horizontal loading which in turn resulted in considerable loss of their bearing capacity. At collapse the columns exhibited internal failure modes such as shear and bending failure (Figure 2.36). An external tilting failure mode was

observed for high strength columns which did not exhibit internal failure. Slip failure surfaces were observed in the improved region and extended outward into the unimproved region (Figure 2.37).

Based on these observations a number of conclusion's can be drawn regarding the failure modes of individual columns in a group: The failure modes were dependent on the external loading conditions as well as the column strength. The columns failed in different ways depending on their location relative to the superstructure and the active, transitional and passive zones in the foundation (Kitazume & Terashi, 2013b). Columns failed internally due to bending and shear. There was an external failure mode due to excessive tilting of high strength columns.

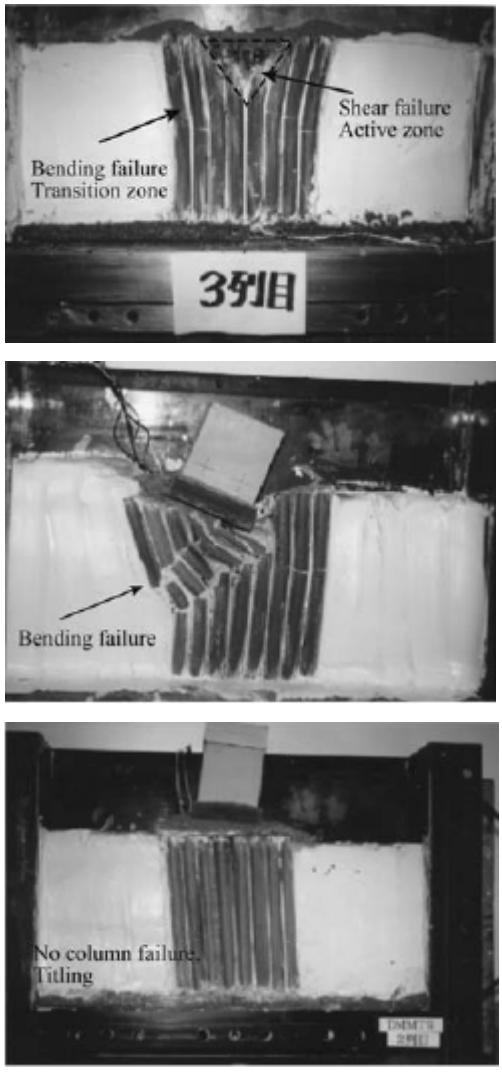

Figure 2.36 – Various failure modes for a group of individual columns during centrifuge tests (Kitazume & Terashi, 2013b)

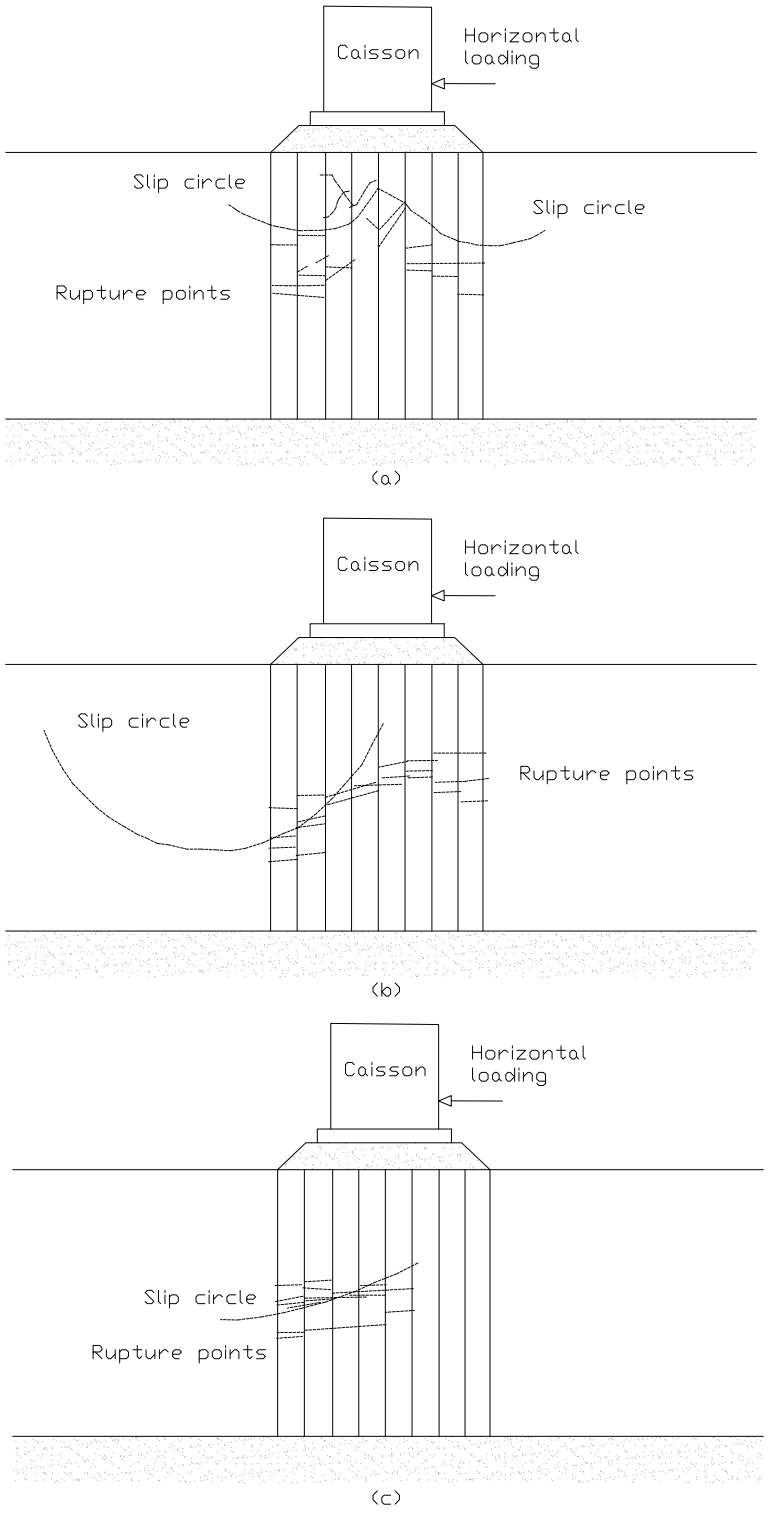

Figure 2.37 – Ground deformation during centrifuge tests (Kitazume, Okano & Miyajima, 2000)

The stability of embankments on a group of individual columns:

Since the middle of the 1990s The Port and Airport Research Institute has studied the modes of failure of individual columns in a group under embankment type loading (Kitazume & Terashi, 2013b). Although the test results have been published elsewhere, Kitazume (2008) recently published all the results of these model tests, together with design recommendations (Kitazume & Terashi, 2013b). The centrifuge model tests setup comprised normally consolidated soft clay reinforced with a group of individual columns. The model foundations were overlain by an embankment with a sloping side. The embankment fill was placed rapidly during testing until the foundation failed. The strength of the columns in terms of unconfined compressive strength, was 0.4 MPa, 1.1 MPa and practically infinite where an acrylic pipe was used (Kitazume & Terashi, 2013b). The area replacement ratios were 28% and 56%.

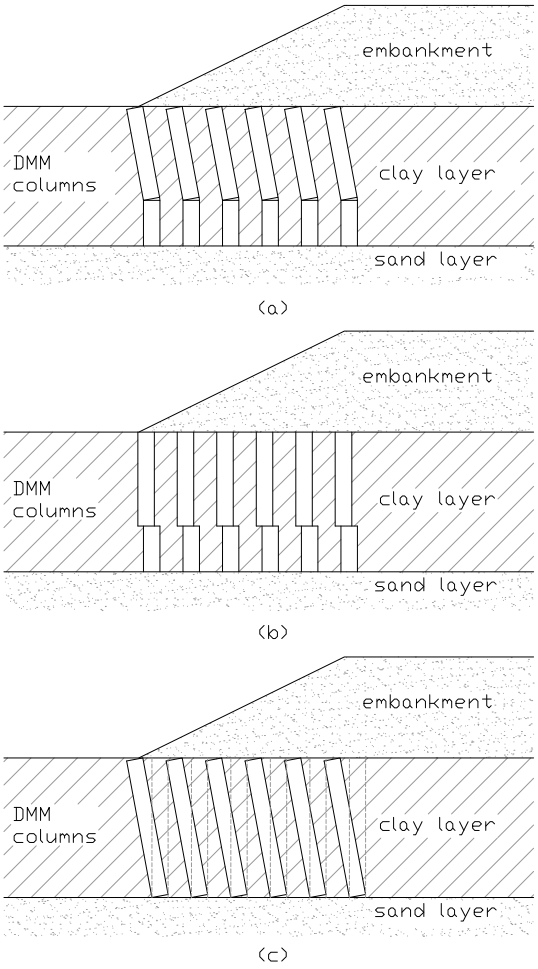

Figure 2.38 – Failure modes of a group of individual columns under embankment loading (Kitazume, 2008)

It was observed during embankment collapse that the columns tilted and bent outwards. The lower strength columns failed by bending, exhibiting tensile cracks at two different locations. The high strength columns failed by tilting outwards. No slip circle failure or sliding failure was observed. One of the important observations from these tests was the progressive mode of failure.

Based on these results Kitazume (2008) proposed embankment stability be evaluated for shear, bending and tilting failure, in additional slip circle and sliding failure. It was concluded that individual columns do not fail simultaneously but rather progressively. In addition, analytical and numerical calculations were carried out and Kitazume (2008) concluded that embankment stability can be overestimated by assuming a slip circle shear failure mode without considering other internal failure modes.

2.2.7.3 Theoretical consideration of failure modes

Nordic engineers also acknowledged the possible overestimation of embankment stability due to the assumption of a single slip circle shear failure mechanism. Kivelo (1998) examined the resistance of individual lime/cement columns when they function as dowels in the shear zone of the assumed slip surface. This theoretical analysis is based on the method proposed by Broms (1972). Broms (1999) extended this work to take into account the reduction in bearing capacity of the columns caused by progressive failure. Both methods assume a slip surface passes through the group of columns and their failure mode is dependent on their location relative to this failure plane (Figure 2.39 and Figure 2.40).

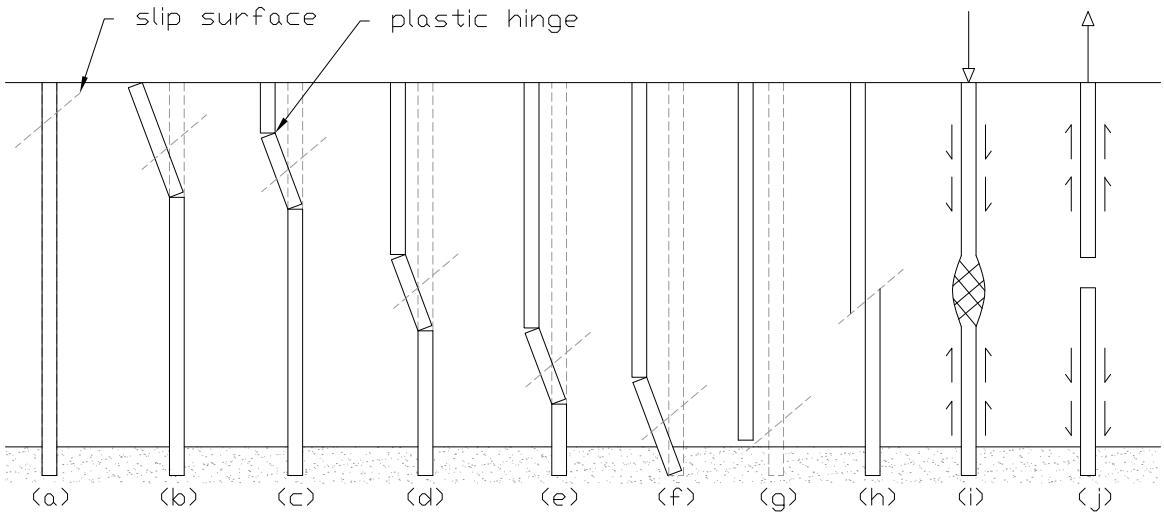

Figure 2.39 – Failure modes of single columns (Broms, 2004)

Analysis of single columns under combined loading:

The assumed slip surface passing through the columns is divided into an active, shear (transitional zone) and passive zone (Figure 2.40). The main function of the columns is to carry the vertical self-weight loading of the embankment fill (Broms, 1999). The columns must support the weight of the embankment through the slip surface (Broms, 1999). The resistance of the columns depends mainly on the axial load in the column at the location of the slip surface (Broms, 1999). The moment capacity of the columns will be low when the axial load is low. Columns fail when the bending moment exceeds the moment capacity of the columns. Broms (1999) suggests that single columns should only be used where the axial load in the columns will be high and lateral displacements are low. This corresponds to the active zone nearer the centre of an embankment. Single columns located in the shear or passive zones are very inefficient by comparison (Broms, 1999).

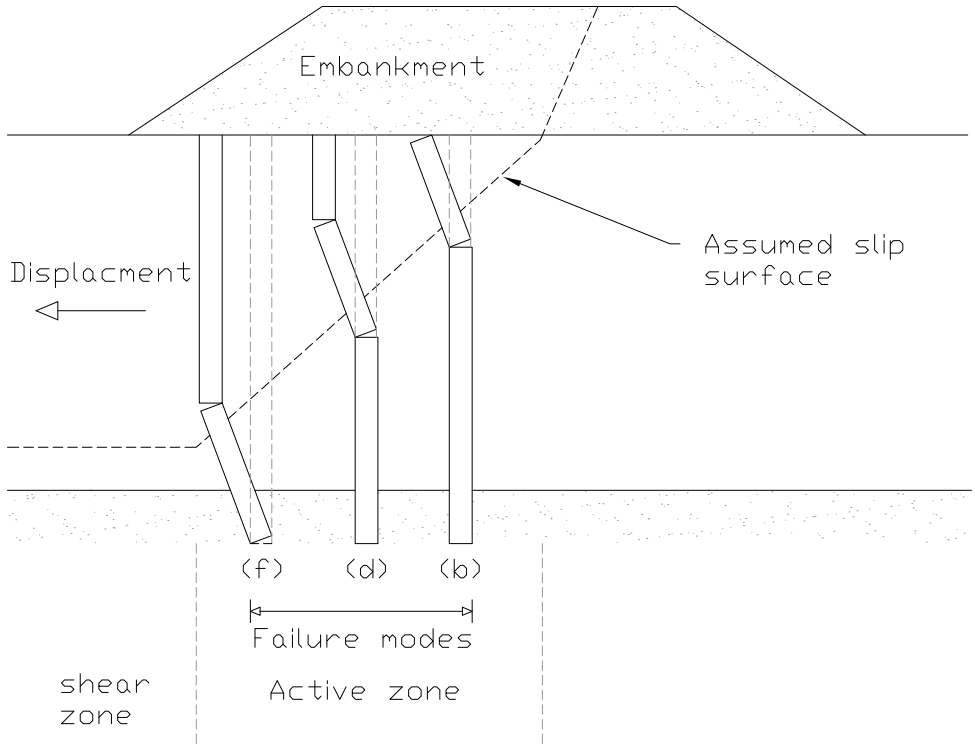

Figure 2.40 – Failure modes of single columns in the active zone (Broms, 2004)

Lateral ground movements and associated lateral displacement of the columns will reduce the bearing capacity of the columns. High strength unreinforced columns with a low failure strain, exhibit brittle behaviour and are most sensitive to this reduction in bearing capacity. In this regard the reduction in bearing capacity is related to the ductility of the columns and thus to the failure strain (Broms, 1999).

Failure modes:

Broms (1999) describes a number of possible failure modes of single columns (Figure 2.39) as follows:

- 3a: Shallow slip surface where the displaced soft soil will flow past the column. The moment capacity of the column is sufficient in this case to resist the lateral earth pressure.
- 3b: The failure mode of the column when the depth of the slip surface is increased. This failure mode occurs when one plastic hinge develops at the location of the maximum bending moment in the column.
- 3c, 3d, 3e: The failure modes when two plastic hinges develop at the location of the maximum bending moments in the columns.
- 3f: The failure mode for a single column which extends into a firm layer. This failure mode occurs when the slip surface is located close to the bottom of the soft soil.
- 3g: Failure mode for a column when the slip surface is located close to the bottom of a column and the column moves through the soft soil as a rigid member.
- 3h: The failure mode when the internal shear resistance of the column section governs.
- 3i: Compression failure of the columns.
- 3j: The columns located in the passive zone will be governed by the tensile strength of the columns.

2.2.7.4 Observed failure modes from numerical simulation

Relatively few numerical simulations focus on the failure modes of a group of rigid inclusions compared with simulations dealing primarily with vertical loading and settlement control. Of particular interest are the numerical simulations performed by Navin (2005), of the centrifuge model tests described in section 2.2.7.2. The centrifuge test data was used to verify the numerical analysis method which was then used to analyse the complex soil structure interaction up to failure.

Navin (2005) performed 2D plane strain numerical simulations using the finite difference method (FDM). The centrifuge models test performed by Kitazume et al. (1996) were simulated. These model tests and numerical simulations are an excellent example of a group of columns subjected to combined loading from a rigid structure. The FDM simulations were able to replicate tilting and bending failure and match the horizontal load displacement behaviour of the model caisson. In order to capture the bending failure of the low strength columns a constitutive model for the columns with

material specific failure criteria was required. In these analyses the Mohr-Coulomb model was used to model the columns.

Navin (2005) performed 2D plane strain and 3D numerical simulations using the finite difference method (FDM). The centrifuge models test performed by Inagaki et al. (2002) were simulated.. These model tests and numerical simulations are an excellent example of the behaviour of individual columns in a group subjected to embankment loading. The columns were modelled as continuous walls for the case of 2D plane strain conditions. The numerical analyses were able to replicate the lateral deflections and bending stresses within the columns. Navin (2005) concluded that although the lateral deflections from two-dimensional analyses are in relatively good agreement with lateral deflections from the three-dimensional analyses, the 2D analyses under predict the bending stresses in the columns for the same area replacement ratio.

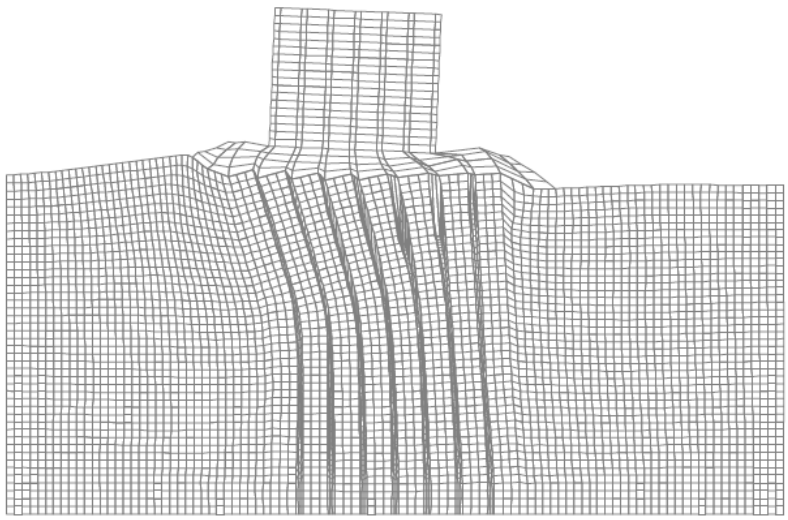

Figure 2.41 – Deformed mesh corresponding to low strength column (Navin, 2005)

Filz & Navin (2006) modelled a hypothetical embankment overlying 8.5 m of soft clay, reinforced with a grid of individual inclusions terminating in sand. The numerical simulations were performed using the 2D plane strain FDM. The rigid columns were 0.9 m in wide and space at 1.8 m in a square grid resulting in an area replacement ratio of 20%. The columns had an unconfined compressive strength of 689 kPa and were modelled with equivalent Mohr-Coulomb properties. The strength of the clay varied linearly from 10 kPa to 20 kPa at the bottom. Figure 2.42 shows the analysis results where shear strains developed in the soil and tension failure in the columns. Filz & Navin (2006) concluded

that the columns failed in bending as the soil between the columns experienced shear distortions and the failed portions of the columns tilted (Navin, 2005). The FOS determined by numerical simulation was compared with that determined by limit equilibrium slip circle analyses. Numerical procedures resulted in a FOS of 1.4 which is significantly lower than the 4.4 determined by LE procedures.

Han et al. (2005) conducted a 2D plane strain numerical study using the FDM to evaluate deep seated slope failure of embankments supported by a group of individual columns. The column width was either 1m or 2 m and the spacing varied resulting in an area replacement ratio varying from 33% to 50%. The column strength in terms of unconfined compressive strength was 200 kPa. A Mohr Coulomb failure criterion was used for the columns. Figure 2.43 showing a circular slip failure plane for the case of an embankment over soft clay without reinforcement. This was selected as the baseline case for the study. Figure 2.44 shows the shear strain rate contours for the embankment supported by a group of inclusions. There is no continuous shear-strain rate plane due to the presence of the inclusions; however this may be the result of the columns being modelled as continuous walls. High strain rates are observed in front and behind the columns. Han et al. (2005) comments that the failure surface can be approximated by a three part wedge rather than circular slip.

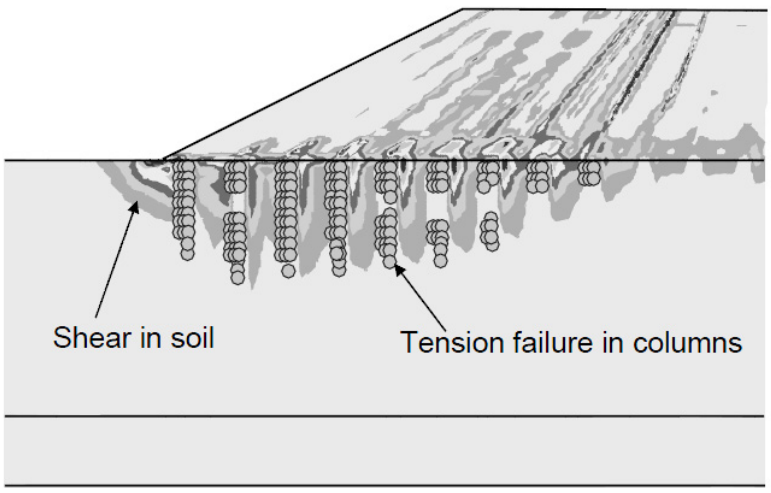

Figure 2.42 – Results of numerical analyses (FDM) of an embankment supported on isolated columns (Filz & Navin, 2006)

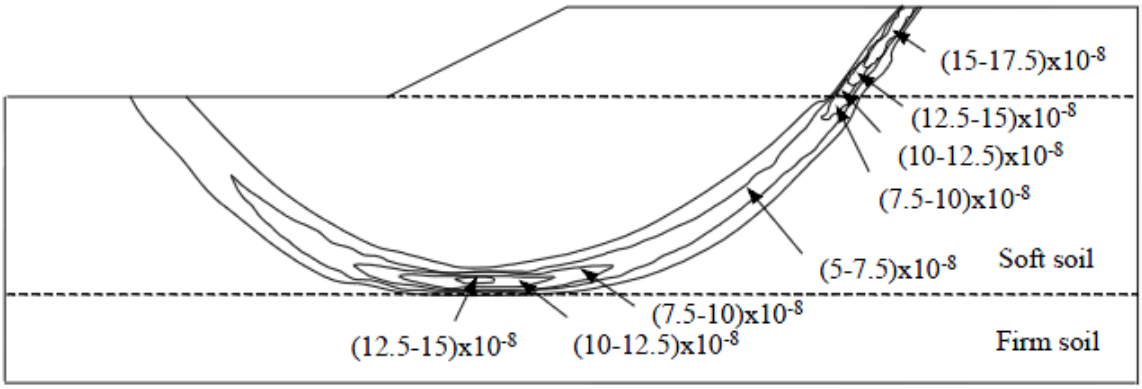

Figure 2.43 – Shear strain developed in an unreinforced embankment (Han et al., 2005)

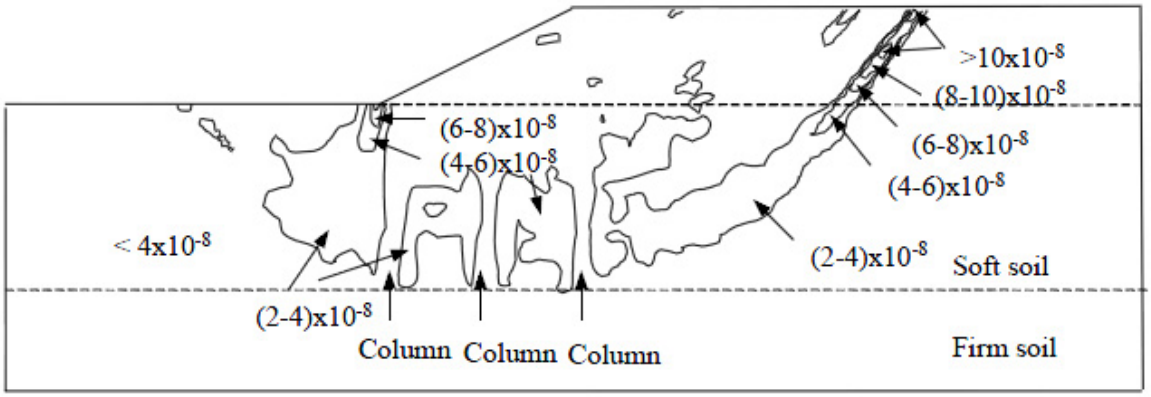

Figure 2.44 – Shear strain in an embankment reinforced with a group of individual inclusions (Han et al., 2005)

2.2.7.5 Summary

Observed failure modes from centrifuge model testing:

- Individual columns in a group may fail in different ways depending on the external loading conditions; column geometry, spacing and strength; column location relative to the superstructure and location relative to the active transitional and passive zones in the foundation.
- Internal failure modes for columns include bending and shear failure.

- There is an external failure mode due to excessive tilting of high strength columns.
- There is an external failure mode to bearing failure and slip circle shear failure.
- Columns fail progressively rather than simultaneously.
- Stability can be overestimated by considering only a slip circle shear failure mode without considering the other failure modes.

Theoretical consideration of failure modes:

- The failure of a group of columns can be analysed on a theoretical basis according to the methods outlined by Broms (1972), Kivelö (1998) and Broms (1999).
- Broms (1999) accounts for internal failure modes such as bending and shear, external failure modes such as slip failure, as well as and progressive failure of the columns.
- Assuming a slip circle passes through a group of columns, their mode of failure depends on their location relative to the slip failure plane.
- The resistance of columns depends mainly on the axial load in the column at the location of the slip surface; their moment capacity will be low when the axial load is low.
- Single columns should only be used where the axial load in the columns will be high and lateral displacements are low
- Lateral displacement of the columns will reduce the bearing capacity of the columns
- The reduction in bearing capacity is related to the ductility of the columns and thus to the failure strain

Observed failure modes from numerical simulation:

- Numerical simulations reproduced internal failure modes such as bending and shear failure as well as external failure modes such as tilting and excessive soil shear strain forming slip surfaces.
- For internal failure modes to be captured the columns require a constitutive model with failure criteria such as the Mohr Coulomb model.
- Three dimensional analysis models the column behaviour most accurately.
- Numerical analysis confirmed that stability can be overestimated by considering a slip circle shear failure mechanism without consider the other failure modes.

2.2.8 Analytical models for the analysis of RI ground improvement

A variety of analytical models are available in literature for the analysis of rigid inclusion ground improvement. Many of these models relate to basal reinforced piled embankments. The following subsections only provide an overview of the available models; the detailed load transfer mechanisms relating to these models have already been presented in the previous sections. For a detailed description of the model formulae and implementation the reader is referred to the latest revisions of the British, Dutch, French and German guidelines for the design of basal reinforced piled embankments.

2.2.8.1 Models for calculating the arching behaviour in piled earth embankments

The majority of the available analytical models for calculating arching behaviour relate to flexible structures; in particular basal reinforced piled embankments. These models typically involve two calculation steps. The first calculation step describes the arching behaviour in the fill and is discussed in this section (Figure 2.45). The second calculation step describes the effect of the residual load and associated load-deflection behaviour of the basal reinforcement (van Eekelen, Bezuijen & van Tol, 2015). The second step is discussed in the following section.

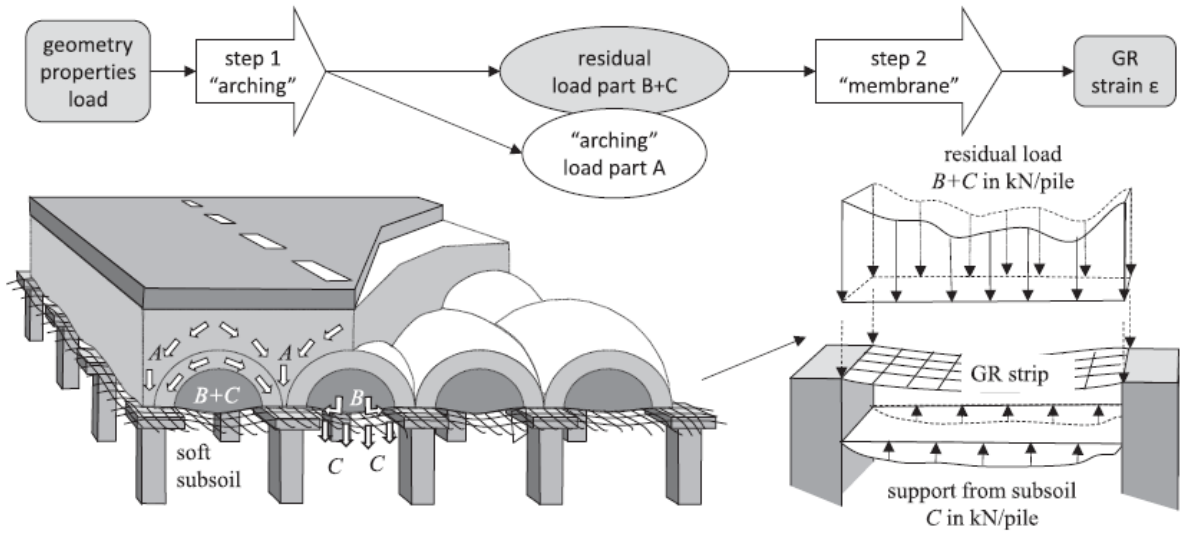

Figure 2.45 – Load parts applicable to calculation step 1 and step 2 (van Eekelen, Bezuijen & van Tol, 2015)

Table 2.3 – Arching models implemented in various design guidelines.

Guideline	Model Type	Arching Model
British; BS 8006 (2016)	Frictional model	Marston and Anderson (1913); modified by Jones et al. (1990)
	Equilibrium model	Hewlett & Randolph (1988)
Dutch; CUR226 (2010)	Equilibrium model	Zaeske (2001); also described in Kempfert et al. (2004)
Dutch; CUR226 (2015)	Equilibrium model	Concentric Arches, Van Eekelen et al. (2013)
French; ASIRI (2012)	Equilibrium model	Hewlett & Randolph (1988)
German; EBGEO (2010)	Equilibrium model	Zaeske (2001); also described in Kempfert et al. (2004)

The first step calculates the proportion of the total vertical load that is transferred directly from the overlying structure to the pile heads by an arching mechanism. Van Eekelen et al. (2013) describes this component as load part A, or 'arching A' (Figure 2.45). There are a number of analytical models for calculating this arching behaviour. They include frictional models, rigid arch models, models using mechanical elements and limit equilibrium models (Van Eekelen et al. 2015). The various models available in literature are explained in more detail by Van Eekelen et al. (2013, 2015) and are also presented in the various national guidelines (Table 2.3). Van Eekelen et al. (2015) suggests that the application of the arching models should be limited to situations where the distance between the piles is similar to the conditions for which the models have been validated.

2.2.8.2 Models for calculating the load-deflection behaviour of geotextile reinforcement in piled earth embankments

The component of vertical load not directed to the pile head is referred to as the 'residual load' (van Eekelen, Bezuijen & van Tol, 2015). Figure 2.45 shows that this residual load is applied to the GR strip and in situ soil between the piles. The second calculation step is concerned with the load-defection behaviour of the GR strip under this residual load.

In this step the residual load is divided into load part B and load part C. Load part B is directed through the GR by membrane action to the pile heads and load part C is transferred to the in situ soil between the piles. The GR strain is calculated using membrane theory as discussed in (van Eekelen et al., 2012).

Two assumptions are made in step 2 that have a significant effect on the calculated load-defection behaviour of the geotextile (van Eekelen, Bezuijen & van Tol, 2015). The first is the distribution of load acting over the GR strip. The three most common distributions are uniform, triangular and inverse triangular (Table 2.4). As discussed in section 2.2.4.4 Van Eekelen et al. (2012) concluded that this distribution approximates an inverse triangle.

The second assumption relates to the degree of subsoil support allowed in the calculation (Table 2.4). Consideration should be given to the possibility of loss of subsoil support. Some calculation models consider full support (van Eekelen et al., 2012), others only consider support underneath the GR strip between the piles, while others disregard subsoil support entirely. These assumptions significantly influence the calculated GR strain.

Table 2.4 – Load distribution and degree of support (adapted after van Eekelen et al., 2015)

Guideline	Arching Model	Load Distribution	Support from subsoil
British; BS 8006 (2016)	Hewlett & Randolph Marston and Anderson	Uniform	No support
Dutch; CUR226 (2010)	Zaeske	Triangular	GR strip
Dutch; CUR226 (2015)	Concentric Arches	Inverse triangular	all GR between piles
French; ASIRI (2012)	Hewlett & Randolph	Uniform	No support
German; EBGEO (2010)	Zaeske	Triangular	GR strip

2.2.8.3 Models for calculating the limiting stress in the LTP

ASIRI (2012) proposes the ultimate stress in the LTP at the inclusion head, q_{i0}, is calculated based on the bearing capacity model proposed by Prandtl (1921). Figure 2.46 shows the Prandtl failure diagram comprises three distinct zones; a triangular elastic zone (I) directly above the inclusion head, a radial shear zone (II) bounded by a log spiral curve and a Rankine passive zone (III). The classic bearing capacity equation takes the form:

$$q_{i0} = s_q N_q q_{s0} + S_c N_c \frac{c'}{\gamma_{c'}} - S_y N_y r_p \frac{\gamma}{\gamma_r} \tag{2.6}$$

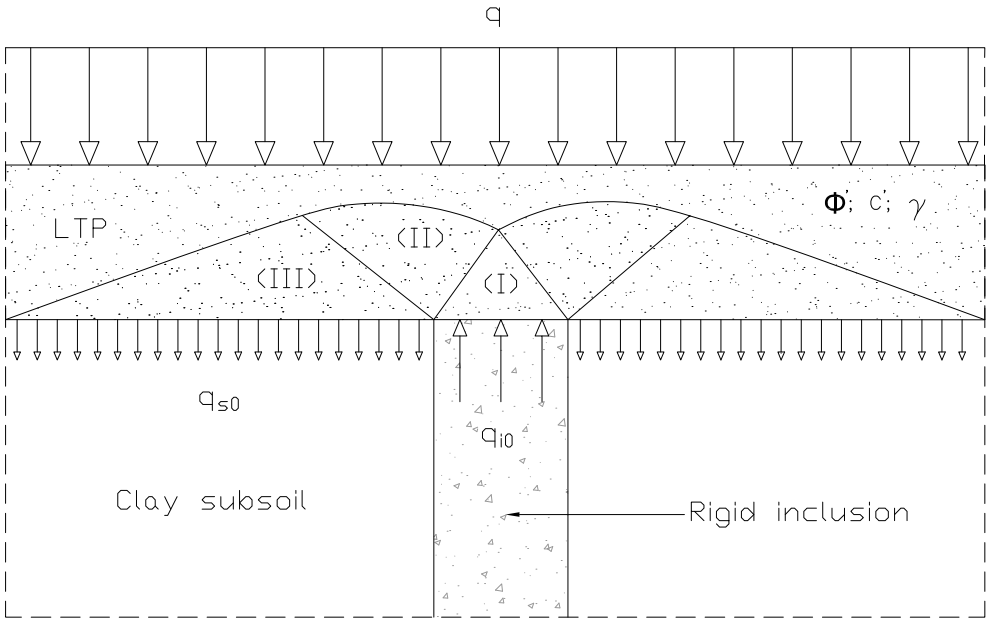

Figure 2.46 – Prandtl failure diagram for calculating the limiting stress in the LTP (ASIRI, 2012)

(ASIRI, 2012) suggest that the $S_y N_y r_p \gamma/\gamma_r$ term is neglected due to its negligible contribution for typical inclusion diameters. Additionally the cohesion term $S_c N_c c'/\gamma_{c'}$ is not applicable to granular LTP materials. According to Terzaghi the inclusion shape factor s_q equals 1 for both axisymmetric and plane strain conditions. Accordingly equation (2.6) simplifies to:

$$q_{i0} = N_q q_{s0} \tag{2.7}$$

The term N_q relates to the friction angle of the LTP. ASIRI (2012) suggests the friction angle is selected as a constant volume value rather than a peak value at LTP relative density values greater than 60%. A constant volume friction angle of 38° is recommended based on a best fit to experimental data. The term q_{s0} is the stress applied to the soil between the inclusions. The Prandtl mechanism is applicable for situations where the LTP thickness allows the full failure mechanism to develop. Further commentary regarding these geometrical considerations is provided in ASIRI (2012).

2.2.8.4 Models for analysing the global load-deflection behaviour of an inclusion

ASIRI (2012) presents various so called analytical models for analysing the load-deflection behaviour of the whole system (RI's, soil, LTP). These models do not allow for basal reinforcement in the LTP. Common features to all of the models include:

- Analytical approach considering an elementary reinforced unit cell.
- Fictitious inclusion extends above the inclusion head after Combarieu (1988, 2007, 2008).
- Unit cell model assimilated to a cylinder composed of two domains,
- Pile and its fictitious inclusion domain; remaining soil volume domain.
- Appropriate stiffness moduli need to be defined for inclusion, LTP and soil.
- Frank and Zhao (1982) mobilisation laws for resistance of tip of inclusion.
- Frank and Zhao (1982) mobilisation laws for shaft friction, or
- Combarieu (1988) mobilisation laws for shaft friction.
- Interaction between both domains is described by the shear stress developed on the common boundary between domains and reference to t-z curves.
- Equilibrium equations express the variation in forces with depth.
- Boundary conditions imposed at head and base for flexible and rigid structures.

This approach can be used to analyse the load-deflection behaviour of a rigid inclusion beneath the centre of a flexible or rigid structure under vertical loading. These models provide the settlement of the inclusion with depth, the average soil settlement with depth, the mobilised shaft friction, the vertical stress in the soil and the axial force in the inclusion. These models, together with the design requirements of ASIRI (2012), have been implemented in the multi-purpose foundation design software FOXTA V3, developed by Terrasol (Cuira & Simon, 2009).

This analytical approach has been extended to the case of a spread footing. This is a special case where the limited number of inclusions means that the assumption of a large number of identical adjacent grids is no longer possible. In this case the interaction with the surrounding unreinforced soil needs to be considered. ASIRI (2012) presents analytical models MV1, MV2 and MV3 which deal with vertical loading and MH1, MH2 and MH3 which deal with lateral loading or an inclined force. Each model yields an increasing volume of information but requires an increasing number of computation steps.

2.2.8.5 Models for analysing global stability

Various analytical methods are available for assessing the collapse load in a stability problem. Two of these methods which have been applied to the problem of rigid inclusion ground improvement are the limit equilibrium method and methods based on yield design theory.

Limit equilibrium methods first involve assuming a failure surface of various simple shapes such as planar, circular or logspiral. This simplified mode of failure then makes it possible to solve the problem by simple statics. Several analytical models based on a Prandtl logspiral failure diagram (Figure 2.46) have been proposed to determine the ultimate bearing capacity of a shallow foundation. Terzaghi and Meyerhof's bearing capacity models are commonly used models.

Limit equilibrium slope stability models divide the problem into vertical slices or wedges and consider the equilibrium of each slice or wedge. The Bishop (1955) method is commonly used and assumes a circular failure surface divided into a number of slices. The assumption of a shear failure mode irrespective of the location along the slip surface has been shown in certain cases to overestimate the stability.

Yield design theory (Salençon, 1983) provides a theoretical framework for evaluating the collapse load of structures overlying soil reinforced by rigid inclusions. ASIRI (2012) describes two approaches based on Yield design theory. The simplified approach involves using a restricted part of the theory, by only considering a kinematic approach; Mohr-Coulomb failure criterion; and the motion of rigid blocks as defined by a succession of logarithmic spiral arcs. With this approach it is possible to take the bending strength of inclusions into consideration in addition to their compressive strength. The comprehensive approach involves applying yield design theory within its general framework, by considering both static and kinematic approaches and an unrestricted displacement field. This approach is capable of processing any combination loads and determining the associated failure mode. ASIRI (2012) recommends this comprehensive approach only for exceptional structures. This method was applied by Pecker (1998) to the foundations for the Rion Antirion bridge (Figure 2.12 and Figure 2.13).

2.2.8.6 Methods to estimate horizontal ground movement due to embankment loading

Various analytical methods have been developed to estimate horizontal ground movements due to embankment construction or backfilling behind a retaining wall. Seaman (1994) provides a summary of the available models for the different calculation methods. The simplest approach utilises empirical calculation models. Table 2.5 summarises a number of the available empirical models and their input data.

Table 2.5 – Empirical models to estimate horizontal ground movement (Seaman, 1994).

Reference	Method	Soil data required
Bourges and Mieussens (1979)	Maximum horizontal movement at varying distance from embankment crest or for different embankment widths. Profile of movement with depth.	Undrained shear strength
Marche and Chapuis (1974)	Maximum horizontal movement at embankment toe for varying embankment width.	Undrained Young's modulus
Suzuki (1988)	Depth of maximum lateral movement for varying embankment width.	None
Tavenas et al (1979)	Relationship between horizontal and vertical movements during consolidation. Influence of slope angle and factor of safety.	Undrained shear strength

2.2.8.7 Methods to estimate the effects of moving soil on piles

Stewart et al. (1994b) provides a summary of the various analytical methods available to estimate the effects of lateral soil movement on piled foundations. The empirically based methods are useful as a first order estimate of the behaviour of a pile in moving soil as they are relatively quick and easy to implement. They are generally restricted to assessing maximum pile bending moment and deflection. Table 2.6 summarises two of the available empirical models and their input data and output data.

Table 2.6 –Empirical models to estimate the effect of moving soil on piles (adapted after Stewart et al. 1994)

Reference	Method	Output
Oteo (1977)	Maximum pile bending moment related to relative pile length, with correction for embankment geometry. Undrained Young's modulus of soil required.	Max bending moment
Stewart et al (1992, 1994)	Maximum pile bending moment and pile head deflection related to relative soil-pile stiffness and current loading level. Undrained shear strength and undrained Young's modulus of soil required.	Max bending moment and pile head deflection

2.2.9 Numerical methods for the analysis of RI ground improvement

2.2.9.1 Introduction

Numerical analysis methods attempt to satisfy all theoretical requirements, include realistic soil constitutive models and incorporate boundary conditions that realistically simulate field conditions (Potts & Zdravkovic, 1999). The finite element (FEM) and finite difference methods (FDM) are the most widely used approaches. The discrete element method (DEM) is sometimes used for research purposes. A more detailed description of the implementation of the finite element method is provided in the next chapter. This section provides an overview of the application of numerical methods for analysing foundations reinforced with rigid inclusions.

2.2.9.2 Application of numerical methods in research

Table 2.7 presents a summary of research where numerical methods have been used to analyse rigid inclusion ground improvement. The choice of constitutive model, numerical method and modelling approach will be discussed in the following sections.

Table 2.7 – Summary of research which utilised numerical methods for analysing rigid inclusions

Reference	Constitutive Model			Numerical Method	Structure / Loading
	LTP	Column	Subsoil		
Kitazume et al. (2000)	MC	LE	MC	FEM (2D-PS)	Caisson / V & H
Ellis & Springman (2001)	MC	LE	MCC	FEM (2D-PS)	Piled Bridge Abutment / V& H
Inagaki et al. (2002)	LE	LE	SO	FEM (2D-PS)	Embankment / V & H
Navin (2005); Filz & Navin (2006)	MC	LE; MC	MCC	FDM (2D-PS; 3D)	Caisson & embankment / V & H
Miao et al. (2006)	-	LE	MC	FEM (3D)	Pile / H
Farag (2008)	HS	LE	LE	FEM (2D-PS; 3D)	Embankment / V & H
Satibi (2009)	HS; HSS	LE	HS; HSS	FEM (2D-AS; 2D-PS; 3D)	Embankment / V
Villard et al. (2009); Chevalier et al. (2010);	-	-	-	DEM-FEM (3D)	Embankment; Slab / V
Balasubramaniam et al. (2010)	MC	LE	MC	FEM (2D-AS; 2D-PS)	Embankment / V & H
ASIRI (2012)	Various	Various	Various	Various	Various
Kelesoglu & Springman (2011)	MC	LE	SSC	FEM (3D)	Piled Bridge Abutment / V& H
Den Boogert (2011)	MC; HS	LE	LE	FEM (2D-AS; 2D-PS; 3D)	Embankment / V
Dias et al. (2012)	MC	LE	SS	FEA (2D-AS)	Slab / V
Dias & Simon (2012)	CJS2	LE	MCC	FDM (3D)	Footing / V & H
Girout et al. (2014)	HS; HYP	LE	-	FEM (2D-AS; 2D-PS; 3D)	Embankment / V
Peet (2014)	MC	LE	MC	FEM (2D-PS; 3D)	Embankment / V

MC = Mohr Coulomb Model; HS = Hardening Soil Model; HSS = Hardening Soil Model with Small Strain Stiffness; LE = Linear Elastic; HYP = Hypo-plastic Model; MCC = Modified Cam Clay Model; SS = Soft Soil Model; SSC = Soft Soil Creep Model; SO = Sekiguchi - Ohta Model

2D-AS = 2D Axisymmetric; 2D-PS = 2D Plane Strain; DEM-FEM = Coupled DEM-FEM model

V& H = Vertical and Horizontal loading

2.2.9.3 Idealisation of problem geometry

In order to apply numerical analysis methods to real geotechnical problems certain assumptions and idealisations of the geometry and boundary conditions must be made. The various structural applications listed in Table 2.7 have been approximated to either plane strain, axi-symmetric or three-dimensional conditions. The different approaches have varying degrees of idealization depending on the size of the problem domain considered.

Plane strain conditions:

Embankments and retaining walls have one very large dimension compared to the other two (Figure 2.48). The assumption of plane strain conditions is suitable when the ground profile, stress state and loading conditions are uniform in this long dimension. Individual rigid inclusions in a group pattern are not suited to this idealisation. For plane strain conditions they are modelled as continuous walls. ASIRI (2012) recommends the following adaptions to ensure realistic behaviour:

- Adapting the width of the wall to maintain a constant area replacement ratio
- Deriving an equivalent EA relative to the axial load and EI relative to the bending stiffness
- Adapt the interface parameters to mobilise the correct shaft friction

The in-plane section analysed can be global, incorporating the entire structure and a number of inclusions, or a simplified unit cell model. ASIRI (2012) comments that while the plain strain approach offers an acceptable approximation of the behaviour of the inclusions, it is not well suited to predicting the stresses in the LTP and the overlying structure. The plane strain model should be verified with an axisymmetric model.

Axisymmetric conditions:

Rigid inclusions located under the central footprint of a structure are suited to axisymmetric conditions provided the loading is uniform and vertical. A single unit cell from this central area of the grid can be assimilated to a cylinder of soil by maintaining the area replacement ratio (Figure 2.47). Under these conditions the problem possesses rotational symmetry. The model is simplified to axisymmetric conditions defined by a vertical section where one vertical side has rotational symmetry. Under these conditions the 3D model geometry is simplified to a single 2D plane where only half the geometry is modelled. These models are ideal for verifying the behaviour of rigid inclusions under vertical loading, as well verifying aspects of larger global models.

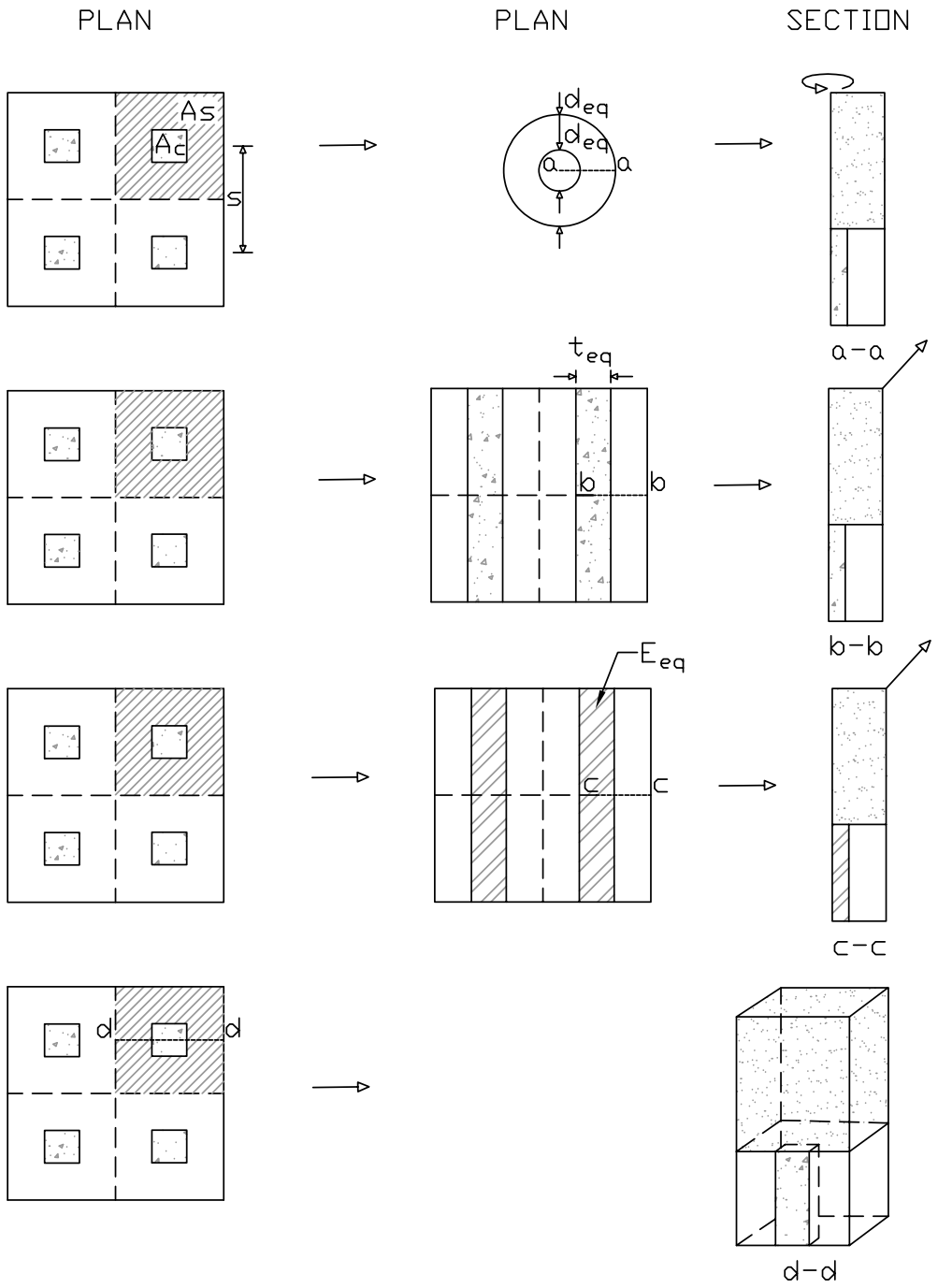

Figure 2.47 – Geometric idealisations for a unit cell: (a-a) axisymmetric conditions (b-b & c-c) plane-strain (d-d) three-dimensional (adapted from Satibi, 2009)

Three-dimensional models:

Although there are aspects of the problem that can be approximated by either plane strain or axisymmetric conditions, a grid of rigid inclusions remains a three dimensional problem. To accurately model the problem in a comprehensive global manner full three dimensional numerical analysis is required. However, the computer recourses and time required for this type of analysis are considerable. One strategy to keep the resources and run time within acceptable limits is to take advantage of the geometric symmetries that exist for the case of a grid of inclusions; there is often a vertical plane of symmetry perpendicular to the long axis of the problem. Consequently only half a unit cell needs to be discretised into finite elements to fully represent the problem. This defines the width of the 3D model in the out-of-plane direction. This type of model still requires a uniform ground profile, stress state and loading condition in the long dimension.

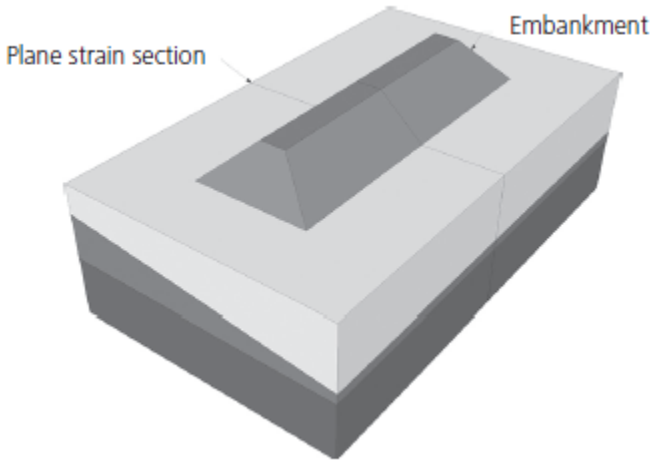

Figure 2.48 – Suitable geometries for plane-strain conditions (Lees, 2016)

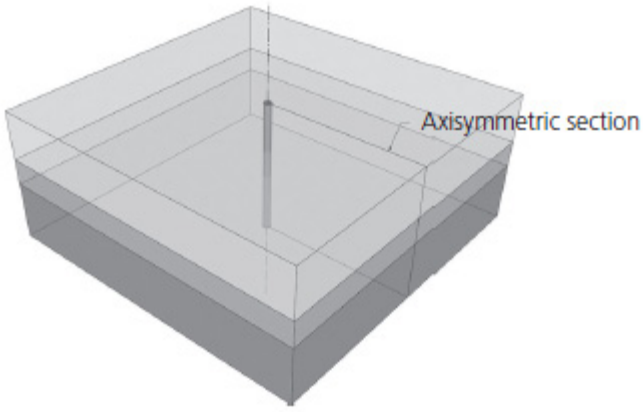

Figure 2.49 – Suitable geometries for axisymmetric conditions (Lees, 2016)

2.2.9.4 Constitutive models

Constitutive models are mathematical formulations which describe the behaviour of the in situ soil and rock, engineered fill and structural elements. All constitutive models are an approximation of the real soil behaviour. For accurately modelling soil behaviour the main aspects of real soil behaviour need to be captured. Additionally for accurately modelling the problem of a structure supported by soil reinforced by rigid inclusions, the mechanisms highlighted in sections 2.2.4 to 2.2.7 need to be captured. Table 2.7 presents a range of models which have been used to represent the behaviour of the in situ fine soil, load transfer platform and rigid inclusions.

Modelling aspects of real soil behaviour:

Soil is a multi-phased material comprising a soil skeleton with grain to grain contacts and voids filled with water or air. When subjected to stress changes soil behaves in a highly non-linear manner which is often time dependent. The rigid inclusion system comprises two different types of soil, namely granular soil characterising the fill, load transfer platform and bearing stratum and in situ clay requiring reinforcement. The most important aspects of real soil behaviour of these soils are discussed below. This enables an evaluation of the extent to which the constitutive soil models are capable of describing these aspects. However, it should be remembered that no constitutive model can take account of all of these aspects of soil behaviour.

- **Undrained behaviour of clays:** Generation of excess pore pressure; undrained failure of clays.

- **Consolidation and creep behaviour of clays**
- **Strength changes during shear:** Contractant and dilatant behaviour of clays; residual shear strength; softening of clays.
- **Stress-dependency of stiffness:** In general the higher the confining stress level (deeper) the larger the stiffness. On the other hand the larger the shear stress levels the smaller the stiffness.
- **Stress-dependency of strength:** In general the higher the confining stress level (deeper) the larger the strength.
- **Stress-path dependency of stiffness:** Unloading and reloading is stiffer than primary loading.
- **Strain-dependant stiffness:** At small strains soil stiffness is high and decays as strains increase.
- **Permanent deformation as a result of loading:** Most soils only have a very small elastic region.
- **Soil fabric and inter-particle bonding**
- **Soil anisotropy**

Constitutive Models:

The four most common types of models used to represent the granular fill, soft clay and rigid inclusions in Table 2.7 are elastic models, simple elastic-plastic models, critical state models and double hardening models. Table 2.8 summarises the features of these models.

Hooke's Law (LE):

The linear isotropic elastic model by Hook defines a simple relationship between increments of stress and increments of strain. It is a two-parameter model defined by Young's Modulus and Poisons ratio. It has been widely applied in geotechnical problems due to its simplicity however it cannot simulate the most important features of real soil behaviour. To some extent, Hooke's law can be used to model rigid materials such concrete or rock layers or far-field areas where plasticity does not play a role, but it is not suitable to model soil in general (Brinkgreve, 2005).

Mohr-Coulomb Model:

The Mohr-Coulomb model is an elastic-perfect plasticity model where the yield/failure surface remains unchanged during yielding. Being a perfectly plastic model there is no hardening or softening

law. The model has been formulated for non-associated plasticity. It is a five-parameter model and requires simple laboratory tests for calibration.

Within the yield surface in the $p' - q$ stress space the behaviour is linear elastic and on the yield surface the behaviour is perfectly plastic. Consequently it cannot accurately predict changes in stress/strain path (primary loading, unloading, reloading) or the significant rotation of principal stress axes. Notwithstanding these limitations the elastic perfectly plastic model still remains suitable for problems with monotonic stress/strain paths provided a careful selection of parameters is made (Potts, 2002).

Modified Cam Clay Model:

The Modified Cam Clay (MCC) model based on the critical state concept was presented by Roscoe & Burland (1968). The failure surface is defined by an elliptical yield locus, together with an associated flow rule, isotropic hardening and softening and linear stress-dependent stiffness. It is a five-parameter model and requires simple laboratory tests for calibration.

The MCC model is able to capture many aspects of real soil behaviour such as yield behaviour, consolidation and shear-induced contraction and dilatation. Limitations of this model relate mainly to the associated flow rule and consideration of only volumetric hardening. The model cannot accurately predict cyclic behaviour, sharp changes in stress/strain paths or the significant rotation of principal stress axes (Potts, 2002). Lees (2016) comments that the MCC model is best suited to predicting the deformation behaviour of soft soils under compression.

The Soft Soil Model (Stolle, Bonnier & Vermeer, 1997) incorporate concepts of Modified Cam Clay Model and Soft Soil Creep Model (Vermeer & Neher, 1999) adds the concept of viscoplasticity to model creep behaviour.

Hardening Soil Model:

The Hardening Soil model (Schanz, Vermeer & Bonnier, 1999) is a double hardening model. Friction hardening models irreversible plastic shear strain. Cap hardening models irreversible plastic volumetric strain. Failure is defined by means of the Mohr Coulomb failure criterion. Stress-dependent stiffness is modelled by a power law formulation. Frictional hardening follows a non-associated flow rule, whereas cap hardening follows an associated flow rule (Schanz, Vermeer & Bonnier, 1999). The Hardening Soil model is an 11-parameter model and requires simple laboratory tests for calibration.

One of the main advantages of this model is its ability to model the dependency of soil stiffness on stress (Schanz, Vermeer & Bonnier, 1999). Additionally in undrained loading the model is able to show a reduction in mean effective stress for soft soils (contractant) and an increase in mean effective stress for stiffer soils (dilatant) (Schanz, Vermeer & Bonnier, 1999). It cannot model anisotropic strength and stiffness or creep behaviour but is an accurate soil model for all the applications listed above. Benz (2007) implemented a small strain overlay for this model (HS small model).

Table 2.8 – Constitutive models, their attributes and their capabilities (adapted from Lade, 2005)

Type of model	**Model**	**Reference**	**Suitable soil types**			**Failure surface / Yield Surface**	**Plastic Potential**	**Hardening Parameter**
			Sand	**Clay**	**Cem***			
Elastic	Hook's Law	Zienkiewicz et al. (1977)	Yes	Yes	Yes	NA	NA	NA
Simple Elastic Plastic	Mohr-Coulomb	Brinkgreve et al. (2016)	Yes	Yes	Yes	Mohr-Coulomb / Equal to Failure Surface	Non-associated	None
Critical State	Modified Cam Clay	Roscoe & Burland (1968)	No	Yes	No	Extended von Mises / Elliptical Cap	Associated	Plastic volumetric strain
Double Hardening	Hardening Soil Model	Schanz et al. (1999)	Yes	Yes	Yes	Mohr-Coulomb / Curved Mohr-Coulomb & Elliptical Cap	Non-associated and associated	Plastic volumetric & shear strain
*Cemented								

Summary of important features of constative models for the load transfer platform and fill:

- Second order model such as double hardening model which captures the rotation of principal stresses and improved prediction of lateral deflection.
- Stress-dependent stiffness and strength due to large stress ranges.
- Non-linear stress path dependent stiffness for improved deflection predictions.
- Strain-dependent stiffness for improved deflection predictions.

Summary of important features of constative models for clay:

- Second order model such as double hardening model required for capturing rotation of principal stresses, plastic straining pre-failure and accurate lateral deflection predictions.
- Stress-dependent stiffness due to large stress ranges.
- Non-linear stress path dependent stiffness for improved deflection predictions.
- Strain-dependent stiffness for improved deflection predictions.
- Models incorporating softening behaviour may be important.
- Models incorporating creep behaviour may be important.
- Models incorporating anisotropic behaviour may be important.

Summary of important features of constative models for rigid inclusions:

- A constitutive model with material-specific failure criterion.
- Simple linear elastic models are acceptable for certain applications provided an appropriate modulus is selected.

2.2.9.5 Modelling structures and interfaces

Modelling Rigid Inclusions:

Structures that have significant volume such as rigid inclusions can be modelled with either volume elements (continuum elements) or with linear elements such as beams or plates (Non-continuum elements). Due to the complex behaviour of rigid inclusions, continuum elements are generally used to accurately model the load transfer mechanisms at the head and along the shaft as well as structural behaviour up to failure. Many researchers introduce a soft beam element into the volume element to facilitate the extraction of inclusion forces and moments.

Modelling Basal Reinforcement (Membrane Element):

Flexible reinforcing strips such as geotextiles and geogrids are modelled as membrane elements which cannot transmit bending moments or shear forces and can only sustain tensile forces (no compression).

Modelling Interfaces:

Interface elements can be used to model the boundary between soil and structure. They allow differential movement of the soil and the structure including slip and separation. Of the various

methods used to model interfaces, the special interface or joint elements of zero thickness are the most popular. A Coulomb failure criterion often defines the elastic-plastic behaviour in terms of effective stress, while a simple limiting shear stress is used for undrained analyses (Lees, 2016).

2.2.9.6 Boundary conditions

The term boundary condition is used to cover all possible additional conditions that may be necessary to fully describe a particular problem. Numerical analysis allows for loading conditions such as point loads, boundary stresses, body forces (gravity loading), prescribed displacements, hydraulic conditions, seepage flows, pore pressures, initial conditions and construction and excavation.

2.2.9.7 Advantages and limitations

Advantages:

- Numerical analysis is a complete theoretical solution which accounts for equilibrium, compatibility of force and displacement, material constitutive behaviour and boundary conditions.
- It has the ability to provide information on local and global stability, structural forces, movements of the structure and adjacent ground and movements and structural forces in adjacent structures.
- It has the ability to predict the behaviour of complex three dimensional field situations.
- Accounts for in situ stress conditions.
- Accounts for large displacements.
- Can simulate construction and excavation.
- Can be used to investigate soil-structure interaction.
- Has the ability to vary the behaviour of the soil-structure interface and to allow differential movement of the soil and structure.
- Identifies the most critical failure mechanism.
- Can be used to calibrate other methods of analysis.

Limitations:

- Requires specialist knowledge in a range of subjects such as soil mechanics, geotechnical engineering and the theory behind numerical methods.

- Constitutive models are limited in their ability to describe real soil behaviour.
- Require large amounts of computing resource and calculation time.

2.2.10 Construction

2.2.10.1 Introduction

Rigid inclusion ground improvement typically involves three main execution phases, namely construction of a working platform, installation of a grid of rigid inclusions and installation of the load transfer platform. The sequence of the works depends on the engineering application. Rigid inclusions can be installed by either extraction techniques or displacement techniques. Displacement techniques can be further subdivided on the basis of whether the inclusion is prefabricated or cast in situ. Table 2.9 provides a list of the main types of rigid inclusions and some of their characteristics.

2.2.10.2 Execution of rigid inclusions

Rigid inclusions can be installed before or after the construction of the working platform. The following sections only deal with augured and vibro-driven cast in situ displacement methods.

Augured cast in situ soil displacement method:

This technique involves a specially designed auger with a reverse pitch, meaning it is screwed into the soil. The soil is displaced laterally without any excavation or vibration. The auger is screwed into the soil to the required depth using equipment with high torque capacity. The inclusion is formed during the extraction process by pumping a grout-cement mix through the centre of the auger. The mixture is often pumped under slight pressure. The grout-cement mix design can be carefully controlled to provide the required strength and stiffness column suited to the project. This type of inclusion is often referred to as a controlled modulus column (CMC). Typical diameters range from 250 mm to 450 mm (Menard, 2016).

Vibro-driven cast in situ soil displacement method:

This techniques involves the use of a bottom feed vibrator, also called a vibroflot or vibro-probe. The probe is supported by custom built machine or crane hung assembly. The installation process involves positioning the probe at the column location, followed by pumping of concrete into the internal tube.

The probe is then vibrated into the ground to the required depth. The inclusion is then formed during the extraction process by pumping concrete through the centre of the probe. The probe can be raised and lowered several times to create an expanded base. This type of inclusion is often referred to as a vibro-concrete column (VCC). Typical diameters range from 250 mm to 420 mm (ASIRI, 2012); but columns as large as 800 mm can be achieved (Menard 2015, pers. comm., 31 March). The VCC is techniques is capable of production rates of 200 – 300 linear meters per day, depending on the soil type (Menard, 2016).

Figure 2.50 – Vibro concrete column installation (Menard, 2016a)

Figure 2.51 – Vibro concrete column crane hung assembly (Menard, 2016a)

Offshore crane-hung assembly:

The vibro-driven method can be used offshore. A crawler crane of sufficient capacity is used to support the vibrator. A barge or pontoon serves as a working platform on which a crawler crane is mounted to support the assembly. Positioning is performed with the assistance of a global positioning system. Driving to the required depth is often assisted by vibrations and air jetting.

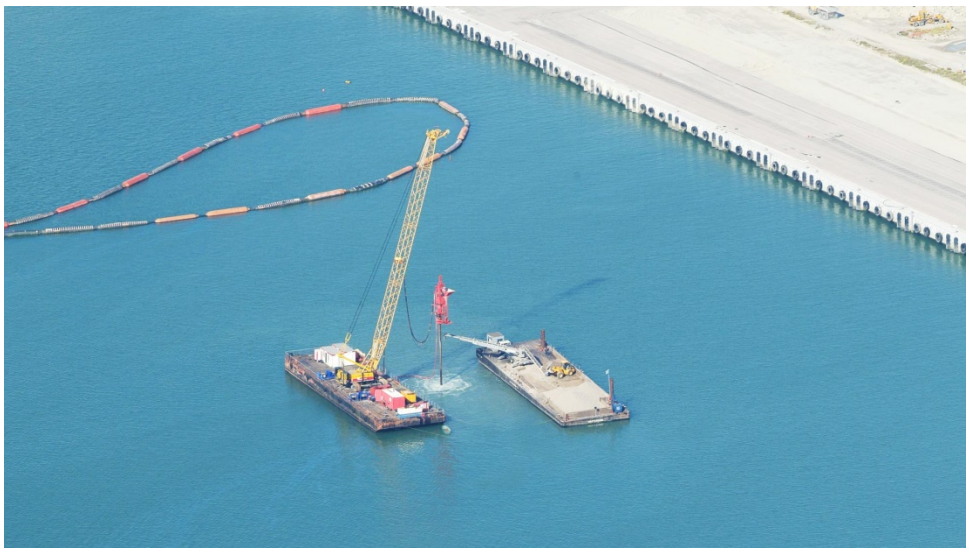

Figure 2.52 – Offshore crane hung assembly (Menard, 2016a)

In situ casting methodology:

It is important that the installation method does not collapse the hole or cause necking of the RI. This typically means the inclusion is formed in a single pour with the inclusion head terminating in a good quality material above the desired cut-off level.

Preparation of the inclusion head:

The head of the inclusion needs to be set at an appropriate level and the quality of the concrete at the inclusion head needs to be intact. This can be achieved by cutting the rigid inclusion head to the required level and quality. Under certain circumstances it may either not be necessary or practically possible to cut the inclusion head.

Table 2.9 – Various characteristic of main rigid inclusion types (ASIRI, 2012)

Type of inclusion			**Vibrations**	**Noise**	**Excavation**	**Estimated long-term modulus (MPa)**
Prefabricated	wood		yes	yes	no	10000 - 15000
	steel		yes	yes	no	210000
	concrete		yes	yes	no	10000 – 20000 (1)
Fabricated in situ	Driven, hammered or bored	Drilled by percussion	yes	no		Mortar: 5000 – 10000 (2) Concrete C15: 9000 (2) Concrete C25: 11000 (2)
		Vibro-driven	yes	no	shallow	
		Simple bored	no	no	yes	
		Drilled cased or sludge drilled	no	no	yes	
		Bored with continuous auger	no	no	yes	
		Bored with displacement	no	no	shallow	
	Treated soil columns	Soil mixing	no	no	shallow	Variable: 250 – 9000 (3)
		Jet grouting	no	no	shallow	500 – 1000 $\times$ *compressive strength*
1 - Depends on type of concrete and reinforcing; 2 - Depends on type of grout / concrete; 3 - Depends on type of binder and soil						

Minimum grid spacing to limit interference:

The sequence or spacing of rigid inclusions should prevent damage caused by the installation of adjacent inclusions before the concrete has gained sufficient strength. ASIRI (2012) recommends a minimum distance of four diameters for inclusions installed by displacement techniques.

Summary of inclusion types by execution method:

For a detailed description of the various installation methods the reader is referred to ASIRI (2012) and the state-of-art report on construction processes by Chu et al. (2009). Table 2.9 lists the various characteristics of the main types of rigid inclusions.

2.2.10.3 Execution of load transfer platform

The load transfer platform is defined as the layer between the inclusion head and the base of the overlying structure. The LTP material is typically granular but may include binders or basal reinforcement within its layer works (Figure 2.53). The LTP material, geometry and the addition of binders or reinforcement, are a function of the engineering application and the performance requirements for the project.

Figure 2.53 – Steel reinforcement cage under embankment LTP for LGV project Paris, Bordeaux (Coghlan, Plomteux & Racinais, 2016)

Working platform:

A working platform is typically constructed before the RI works to provide a stable base for the installation equipment and to protect the inclusion from construction activity. The working platform is typically constructed from the same material as the LTP and may in fact form part of the LTP.

Sequence of load transfer platform installation:

Depending on the engineering application, the LTP can be installed prior to or after the installation of the rigid inclusions. Benefits of prior installation are the ability to compact the LTP without damaging the inclusions, termination of the inclusion in a good quality material and limiting heave of the surrounding soil caused by the displacement method.

Execution of the load transfer platform:

The execution of the load transfer platform involves typical earth works activities and equipment related to forming granular layer works. The works typically includes excavation, initial grading,

compaction and finish grading. Compaction and quality control measures are required. Specialist works may include the addition of binders and the installation of basal reinforcement.

The construction process typically involves grading the fill to the line and grade required by the drawings. The fill is compacted with the addition of water to achieve the optimum moisture content for compaction. Finally, soft spots are identified, replaced and recompacted.

For execution in the marine environment, speciality screeding and compaction equipment may be needed. Marine screeding equipment may include travelling screed hoppers, screeding beams and stone tremie tubes. Marine compaction equipment may include a vibrating plate, a dynamic compaction pounder or a vibroflot.

Minimum characteristics and thickness of the material used for the LTP

The LTPs ability to direct load to the inclusion head by an arching mechanism is a function of the granular materials strength of relative density. The material characteristics, strength and compaction are justified by typical testing standards. Only unstablised materials are considered here.

Unstablised (granular) LTPs may comprise a wide range of soils and aggregates. Typical materials include crushed stone, sand-gravels, sands and recycled crushed concrete. The following should be considered when selecting a suitable material (with typical values): maximum particle size (of no more than one third the layer thicknesses); fines content (Less than 15% passing μm sieve); plasticity index (6 or less); liquid limit (25 or less); Los Angeles abrasion resistance of 50 or less; permeability (45m/day). Additional considerations for aggregate materials include aggregate uniformity (D_{85}/D_{15}), density ($> 2600\ kg/m^3$), water absorption (> 2%), strength and durability (AIV < 30%; 10% FV > 120 kN; AAV < 15%).

ASIRI (2012) established the shear parameters for an LTP composed of industrial gravel under rigid loading. At a relative density of 85% the peak friction angle was 42° reducing to 38° at the maximum load. At a RD of 65% no peak was observed and it was concluded that a friction angle of 38° was representative of the critical state.

ASIRI (2012) recommends a minimum thickness of 400 mm for the LTP of a raft or ground slab and 300 mm under a footing.

Basal Reinforcement:

The LTP may include one or more layers of geotextile within its layer works. Although the geotextile typically performs a reinforcing function it may also be used for separation and filtration. There are various standard specifications governing the characteristics, implementation and quality control of geotextile related products such as:

- BS EN 13251:2014+A1:2015. Geotextiles and geotextile-related products. Characteristics required for use in earthworks, foundations and retaining structures.
- PD CEN/TR 15019:2005. Geotextiles and geotextile-related products. On-site quality control

Table 2.10 provides an example of the required parameters for a geotextile used for reinforcement, separation and filtration, in construction of earthworks, foundations and retaining structures.

Table 2.10 – Geotextile properties (adapted from BS EN 13251, 2015)

Product:	**Composite geotextile and geotextile related products**		
Intended use	**For reinforcement, separation and filtration, in construction of earthworks, foundations and retaining structures.**		
Tensile strength (T_{MAX})	Machine direction (MD)	kN/m	BS EN 13251 EN ISO 10319
	Cross machine direction (CMD)	kN/m	
	Elongation (ε_{MAX})	%	
	Creep limited strength (120 years)	kN/m	BS EN 13251 EN ISO 10319
Resistance to static puncture	CBR test	kN/m	BS EN 13251 EN ISO 12236
Water permeability	Normal to Plane	l/m^2s	BS EN 13251 EN ISO 11058
Characteristic opening size	O_{95W}	µm	BS EN 13251 EN ISO 12956
Durability	To be declared in accordance with the relevant clause of EN 13251, Annex B	-	BS EN 13251 Annex B
Release of dangerous substances	Less than required by national regulations	-	National Regulations in force

2.2.10.4 Testing and Monitoring

In order to guarantee the quality of the rigid inclusions and the quality and thickness of the load transfer platform, various tests, controls and monitoring activities are required, some of which include:

- Static load tests on a group of working or trial inclusions.
- Field tests conducted before the general works.
- Structural integrity tests along the shaft.
- Execution controls relating to layout and positioning of inclusions.
- Execution controls for the LTP thickness and compaction.
- Execution controls relating to the placement and protection of the geotextile.

It is beyond the scope of this review to discuss these tests, controls and monitoring activates. The reader is referred to ASIRI (2012) for a general discussion of each topic.

2.2.11 Summary

The topic of RI ground reinforcement has been covered broadly and in this regard this part of the literature review serves as an overview of the topic for various fields of application. Emphasis was placed on the mechanics of the problem which are covered in sections 2.2.4 to 2.2.7; a summary has been provided at the end of each section.

The following summarises the key findings for the specific structural application of a caisson quay wall supported by RIs:

- A caisson quay wall imposes a rigid boundary condition at the base of the structure.
- For the case where RIs are extended behind the caisson to support the backfill, as is suggested in the next section, the problem includes an upper flexible boundary condition.
- The presence of both boundary conditions means all the load transfer mechanisms presented in sections 2.2.4 to 2.2.7 are relevant to this problem.
- The embankment type loading from the caisson backfill has the potential to produce significant lateral ground movements.
- Unreinforced RIs are vulnerable to lateral loading from ground movements due to their brittle behaviour.

- The behaviour of individual inclusions beneath a caisson subjected to lateral ground movements depends on the relative inclusion-soil flexibility, free-head condition, soil movement distribution and failure mode of the soil.
- Under combined vertical and lateral loading from the caisson, internal failure modes for columns such as bending and shear failure should be considered. Additionally there is an external failure mode due to excessive tilting.
- Various analytical models are available for analysing the behaviour of RIs. Most focus on vertical loading and are therefore are limited for this application.
- Various analytical models are available for estimating lateral ground movements and the effects on inclusions. These models are useful as a first order estimate of behaviour due to the embankment type loading from the caisson backfill.
- Three-dimensional numerical modelling has the ability to predict the behaviour of this complex three dimensional field situation.
- The vibro-driven cast in situ soil displacement method is suitable for marine execution using an offshore crane-hung assembly.

2.3 Strategies for Limiting and Accommodating Lateral Loading of Piles

2.3.1 Introduction

The Transport Research Laboratory (TRL) produced a report identifying a number of strategies to avoid structural damage to highway bridge abutments and their foundations due to lateral soil movement caused by embankment construction (Seaman, 1994). These strategies are categorised into those which limit ground movement and those which accommodate ground movement. The report also identifies the various factors affecting ground movement and the factors affecting the behaviour of piles in moving soil. The report concludes that not all of the solutions are suitable for every site and that many of the solutions are most effective when used in combination with one another (Seaman, 1994).

Caisson quay walls retaining backfill supported by RIs, are analogous to piled bridge abutments retaining embankments. It is therefore argued that the strategies to limit and accommodate lateral loading are directly applicable. The following sections are a summary of the TRL guidelines.

2.3.2 Factors affecting horizontal ground movement

The load transfer mechanisms and primary factors affecting lateral horizontal ground movements have been highlighted in section 2.2.6. They are the vertical self-weight of the structure, outward lateral thrust in the structure and the strength and stiffness of the clay subsoil. Table 2.11 from the TRL report highlights these factors, as well as others, and further distinguishes those which have a direct effect on lateral soil movements from those which have a less directly quantifiable relationship.

Table 2.11 – Factors influencing lateral soil movements (Seaman, 1994)

Factor influencing soil movement			
Increase in magnitude of factor cause lateral soil movement to:	**Decrease**	**Increase**	**Relationship not directly quantifiable**
Vertical stress applied to the soil due to weight of fill		●	
Shear stress applied to the soil due to active thrust from the fill		○	
Shear stress applied to the soil due to compaction pressures on abutment		○	
Stiffness of fill	○		
Strength of fill	○		
Width of the embankment		●	
Length of the embankment		○	
Embankment slope angle		●	
Distance from the embankment toe	●		
Thickness of soil layer(s) affected by soil movements			■
Stiffness of the soil	●		
Variation of stiffness with depth			■
Adhesion between the fill and the soil	○		
Variation of vertical and horizontal stiffness of the soil (anisotropy)			■
Relationship between stress and strain in the soil			■
Strength of the soil	●		
Variation of strength with depth			■
Initial state of stress in the soil			■
Poisson's ratio of the soil		●	
Consolidation properties of the soil			■
Rate of loading		○	
Time after application of loading	●		
Creep effects			■

● Very significant effect; ○ less significant effect

2.3.3 Strategies to limit ground movements

The lateral loading of RIs and piles can be reduced by limiting the magnitude of lateral ground movements. This can be achieved by a reducing the disturbing forces causing the movement and increasing the forces resisting the movement. Various construction methods or combinations of methods are suited to this purpose. Seaman (1994).divides them into three broad categories:

- modification of the embankment load,
- provision of additional structural support to the embankment or structure,
- improvement of the ground itself.

2.3.3.1 Summary of construction methods to modify the embankment load

Table 2.12 summarises the various strategies for modifying the embankment load. They include the use of light-weight fills, the use of stronger stiffer fills and changes to the structures geometry. For a more detailed discussion on each of these methods the reader is referred to Seaman (1994).

Table 2.12 – Construction methods to modify the embankment loading (Seaman, 1994).

Method	Brief Description	Advantages	Disadvantages	Special Requirements
Lightweight Fills	Use of material of lower density than conventional fills e.g expanded or extruded polystyrene, PFA and expanded clay.	Requires lower bearing capacity to support embankment. Reduced settlement and lateral movements. Reduced earth pressures on structure.	Expanded polystyrene requires protection from petrol, fire and UV light. PFA is frost susceptible and may inhibit plant growth. PFA difficult to handle when wet. Expanded Clay difficult to compact in unconfined situations.	Materials testing usually required to confirm design parameters of lightweight fills.
Stronger stiffer fills	Use of material of a higher strength and stiffness. e.g rock fill or densified sand.	Reduced earth pressures on structure.	Additional construction activity.	In situ testing if compaction measures are undertaken.
Change in structure geometry	Flatten slopes or use berms to counter balance potential failure zones	Requires lower bearing capacity. Reduced settlements and lateral movements.	Changes to structure may not suit the design requirements, may not be practical and may be costly.	None.

2.3.3.2 Summary of construction methods to provide additional structural support

Two primary methods of embankment support are presented in section 2.2.6 namely basal reinforcement and embankment support using rigid inclusions or piles. Table 2.13 summarises these two strategies.

Table 2.13 – Construction methods to provide additional structural reinforcement to the embankment (Seaman, 1994).

Method	Brief Description	Advantages	Disadvantages	Special Requirements
Reinforcement of the Embankment Fill	Incorporation of tensile reinforcement within the fill, usually at the base.	Increases bearing capacity by reducing lateral stresses on soil from embankment fill. Recues lateral movement adjacent to embankment, Can reduce differential settlements.	Total settlements may not be reduced. Creep may reduce long terms reinforcement strength. Need to avaoid damage by construction plant. Requires protection from UV light and some chemicals.	Long terms testing needed to determine creep characteristics of reinforcement. Need to establish friction between reinforcement and fill and soil.
Embankment Support Piles	Piles carry some or all of the weight of the fill. Geotextile can assist arching action if isolated piles are used instead of a raft.	Settlement of embankment greatly reduced. Reduction of lateral loads on abutment piles due to soil improvements.	Pile driving may affect stability of existing structures or embankments. Piles are likely to be affected by negative skin friction. Geotextile may need to be used to provide lateral restraint at edges of embankment.	Internal angle of friction of fill needs to be established to confirm effectiveness of arching action. Pile test required to confirm bearing capacity. Negative skin friction potential should be assessed.

2.3.3.3 Summary of construction methods to improve the ground

Ground improvement methods can be used to increase the strength and stiffness of the sub-soil prior to or during embankment construction. Seaman (1994) subdivides these methods into non-intrusive methods requiring no excavation or insertion into the ground; these include preloading, surcharging and staged construction. Intrusive methods require excavation or treatment using a probe, such as, excavation and replacement, soil displacement, vertical drains, granular inclusions and rigid inclusions. Table 2.14 summarises these methods.

Table 2.14 – Summary of construction methods used to improve the ground (Seaman, 1994)

Method	Brief Description	Advantages	Disadvantages	Special Requirements
Pre-loading	Application and removal of load to ground before construction of permanent works to deliberately cause settlement to occur.	Reduction of proportion of consolidation and secondary settlements. Soil strength increases. Low grade fill can be used for pre-loading.	Can be time-consuming. Double handling of fill required. Confidence in design parameters to time pre-loading required.	Good knowledge of consolidation characteristics needed from laboratory and in situ tests. Full scale trial may be required if timing is critical.
Surcharging	Application of load in excess of permanent load to accelerate rate of settlement.	Reduction of proportion of consolidation and secondary settlements.	Can be time consuming. Bearing capacity should be sufficient to tolerate increased height of fill. Confidence in design parameters to time duration of surcharge required.	Good knowledge of consolidation characteristics needed from laboratory and in situ tests. Full scale trial may be required if timing is critical.
Staged Construction	Embankment filling rate limited by soil strength increase due to consolidation.	Increased embankment heights and steeper slope angles can be achieved.	Can be time-consuming. Instrumentation in soil required. Regular monitoring of data needed.	Comprehensive site investigation and laboratory testing to establish consolidation characteristics and the anticipated increase in soil strength during construction.
Excavation and replacement	Removal of soft ground and replacement with better quality material.	Increased bearing capacity. Reduction in ground movements.	Excavation may be difficult below ground water level. Remaining soft soil may cause differential settlements. Disposal of excavated soil may be a problem. Placement of fill below the water table requires careful consideration. Effects of temporary excavation on nearby structures should be considered.	No special testing other than to determine stability of excavation and stability and settlement of embankments.

Table 2.21 continued – Summary of construction methods used to improve the ground (Seaman, 1994)

Method	Brief Description	Advantages	Disadvantages	Special Requirements
Soil Displacement	Displacement of soft soil from beneath embankment by weight of fill.	No excavations required. Heaved material at sides of embankment can enhance bearing capacity.	Large quantities of fill required. Unsuitable for thick deposits of soft ground. Pockets of soft soil may become trapped and cause differential settlement.	Ability to ensure failure and displacement of soil at tip face should be demonstrated. Post construction testing may be required to identify zones of trapped soft soil.
Vertical Drains	Installation of a grid of drainage elements to increase rate of consolidation of soft soil.	Reduction in time for ground movements to occur after fill has been placed.	Must be in conjunction with application of load to the soil. Effects of heave, smear, clogging and discharge capacity need to be considered	Good knowledge of consolidation characteristics needed from laboratory and in situ test. Full scale trials may be required if timing is critical.
Stone Columns	Columns of granular material formed in soil using vibrating poker.	Increased bearing capacity and reduced ground movement. Stone columns act as vertical drains increasing rate of consolidation.	Wet methods produce large quantities of efferent. Dry method not suitable in very soft soils.	No special soil testing requirements. Zone tests of several stone columns recommended to confirm performance.
Vibro Concrete Columns	Columns of concrete formed in the soil while with drawing vibrating poker.	Increased bearing capacity and reduced ground movements.	Access required for supply of concrete.	No special soil testing requirements. Concrete supply should be monitored during formation of columns. Individual columns may be load tested.
Lime Columns	Lime mixed in situ with existing soil by an auger to produce columns with greter strength and stiffness than the surrounding soil.	Increased bearing capacity and reduced ground movements. Columns act as drains to increase rate of settlement.	Strength of the column sensitive to soil chemistry, particularly pH, and high water contents. Strength measured in field and laboratory may differ.	Laboratory testing of lime and soil mixture needed to establish required quantities of lime to be added. Zone tests of several lime columns recommended confirming performance. Individual columns can be tested using penetrometer devices.
Jet Grout Columns	Erosion of soil by high pressure jets of water or grout and subsequent mixing with grout to form columns with greater strength than the surrounding soil.	Increased bearing capacity and reduced ground movements. Interlocking columns can provide foundations of greater bearing capacity.	End product dependant on properties of existing soil. Disposal of effluent required.	Testing required to assess quantities of grout required. Strength of finished columns should be confirmed by testing samples of the grout-oil mix and by zone tests of the finished columns.

2.3.4 Factors affecting the behaviour of piles in moving soil

The principal factors affecting the behaviour of RIs or piles in moving soil are:

Soil related factors:

- variation in magnitude of soil movements with depth at the foundation location,
- relationship between soil stiffness and strain,
- strength of the soil,
- relationship between earth pressures on the pile and soil strength,
- rate of movement of soil.

Inclusion / Pile related factors:

- lateral restraint offered to the pile by deeper soil layers,
- pile diameters,
- pile length,
- pile rake,
- pile stiffness,
- pile ductility,
- pile group layout and spacing,
- pile group interaction,
- pile head restraint.

Construction related factors:

- time of pile installation in relation to embankment construction;
- reduction of soil movement due to reinforcing effects of piles.

2.3.5 Strategies to accommodate ground movements

Constraints on the construction of the structure may be such that the measures described in the previous sections cannot significantly reduce the ground movements. It may prove necessary to adopt additional measures to supplement those already chosen to limit ground movements. A number of techniques are available to accommodate ground movement. Seaman (1994) describes a number of basic approaches, which are listed here and summarised in Table 2.15:

- Modify the construction sequence so that piles are installed when the remaining ground movements will not adversely affect the foundation or structure.
- Accept that the piles will be subjected to extreme earth pressures and design them accordingly.
- Physically isolate the piles from the moving soil.
- Revise the layout of the foundations.
- Adopt a different superstructure arrangement.

Table 2.15 – Summary of strategies to accommodate ground movements (adapted from Seaman, 1994).

Method	Brief Description	Advantages	Disadvantages	Special Requirements
Modify construction sequence	Postpone construction of foundations or superstructure until remaining ground movements cannot cause damage.	No additional construction or special techniques required.	Delay to scheme programme.	Installation of instrumentation to monitor movements. Contract may need to provide for movement continuing longer than anticipated.
Design piles to withstand earth pressures.	Increase strength of foundations so that damage does not occur.	No delays to construction programme.	Increase cost of foundation.	None.
Isolate piles from ground movements	Provide soft barrier between pile and moving soil to accommodate movement.	Reduce delays to construction programme.	Additional expense of barrier systems. Loss of lateral support to piles.	Equipment for installation of barrier system.
Modify the foundation layout	Arranging piles to reduce overall earth pressure on foundation.	Reduce delays to construction programme.	Substructure may require modification.	None.
Modify the structure	Change overall geometry or details of the superstructure.	Reduce delays to construction programme. Modifications to foundations may be avoided.	Increased cost of superstructure.	None.

2.3.6 Summary

The TRL Report 71 by Seaman (1994) focusing on piled bridge abutments provides a valuable overview of strategies limiting or accommodating soil-induced lateral ground movements. A caisson quay wall supported on RIs is analogous to a piled bridge abutment and therefore these strategies are directly applicable.

Significant factors affecting horizontal ground movement include:

- Vertical stress applied to the subsoil due to the weight of the backfill,
- Shear stress applied to the subsoil due to active thrust from backfill,
- Strength and stiffness of the backfill,
- Strength and stiffness of the clay subsoil,
- Rate of loading.

Significant factors affecting the behaviour of the inclusions in moving soil for this problem include:

- Inclusion diameter, length and rake;
- Inclusion strength, stiffness and ductility;
- Inclusion group layout and spacing;
- Lateral restraint offered to the pile by deeper soil layers;
- Reduction of soil movement due to reinforcing effects of piles.

Suitable strategies for limiting lateral ground movement for this problem include:

- Strengthening and stiffening the backfill material,
- Basal reinforcement,
- Supporting the backfill using RIs,
- Excavation and replacement,
- Reducing the rate of loading.

Suitable strategies for accommodating lateral ground movement for this problem include:

- Designing the inclusions to withstand earth pressures,
- Revising the layout of the foundations.

Chapter 3 Development of the Ground Improvement Strategy

3.1 Introduction

This section begins with a description of the caisson superstructure, its construction, intrinsic loading and the subsoil conditions for this problem. Simple analytical calculations are presented which were firstly used to justify the requirement for RI ground improvement and secondly, provided a first order estimate of the magnitude of lateral ground movement. Lateral loading of the RIs was identified as a problem and suitable strategies for limiting this movement were selected. The overall ground improvement scheme which was implemented in the numerical models is described in detail in this section.

3.2 Superstructure

3.2.1 Caisson quay wall

The superstructure is a gravity caisson functioning as a quay front structure for a port container terminal (Figure 1.1 and Figure 3.1). The subsoil condition is characterized by a significant thickness of clay which requires ground improvement. The caisson capping beam and piled rear crane beam support the front and rear legs of a ship-to-shore crane. The caisson retains engineered fill which is used to reclaim the land behind the structure. The reclamation area is used for port operations and storage.

The caisson selected for this study was adopted as part of the quay front structure for a container terminal port in Singapore (Leung & Shen, 2008). It is applicable to this study for two reasons; it was designed to function as a container terminal quay and its size accommodates Post Panamax sized vessels and STS quay cranes. Only ten percent of the current global container vessel fleet are larger

than this size (WSC, 2015). In a case study published by Leung & Shen (2008) the dimensions and weight of the caisson were described in detail. Each caisson is 29.9 m long (along the quay wall line), 16 m wide (20 m wide at the base) and 19.15 m high (Figure 3.1). The caisson and capping beam retain approximately 22 m of fill and support a 30 m gauge ship-to-shore crane, which is typical for Post Panamax sized vessels (EAU, 2015).

3.2.2 Construction and operational loading

The construction of this type of marine superstructure typically occurs in a number of sequential stages (Davies & McIlquham, 2011). Table 3.1 and Figure 3.2 detail the construction stages considered in this study. Conservative estimates of time were calculated for the various stages after execution of the ground improvement works; the basis for these calculations is presented in annexure B.2.

Table 3.1 – Typical construction stages (adapted from Davies & McIlquham, 2011)

Stage	Description	Duration
1	Existing condition before construction commences.	-
2	Dredging to founding elevation.	-
3	Preparation of the foundation, including any ground improvement.	-
4	Caisson placement and filling.	40 days
5	Backfilling behind the caisson and vibrocompaction of the backfill.	80 days + 60 days
6	Construction of the capping beam, layer works and piled rear crane beam.	170 days
7	Operational conditions.	-

In addition to the loading arising from the ground during construction, the intrinsic loads imposed on a container terminal structure include environmental loads due to wind, waves, currents and tides; live loads due to berthing and mooring vessels; live loads due to cranes, traffic and container handling and stacking (EAU, 2015). The most unfavourable load combinations that could reasonably coexist for this type of structure were derived for a recent port expansion project and have been adopted in this study (ZAA, 2015); they are in line with those specified in similar projects (Davies & McIlquham, 2011). The load combinations used in this study are summarised in Table 3.2 and illustrated in Figure 3.3.The mooring load was based on a mooring analysis of a Post Panamax vessel (ZAA, 2015). The STS crane loads were based on an 80 tonne, 30 m gauge STS crane (ZAA, 2015). The operational surcharges were based on container handling and stacking up to four high (ZAA, 2015). A tidal lag of 1 m was selected (ZAA, 2015).

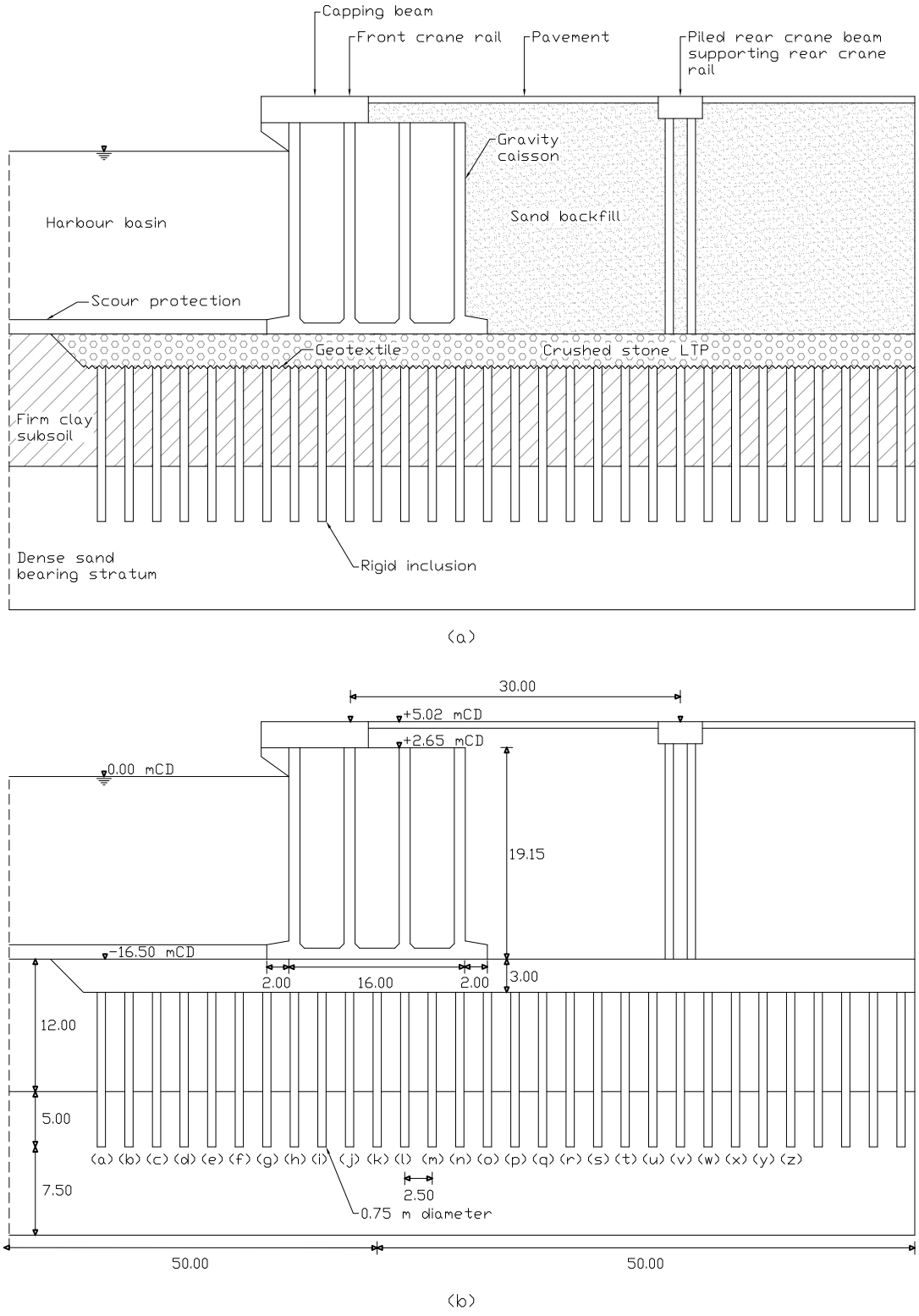

Figure 3.1 – Model description and dimensions (adapted from Leung & Shen, 2008)

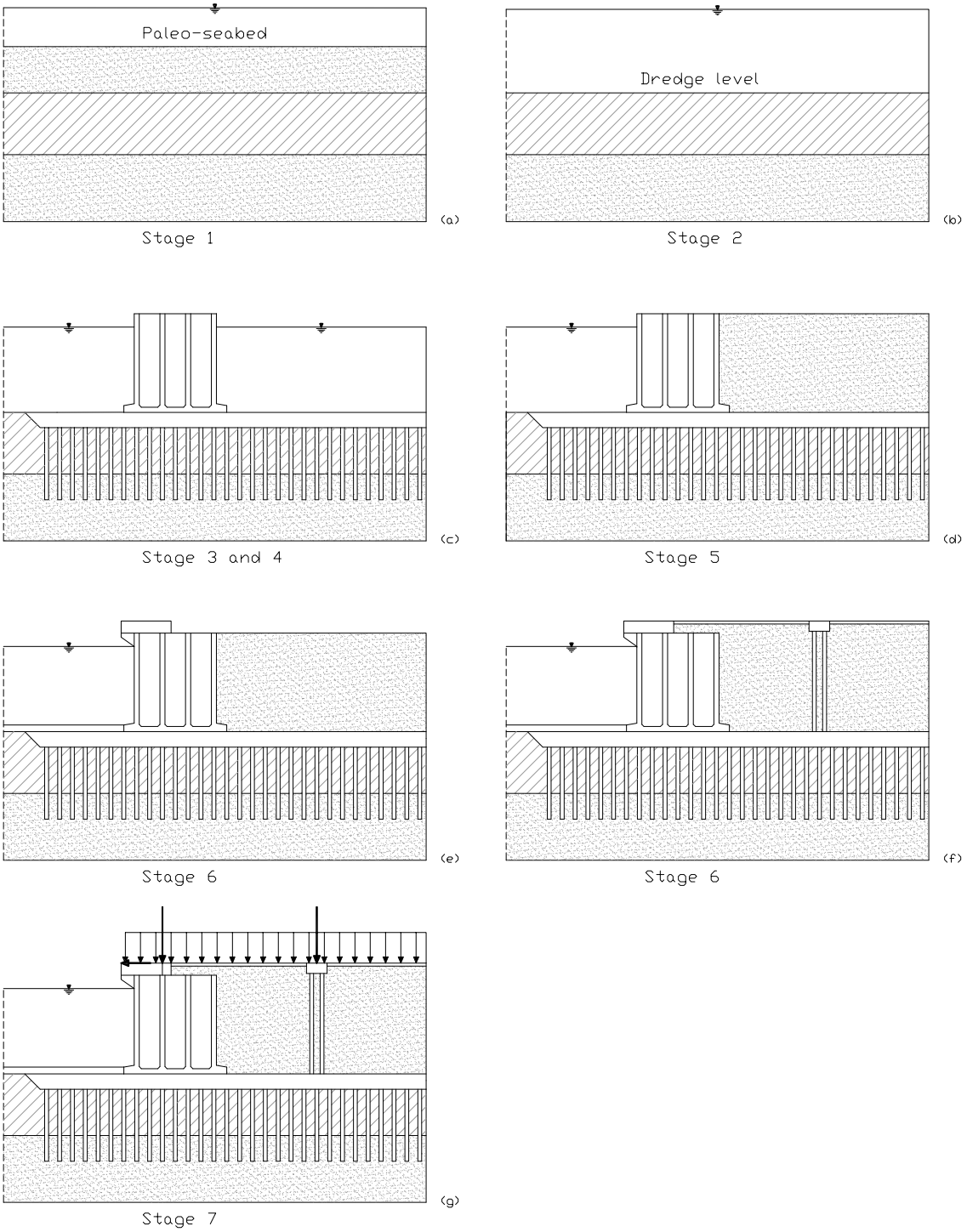

Figure 3.2 – Model construction stages

Table 3.2 – Characteristic transient load combinations

Description	**Transient load combinations (kN/m)**	
	Vertical	**Horizontal**
Front crane load and horizontal wind load	-746	-46
Rear crane load and horizontal wind load	-438	-46
Mooring load	-	-98
Operational surcharge between front and rear crane rail	-20	-
Operational surcharge behind rear crane rail	-40	-
Tidal lag of 1 meter	-	-
*negative is downwards and towards the basin		

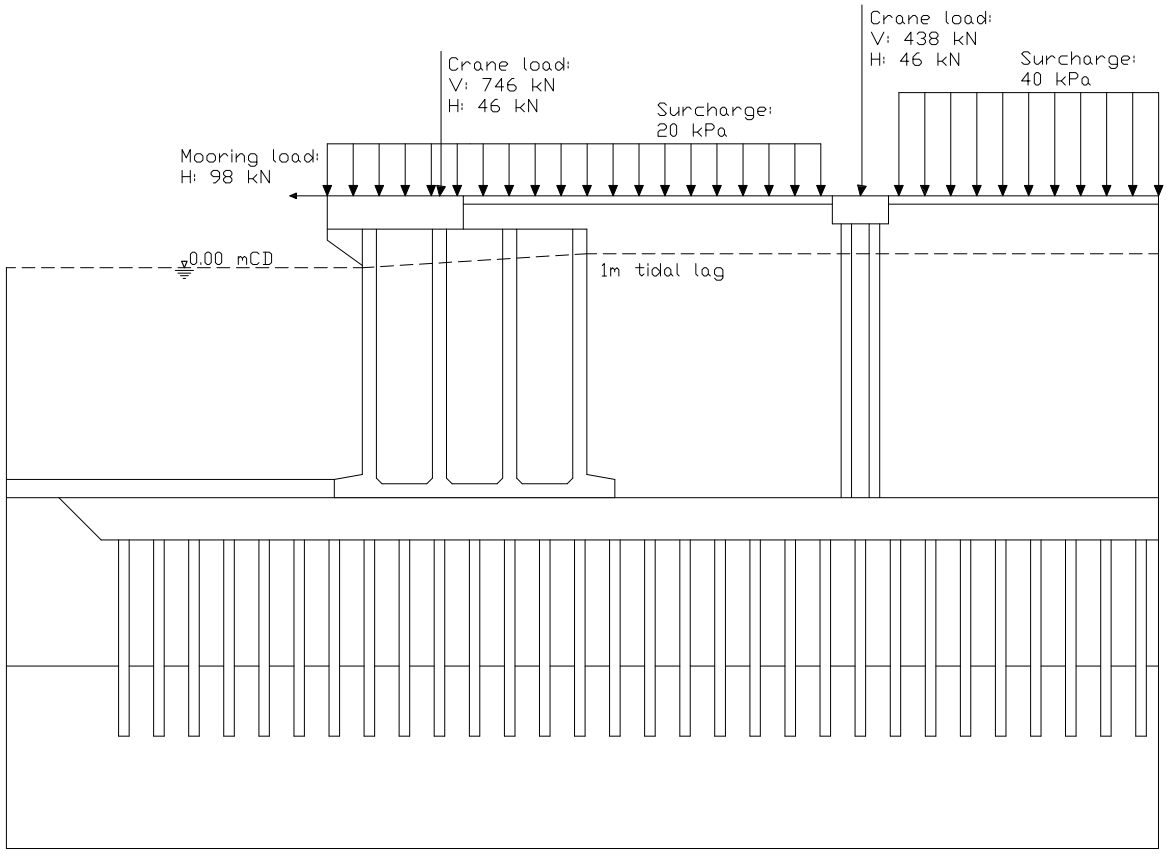

Figure 3.3 – Transient load combinations

3.3 Subsoil Condition

The hypothetical subsoil condition selected for this study comprises 12 m of soft to firm clay underlain by a stable bearing layer comprising dense sand (Figure 3.1). This ground profile has been selected for a number of reasons. Firstly, it is generally understood that soft to firm clay constitutes poor founding conditions due to its low shear strength, compressibility and time related deformation problems (Jones & Davies, 1985). Secondly, the locations of many ports coincide with rivers, deltas and estuaries which are associated with these poor soil conditions, which often require ground improvement (Hill, 2013). Lastly, in practice, the application of RI ground improvement remains economically competitive in soft to firm clays (ASIRI, 2012). The subsoil condition is defined as follows:

Soft to firm clay subsoil:

A saturated unit weight of 17.5 kN/m^3 was selected based on the recommendations in EAB (2008) for high plasticity soft clays. The over consolidation ratio (OCR) in the clay subsoil is 2.6 near its surface which reduces to 1.9 nears its base. Similarly, the lateral earth pressure coefficient (K_0) in the clay subsoil ranges from 1.0 to 0.75. These values have been selected to be consistent with lightly over-consolidated clay which typically has an OCR < 3 and K_0 between 0.5 and 1.0 (Bowles, 1996).

The undrained shear strength profile increases linearly with depth from 30 kPa to 60 kPa. This profile has been selected to be consistent with a soft to firm clay which is defined by an undrained shear range from 20 kPa to 70 kPa (Head, 1992).

The clay subsoil has a constrained modulus (M) of 5 MPa at a reference minor principle stress of 100 kPa. This modulus has been selected to be consistent with a firm clay which is typically characterised by constrained moduli in the range from 3.3 MPa to 10 MPa (Carter & Bentley, 2016).

The clay has a permeability of $4.5 \times 10^{-10} m/s$ which was selected to be consistent with typical values for clay, which range from $10^{-9} m/s$ to $10^{-11} m/s$ (Carter & Bentley, 2016).

Dense sand bearing layer:

Brinkgreve, Engin & Engin (2010) validated the material properties of clean quartz sand for a range of relative densities. The following properties corresponding to dense sand (RD of 80%) were used in this study: saturated unit weight of 20 kN/m^3; effective friction angle of 38°; constrained modulus of 48 MPa at a reference minor principal stress of 100 kPa. A dilation angle of 8° was specified ($\psi = \varphi' - \varphi'_{cv}$). The sand has a permeability of $7 \times 10^{-5} m/s$ which was selected to be consistent with typical values for clean sand, which range from $10^{-3} m/s$ to $10^{-5} m/s$ (Carter & Bentley, 2016).

3.4 Justification of the Ground Improvement Strategy

The following sections describe the development of the ground improvement strategy. Figure 3.4 illustrates the various phases that were followed in this process.

3.4.1 Requirement for ground improvement

In order to establish whether the foundation required ground improvement it was necessary to define what ground behaviour was required for this particular structural application. Firstly, the foundation was required to have sufficient resistance to failure (stability) and, secondly, deform within accepted limits under the imposed loads. Port engineers typically place stringent limits on the allowable total and differential deflections of the structure to ensure efficient port operations. For example, the operational deflection limit specified for the Post-Panamax quay crane used in Singapore was 30 mm (Leung & Shen, 2008). Therefore the foundation was first checked for sufficient resistance to failure and then acceptable movements under the imposed loads.

Preliminary assessment of stability:

The concept of bearing capacity relates to stability. An analytical bearing capacity model was used to provide a first order estimate of the adequacy of the foundation without ground improvement. The calculation is presented in annexure A.1. Under centric vertical loading during caisson placement and filling, the caisson exerted a uniform pressure on the foundation of approximately 220 kPa. During reclamation and backfilling a lateral earth pressure is imposed on the caisson (Figure 3.4a). This results in an inclined eccentric load on the foundation and a change in the vertical stress distribution with a maximum stress of 290 kPa at the toe and a minimum stress of 240 kPa at the heel. The calculated ultimate bearing resistance of the caisson under purely vertical loading was 169 kPa which reduced by 27% to 123 kPa under inclined eccentric loading. The calculated resistance is insufficient to prevent bearing failure and excessive deformation. Although there is uncertainty in predictions using analytical models, it is suggested they are still useful as a first step in the process of considering ground improvement. Based on this preliminary assessment it was concluded that either the ground needed to be strengthened and stiffened or the imposed load needed to be reduced; or a combination of these. Additionally, it was concluded that the inclined eccentric nature of the load significantly reduces the foundation resistance and in this regard a reduction in the lateral component of the loading is beneficial.

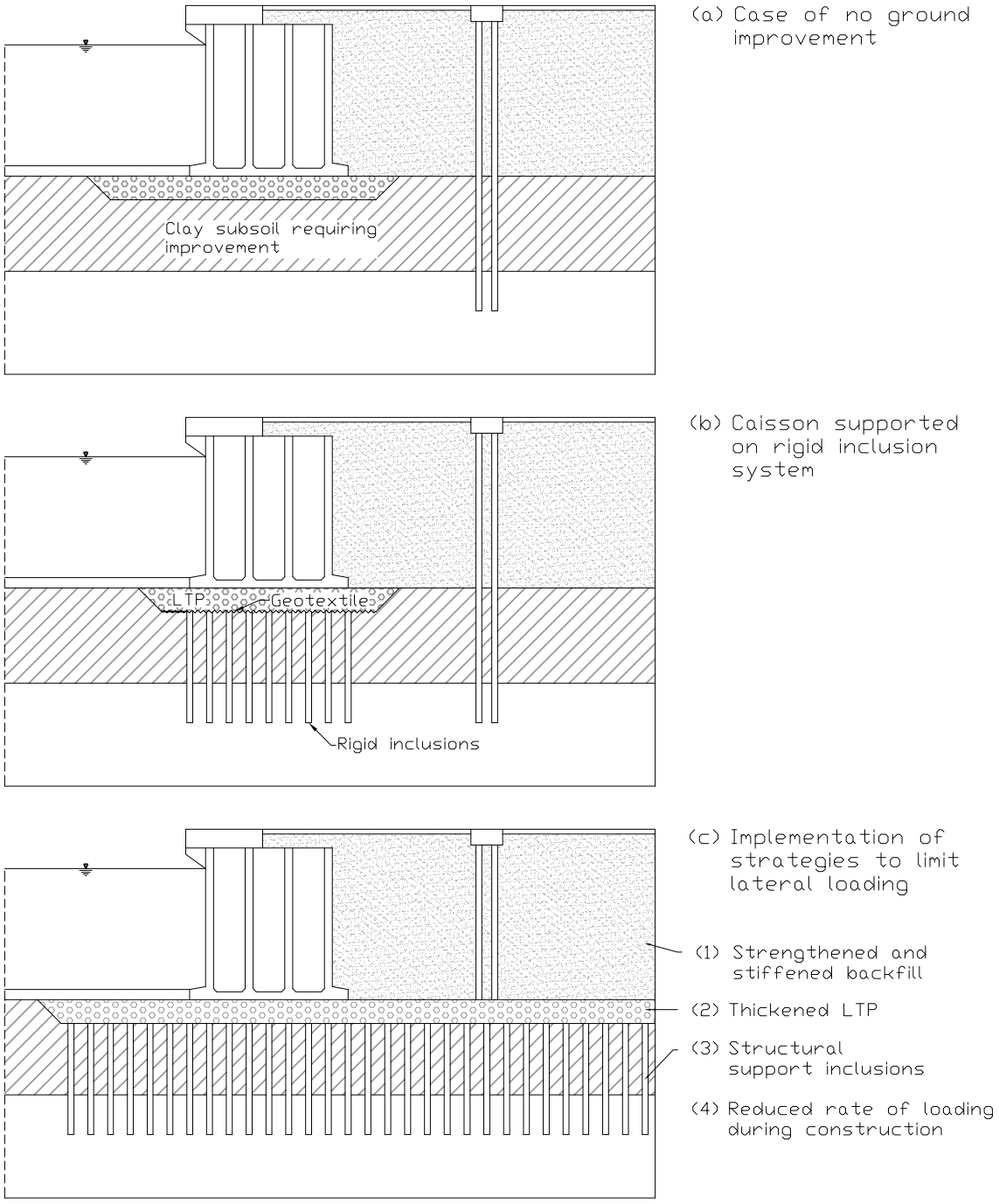

Figure 3.4 – Development of ground improvement strategy

3.4.2 Selection of a suitable ground improvement strategy

After establishing that ground improvement was required in terms of stability, an appropriate technique needed to be selected. The Strategic Highway Research Program 2 (SHRP2) developed a framework for determining the applicability of specific ground improvement technologies for specific applications. Table 3.3 details this procedure for the problem of a caisson quay wall constructed over unstable soil conditions. Ground reinforcement using inclusions was identified as the most suitable category of techniques. This included aggregate columns, continuous flight auger piles, deep mixing methods, sand compaction piles, and vibro-concrete columns. RI ground reinforcement installed by the vibro-concrete column (VCC) method was selected as a suitable technique for the following reasons:

- Well suited to saturated weak fine grained soils (ASIRI, 2012).
- Can be used offshore. A crawler crane of sufficient capacity is used to support the vibrator. A barge or pontoon is used as a working platform on which a crawler crane is mounted to support the assembly (Coghlan, Plomteux & Racinais, 2016).
- Capable of treatment depths in excess of 15 m below seabed level (Coghlan, Plomteux & Racinais, 2016).
- Increases the bearing resistance by reducing the forces causing failure and increasing the forces resisting failure.
- Reduces consolidation settlement by reducing the magnitude of load on the soil between the inclusions.
- High production rate in the marine environment (Menard, 2016b).
- Well suited to large areas requiring ground improvement (ASIRI, 2012).
- The method allows for an accelerated schedule for a number of reasons: the inherent strength and stiffness of the columns and high proportion of load directed to the columns; a preload is not typically required; the reduced load on the in situ soil means a reduced time to 90 % consolidation.
- The vibro-driven cast in situ soil displacement method produces very little spoil which is beneficial in terms of environmental considerations such as the impact of the disposal of spoil and water pollution (Menard, 2016b).

Table 3.3 – Selection of applicable ground improvement technique based on the SHRP2 framework

Techniques applicable to construction over unstable ground requiring ground improvement	Unstable soil condition: Saturated, weak, fine grained soils	Treatment depth below ground surface: Greater than 15 meters	Purpose of improvement: Increase bearing capacity	Purpose of improvement: Reduce consolidation settlement	Size of area to be improved: Greater than 4600 m2	Accelerated Schedule	Undrained shear strength of soil less than 30 kPa
Aggregate Columns	●	●	●	●	●	●	
Blast Densification							
Bulk-infill Grouting							
Compaction Grouting							
Continuous Flight Auger Piles	●	●	●	●	●	●	
Deep Dynamic Compaction							
Deep Mixing Methods	●	●	●	●	●	●	●
Excavation and Replacement	●	●	●	●	●	●	●
Geosynthetic Reinforcement	●	●	●				
Geotextile Encased Columns	●						
High-Energy Impact Rollers							
Jet Grouting	●	●	●	●			
Lightweight Fill	●	●					
Mass Mixing Methods	●						
Micropiles	●	●	●	●			
Prefabricated Vertical Drains and Preloading	●	●					
Rapid Impact Compaction							
Sand Compaction Piles	●	●	●	●	●	●	
Vacuum Preloading with Prefabricated Vertical Drains	●	●					
Vibrocompaction							
Vibro concrete columns	●	●	●	●	●	●	●

3.4.3 Description of the Proposed RI System

The overall system comprises the in situ soil reinforced with rigid columns and the load transfer platform which includes basal reinforcement (Figure 3.4b). The selection of the system geometry, extent of the reinforcement and material properties, are described below and were based on best practice as discussed in section 2.2 and 2.3 of the literature review.

Rigid Inclusions:

Rigid inclusions are defined by geometrical parameters such as their diameter, centre-to-centre spacing, grid pattern, length and extent. The RI diameter was selected as 750 mm which is a conservative estimate of the maximum diameter (800 mm) for the VCC method (Menard 2015, pers. comm., 31 March). The large diameter was chosen due to the nature of the load from the overlying structure (large, inclined and eccentric) and the requirement of the RIs to ensure stability. The spacing between inclusions was chosen to limit interference between fresh inclusions during installation. The centre-to-centre spacing was selected as 2.5 m, arranged in a square grid pattern, which is close to the minimum value (3 to 4 diameters) recommend by ASIRI (2012). The resulting area replacement ratio is 7%, which falls within the typical range for VCCs in similar applications such as high earth embankments (van Eekelen, Bezuijen & van Tol, 2013).

The length of the inclusions, and in particular the length of embedment into the bearing stratum, has a significant effect on the behaviour of the inclusion under lateral load. According to Poulos & Davis (1980), under lateral load the largest moment in the inclusion is generated when the soil strength is fully mobilised in the unstable and stable zone. Therefore, in order to mobilise the largest moment the RIs were embedded 5 m into the stable bearing layer.

Material properties for concrete are dependent on the concrete mix design and are categorised according to strength class. Due to the large inclined and eccentric load a relatively high strength class (C35/45) was selected for this study; the concrete is unreinforced. Table 3.4 details the material properties.

Table 3.4 – Material properties for concrete (Eurocode 2, part 1 (ENV 1992-1-1:1993))

Strength class	f_{ck}	f_{cm}	f_{cd}	f_{ctm}	$f_{ctk\ 0.05}$	$f_{ctk\ 0.95}$	E_{cm}	E_{cd}
(N/mm^2)								
C35/45	35	43	23.3	3.2	2.2	4.2	33500	22300
$f_{ck;\ cm;\ cd}$ = characteristic, mean, design compressive cylinder strength at 28 days; f_{ctm} = mean value of the axial tensile strength of concrete at 28 days; $f_{ctk\ 0.05}$ = lower characteristic axial tensile strength (5%-fractile) of concrete at 28 days; $f_{ctk\ 0.95}$ = upper characteristic axial tensile strength (95%-fractile) of concrete at 28 day; $E_{cm;\ cd}$ = mean, design value of the secant modulus of elasticity								

Load transfer platform:

The geometric and material parameters of the LTP were selected to ensure maximum arching efficiency and load transfer to the inclusion head. A 3 m LTP thickness was selected for this study; this is greater than the calculated critical height of 1.2 m which ensures maximum arching efficiency (BS 8006, 2010). A well graded gravel was chosen for the LTP due to its high shear strength characteristics (Nicks & Adams, 2013). A friction angle of 42° was selected based on a compacted relative density of 80% and considering large strain effects (Araei, Soroush & Rayhani, 2010; Nicks & Adams, 2013). The compacted gravel has a saturated unit weight of 21 kN/m^3 and constrained modulus of 100 MPa at a reference minor principal stress of 100 kPa (Araei, Soroush & Rayhani, 2010). A permeability of $7 \times 10^{-5} m/s$ was selected to be consistent with typical values for gravels, which range from $10^{-1} m/s$ to $10^{-5} m/s$ (Carter & Bentley, 2016).

Basal Reinforcement in the LTP:

RockGrid© PC 200/200 was selected for reinforcement of the LTP due to its high strength and modulus characteristics. Its material properties are presented Table 3.5 and deformation properties in Table 6.10 in annexure B.1.

Table 3.5 – Material properties for RockGrid© PC 200/200 composite geotextile (Kaytech, 2016)

Product:	RockGrid© PC 200/200: High strength composite geotextile			
Intended use	For reinforcement, separation and filtration, in construction of earthworks, foundations and retaining structures.			
Material	Polyester, stable fibre 150g/m2 needle punched nonwoven / high strength polyester yarns.			
Short term tensile strength (T_{MAX})	Machine direction (MD)	200	kN/m	BS EN 13251 EN ISO 10319
	Cross machine direction (CMD)	200	kN/m	
	Elongation (ε_{MAX})	10	%	
Creep limited strength (120 years)		120	kN/m	BS EN 13251 EN ISO 10319
Long term design strength at 120 years		105	kN/m	EN ISO 10319
Water permeability	Normal to plane	150	l/m^2s	BS EN 13251 EN ISO 11058

3.4.4 The effects of lateral ground movements

A preliminary analytical assessment was undertaken to determine the effects of lateral ground movement due to backfilling behind the caisson (Figure 3.4b). Estimates of the magnitude of ground movement, inclusion bending moment and inclusion head defection, were calculated using the methods presented in Table 2.5 and Table 2.6 in section 2.2.8. The calculations are presented in annexure A.2 and A.3.

The empirical method by Bourges & Mieussens (1979) indicated a maximum immediate undrained horizontal ground movement at the caisson toe of 333 mm. The relatively large movement is due to the low shear resistance of the clay under the imposed load (i.e. F_s approaches 1). The empirical data presented in Figure 6.1 in annexure A.2 suggests that the magnitude of lateral movement is significantly reduced when the factor of safety on undrained strength is greater than 2.0. For an embankment load corresponding to $F = 2$ $(84\ kPa)$ the horizontal ground movement reduced to 45 mm.

For a free head condition, the empirical design charts by Stewart et al. (1994) provided an estimate of the maximum inclusion bending moment of $2104\ kN.m$. The corresponding maximum inclusion head deflection was 291 mm. Similarly to Bourges & Mieussens (1979), the large moments and deflections relate to post-threshold load levels, which correspond to low factors of safety on the undrained shear strength of the clay subsoil. For a pre-threshold load level equal to three times the undrained shear strength (99 kPa) the maximum estimated bending moment reduced to $406\ kN.m$ with a corresponding maximum head deflection of 32 mm.

These empirical estimations indicated that the foundation defection tolerances and limiting bending moments were likely to be exceeded for the GI strategy presented in Figure 3.4b. It was concluded from these results that there was likely to be a requirement to adopt strategies to limit or accommodate lateral loading. The most suitable strategies are presented in the next section. There is considerable uncertainty in the accuracy of these preliminary results as the behaviour of the ground and RIs may follow different tends to those indicated by the authors for this structural application. In this regard a more detailed assessment was required to confirm these findings. The basis for a finite element analysis of the problem is presented in Chapter 4.

3.4.5 Strategies to limit lateral loading

The following sections describe the implementation of the various strategies for limiting lateral loading recommended in section 2.3.6.

3.4.5.1 Construction methods to modify the backfill load

Densifying granular backfill is a well-established strategy for modifying the backfill load in marine projects, and was therefore selected for this study (Hamidi et al., 2013). The vibro-compaction technique was chosen as the most suitable technique due to its treatment depth in excess of 15 m. This strategy only modifies the lateral component of the load acting on the back of the caisson. The aim of this strategy was to reduce the outward shear stress applied to the subsoil along the base of the caisson due to the lateral earth pressure on the back of the caisson. Rankine theory relates the lateral earth pressure in the active condition to the effective angle of friction of the backfill; therefore this is a controlling parameter in terms of the performance of this strategy.

Hydraulically placed backfill material is typically in a loose state prior to vibro-compaction, with a relative density in the range 20% to 40% (van ‘t Hoff & van der Kolff, 2013). Brinkgreve, Engin & Engin (2010) validated the material properties of clean quartz sand for a range of relative densities. The following properties corresponding to loose sand (RD of 25%) were conservatively used in this study: saturated unit weight of 19.4 kN/m^3; effective friction angle of 31°; constrained modulus of 15 MPa. The sand has a permeability of $7 \times 10^{-5} m/s$ which was selected to be consistent with typical values for clean sand, which range from $10^{-3} m/s$ to $10^{-5} m/s$ (Carter & Bentley, 2016).

Vibro-compaction is capable of densifying clean sands to relative densities in excess of 80% (Han, 2015). Properties corresponding to very dense sand (RD of 80% to 100%) were used in this study: saturated unit weight of 20.5 kN/m^3; effective friction angle of 40° which is within the typical range (37° to 43°) for a relative density of 80% (Brinkgreve, Engin & Engin, 2010; Carter & Bentley,

2016); constrained modulus of 100 MPa at a minor principal stress of 100 kPa. The sand has a permeability of $7 \times 10^{-5} m/s$ which was selected to be consistent with typical values for clean sand, which range from $10^{-3} m/s$ to $10^{-5} m/s$ (Carter & Bentley, 2016).

Execution of ground improvement works is generally understood to be more economical overland. The vibro-compacted properties were therefore implemented in the model once the backfill reached an elevation of 2.65 m CD, allowing execution in the dry Figure 3.2d.

3.4.5.2 Construction methods to provide additional structural support to the backfill

For the case of a piled bridge abutment Reid & Buchanan (1984) proposed supporting the backfill on piles, in what is termed structural embankment support piling. For this study, RIs were used to support the caisson backfill reducing the vertical load on the clay subsoil. Figure 3.4c shows overall system comprising the in situ soil reinforced with RIs and the load transfer platform with basal reinforcement extended behind the caisson. The reinforcement mechanics for both structural elements are discussed in section 2.2.6 and are not covered in any detail here. The system geometry and material properties are described in section 3.4.3.

3.4.5.3 Construction methods to improve the subsoil

Ground improvement methods can be used to increase the strength and stiffness of the subsoil prior to or during construction. Controlling the rate of loading during the various construction stages was selected as the most suitable non-intrusive method. A reduced rate of loading allows the clay sub-soil to consolidate, strengthen and stiffen. However, a significant benefit of the rigid inclusion system is the removal of any restriction on the rate of loading behind the caisson. Therefore the rate of loading used in this study was selected as the typical duration for the various construction activities described in section 3.2.2. Conservative estimates of time were calculated for the various stages after execution of the ground improvement works; the basis for these calculations is presented in annexure B.2.

Of the various intrusive methods, reinforcement and excavation and replacement were considered the most suitable techniques for improving the ground, while keeping the system economically competitive. In order to improve the strength and stiffness of the clay subsoil the overall system was extended ahead of the caisson toe (Figure 3.4c). Two of the main disadvantages of excavation and replacement are the disposal of the excavated material and the cost of the replacement material. For these reasons a maximum LTP thickness of 3 m was selected for this study.

Chapter 4 Finite Element Modelling

4.1 Modelling Approach

4.1.1 Description of the numerical model

Finite element analysis was performed with PLAXIS 3D 2016 version 2016.0. This section provides a description of the numerical model (Figure 4.1).

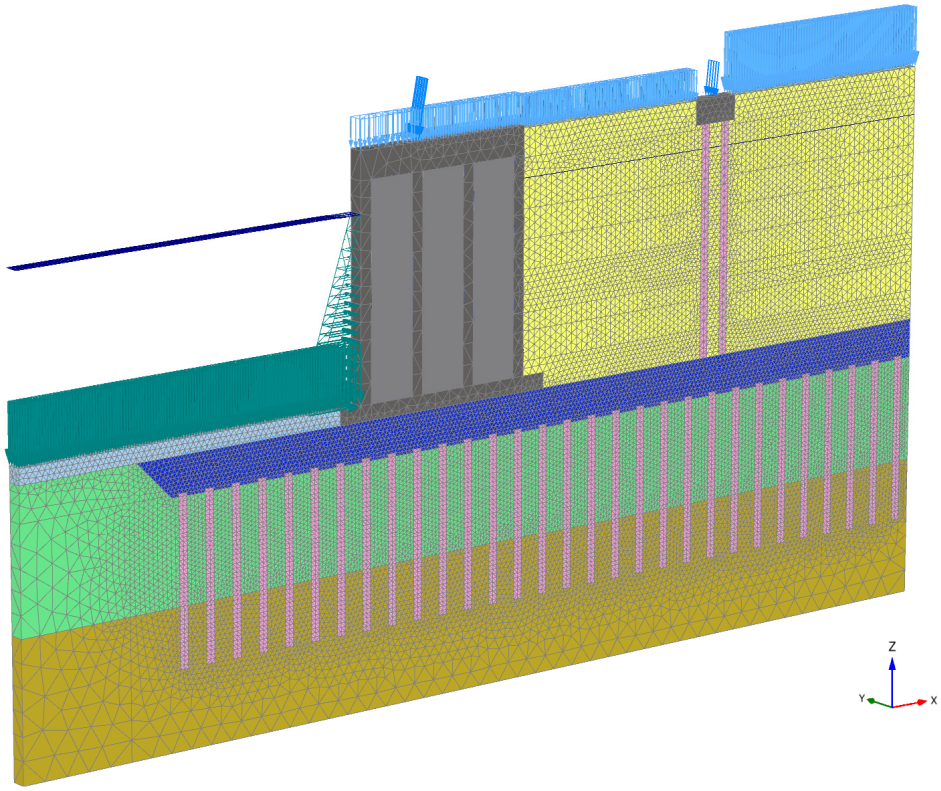

Figure 4.1 – 3D finite element model of the problem (Dimensioned in Figure 3.1)

4.1.1.1 Geometric idealization and model geometry

Three-dimensional finite element analysis was chosen to accurately model the problem. The vertical plane of symmetry perpendicular to the long axis of the quay wall means that only half a unit cell (1.25 m) needed to be discretised into finite elements to fully represent the problem. This defined the width of the 3D model in the out of plane direction (Figure 4.2b). The finite element model geometry is presented in Figure 3.1.

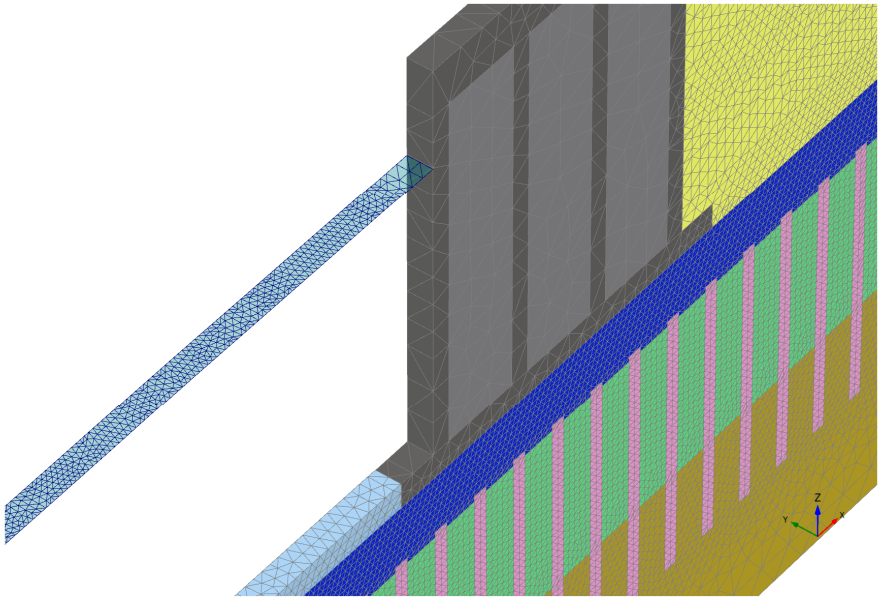

(a)

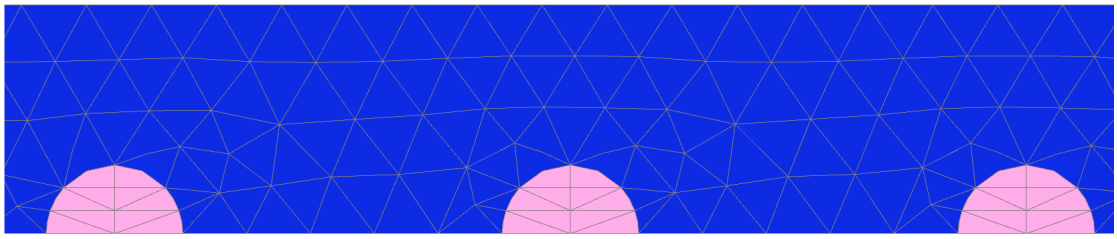

(b)

Figure 4.2 – 3D model width defined by half a unit cell (1.25 m)

4.1.1.2 Constitutive models for soils and structural elements

The various constitutive models used to describe the behaviour of clay, the LTP and the rigid inclusion elements have been summarised in section 2.2.9. For this particular problem a second order model such as a double hardening model was required to accurately describe the behaviour of the clays and LTP. The Hardening Soil Model with Small Strain Stiffness (HS-Small) was selected to model the in situ clays and sands, the LTP and the engineered fill. Additionally a constitutive model

with material-specific failure criterion was required to model the rigid inclusions. In this regard, in addition to modelling the RIs with a linear elastic model, an elastic plastic Mohr-Coulomb model was used.

Hardening Soil model with Small Strain Stiffness (HS-Small):

In addition to general soil parameters defining the weight and flow properties of soil, the Hardening Soil Model requires a total of 11 input parameters and a further two parameters for the small strain overlay. The basic strength and stiffness parameters and advanced parameters for the HS-Small Model are summarised in Table 4.1.

Table 4.1 – Input parameters for the HS-Small Model

Parameter	Description
φ'	Internal friction angle
c'	Cohesion
R_f	Failure ratio
ψ	Dilatancy
E_{50}^{ref}	Reference tangent stiffness from drained triaxial test
E_{oed}^{ref}	Reference tangent stiffness for oedometer primary loading
E_{ur}^{ref}	Reference unloading / reloading modulus
m	Exponential power
v_{ur}	Unloading / reloading Poisson's ratio
P_{ref}	Reference pressure (Minor principal stress)
K_0^{nc}	Coefficient of earth pressure at resr (NC state)
G_{max}^{ref}	Reference small strain shear modulus
$\gamma_{0.7}$	Shear strain amplitude at $0.7G_{max}$

HS-Small model parameters for soft to firm clay:

Table 4.2 provides the basis for the HS-Small model parameters selected for the soft to firm clay subsoil. The values used in this study are presented in Table 6.5 in annexure B.1.

Table 4.2 – HS-Small model parameters for firm clay

Parameter	Unit	Comment
γ_{unsat}	kN/m^3	Refer to section 3.3
γ_{sat}	kN/m^3	Refer to section 3.3
e_{imt}	-	Stiff clay = 0.6; soft clay = 1.9 (Terzaghi, Peck & Mesri, 1996)
$k_{x,y}$	m/day	Refer to section 3.3-
φ'	°	$\varphi' = 29°$ (Surarak et al., 2012a) S_u is a model output; S_u increases linearly with depth (30 kPa to 60 kPa)
c'	kPa	$c' = 0$ (Surarak et al., 2012a)
R_f	-	Failure ratios for various soils range from 0.75 to 1.0 (Lees, 2012)
ψ	°	-
E_{50}^{ref}	kPa	$E_{50}^{ref} \approx E_{oed}^{ref}$ (Benz, 2007)
E_{oed}^{ref}	kPa	$E_{oed}^{ref} \approx M^{ref}$ Refer to section 3.3
E_{ur}^{ref}	kPa	$E_{ur}^{ref}/E_{50}^{ref} \approx 3$ (Benz, 2007)
m	-	Exponential power (m) is close to unity for clay (Benz, 2007)
v_{ur}	-	0.2 for clays (Lees, 2012)
P_{ref}	kPa	Minor reference principal stress
K_0^{nc}	-	$K_0^{nc} = 1 - \sin\varphi'$; Jaky's equation (Lees, 2012)
POP	kPa	Pre-overburden pressure
G_0^{ref}	kPa	Soft to firm clays = 46000 kPa (Benz, 2007)
$\gamma_{0.7}$	-	Soft to firm clays = 0.00024 (Benz, 2007)

Sands and gravels (HS-Small):

Table 4.3 provides the basis for the HS-Small model parameters selected for the granular materials. The values used in this study are presented in Table 6.5 to Table 6.8 in annexure B.1.

Table 4.3 – HS-Small model parameters for sands and gravels

Parameter	Unit	Comment
γ_{unsat}	kN/m^3	Refer to section 3.3 and section 3.4.5
γ_{sat}	kN/m^3	Refer to section 3.3 and section 3.4.5
$e_{min;max;in}$	-	$e_{min} = 0.51;\ e_{max} = 0.85$ (Terzaghi, Peck & Mesri, 1996)
$k_{x,y}$	m/day	Refer to section 3.3 and section 3.4.5
φ'	°	Refer to section 3.3 and section 3.4.5
c'	kPa	Refer to section 3.3 and section 3.4.5
R_f	-	Failure ratios for various soils range from 0.75 to 1.0 (Lees, 2012)
ψ	°	$\psi = \varphi' - \varphi'_{cv}$ (Bolton, 1986); $\varphi'_{cv} = 30°$ (Brinkgreve, Engin & Engin, 2010).
E_{50}^{ref}	kPa	$E_{50}^{ref} \approx E_{oed}^{ref}$ (Benz, 2007)
E_{oed}^{ref}	kPa	$E_{oed}^{ref} \approx M^{ref}$ Refer to section 3.3
E_{ur}^{ref}	kPa	$E_{ur}^{ref} / E_{50}^{ref} \approx 3$ (Benz, 2007)
m	-	Exponential power (m) is close to 0.5 for sand (Benz, 2007)
v_{ur}	-	0.25 for loose sands and 0.2 for dense sands (Lees, 2012)
P_{ref}	kPa	Minor reference principal stress
K_0^{nc}	-	$K_0^{nc} = 1 - \sin\varphi'$; Jaky's equation (Lees, 2012)
POP	kPa	Pre-overburden pressure
G_0^{ref}	kPa	Correlated with RD (Brinkgreve, Engin & Engin, 2010)
$\gamma_{0.7}$	-	Correlated with RD (Brinkgreve, Engin & Engin, 2010)

Rigid Inclusions (LE and MC):

The behaviour of the concrete RIs was described using two different constitutive models. A simple linear elastic model was used to estimate the maximum structural forces in the RIs. In order to capture accurately the behaviour of the RIs up to failure, a Mohr-Coulomb model was used in a subsequent analysis. Concrete strength class C35/45 was used in this study. The mean design value of the secant modulus of elasticity $(E_{cm;\,cd})$ was used for both models.

A Mohr-Coulomb model with a tension cut-off was implemented. The tension cut-off was conservatively set as the lower characteristic axial tensile strength, $f_{ctk\,0.05}$. A friction angle of 35° and cohesion of 585 kPa was derived according to (Dusko, 2009). The state, strength and deformation properties are summarised in Table 6.2 and Table 6.3 in annexure B.1.

4.1.1.3 Modelling structures and interfaces

The rigid inclusions were modelled with volume elements (continuum elements) in order to accurately capture the load transfer mechanisms at the head and along the shaft, as well as the structural behaviour up to failure. A soft beam element was placed through the centre of the volume element to facilitate the extraction of inclusion forces and moments. Figure 4.3 shows the 0.75 m diameter, 14 m long volume elements. As discussed in Section 4.1.1.1 only half the RI is modelled due to the symmetry conditions of the problem.

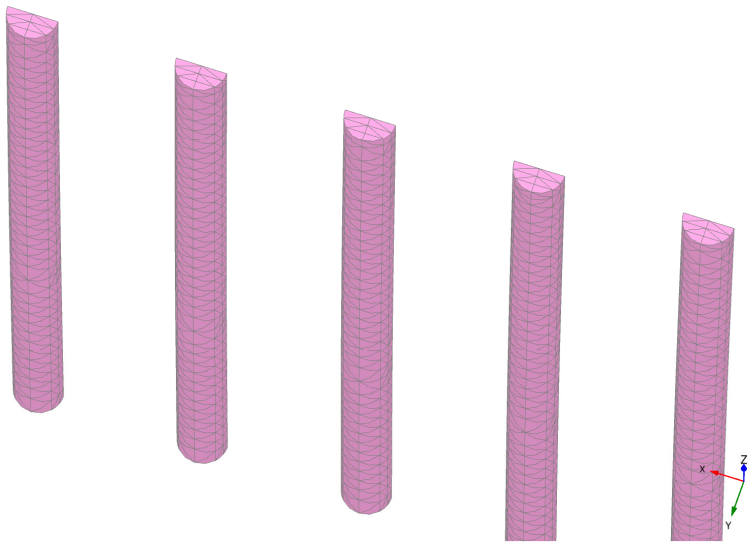

Figure 4.3 – RIs modelled using 3D volume elements

The interface behaviour was described by the Mohr-Coulomb model which is defined by five input parameters, c_{in}, φ_{in}, ψ_{in}, v_{in} and E_{in}. The interface properties use the properties of the surrounding soil, with the so-called interface strength reduction factor parameter R_{inter}. This accounts for the reduced strength observed at the soil-structure boundary. For RIs installed by displacement methods, R_{inter} was selected as 0.9 and for all other interfaces R_{inter} is 0.67 (BS 8004, 2015).

4.1.1.4 Conditions at model boundary

The model boundaries were chosen so as not to have an effect on the model results. The standard fixities applied at the model boundaries were zero displacement in all directions at the bottom boundary and zero displacement on the vertical sides in the horizontal direction perpendicular to those boundaries, including on axes of symmetry (Potts 2002). This implies that normal stresses were allowed but no shear stresses. The top surface had no fixities. The depth of the bottom boundary relative to the base of the inclusions was chosen so as not to influence the group effect of the inclusions which results in settlements in the bearing stratum. The hydraulic boundary conditions at all vertical model boundaries were set to zero dissipation of excess pore pressures. This is realistic as the shortest flow path from the centre of the clay layer is vertical to the underlying or overlying granular layers.

4.1.1.5 Initial conditions

The initial stress conditions were generated according to the K_0 procedure. This is acceptable due to the horizontal soil layering and water levels.

For the firm clay subsoil condition the initial stress state was described using a pre-overburden pressure (POP) which is an alternative way of describing the over-consolidation ratio. The pre-overburden pressure is defined as (Brinkgreve, Kumarswamy & Swolfs, 2016):

$$POP = \left|\sigma_p - \sigma'_{v0}\right| \tag{4.1}$$

Where, σ_p is the greatest effective vertical stress previously reached and σ'_{v0} is the in situ effective vertical stress. A POP of 100 kPa was selected for the soft to firm clay which corresponds to a paleo seabed 10 m higher than the current seabed (Figure 3.2a).

4.1.1.6 Loading conditions

The load combinations used in this study are presented in Table 3.2 and are typical of a 30 m gauge STS cane servicing Post Panama size vessels (ZAA, 2015). The transient load conditions were used for stability analyses and deformation analyses.

4.1.1.7 Mesh

The basic soil elements of the 3D finite element mesh are 10-node tetrahedral elements. Sufficiently small elements were required due to the large stress concentrations and zones of rapid stress (including pore pressure) and strain change. Additionally, in order to accurately predict the collapse load a sufficiently fine mesh was required. Meshing analyses were carried out to determine the appropriate mesh coarseness. The resulting model consisted of approximately 300000 elements with an average element size of approximately 0.3 m. The global mesh density and local refinement near the inclusions are shown in Figure 4.2b and Figure 4.4. The influence of geometry changes in the mesh due to large deformations were accounted for using an Updated Lagrangian formulation approach (Updated mesh). This also accounted for the change in stiffness in the GR during deformation.

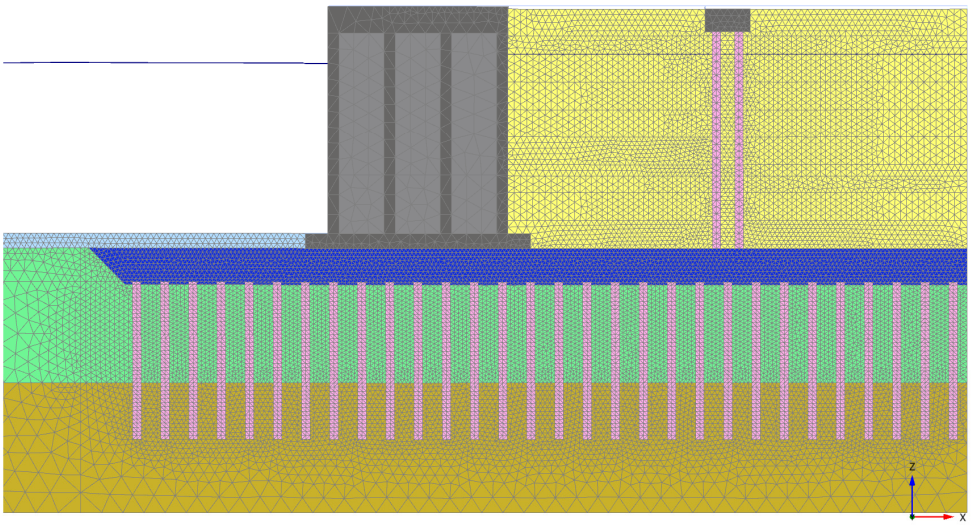

Figure 4.4 – Global mesh density; average element length approximately 0.3 m

4.1.1.8 Simulating the construction process and operational conditions

The finite element calculation was divided into several sequential calculation phases. The calculation phases correspond to particular construction or loading stages (Figure 3.2). Conservative estimates of time were calculated for the various stages after caisson placement; the basis for these calculations is presented in annexure B.2. Details of the model phases are presented in Table 4.4 and are discussed in more detail in annexure B.2.

Table 4.4 – Model calculation phases

Stage	Phase description	Construction duration
1	Phase 0: Initial conditions	-
2	Phase 1: Dredge to foundation trench elevation	-
3	Phase 2: Installation of rigid inclusions system	-
4	Phase 3 to 5: Caisson placement and filling with sand	40 days
5	Phase 6 to 13: Hydraulically place sand behind caisson	80 days
	Phase 14: Tidal lag	-
	Phase 15: Vibro-compact backfill	60 days
6	Phase 16: Construct capping beam, service tunnel and quay furniture etc	50 days
	Phase 17: Construct piled rear crane beam and concrete pavement	120 days
	Phase 18 to 19: Unload tidal lag and plastic nil step	-
7	Phase 20to 26: Activate operational transient loads including crane load, bollard load, surcharge load, tidal lag	-
	Phase 27 to 28: Dissipation of excess pore water pressure	100 % consolidation

4.1.1.9 Modelling undrained and time dependent behaviour

The clay subsoil has a low permeability which means during loading very little water movement takes place, resulting in the build-up of excess pore pressures. This behaviour was modelled using an undrained effective stress analysis, the so called “Method A”. The development and dissipation of excess pore pressure with time and the effects of consolidation were simulated using a consolidation analysis.

Undrained Method A:

A bulk modulus for water is added to the stiffness of the soil. Excess pore water pressure is generated due to the small volumetric strain occurring during plastic calculations and the low compressibility of the pore water. Estimations of excess pore pressure are reasonable when an advanced constitutive model such as the HS-Small model is used in conjunction with this method. Effective stiffness and strength parameters are model inputs. Undrained shear strength is an output of the constitutive model.

Consolidation analysis:

Consolidation analyses were performed using "Method A" which allows for the strength to be updated automatically due to the effects of consolidation. The dissipation of pore pressure depends on the soils permeability and the hydraulic boundary conditions.

4.1.1.10 Stability analysis by strength reduction

Global stability was assessed using the "shear strength reduction technique" which has been validated by various authors (Brinkgreve & Bakker, 1991; Dawson, Roth & Drescher, 1999; Griffiths & Lane, 2001; Tschuchnigg et al., 2015). The resulting factor of safety is the ratio of the soil's actual shear strength to that of the reduced strength at failure (Dawson, Roth & Drescher, 1999). This technique has the significant advantage over other methods of stability analysis because the critical failure surface is found automatically.

In the shear strength reduction technique the strength parameters $tan\,\varphi'$ and c' of the soil are successively reduced until failure occurs. The strength of the interfaces is reduced in the same way. The HS-Small Model behaves as a standard Mohr-Coulomb model during this type of stability analysis, since stress-dependant stiffness behaviour and hardening effects are excluded.

4.1.2 Validation of the numerical model

4.1.2.1 Validation of soil parameters

In order to determine whether the constitutive models and their parameters accurately describe real soil behaviour, appropriate validation was required. One method of validation is to use the FE method to simulate common laboratory tests. The constitutive model and model parameters can be checked to ensure that the simulated soil behaviour is representative of measured laboratory test data.

Surarak et al. (2012) analysed a comprehensive set of experimental data on Bangkok clays in order to determine the stiffness and strength parameters for the Hardening Soil Model. Parameters for soft and

stiff Bangkok clays were numerically validated by simulating drained and undrained triaxial tests and calibrating the models using laboratory triaxial data (CIDC & CIUC).

These validated HSM parameters for Bangkok soft and stiff clays were evaluated in this study. The HSM model was updated to an HS-Small model by deriving two additional parameters for the small strain overlay. This updated model was validated by simulating undrained traixal tests and comparing the results with the laboratory data published by Surarak et al. (2012). A hypothetical firm clay dataset was derived which is the average of the strength and stiffness parameters derived for the soft and stiff clays. The validation results are presented in annexure B.3.1.

4.1.2.2 Validation of initial conditions

Initial state parameters such as the in situ stress ratio ($K_{0\,nc}$) and pre-overburden stress (POP), were used to setup the initial stress state, stress history and undrained shear strength profile. Model outputs in the initial conditions phase, such as the stress ratio (K_0) and undrained shear strength profile, were checked to ensure that they were appropriate for a lightly overconsolidated soft to firm clay i.e. OCR < 3.0 and undrained shear strength profile in the range of 20 kPa to 70 kPa. The validation results are presented in annexure B.3.2.

4.1.2.3 Validation of mesh

Mesh tests were carried out to ensure the coarseness of the mesh did not affect the accuracy of the model results. In addition to the accuracy of the mesh, the element quality was checked. Element quality is defined as the radius of the maximum inner circle of the soil element divided by the radius of the maximum outer circle, where an ideal tetrahedral element is normalised at 1.0. The minimum element quality was set as 0.1.

4.1.2.4 Validation of load transfer mechanisms

The global load deflection behaviour of an inclusion under the centre of the caisson was evaluated using the analytical models presented section 2.2.8, as implemented in the commercially available software FOXTA V3. Only vertical loading during caisson placement and filling was considered. The analytical model results were compared with numerical simulation results. The validation results are presented in annexure B.3.3.

4.1.3 Reference Models

The modelling approach for this study corresponded with the three phases in the development of the ground improvement strategy, as illustrated in Figure 3.4.

4.1.3.1 Reference case without ground reinforcement

This model (FE Model 1) established three important foundation performance criteria without ground reinforcement (Figure 3.4a):

- The mode of failure and the collapse load.
- Whether the inclusions were required for stability or purely as settlement reducing elements.
- The virgin settlement and lateral deflection without reinforcement.

The terminology used by ASIRI (2012) was adopted for this study: The foundation was classified as either “Domain 1” where the inclusions are required for stability, or “Domain 2” where the inclusions are used to reduce settlements and not required for stability.

The magnitude of virgin settlement and lateral deflection were used to quantify the settlement and lateral deflection efficiency of the ground improvement strategy (section 2.2.4).

4.1.3.2 Caisson supported by RI ground reinforcement

An analytical assessment of this case (Figure 3.4b) is presented in section 3.4. The calculations predicted excessive lateral ground movement and high inclusion bending moments. This behaviour was confirmed with this model (FE Model 2) and the requirement for strategies to limit lateral loading were justified.

4.1.3.3 Implementation of strategies for limiting lateral loading

In the final model (FE model 3), the various strategies to limit lateral loading were implemented in combination (Figure 3.4c). There were two iterations of this model which used different constitutive models for the RIs. A linear elastic material model was used in the first iteration (FE model 3-1). This allowed the maximum RI forces and moments to be generated. The second iteration (FE model 3-2) evaluated the mode of failure using an RI constitutive model with material specific failure criterion. This model captured the progressive failure of the RIs and the associated deformation. Both models were used to evaluate the performance of the proposed GI scheme in accordance with the performance requirements described in the following section.

4.2 Performance Requirements

4.2.1 Performance requirements in terms of stability

In terms of stability, it was verified that the foundation and structural elements did not fail; importantly the RIs are considered as structural elements and not purely settlement reducing elements. An external geotechnical stability check was carried out to verify that there was sufficient resistance to failure or excessive deformation of the ground. This is relevant to the proposed ground improvement strategy where the strength of the ground is significant in providing resistance. External stability was assessed using the "shear strength reduction technique". According to ASIRI (2012) for this structural application, a factor of safety of 1.25 is required on strength parameters $tan\ \varphi'$ and c'; a factor of 1.5 is applied to the unfavourable variable external actions (Table 3.2). The critical mode of failure was determined automatically. The model output at a factor of safety of 1.25 was used to verify the internal structural integrity of the RIs.

Internal structural integrity of the RIs was assessed according to the following recommendations from the ASIRI (2012) guidelines:

- "Where inclusions are required to guarantee stability (Domain 1), the inclusions must be reinforced over the length where they are not fully compressed".
- "Where inclusions are not required to guarantee stability (Domain 2), it is proposed not to reinforce the inclusions, provided the maximum tensile force in the concrete can be justified".

4.2.2 Performance requirements in terms of crane rail deflection tolerances

In terms of deflections it was verified that the foundation and superstructure deform within accepted limits. The critical settlement and deflection criteria for a container terminal structure relate to the STS crane rail tolerances. Table 4.5 details the various tolerance checks that were carried out in this study. A vertical and horizontal differential deflection limit of 30 mm was adopted for this study which is in line with industry practice (Leung & Shen, 2008).

Table 4.5 – STS crane rail tolerances for 30.480 m gauge

Tolerance Check	Description of tolerance check	Type
1 – Track gauge or span	The actual value of the span may not vary by more than ± 30 mm.	Horizontal
2 – Crane rail alignment	The overall alignment must not differ by more than ± 30 mm from the true length of rail.	Horizontal
3 – Crane rail level	The crane rail level (allowable undulation) must not vary by more than ± 30 mm over the total length of rail.	Vertical
4 – Relative crane rail heights	The deviation from specified heights between seaside and landside rails must not exceed ± 30.	Vertical

Chapter 5 Results

5.1 Numerical Modelling Results

The following sections present the numerical modelling results. The validation results are presented in annexure B.3.

5.1.1 FE Model 1: Reference case without ground reinforcement

The reference case of a caisson founded on firm clay without ground reinforcement is illustrated in Figure 3.4a. The load-deflection behaviour of the caisson during placement and filling is shown in Figure 5.1 and Figure 5.2. As the pressure under the base increased, there was a corresponding linear increase in caisson settlement. With increasing pressure, the ultimate bearing capacity q_u was reached at approximately 146 kPa. This resulted in a sudden increase in settlement immediately after reaching q_u, indicating collapse. Total deformations of up to 960 mm were observed at failure. The load-deflection curve is characteristic of both general shear failure and local shear failure with a well-defined yield point, yet no distinctive peak in the load displacement curve. This is most likely due to the two layered profile, with a strong granular trench overlying a weak cohesive layer. Figure 5.3 and Figure 5.4 show the failure surface extending to the ground surface and Figure 5.1 highlights the heave at ground level on either side of the caisson. Both of these features are characteristic of general shear failure.

The following was concluded from the results of FE Model 1:

- The caisson fails by general shear at an ultimate bearing pressure of approximately146 kPa.
- The RIs are required to ensure stability and the problem was classified as “Domain 1” according to ASIRI (2012).
- The virgin settlement without ground reinforcement is in excess of 600 mm.

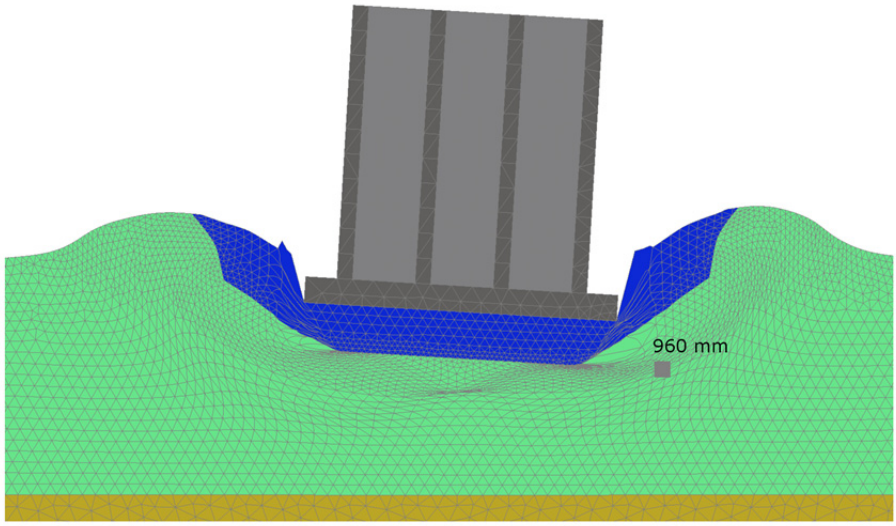

Figure 5.1 – FE model 1 deformed mesh showing general shear failure; scaled up 5 times $\left(\delta_{t;max} = 960\ mm\right)$

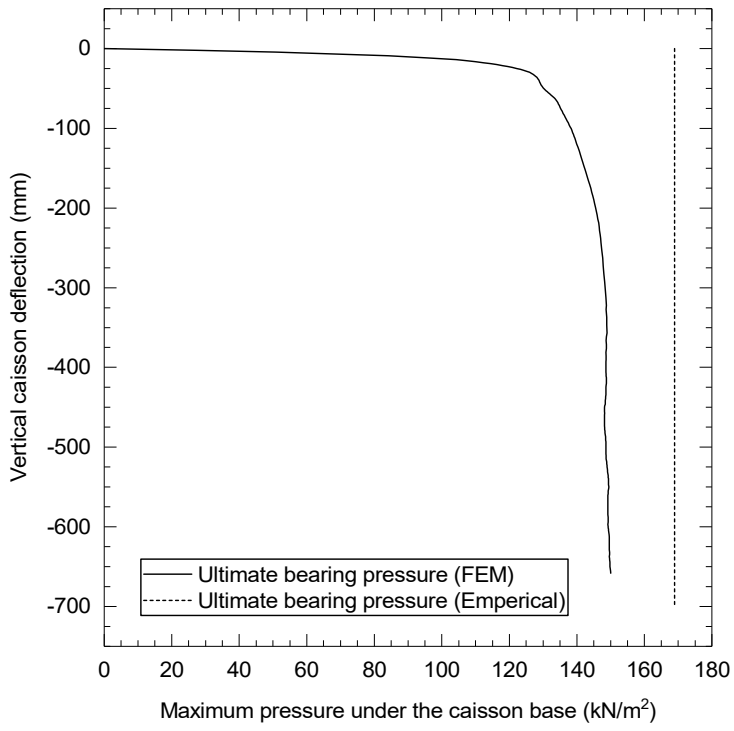

Figure 5.2 – Load-defection behaviour of the caisson up to failure

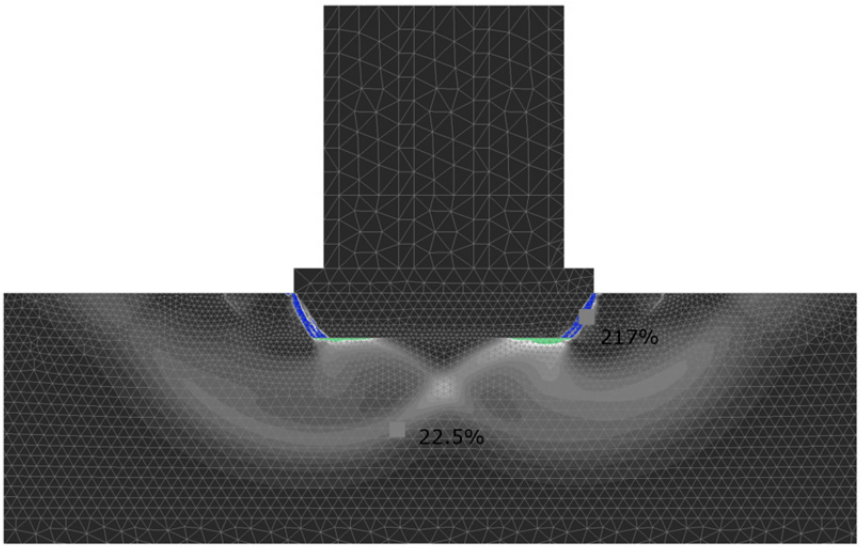

Figure 5.3 – Contours of shear strain highlighting the failure surface ($\varepsilon_{max} = 217\%$)

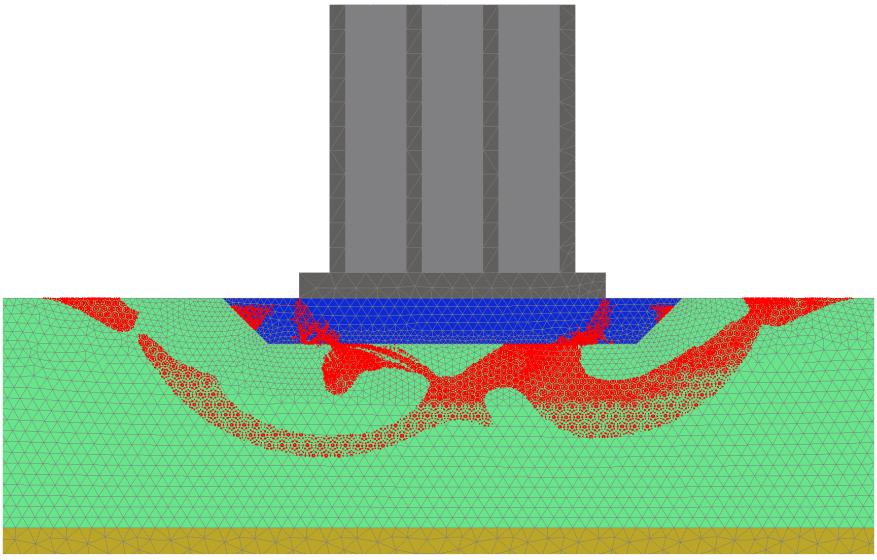

Figure 5.4 – Plastic points showing the stress points that are in a failure state

5.1.2 FE Model 2: Caisson supported on RI ground reinforcement

5.1.2.1 Behaviour of the caisson

In FE Model 2 the firm clay was reinforced with RIs beneath the footprint of the caisson. Figure 3.4b and Figure 5.6 illustrate the problem. The model results presented in Figure 5.5 show that the RIs reduced the settlement of the caisson by 95% when compared to FE model 1 during caisson placement and filling. The high settlement efficiency was largely due to the RIs ensuring stability under vertical loading. At this construction phase the caisson had settled 36 mm. However, Figure 5.5 shows that during backfilling the caisson settled an additional 10 mm to 46 mm and deflected laterally 213 mm.

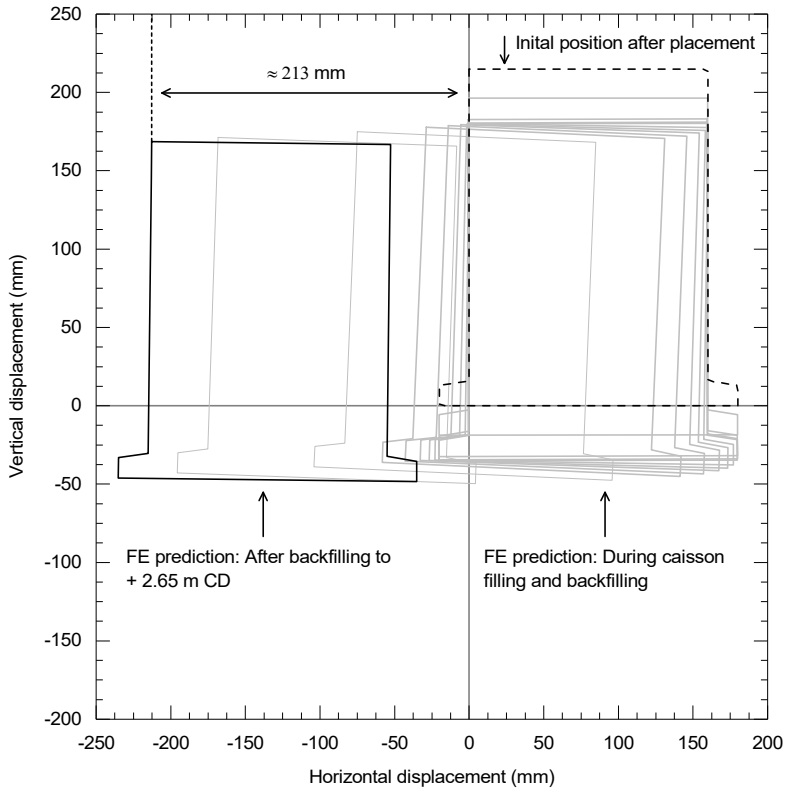

Figure 5.5 – FE Model 2 prediction of caisson displacement during construction and operational conditions

5.1.2.2 Behaviour of the rigid inclusions

The magnitude and distribution of loads, moment and deflection in individual inclusions within the group supporting the caisson are presented in Figure 5.8 and Table 5.2. The free-field lateral soil movement profile is presented in Figure 5.7.

The lateral soil movement profile behind and beneath the caisson is characterised by a triangular distribution with relatively small movements at or near the base of the clay layer and the maximum movement at the top of the layer. Figure 5.7 shows that the lateral deflection of the relatively flexible RIs was dependent on the soil movement profile, particularly at the head where the maximum movement occurred. The following observations were made from Figure 5.8: (i) the maximum shear forces in the RIs developed at the inclusion head and at the base of the zone of moving soil (at or near base of clay layer); (ii) the maximum moment occurred above the stable layer in the moving soil (iii) the lateral RI defection at all RI positions was approximately 213 mm The predicted maximum compressive stress in the RIs ranged from 25100 to 32670 kPa and maximum tensile stress from 18840 to 29860 kPa.

The analytical calculations presented in annexure A.2 and A.3 predicted lateral RI deflections of 291 mm and 333 mm and a maximum bending moment of 2104 $kN.m$. These results are in fair agreement with the FE model results considering the complexity of the problem.

Table 5.1 – Table of forces for RIs after backfilling to + 2.65 m CD

	RIs supporting the caisson								
RI reference	**g**	**h**	**i**	**j**	**k**	**l**	**m**	**n**	**o**
Dist. from center of caisson	**-10**	**-7.5**	**-5**	**-2.5**	**0**	**2.5**	**5**	**7.5**	**10**
Loc. of max. bending moment	-28.2	-28.2	-28.2	-28.2	-28.5	-28.5	-28.5	-28.9	-28.9
Max. bending moment	1304	1172	1076	1004	917	917	903	916	997
Axial force at Mmax	457	-1235	1151	1190	1284	1284	1288	1156	1073
Max compressive stress	-32670	-31180	-29090	-27490	26410	-25440	-25100	-25240	-26620
Max tension	29860	25520	23000	21240	19900	19170	18840	19140	21130
Loc of max shear force	-29.6	-19.5	-19.5	-19.5	-19.5	-19.5	-19.5	-19.5	-19.5
Maximum shear force	-398	-736	-781	-798	-841	-825	-854	-908	-688

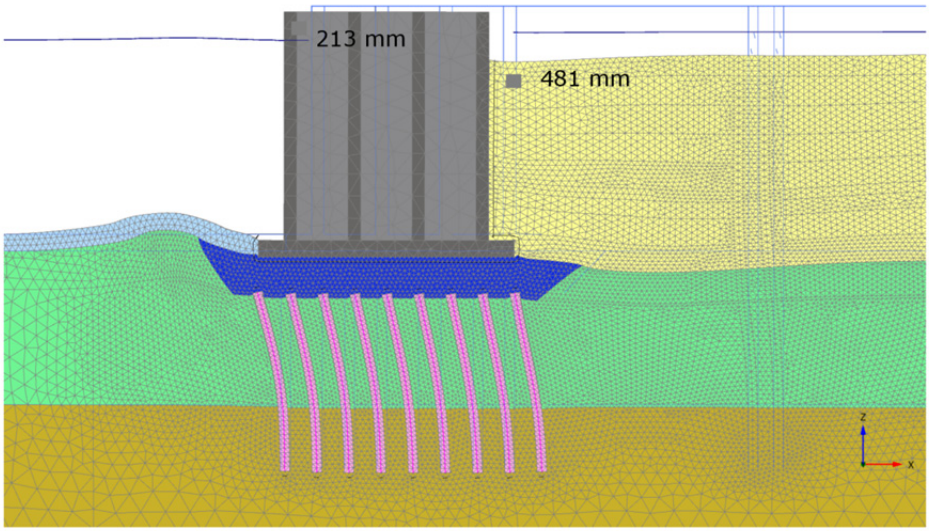

Figure 5.6 – FE Model 2 deformed mesh after backfilling; scaled up 5 times $\left(\delta_{t;max} = 481\ mm\right)$

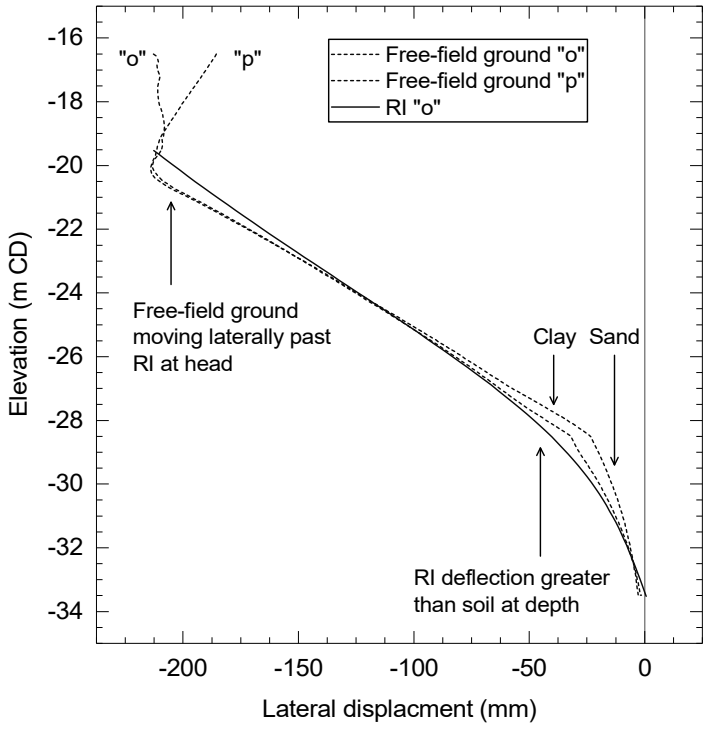

Figure 5.7 – FE Model 2 prediction of free-field lateral ground movement beneath and behind the caisson

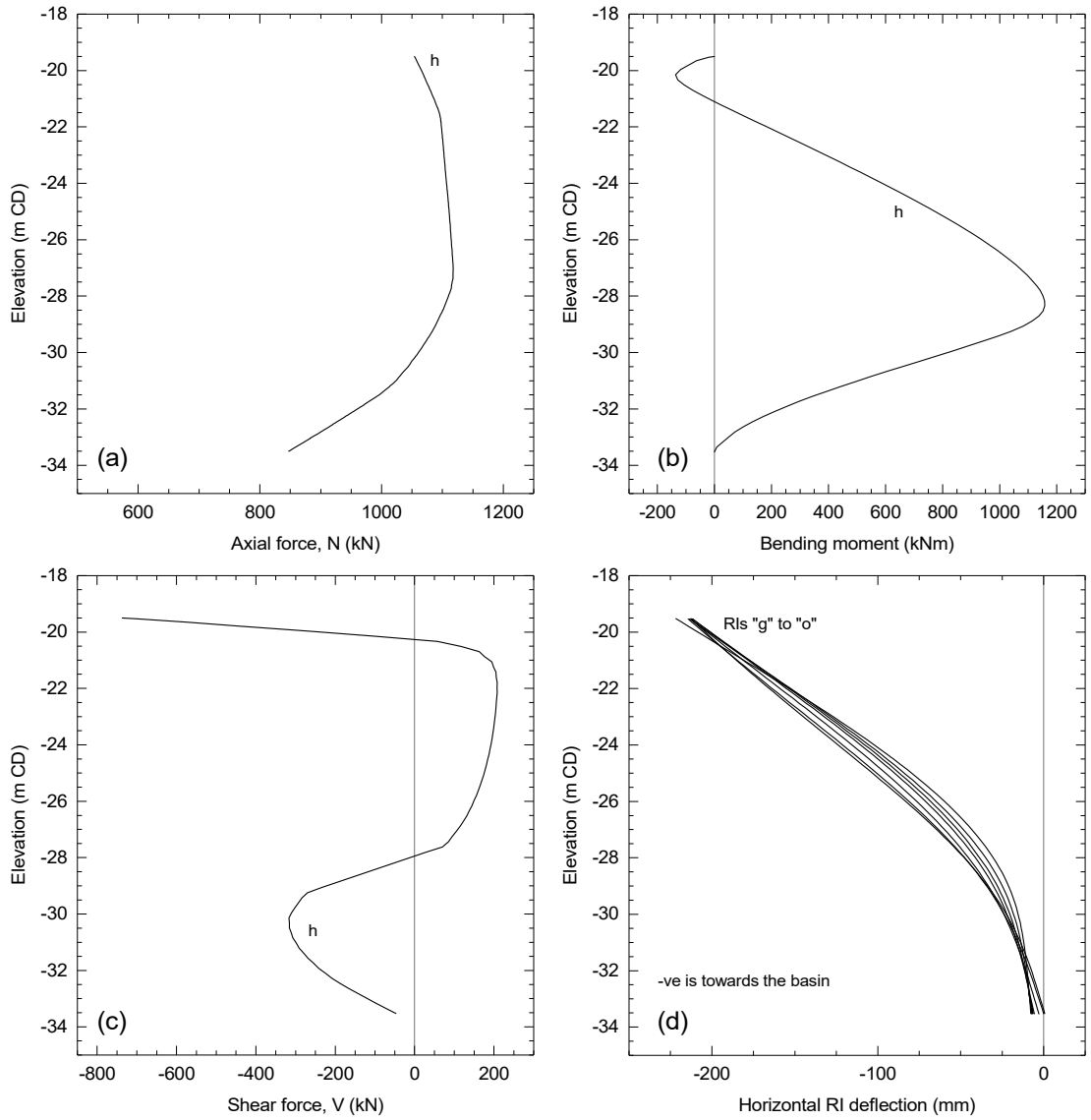

Figure 5.8 – FE Model 2 force diagrams for RIs supporting the caisson after backfilling

5.1.2.3 Conclusions

The following was concluded from the results of FE Model 2:

- The RI ground reinforcement reduced the settlement of the caisson by ≈ 95% when compared to FE Model 1.
- The embankment type loading due to backfilling behind the caisson resulted in large free-field lateral ground movements.
- The relatively flexible RIs deform laterally with the moving soil, resulting in the development of additional bending moments and high compressive and tensile stresses.
- There is fair agreement between analytical and FE estimations of the magnitude of free-field lateral ground movement and associated RI bending moments.
- FE model 2 confirms the requirement for strategies to limit lateral loading and the effects of lateral loading.

5.1.3 FE Model 3: Implementation of strategies for limiting lateral loading

5.1.3.1 Behaviour of the caisson

The various strategies for limiting lateral loading described in section 3.4.5 were implanted in FE Model 3. Figure 3.1 illustrates the problem and Figure 5.9 shows the numerical model deformed mesh for the operational load case.

Lateral deflection efficiency of strategies to limit loading:

The effect of the strategies to limit lateral loading was to reduce the lateral deflection of the caisson by ≈ 88% when compared to FE model 2 after backfilling to 2.65 m CD (Figure 5.10). At this construction phase the caisson had deflected laterally towards the basin ≈ 30 mm and settled ≈ 46 mm.

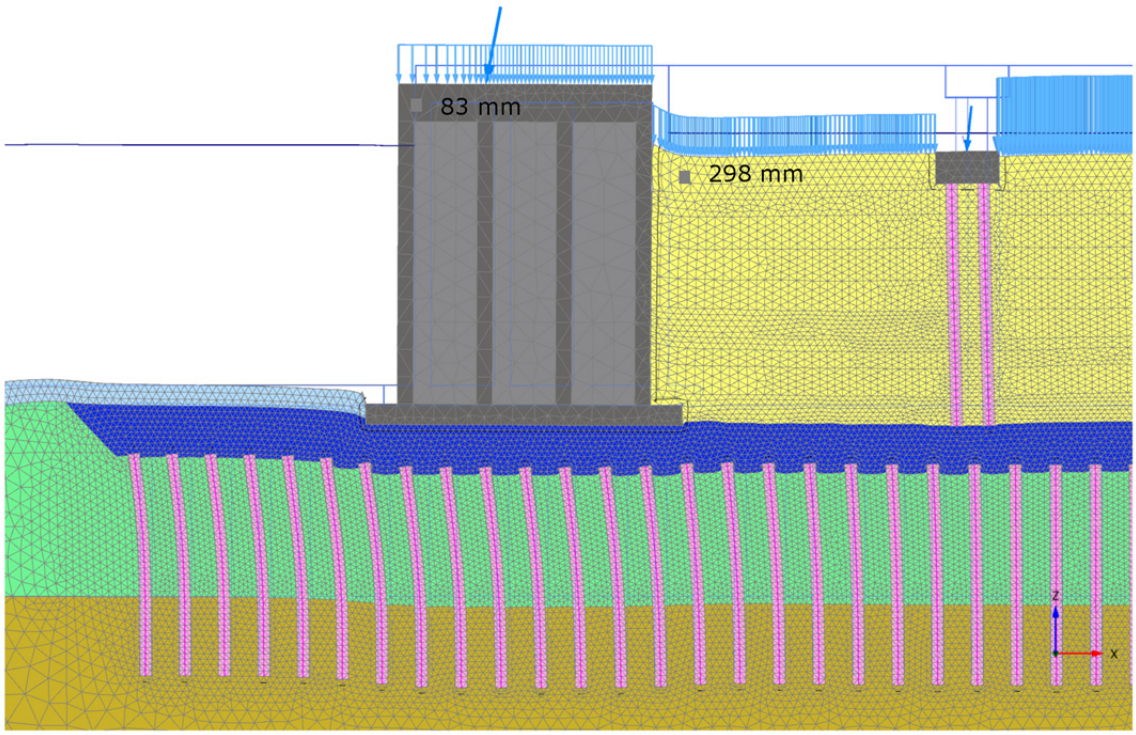

Figure 5.9 – FE Model 3 deformed mesh for operational loading phase ; scaled up 5 times $(\delta_{t;max} = 298\ mm)$

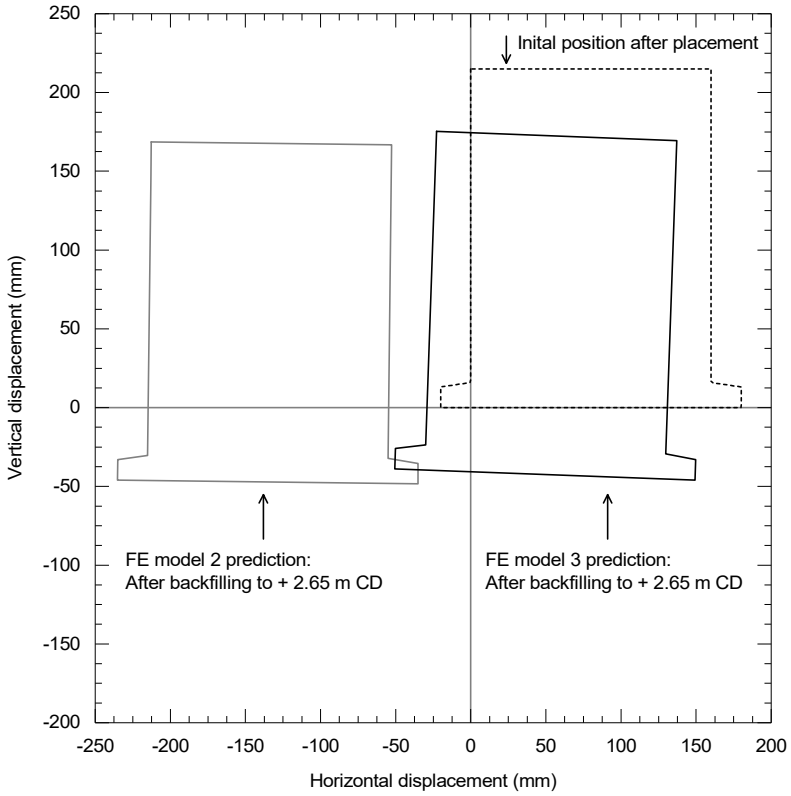

Figure 5.10 –Deflection predictions for FE model 2 and model 3 after backfilling to 2.65 m CD

Behaviour of the caisson during construction:

During construction the caisson settled and deflected laterally with a slight backward rotation (Figure 5.11). At the end of construction the caisson had deflected laterally 19 mm to 35 mm along its front wall and settled 44 mm to 60 mm across its base. The average pressure across the base was 270 kPa at the toe which increased to 310 kPa at the heel (Figure 2.15). Stress concentrations in the LTP at the location of each inclusion resulted in peaks in stress across the base (Figure 5.13). The lateral earth pressure profile was generally defined by K_a conditions to near K_0 conditions at depth in the confined wedge near the heel of the caisson.

Behaviour of the caisson during operational conditions into the long term:

During transient operational loading the caisson deflected laterally and rotated forward as the pressure distribution changed to a maximum average pressure of 343 kPa at the toe to 323 kPa at the heel. The lateral earth pressure profile has been described above; however, during unloading in the operational phase, the caisson rebounded and deflected backwards. The resulting increase in lateral earth pressure near the top of the caisson exceeded the K_0 condition. During operational loading the caisson

deflected laterally an additional 22 mm to 31 mm along its front wall and settled an additional 2 mm to 11 mm across its base (Figure 5.11 and Figure 5.12). During consolidation, as the excess pore pressure in the clay dissipated to the long-term drained conditions (Figure 5.15), the caisson deflected less than 2 mm vertically and laterally.

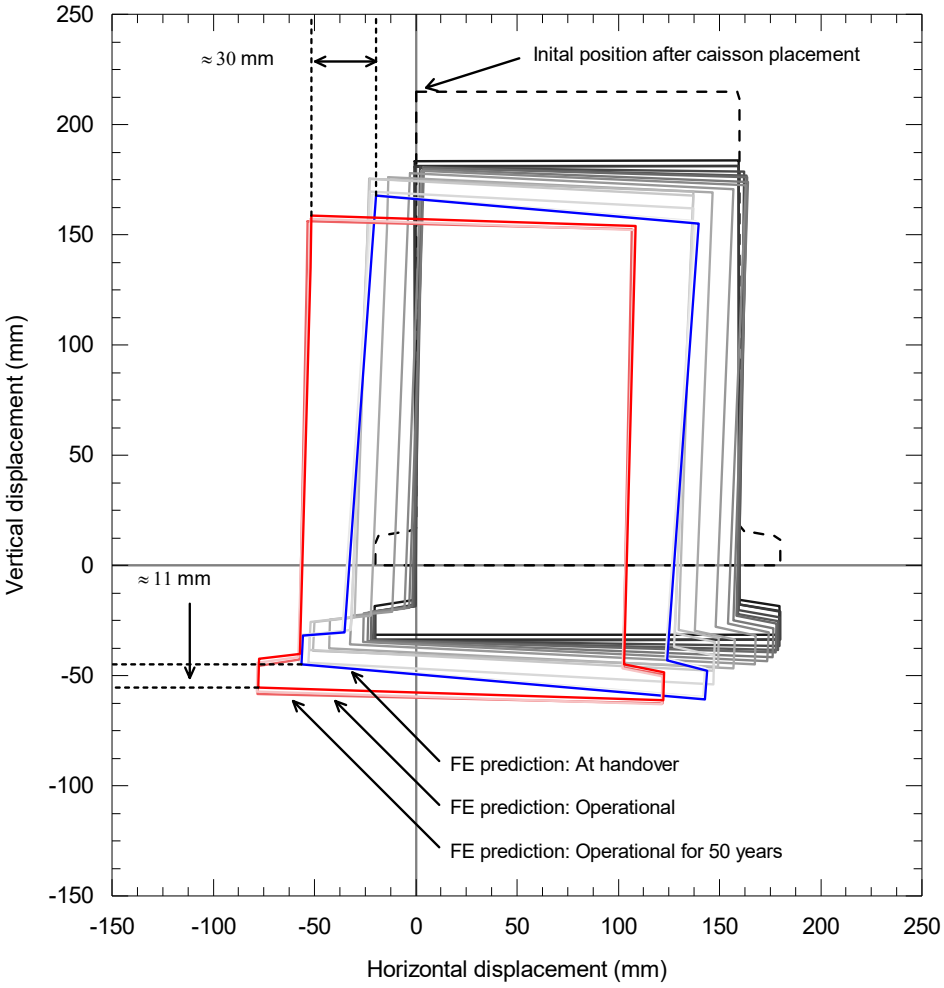

Figure 5.11 – FE Model 3 prediction of caisson displacement during construction and operational conditions

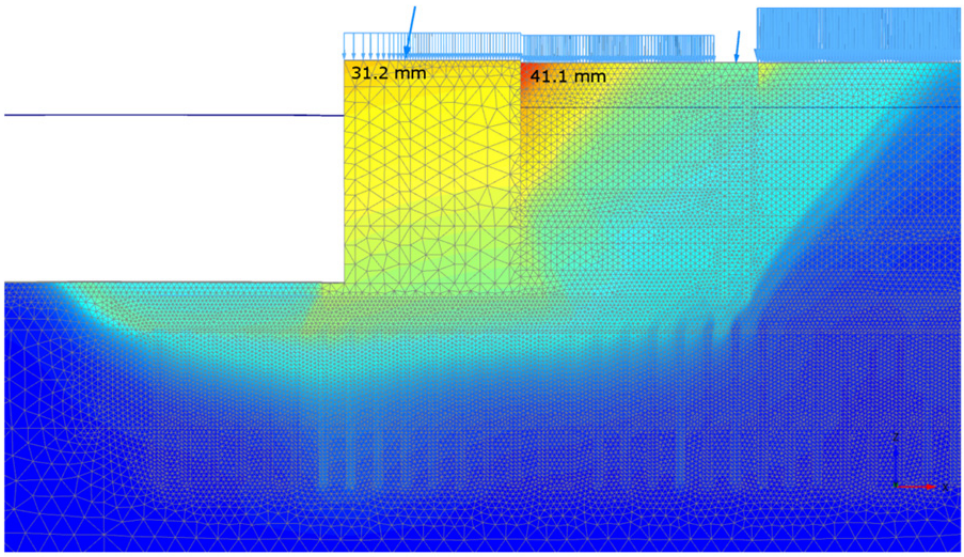

Figure 5.12 – FE Model 3 total displacements for the transient operational phase $(\delta_{t;max} = 41.1\ mm)$

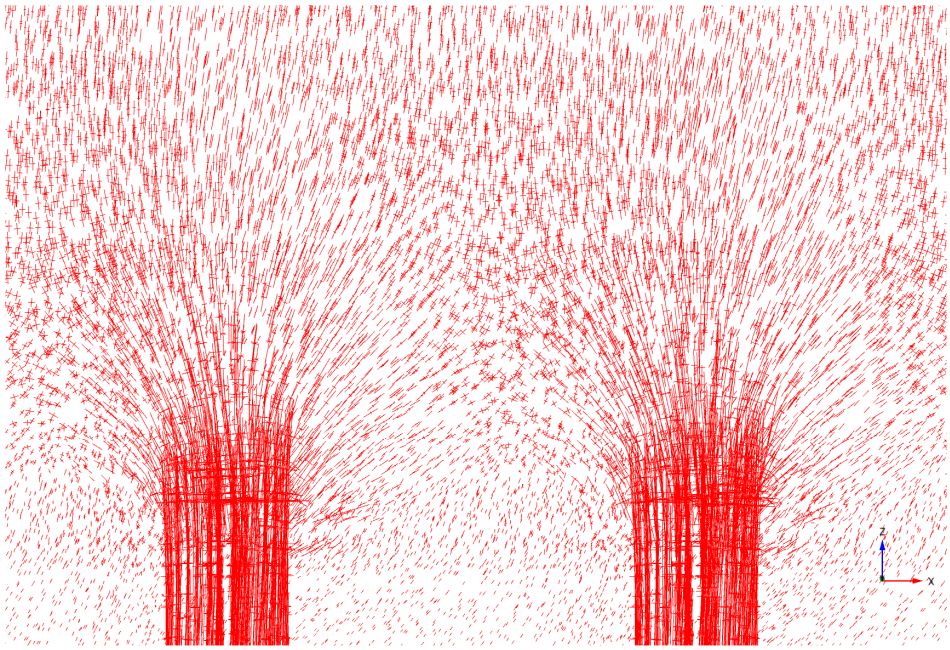

Figure 5.13 – FE Model 3 effective principal stress directions at the RI head for the transient operational phase

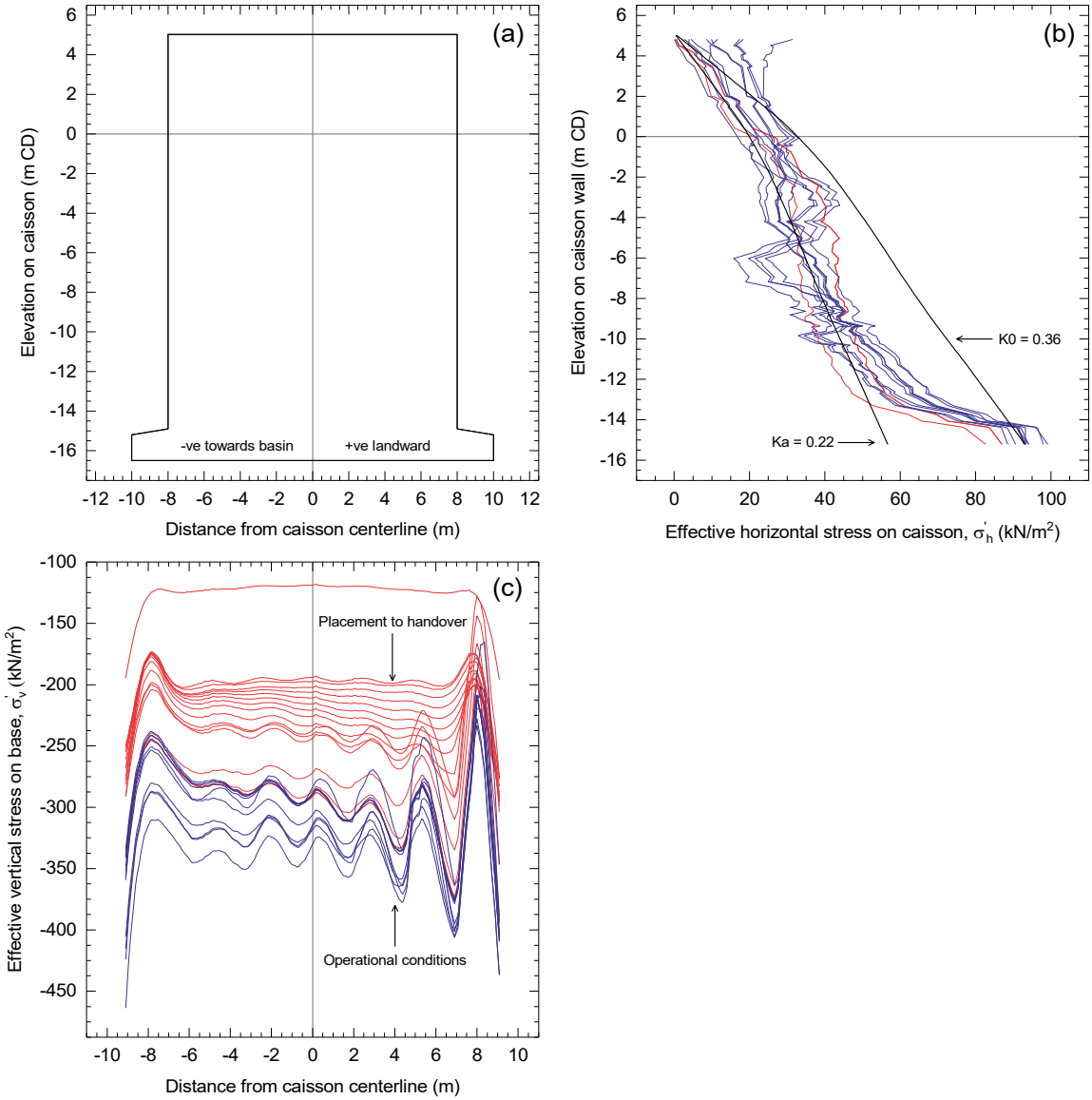

Figure 5.14 – FE Model 3 prediction of lateral earth pressure and bearing pressure for all loading phases

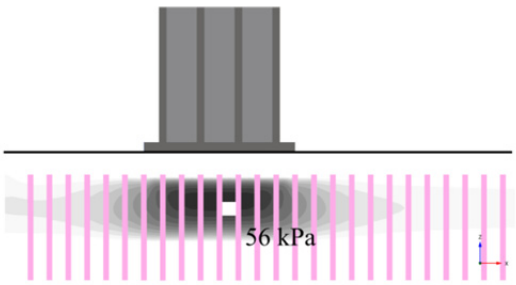

(a) Fill caisson with sand
umax = 56 kPa (Day 20)

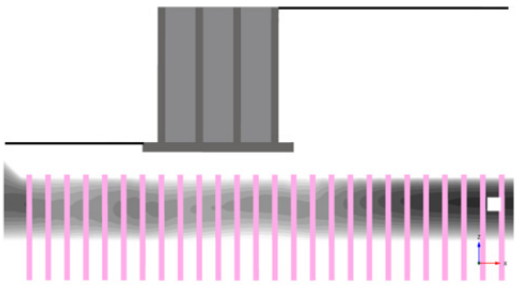

(b) Backfill final lift to 2.65 m CDP
umax = 27 kPa (Day 120)

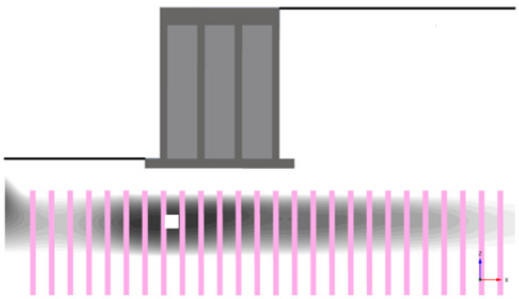

(c) Construct capping beam
umax = 9.5 kPa (Day 170)

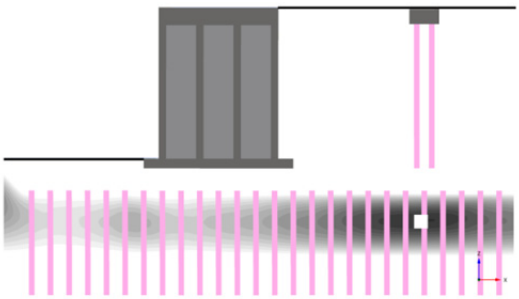

(d) Constuct pavement and piled rear crane beam
umax = 56 kPa (Day 360)

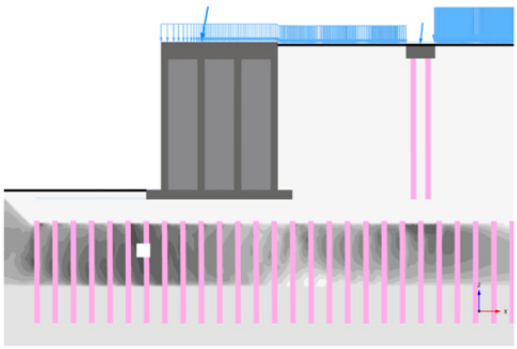

(e) Operational conditions
umax = 42 kPa (Day 360)

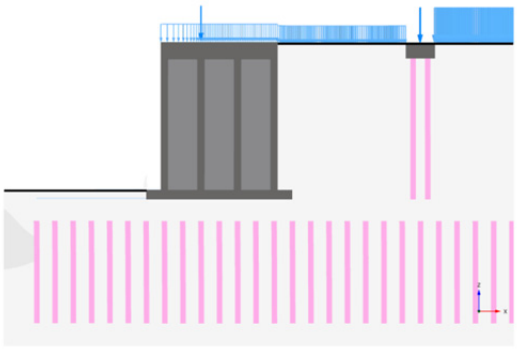

(f) FSustained operational conditions
90% consolidation (Day 500)

Figure 5.15 – FE Model 3 prediction of excess pore pressure for the various construction and loading phases

5.1.3.2 Behaviour of the rigid inclusions

The load-deflection behaviour of the RIs ahead of the caisson ("a" to "f"), supporting the caisson ("g" to "o") and supporting the backfill ("p" to "z"), are presented separately in this section. The results are taken from the transient operational load case.

Boundary conditions and relative pile-soil flexibility:

The results presented below show that RIs were subjected to the combined effects of vertical and horizontal loading and lateral ground movements. The RIs have a free-head condition whereas the toe is effectively pinned due to the restraint offered by the stable bearing layer. The loading can be generalised as follows:

- Vertical load acting on the inclusion head,
- Drag load due to negative skin friction caused by free-field vertical soil movements,
- Shaft resistance due to positive shaft friction in the vertical direction,
- Bearing resistance at the base.
- Horizontal load due to shear on the inclusion head,
- Horizontal load due to free-field horizontal ground movements (lateral-load analogue of negative skin friction),
- Shaft resistance due to positive shaft friction in the horizontal direction,
- Shear resistance at the base.

Behaviour of RIs "a" to "f" ahead of the caisson:

The magnitude and distribution of loads, moment and deflection in individual inclusions within a group ahead of the caisson are presented in Figure 5.16 and Table 5.2. The free-field lateral soil movement profile is presented in Figure 5.17.

The lateral soil movement profile ahead of the caisson is characterised by a triangular distribution, with relatively small movements at or near the base of the clay layer and the maximum movement at the top of the layer. The greatest magnitude of lateral soil movement occurred at position "f" and decreased away from the caisson toe. The greatest depth of soil movement occurred at position "f" and decreased by approximately 3 meters to position "a". The soil movement distribution is similar to "case 2" described by Poulos & Davis (1980) which produced the lowest moment and largest lateral deflections of the three cases considered (Figure 2.34). Figure 5.17 shows that the lateral deflection of

the relatively flexible RIs was dependent on the soil movement profile, particularly at the head where the maximum movement occurred. The following observations were be made from Figure 5.16: (i) the maximum shear forces in the RIs developed at the inclusion head and at the base of the zone of moving soil (at or near base of clay layer); (ii) the maximum moment occurred above the stable layer in the moving soil; (iii) RIs ahead of the caisson were characterised by low axial loads; the maximum axial load occurred at position "f" at the base of the clay layer due to the drag load caused by negative skin friction; (iv) the lateral RI defection at the head ranged from 40 mm at "a" to 58 mm at "f". The RI settlement ranged from 2 mm at "a" to 14 mm at "f". The predicted compressive stress in the RIs ranged from 6847 kPa to 9938 kPa and tensile stress from 6847 kPa to 8072 kPa. Tensile loads in the geotextile were less the 1 kN/m.

Table 5.2 – FE Model 3 table of forces for RIs and geogrid ahead of the caisson toe

	RIs in the passive zone ahead of the caisson toe					
RI reference	**a**	**b**	**c**	**d**	**e**	**f**
Distance from the center of the caisson	**-25**	**-22.5**	**-20**	**-17.5**	**-15**	**-12.5**
Max tensile force in geogrid (kN/m)	<1	<1	<1	<1	<1	<1
Location of maximum bending moment	-24.3	-25.2	-26.1	-27.2	-28.1	-28.1
Maximum bending moment, Mmax	339	312	296	298	321	353
Axial force at Mmax	83	96	111	159	295	552
Maximum compressive stress	-8491	-7806	-7461	-7635	-8412	-9938
Maximum tension	8072	7329	6905	6847	7010	7157
Location of maximum shear force	-19.9	-20.1	-29.0	-29.6	-19.5	-19.5
Maximum shear force (kN)	119	96	-86	-87	-122	-267

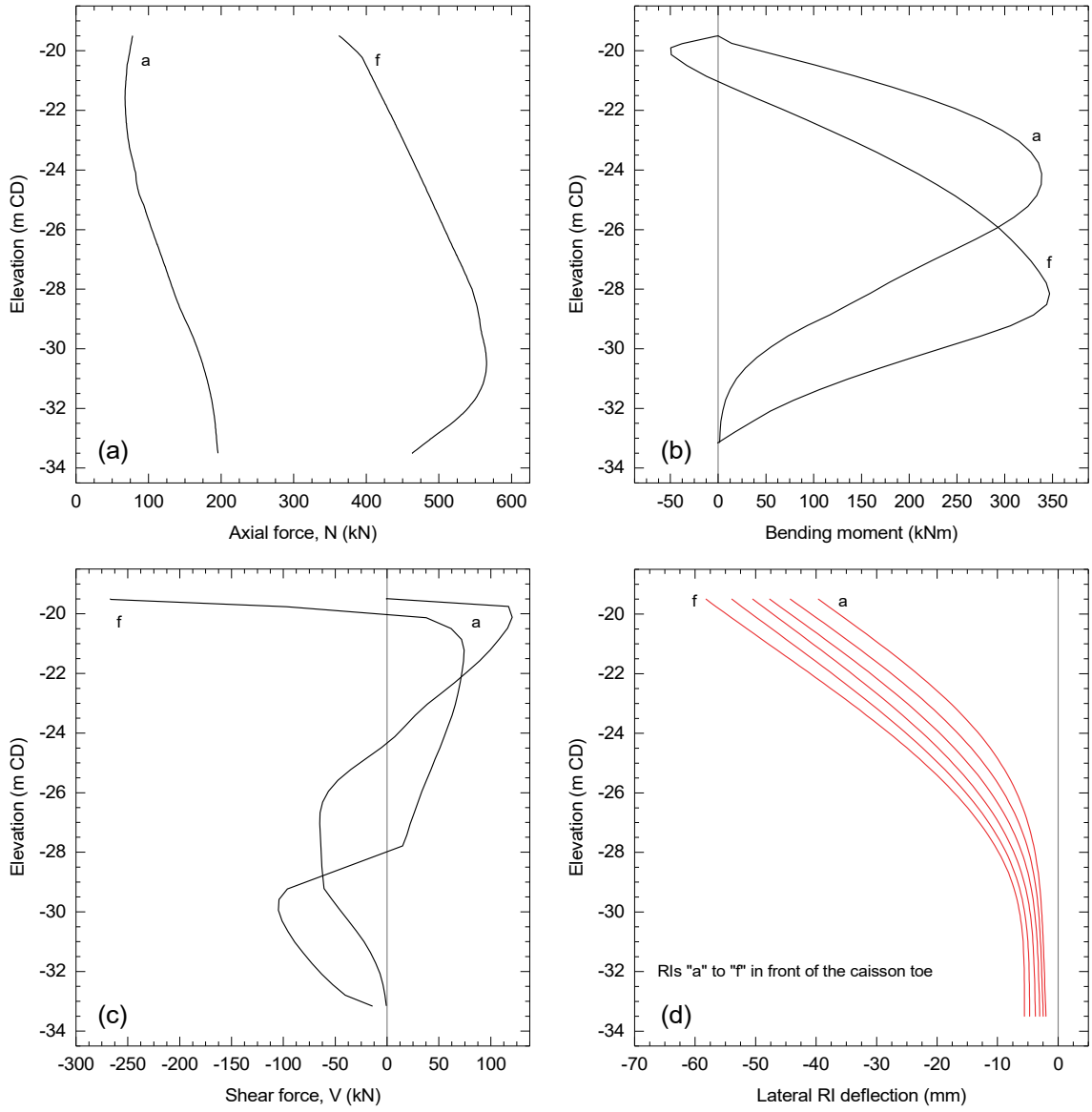

Figure 5.16 – FE Model 3 force diagrams for RIs ahead of the caisson toe under operational load conditions

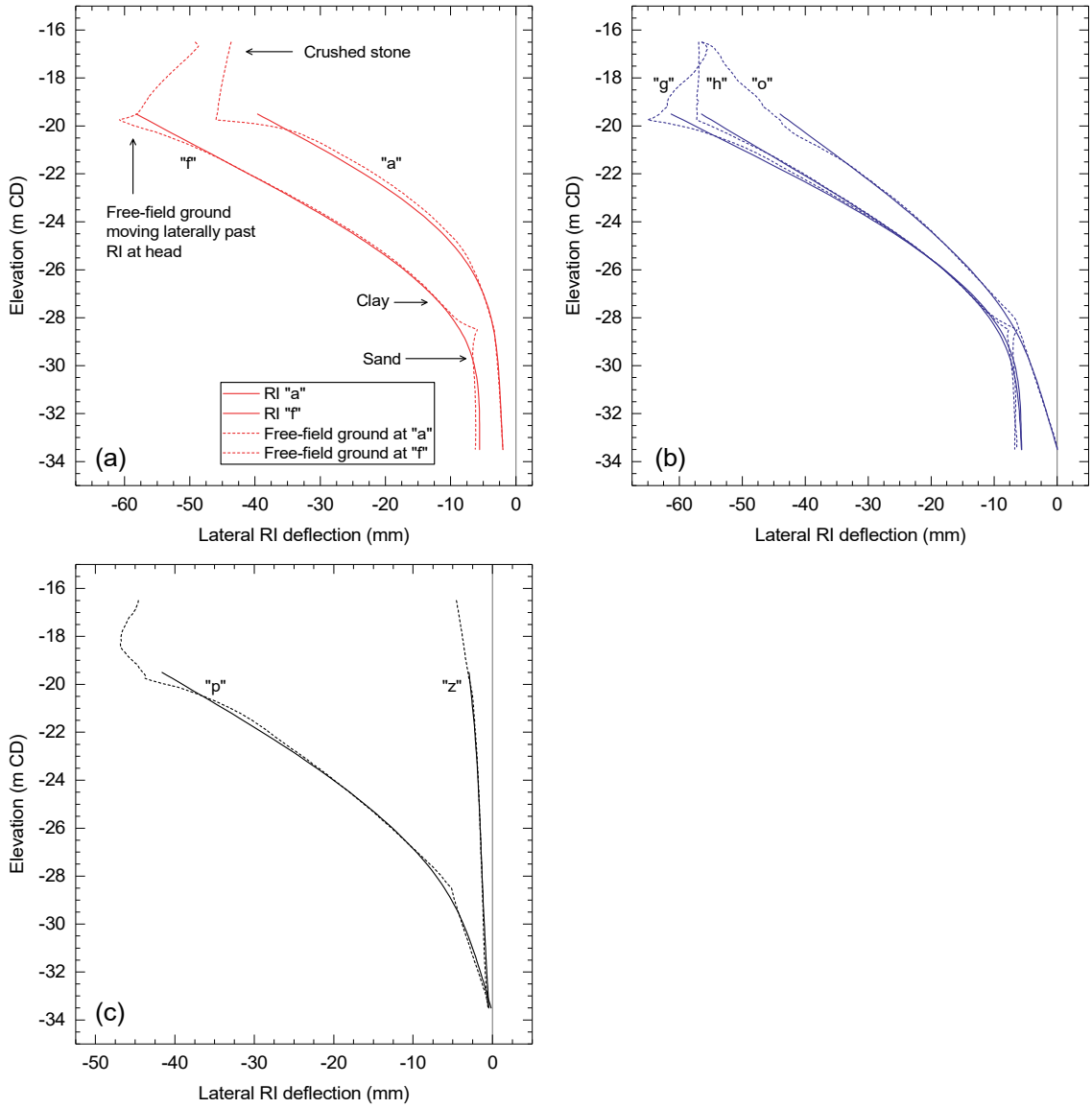

Figure 5.17 – FE Model 3 prediction of free-field lateral ground movement at selected positions ahead, beneath an behind the caisson

Behaviour of RIs "g" to "o" supporting the caisson:

The magnitude and distribution of loads, moment and deflection in individual inclusions within a group supporting the caisson are presented in Figure 5.18 and Table 5.3. The free-field lateral soil movement profile is presented in Figure 5.17.

The lateral soil movement profile beneath the caisson is characterised by a triangular distribution with relatively small movements at or near the base of the clay layer and maximum movement at the top of the layer. The greatest magnitude of lateral soil movement occurred at position "g" and decreased towards the caisson heel. The depth of soil movement was fairly uniform beneath the caisson. Figure 5.17 shows that the lateral deflection of the relatively flexible RIs was dependent on the soil movement profile, particularly at the head where the maximum movement occurred. The following observations were made from Figure 5.16: (i) the maximum shear forces in the RIs developed at the inclusion head and at the base of the zone of moving soil (at or near base of clay layer); (ii) the maximum moment occurred in the moving soil at the boundary between the clay and the stable bearing layer; (iii) RIs beneath the caisson developed significant axial load due to arching in the LTP above the head and negative skin fraction along the shaft; the maximum axial load occurred at position "h" and decreased slightly to position "n" in line with the distribution across the base; inclusions "g" and "o" attracted significantly lower axial load due to the local stress conditions at the edges of the caisson; (iv) the lateral RI defection at the head ranged from 40 mm at "a" to 58 mm at "f". The RI settlement ranged from 31 mm at "o" and "g" to 40 mm at "h". The predicted compressive stress in the RIs ranged from 8193 kPa to 12370 kPa and tensile stress from 1054 kPa to 5340 kPa. The mobilised tension in the geotextile ranged from 9 kN/m to 29 kN/m.

Table 5.3 – FE Model 3 table of forces for RIs and geogrid supporting the caisson

	RIs supporting the caisson								
RI reference	**g**	**h**	**i**	**j**	**k**	**l**	**m**	**n**	**o**
Dist. from center of caisson	**-10**	**-7.5**	**-5**	**-2.5**	**0**	**2.5**	**5**	**7.5**	**10**
Max tensile force in geogrid (kN/m)	29.18	11.73	8.42	12.37	8.68	8.72	9.05	14.14	18.58
Loc. of max. bending moment	-28.2	-28.2	-27.4	-26.7	-26.4	-26.0	-27.1	-28.2	-28.2
Max. bending moment	357	327	287	267	250	235	221	212	207
Axial force at Mmax	1362	1835	1755	1783	1769	1809	1773	1583	1309
Max compressive stress	-12070	-12370	-11390	-10840	-10380	-10120	-9714	-9171	-8193
Max tension	5340	3414	2541	2144	1748	1314	1054	1133	1785
Loc of max shear force	-19.5	-19.5	-19.5	-19.5	-19.5	-19.5	-20.9	-29.6	-29.4
Maximum shear force	-147	-227	-192	-182	-135	-101	75	-64	-70

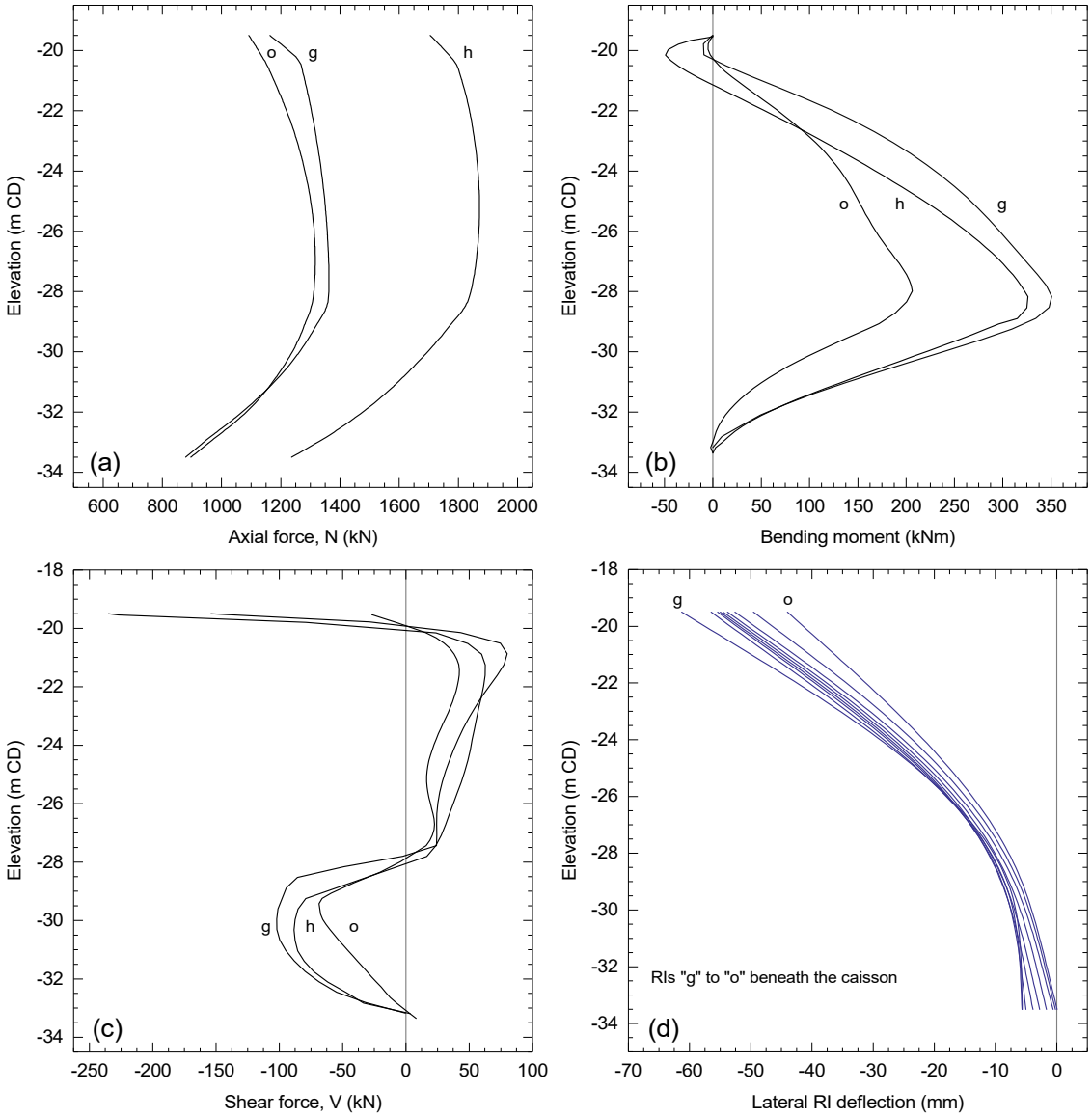

Figure 5.18 – FE Model 3 force diagrams for RIs supporting the caisson under operational load conditions

Behaviour of RIs "p" to "z" supporting the backfill:

The magnitude and distribution of loads, moment and deflection in individual inclusions within a group supporting the backfill are presented in Figure 5.19 and Table 5.4. The free-field lateral soil movement profile is presented in Figure 5.17.

The lateral soil movement profile near the caisson heel is characterised by a triangular distribution with relatively small movements at or near the base of the clay layer and maximum movement at the top of the layer. The greatest magnitude of lateral soil movement occurred at position "p" and decreased away from the caisson. The depth of soil movement decreased gradually away from the caisson. Figure 5.17 shows that the lateral deflection of the relatively flexible RIs was dependent on the soil movement profile, particularly at the head where the maximum movement occurs. The following observations were made from Figure 5.16: (i) the maximum shear forces in the RIs developed at the inclusion head and at the base of the zone of moving soil; (ii) the maximum moment occurred above the stable layer in the moving soil; (iii) RIs supporting the backfill developed significant axial load due to arching in the LTP above the head and negative skin fraction along the shaft; the axial load was fairly uniform in RIs "q" to "z"; inclusions "p" attracted significantly lower axial load due to the local stress conditions at the caisson heel; (iv) the lateral RI defection at the head ranged from 3 mm at "z" to 42 mm at "p". The RI settlement ranged from 28 mm at "p" to 34 mm at "q" to "z". The predicted compressive stress in the RIs ranged from 5022 kPa to 7745 kPa and tensile stress from 1544 kPa to 0 kPa. It is important to note that RIs "s" to "z" were fully compressed over their entire section. The mobilised tension in the geotextile ranged from 6 kN/m to 28 kN/m.

Table 5.4 – FE Model 3 table of forces for RIs supporting the backfill

	RIs supporting the backfill										
RI reference	**p**	**q**	**r**	**s**	**t**	**u**	**v**	**w**	**x**	**y**	**z**
Dist. from centre of caisson	**12.5**	**15**	**17.5**	**20**	**22.5**	**25**	**27.5**	**30**	**32.5**	**35**	**37.5**
Max tension in geogrid (kN/m)	17.65	27.07	24.59	17.09	14.41	28.33	20.07	13.6	9.31	5.92	6.08
Loc. of max. bending moment	-28.2	-28.2	-27.4	-26.3	-24.9	-24.2	-22.7	-21.2	-22.2	-22.7	-22.5
Max. bending moment	191	162	135	120	101	96	41	14	15	20	15
Axial force at Mmax	1240	1450	1477	1495	1615	1495	1511	1485	1508	1555	1488
Max compressive stress	-7689	-7461	-6994	-7099	-6526	-6128	-7745	-6550	-5022	-5510	-6086
Max tension	1544	362	395	-721	-1049	-996	-1184	-1041	-740	-1101	-1068
Loc of max shear force	-29.1	-31.0	-31.0	-21.6	-20.9	-21.6	-20.1	-20.3	-20.1	-20.3	-20.1
Maximum shear force	-57	-42	-35	27	31	27	18	13	10	10	9

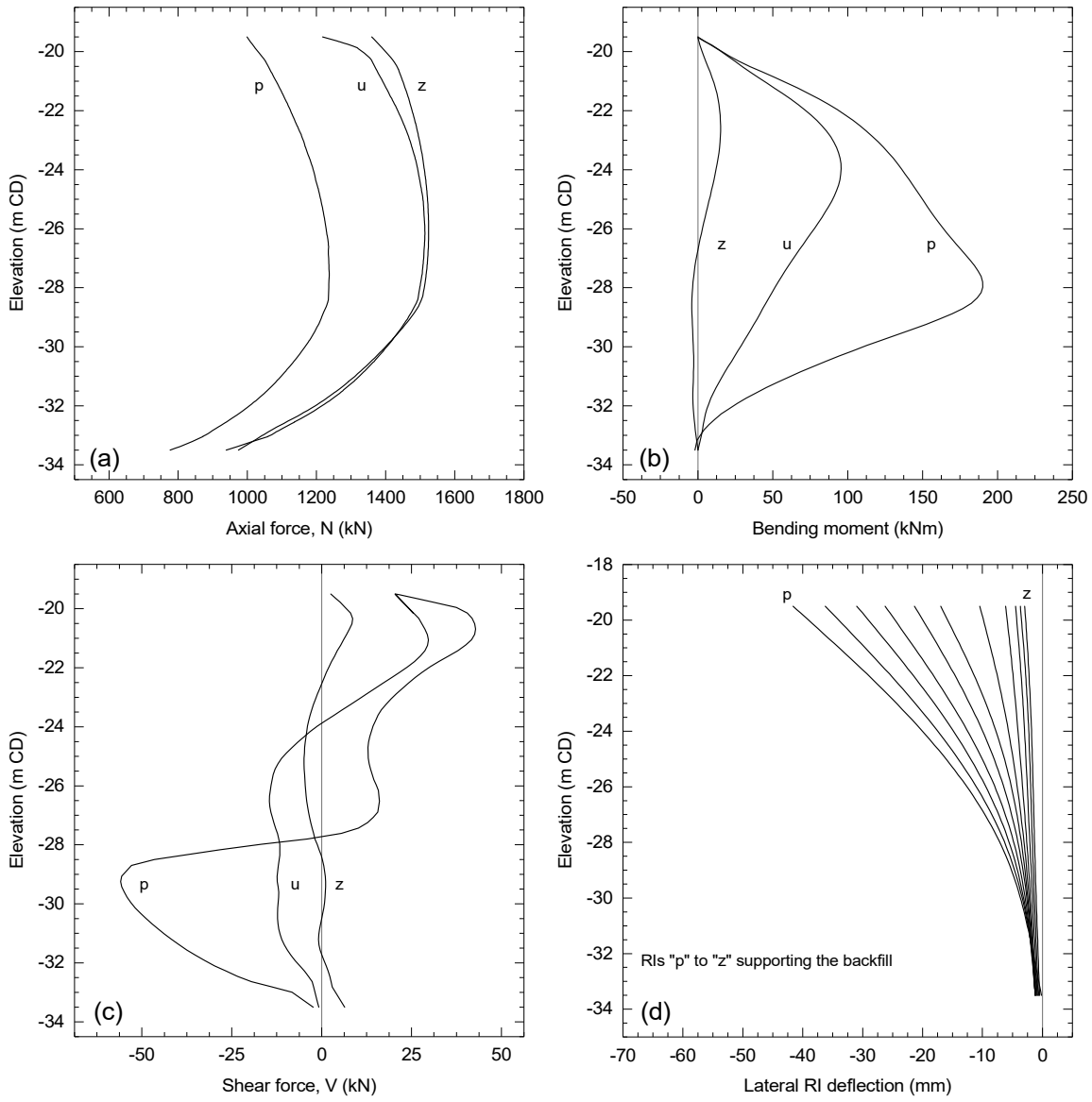

Figure 5.19 – FE Model 3 force diagrams for RIs supporting the backfill under operational load conditions

5.1.3.3 Mode of failure

The mode of failure was evaluated by carrying out stability analyses using the "shear strength reduction technique". The mode of failure in FE-Model 3-2 was evaluated using a Mohr-Coulomb model to model the RIs. The stability analyses were carried out for the transient operational load case.

Figure 5.20 shows the critical slip surface which passed through the RIs daylighting approximately 25 m ahead of the caisson toe. Although there was no continuous shear-strain plane in the vicinity of the inclusions, the shape of the failure surface appeared to approximate a circular slip. This agrees with the theoretical consideration of failure by Kivelo (1998) and Broms (1999). Figure 5.22 shows the lateral deflection profile of the RIs, highlighting the upper "unstable" and lower "stable volume of soil. The failure surface defined by the shear strain contours in Figure 5.20 was reproduced in Figure 5.22 at each RI position. The failure of the RIs was due to the development of bending tensile stresses in excess of the tension cut-off specified in the MC model, resulting in the development of a plastic hinge. It is evident that the specific failure mode of each inclusion was dependent on its location relative to the slip surface.

Figure 5.21 shows the conceptual failure mode based on the results presented in Figure 5.20 and Figure 5.22. The following modes of failure occurred:

- RIs "a" to "g" and "n" to "r" developed one plastic hinge at the location of the maximum bending moment in the column (Mode 3b in Figure 2.39).
- RIs "h" to "m" developed two plastic hinges at the location of the maximum bending moments in the columns (Mode 3c. 3d, 3e in Figure 2.39).
- RI "s" to "z" had a shallow zone of unstable soil near the surface and the moment capacity of the column was sufficient in this case to resist the lateral earth pressure.

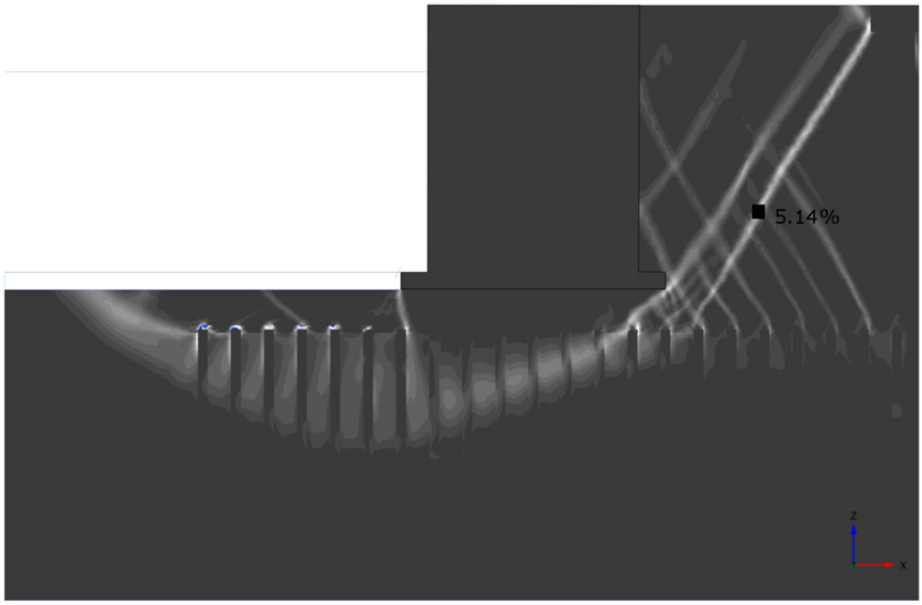

Figure 5.20 – Shear strain contours at failure ($\varepsilon_{max} = 5.14\%$)

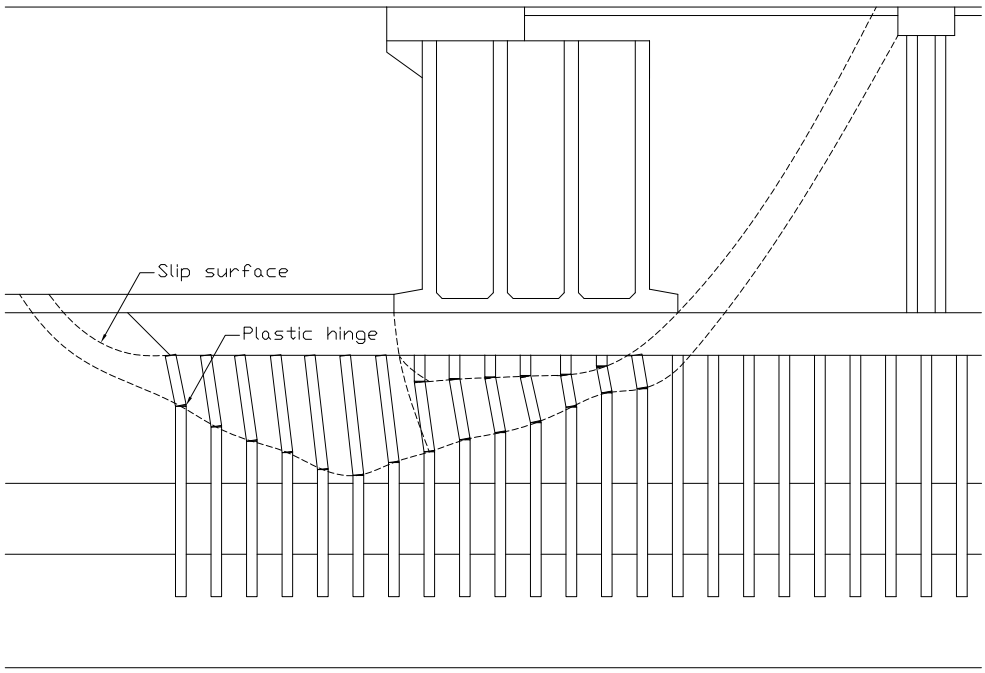

Figure 5.21 – Conceptual failure mode

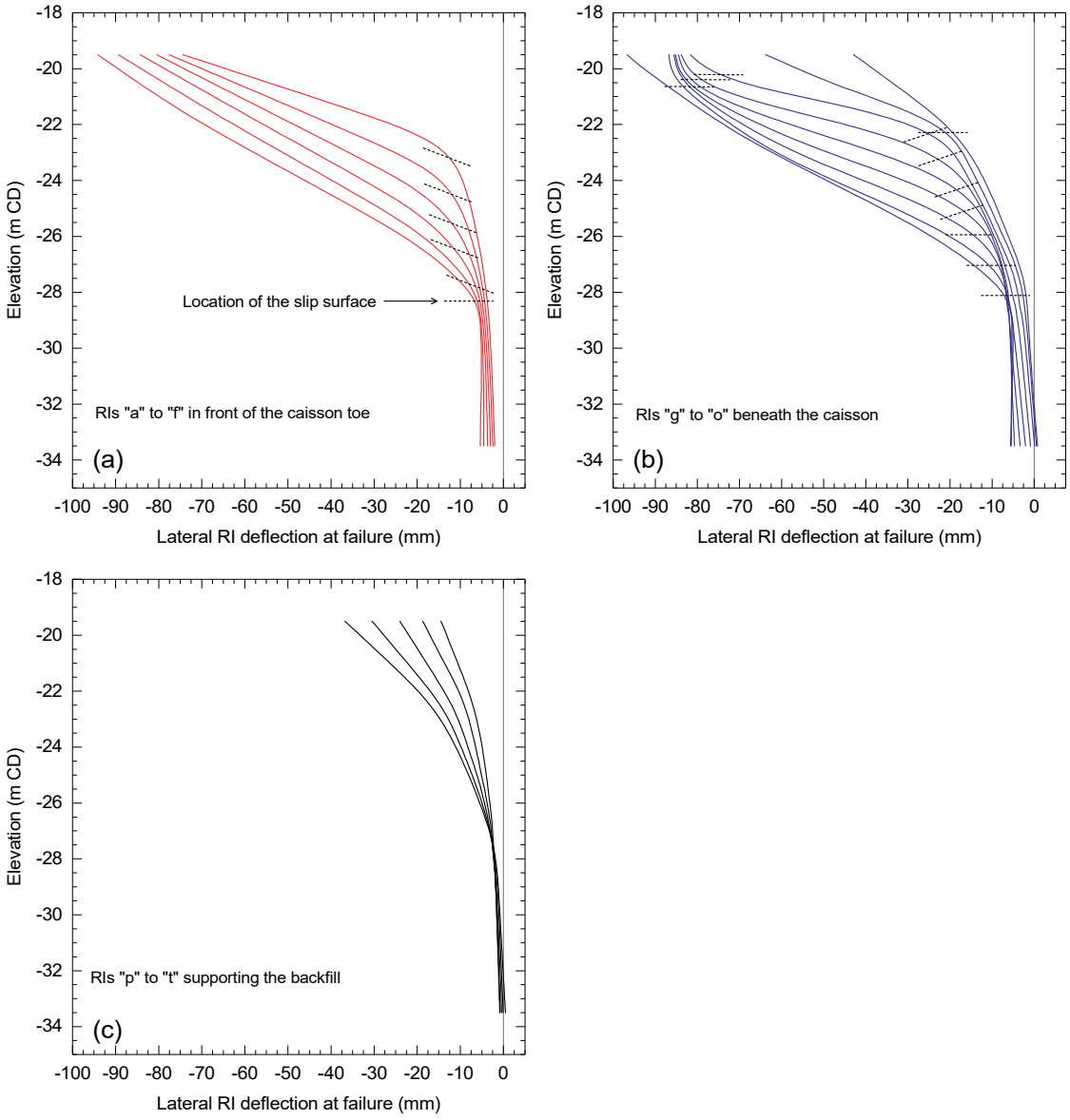

Figure 5.22 – Lateral deflection of RIs at failure

5.1.3.4 Conclusions

The following was concluded from the results of FE model 3:

- The effect of the strategies to limit lateral loading was to reduce the lateral deflection of the caisson by ≈ 88% when compared to FE model 2.
- During transient operational loading the caisson deflected laterally 22 mm to 31 mm along its front wall and settled 2 mm to 10 mm across its base.
- There was sufficient time during construction to dissipate the majority of the excess pore pressure generated in the clay subsoil with the result being negligible long-term deformation.
- Lateral deflections of RIs “a” to “r” resulted in the development of bending tensile stresses.
- RIs “s” to “z” remained in compression over their entire section.
- RIs “g” and “o” at the edge of the structure attracted significantly less axial load resulting in higher moments and bending tensile stresses.
- At failure the critical slip surface approximated a circular slip and passed through the RIs daylighting approximately 25 meters ahead of the caisson toe.
- The specific failure mode of each inclusion was dependent on its location relative to the slip surface.
- The failure of the RIs was due to the development of bending tensile stresses in excess of tension cut-off specified in the MC model, resulting in the development of a plastic hinge.

5.2 Technical Appraisal of FE Model 3 Results

5.2.1 Performance in terms of stability

Geotechnical stability:

Geotechnical stability was evaluated using FE Model 3-2 according to the methodology described in section 4.2.1. The performance requirement was a factor of safety of 1.25 which is the ratio of the soil's actual shear strength to that of the reduced strength at failure. Figure 5.23 shows that the required FOS of 1.25 is achieved.

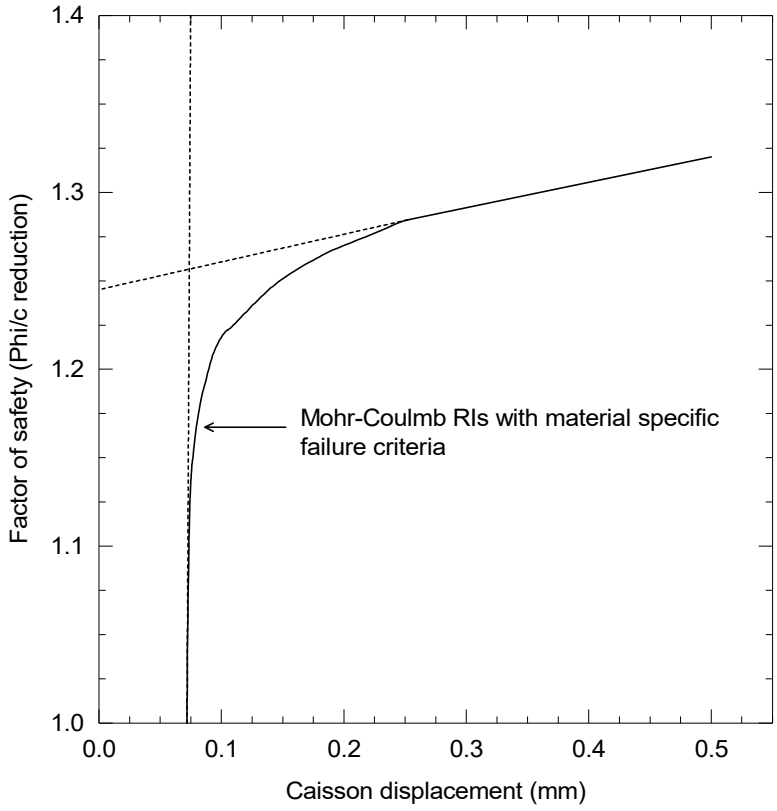

Figure 5.23 – FE Model 3-2 estimation of FOS against failure

Structural integrity of the RIs:

The structural integrity of the RIs was evaluated using FE Model 3-1 according to the methodology described in section 4.2.1. The behaviour of the RIs was evaluated at the ultimate limit state with partial factors on unfavourable actions and material strengths. It was established that the RIs are required to ensure stability. In this case the RIs were required to be reinforced over the length where they were not fully compressed (ASIRI, 2012). Table 5.5 to Table 5.7 present the structural forces, moments and stresses at the ultimate limit state.

The following was concluded regarding the structural integrity of the RIs:

- Lateral deflection of RIs "a" to "u" resulted in the development of bending tensile stresses. The RIs were required to guarantee stability (Domain 1), and therefore they are required to be reinforced over the length where they were fully compressed (ASIRI, 2012).
- RIs "v" to "z" remained in compression over their entire section. Therefore these RIs do not require reinforcement.
- The mobilised tensile force in the basal reinforcement was less than its long term design strength.

Changing the RI layout at edge of structure:

It is proposed that RIs "g" and "o" are repositioned further beneath the caisson toe which will result in the attraction of significantly greater axial load, increasing moment capacity and lowering the bending tensile stresses.

An alternative to conventional RI reinforcement suited to marine execution:

Steel fibre reinforced concrete (SFRC) is suggested as an alternative approach to conventional reinforcing. The conventional approach is to drive a reinforcing cage into the boring filled up with fresh concrete. The main problem with this approach is the difficult and time consuming execution of this operation in the marine environment. Cementitious matrices such as plain concrete have low tensile strength and fail in a brittle manner. Adding short needle-like fibres to such matrices enhances their mechanical properties, particularly their toughness, ductility and energy absorbing capacity under load (ACI, 2002). The addition of steel fibres to the concrete provides the concrete with post-cracking capacity which enables the structural member to develop a post-cracking flexural capacity without brittle failure (ACI, 2002). In terms of constructability Falkner & Henke, (1998) describe the application of SFRC for an underwater concrete slab in Berlin. This case study demonstrates the

handling of SFRC in difficult conditions such as placement underwater and pumping over large distances.

Table 5.5 – Table of forces for RIs ahead of the caisson toe at the ultimate limit state

	RIs in the passive zone ahead of the caisson toe					
RI reference	a	b	c	d	e	f
Distance from the center of the caisson	-25	-22.5	-20	-17.5	-15	-12.5
Max tensile force in geogrid (kN/m)	< 1	< 1	< 1	< 1	< 1	< 1
Location of maximum bending moment	-24.9	-25.9	-27.0	-28.1	-28.1	-28.1
Maximum bending moment, Mmax	366	354	355	411	411	453
Axial force at Mmax	51	66	95	149	223	429
Maximum compressive stress	-9031	-8772	-8861	-9457	-10420	-12010
Maximum tension	8788	8430	8379	8751	9323	9838
Location of maximum shear force	-20.1	-20.1	-29.6	-29.6	-29.6	-19.5
Maximum shear force	116	97	-106	-112	-118	-139

Table 5.6 – Table of forces for RIs supporting the caisson at the ultimate limit state

	RIs supporting the caisson								
RI reference	g	h	i	j	k	l	m	n	o
Dist. from center of caisson	-10	-7.5	-5	-2.5	0	2.5	5	7.5	10
Max tensile force in geogrid (kN/m)	41.41	16.17	10.25	16.92	9.22	10.90	12.45	20.34	18.33
Loc. of max. bending moment	-28.1	-28.1	-27.4	-26.5	-25.9	-25.9	-25.8	-25.9	-27.4
Max. bending moment	464	443	409	393	379	368	352	327	207
Axial force at Mmax	1322	2074	1936	1913	1831	1789	1651	1356	1063
Max compressive stress	-14420	-15720	-14830	-14210	-13660	-13290	-12580	-11390	-9942
Max tension	7953	5576	5051	4880	4727	4556	4517	4503	4752
Loc of max shear force	-20.5	-19.5	-19.5	-19.5	-19.5	-20.8	-20.8	-21.2	-29.6
Maximum shear force	124	-228	-196	-194	-142	110	104	89	-89

Table 5.7 – Table of forces for RIs supporting the backfill at the ultimate limit state

	RIs supporting the backfill										
RI reference	p	q	r	s	t	u	v	w	x	y	z
Dist. from center of caisson	12.5	15	17.5	20	22.5	25	27.5	30	32.5	35	37.5
Max tensile force in geogrid (kN/m)	23.10	33.20	34.37	19.03	19.40	46.29	29.51	26.60	11.30	12.52	6.12
Loc. of max. bending moment	-27.4	-27.4	-27.0	-26.3	-25.8	-24.9	-23.8	-21.6	-21.8	-22.7	-22.7
Max. bending moment	280	252	225	205	187	180	101	26	20	26	21
Axial force at Mmax	1162	1418	1407	1574	1512	1562	1686	1417	1493	1495	1421
Max compressive stress	-9672	-9577	-9008	-8817	-8330	-8334	-9352	-6882	-4893	-5302	-5828
Max tension	3904	2665	1968	1152	730	434	-1337	-1124	-779	-1159	-1104
Loc of max shear force	-20.8	-31.0	-31.0	-30.3	-21.6	-21.2	-20.5	-20.1	-20.1	-20.5	-20.3
Maximum shear force	72	-63	-55	-47	45	53	35	25	15	14	11

5.2.2 Performance in terms of deflections

Performance in terms of deflections was evaluated using FE model 3-1 according to the performance requirements described in section 4.2.2.

5.2.2.1 Crane rail gauge or span

Satisfying the tolerances for the crane rail gauge or span required checking that the horizontal distance between the front and rear crane rail did not vary by more than ± 30 mm. Table 5.8 shows that the deflections were within tolerance.

Table 5.8 – Deflection tolerance check on crane track gauge or span

LOADING PHASE	Front crane rail		Rear crane rail		Tolerance check			
	Incr. Def.*	Cum. Def.*	Incr. Def.*	Cum. Def.*	Tolerance	Guage	Out of guage	Out of tol.
	mm	mm	mm	mm	mm	m	mm	mm
Handover	**0.00**	**0.00**	**0.00**	**0.00**	**± 30**	**30.00**	0.0	0.0
Crane load	-3.25	-3.25	-2.99	**-2.99**	**± 30**	**30.00**	0.3	0.0
Unload crane	1.20	-2.05	1.07	**-1.92**	**± 30**	**30.00**	0.1	0.0
Mooring load	-0.69	-2.73	-0.24	**-2.16**	**± 30**	**30.00**	0.6	0.0
Unload mooring	0.59	-2.14	0.18	**-1.98**	**± 30**	**30.00**	0.2	0.0
Stacking load	0.30	-1.84	0.76	**-1.21**	**± 30**	**30.00**	0.6	0.0
Unload stack	0.39	-1.45	-0.08	**-1.30**	**± 30**	**30.00**	0.2	0.0
All transient loads*	-29.62	-31.08	-16.72	**-18.02**	**± 30**	**30.01**	13.1	0.0
All sustained loads	1.51	-29.57	0.97	**-17.05**	**± 30**	**30.01**	12.5	0.0
Consolidation (100%)	-0.12	-29.69	-0.17	**-17.22**	**± 30**	**30.01**	12.5	0.0
Unload all loads	0.48	-29.21	-0.07	**-17.29**	**± 30**	**30.01**	11.9	0.0

5.2.2.2 Crane rail alignment

Satisfying the tolerances for the crane rail alignment required checking that the overall alignment of the crane rail did not deviate by more than ± 30 mm from the true centre line of the rail. This is a horizontal deflection tolerance check. Table 5.9 shows that the deflections were out of tolerance by 1.1 mm which is considered acceptable.

Table 5.9 – Deflection tolerance check on crane rail alignment

LOADING PHASE	Front crane rail		Tolarance check		
	Incr. Def.*	Cum. Def.*	Tolerance	Crane rail out of alignment	Out of tolerance
	mm	mm	mm	mm	mm
Handover	**0.0**	**0.0**	**± 30**	**0.0**	0.0
Crane load	-3.2	-3.2	**± 30**	3.2	0.0
Unload crane	1.2	-2.0	**± 30**	2.0	0.0
Mooring load	-0.7	-2.7	**± 30**	2.7	0.0
Unload mooring	0.6	-2.1	**± 30**	2.1	0.0
Stacking load	0.3	-1.8	**± 30**	1.8	0.0
Unload stack	0.4	-1.5	**± 30**	1.5	0.0
All transient loads*	-29.6	-31.1	**± 30**	31.1	1.1
All sustained loads	1.5	-29.6	**± 30**	29.6	0.0
Consolidation (100%)	-0.1	-29.7	**± 30**	29.7	0.0
Unload all loads	0.5	-29.2	**± 30**	29.2	0.0

5.2.2.3 Crane rail level or allowable undulation

Satisfying the tolerances for the crane rail level required checking that the level did not vary by more than ± 30 mm over the total length of rail. This is a vertical deflection tolerance check. Table 5.10 shows that the deflections were within tolerance.

Table 5.10 – Deflection tolerance check on crane rail level

Loading Phase	Front crane	Tolerance check			Rear crane	Tolerance check		
	Cum. Def.*	Tolerance	Crane rail out of level	Out of tolerance	Cum. Def.*	Tolerance	Crane rail out of level	Out of tolerance
	mm	mm	mm	mm	mm	mm	mm	mm
Handover	**0.00**	**± 30**	**0.00**	0.00	**0.00**	**± 30**	**0.00**	0.00
Crane load	-5.24	**± 30**	5.24	0.00	-3.94	**± 30**	3.94	0.00
Unload crane	-3.19	**± 30**	3.19	0.00	-2.01	**± 30**	2.01	0.00
Mooring load	-3.43	**± 30**	3.43	0.00	-1.97	**± 30**	1.97	0.00
Unload mooring	-3.19	**± 30**	3.19	0.00	-2.00	**± 30**	2.00	0.00
Stacking load	-3.70	**± 30**	3.70	0.00	-4.94	**± 30**	4.94	0.00
Unload stack	-3.09	**± 30**	3.09	0.00	-3.22	**± 30**	3.22	0.00
All transient loads*	-11.98	**± 30**	11.98	0.00	-14.57	**± 30**	14.57	0.00
All sustained loads	-10.58	**± 30**	10.58	0.00	-14.26	**± 30**	14.26	0.00
Consolidation (100%)	-10.94	**± 30**	10.94	0.00	-15.12	**± 30**	15.12	0.00
Unload all loads	-9.09	**± 30**	9.09	0.00	-11.32	**± 30**	11.32	0.00

5.2.2.4 Relative crane rail heights

Satisfying the tolerances for relative height between crane rails required checking that the deviation between the seaside and landside crane rails did not exceed ± 30 mm. This is a vertical deflection tolerance check. Table 5.11 shows that the deflections were within tolerance.

Table 5.11 – Deflection tolerance check on crane rail level

LOADING PHASE	FRONT CRANE		REAR CRANE		TOLERANCE CHECK		
	Incr. Def.*	Cum. Def.*	Incr. Def.*	Cum. Def.*	Tolerance	Relative crane rail height	Out of tolerance
	mm	mm	mm	mm	mm	mm	mm
Handover	**0**	**0**	**0**	**0**	**± 10**	0.0	0.0
Crane load	-5.24	-5.2	-3.94	-3.9	**± 10**	1.3	0.0
Unload crane	2.05	-3.2	1.93	-2.0	**± 10**	1.2	0.0
Mooring load	-0.24	-3.4	0.04	-2.0	**± 10**	1.5	0.0
Unload mooring	0.24	-3.2	-0.03	-2.0	**± 10**	1.2	0.0
Stacking load	-0.51	-3.7	-2.94	-4.9	**± 10**	1.2	0.0
Unload stack	0.62	-3.1	1.72	-3.2	**± 10**	0.1	0.0
All transient loads*	-8.89	-12.0	-11.35	-14.6	**± 10**	2.6	0.0
All sustained loads	1.40	-10.6	0.31	-14.3	**± 10**	3.7	0.0
Consolidation (100%)	-0.36	-10.9	-0.86	-15.1	**± 10**	4.2	0.0
Unload all loads	1.84	-9.1	3.81	-11.3	**± 10**	2.2	0.0

Chapter 6 Conclusions and Recommendations

6.1 Conclusions

The main objective of this study was to determine whether rigid inclusions are suitable for reinforcement of the foundation of a caisson container quay wall. Their suitability was assessed in terms of caisson deflection criteria and RI structural criteria. For a soft to firm clay subsoil condition the RIs studied met the foundation performance criteria for this structural application provided:

- strategies to limit lateral loading were implemented and
- the RIs were reinforced over the length where they were not fully compressed.

While this study provided insights into the behaviour of RIs for this structural application, ultimately suitability is a function of range of factors, in addition to the limited technical performance criteria derived for this study.

The following can be concluded with respect to the sub-objectives for this study:

The mechanics of the problem, analysis method and execution

- The “rigid” loading from the caisson and “flexible” loading from the backfill affected the way load was transferred to the underlying foundation. The presence of both boundary conditions meant that the all the load transfer mechanisms presented in section 2.2.4 to 2.2.7 were relevant to this problem.
- The reinforced foundation was subjected to combined vertical and lateral loading. The effect of lateral loading was to reduce the ability of foundation to carry the vertical load.
- The main disturbing force was the vertical self-weight of the caisson and backfill. A secondary disturbing force was the outward lateral thrust of the caisson and backfill.

- The main resisting force was the shear resistance of clay and secondary resisting forces were the shear resistance of backfill and the reinforcement elements.
- Reinforcement acted to reduce the forces causing failure and increased the forces resisting failure. Rigid inclusions reduced the vertical load on the foundation and resisted lateral ground movement. Basal reinforcement acted to sustain the outward shear stresses and to restrain the surface of the foundation soil against lateral movement.
- Individual RIs in a group failed in different ways, depending on their location relative to the caisson and relative to the active, transitional and passive zones in the foundation.
- Three-dimensional numerical modelling was able to simulate the behaviour of this complex three dimensional field situation.
- The vibro-driven cast in situ soil displacement method (VCC) was selected as the most suitable technique for marine execution.

Suitable strategies for limiting lateral ground movement:

- Modifying the backfill load by strengthening and stiffening the backfill material.
- Providing additional structural support by using rigid inclusions to support the backfill and adding basal reinforcement in the LTP.
- Improving the subsoil by excavation and replacement with crushed stone; thickening the LTP.
- Improving the subsoil by reducing the rate of loading and allowing the beneficial effects of consolidation to take place.

Foundation performance criteria in terms of stability:

- In terms of stability, it was verified that the foundation and structural elements do not fail; importantly the RIs are considered as structural elements and not just settlement reducing elements.
- Internal structural integrity of the RIs was assessed according to the following recommendations from the ASIRI (2012) guidelines: “Where inclusions are required to guarantee stability (Domain 1), the inclusions must be reinforced over the length where they are not fully compressed”; “Where inclusions are not required to guarantee stability (Domain 2), it is proposed not to reinforce the inclusions, provided the maximum tensile force in the concrete can be justified”.

Foundation performance criteria in terms of deformations:

- The critical settlement and deflection criteria for a container terminal structure relate to the STS crane rail tolerances. A horizontal and vertical deflection tolerance of less than 30 mm was selected for this study. Specific verification checks were carried out for crane rail gauge, crane rail alignment, crane rail level and relative crane rail heights.

Technical appraisal of the numerical model results:

- Lateral deflection of RIs “a” to “u” resulted in the development of bending tensile stresses. The RIs were required guarantee stability (Domain 1), and therefore it was proposed that they are reinforced over the length where they are not fully compressed.
- RIs “v” to “z” remained in compression over their entire section. It was therefore proposed not to reinforce these inclusions.
- Provided the RIs are reinforced the performance requirements in terms of crane rail deflection tolerances are achieved.
- Unreinforced RIs failed due to the development of bending tensile stresses in excess of tensile capacity of the concrete, which resulted in the development of a plastic hinge. The specific failure mode of each inclusion was dependent on its location relative to the slip surface.

An alternative to conventional reinforcement suited to marine execution:

- The use of steel fibre reinforced concrete (SFRC) is suggested as an alternative to conventional reinforcing of the RIs.
- The addition of steel fibres provides the concrete with post-cracking capacity which enables the structural member to develop a post cracking flexural capacity without brittle failure (ACI, 2002).
- It remains to be shown by calculation within the framework of a relevant code that SFRC provides adequate structural capacity to resist the forces and moments presented in Chapter 4.

6.2 Recommendations for Further Research

Physical model testing:

Centrifuge modelling is proposed to validate the numerical model and confirm the load transfer mechanisms and geotechnical behaviour of the caisson and RIs. With any type of physical modelling you should always start out with a prediction of what you expect to happen (Wood, 2003). The numerical model results presented in Chapter 5 are a prediction of the expected behaviour for the problem presented in this study.

Numerical modelling:

A sensitivity analysis is recommended to determine which model input parameters have the most influence on the key model outputs. Additionally based on the results of the sensitivity study a parametric study of the critical input parameters is recommended. The critical input parameters are varied between permissible ranges in order to determine the probable range of critical outputs (Lees, 2016).

Additional suitability criteria:

The suitability of RIs for this structural application should be assessed in terms of economic viability and risk, by comparing the technique with other more established ground reinforcement methods for this structural application.

Structural analysis of SFRC for the application of RIs:

It remains to be shown by calculation within the framework of a relevant code that SFRC provides adequate structural capacity to resist the forces and moments presented in Chapter 5.

References

van ‘t Hoff, J. & van der Kolff, A.N. 2013. *Hydraulic Fill Manual: For Dredging and Reclamation Works*. CRC press.

ACI. 2002. State-of-the-Art Report on Fiber Reinforced Concrete Reported by ACI Committee 544. *ACI Structural Journal*. 96(Reapproved).

API. 2005. *Recommended practice for planning, designing and constructing fixed offshore platforms : working stress design.* Washington, D.C.: American Petroleum Institute.

Araei, a A., Soroush, A. & Rayhani, M. 2010. Large-Scale Triaxial Testing and Numerical Modeling of Rounded and Angular Rock ll Materials. *Civil Engineering*. 17(3).

ASIRI. 2012. *Recommandations pour le dimensionnement, l’execution et le controle de l’amelioration des sols de fondation par inclusions rigides*. Paris: Presses des Ponts.

Balasubramaniam, A.S., Cai, H., Zhu, D., Surarak, C. & Oh, E.Y.N. 2010. Settlements of embankments in soft soils. *Geotechnical Engineering Journal of the SEAGS & AGSSEA*. 41(2):1–19.

Balfour Beatty. 2016. *Balfour Beatty Ground Engineering Vibro Concrete Columns Technical Datasheet*. Balfour Beatty. Available: http://www.balfourbeatty.com/media/28610/vcc-web.pdf.

Benz, T. 2007. Small-strain stiffness of soils and its numerical consequences. Ph.D. Thesis. Mitteilungen des Institutes für Geotechnik. Universität Stuttgart.

Bjerrum, L., Johannessen, I.J. & Eide, O. 1969. Reduction of negative skin friction on steel piles to rock. In *Proc. 7th ICSMFE, Vol. 2*. Mexico City. 27–34.

Blanc, M., Rault, G., Thorel, L., Almeida, M.C.F. & Almeida, M.S.S. 2012. Centrifuge investigation of the load transfer mechanism above rigid inclusions. In *Eurofuge 2012, Delft, The Netherlands, April 23-24*.

Blanc, M., Rault, G., Thorel, L. & Almeida, M. 2013. Centrifuge investigation of load transfer mechanisms in a granular mattress above a rigid inclusions network. *Geotextiles and Geomembranes*. 36:92–105. DOI: 10.1016/j.geotexmem.2012.12.001.

Bolton, M.D. 1986. The strength and dilatancy of sands. *Géotechnique*. 36(1):65–78. DOI:

10.1680/geot.1986.36.1.65.

Den Boogert, T.J.M. 2011. Piled embankments with geosynthetic reinforcement: numerical analysis of scale model tests. MSc Thesis. Delft University of Technology.

Bourges, F. & Mieussens, C. 1979. Déplacements latéraux à proximité des remblais sur sols compressibles. Méthode de prévision. *Bulletin de liaison des Laboratoires des Ponts et Chaussées*. 101:73–100.

Bowles, J.E. 1996. *Foundation analysis and design*. 5th ed. McGraw-hill.

Bozozuk, M. 1972. Downdrag measurements on a 160-ft floating pipe test pile in marine clay. *Canadian Geotechnical Journal*. 9(2):127–136. DOI: 10.1139/t72-014.

Brinkgreve, R.B.J. 2005. Selection of Soil Models and Parameters for Geotechnical Engineering Application. In *Soil Constitutive Models: Evaluation, Selection, and Calibration (Geotechnical Special Publication No. 128)*. Reston, VA: American Society of Civil Engineers. 69–98. DOI: 10.1061/40771(169)4.

Brinkgreve, R.B.J. 2013. *Validating numerical modelling in geotechnical engineering*. National Agency for Finite Element Methods & Standards (NAFEMS).

Brinkgreve, R.B.J. & Bakker, H. 1991. Non-linear finite element analysis of safety factors. In *Proc. 7th Int. Conf. on Computer Methods and Advances in Geomechanics*. Cairns, Australia. 1117–1122.

Brinkgreve, R.B.J., Engin, E. & Engin, H.K. 2010. Validation of empirical formulas to derive model parameters for sands. In *Numerical Methods in Geotechnical Engineering - NUMGE 2010*. T. Benz & S. Nordal, Eds. CRC Press. 137–142. DOI: 10.1201/b10551-25.

Brinkgreve, R.B.J., Kumarswamy, S. & Swolfs, W.M. 2016. *PLAXIS Material Models Manual*. Build B327 ed. Delft University of Technology and PLAXIS bv, The Netherlands.

Broms, B.B. 1972. Stabilization of slopes with piles. In *Proceedings of the 1st International Symposium on Landslide Control*. Kyoto. 115–123.

Broms, B.B. 1999. Keynote lecture: Design of lime, lime/cement and cement columns. In *International Conference on Dry Mix Methods: Dry Mix Methods for Deep Soil Stabilization*. Stockholm, Sweden: Balkema, Rotterdam. 125–154.

Broms, B.B. 2004. Lime and lime/cement columns. In *Ground Improvement*. Second ed. M. Moseley & K. Kirsch, Eds. Oxon: Spon Press. 252–330.

BS 8004. 2015. *Code of practice for foundations (BS 8004:2015)*. British Standards Institution (BSI).

BS 8006. 2010. *Code of practice for strengthened / reinforced soils and other fills (BS 8006-1:2010+A1:2016)*. British Standards Institution (BSI).

Buschmeier, B., Masse, F., Swift, S. & Walker, M. 2012. Full Scale Instrumented Load Test for Support of Oil Tanks on Deep Soft Clay Deposits in Louisiana using Controlled Modulus Columns. In *Proceedings of the 18th International Conference on Soil Mechanics and Geotechnical Engineering*. Paris. 359–372.

Cao, X.D., Wong, I.H. & Chang, M.F. 2004. Behavior of Model Rafts Resting on Pile-Reinforced Sand. *Journal of Geotechnical and Geoenvironmental Engineering*. 130(2):129–138. DOI: 10.1061/(ASCE)1090-0241(2004)130:2(129).

Carlsson, B. 1987. Armerad jord beräkningsprinciper för vertikala väggar, branta slänter, bankar pa lös undergrund, bankra papalar. *Terrateam AB*.

Carter, M. & Bentley, S.P. 2016. *Soil Properties and their Correlations*. John Wiley & Sons.

Chen, Y.M., Cao, W. & Chen, R.P. 2008. An experimental investigation of soil arching within basal reinforced and unreinforced piled embankments. *Geotextiles and Geomembranes*. 26(2):164–174. DOI: 10.1016/j.geotexmem.2007.05.004.

Chevalier, B., Villard, P. & Combe, G. 2010. Investigation of load-transfer mechanisms in geotechnical earth structures with thin fill platforms reinforced by rigid inclusions. *International Journal of Geomechanics*. (June):239–251. DOI: 10.1061/(ASCE)GM .1943-5622.0000083.

Chow, Y.K., Yong, K.Y. & Shen, W.Y. 2001. Analysis of Piled Raft Foundations Using a Variational Approach. *International Journal of Geomechanics*. 1(2):129–147. DOI: 10.1061/(ASCE)1532-3641(2001)1:2(129).

Chu, J., Varaksin, S., Klotz, U. & Mengé, P. 2009. State of the art report: construction processes. In *17th International Conference on Soil Mechanics & Geotechnical Engineering: TC17 meeting ground improvement, Alexandria*. J. Chu, S. Varaksin, U. Klotz, & P. Mengé, Eds. 1–130.

Coghlan, K., Plomteux, C. & Racinais, J. 2016. Execution and Engineering Principels of Controlled Modulus Columns (CMC). In *Proceedings of the First Southern African Geotechnical Conference*. S. Jacobsz, Ed. CRC Press. 19–24.

Cooke, R.W. 1986. Piled raft foundations on stiff clays - a contribution to design philosophy. *Géotechnique*. 36(2):169–203. DOI: 10.1680/geot.1986.36.2.169.

Cuira, F. & Simon, B. 2009. Two simple tools for evaluation the complex interactions in a soil reinforced by rigid inclusions. *Proceedings of the 17th International Conference on Soil Mechanics and Geotechnical Engineering*. 1163–1166.

Davies, P.R.E. & McIlquham, J.D. 2011. Geotechnical design for the Port Botany expansion project, Sydney. *Proceedings of the Institution of Civil Engineers - Geotechnical Engineering*. 164(3):149–167. DOI: 10.1680/geng.10.00052.

Davis, E.H. & Poulos, H.G. 1972. The analysis of piled raft systems. *Australia Geotechnique Journal*. 2(1):21–27.

Dawson, E.M., Roth, W.H. & Drescher, A. 1999. Slope stability analysis by strength reduction. *Géotechnique*. 49(6):835–840. DOI: 10.1680/geot.1999.49.6.835.

Dias, D. & Simon, B. 2012. Spread foundations on rigid inclusions subjected to complex loading : Comparison of 3D numerical and simplified analytical modelling. In *Proceedings of the 18th International Conference on Soil Mechanics and Geotechnical Engineering*. 411–421.

Dias, D., Grippon, J. & Nunez, M. 2012. Behavior of a Pile-Supported Embankment using rigid piles with variable inertia General information. In *Proceedings of the 18th International Conference on Soil Mechanics and Geotechnical Engineering*. 401–410.

Dobry, R., Pecker, A., Mavroeidis, G., Zeghal, M., Gohl, B. & Yang, D. 2003. Damping/global energy balance in FE model of bridge foundation lateral response. *Soil Dynamics and Earthquake Engineering*. 23(6):483–495. DOI: 10.1016/S0267-7261(03)00050-2.

Dusko, A. 2009. Mohr-Coulomb parameters for modelling of concrete structures. *Plaxis Bulletin*. (25):12–15.

EAB. 2008. *Recommendations on Excavations (EAB)*. 2nd ed. German Geotechnical Society. John Wiley & Sons.

EAU. 2015. *Recommendations of the Committee for Waterfront Structures Harbours and Waterways: EAU 2012*. 9th ed. John Wiley & Sons.

van Eekelen, S.J.M., Bezuijen, A. & Oung, O. 2003. Arching in piled embankments; experiments and design calculations. In *Proceedings of Foundations: Innovations, observations, design and practice*. 885–894.

van Eekelen, S.J.M., Bezuijen, A., Lodder, H.J. & van Tol, A.F. 2012. Model experiments on piled embankments. Part II. *Geotextiles and Geomembranes*. 32:82–94. DOI: 10.1016/j.geotexmem.2011.11.003.

van Eekelen, S.J.M., Bezuijen, A. & van Tol, A.F. 2013. An analytical model for arching in piled embankments. *Geotextiles and Geomembranes*. 39:78–102. DOI: 10.1016/j.geotexmem.2013.07.005.

van Eekelen, S.J.M., Bezuijen, a. & van Tol, a. F. 2015. Validation of analytical models for the design of basal reinforced piled embankments. *Geotextiles and Geomembranes*. 43(1):56–81. DOI: 10.1016/j.geotexmem.2014.10.002.

Ellis, E.A. & Springman, S.M. 2001. Modelling of soil–structure interaction for a piled bridge abutment in plane strain FEM analyses. *Computers and Geotechnics*. 28(2):79–98. DOI: 10.1016/S0266-352X(00)00025-2.

Ellis, E. & Aslam, R. 2009a. Arching in piled embankments: comparison of centrifuge tests and predictive methods - part 1 of 2. *Ground Engineering*. 1:1–5.

Ellis, E. & Aslam, R. 2009b. Arching in piled embankments: comparison of centrifuge tests and predictive methods - part 2 of 2. *Ground Engineering*. 2:28–30.

Falkner, H. & Henke, V. 1998. Application of steel fibre concrete for underwater concrete slabs. *Cement and Concrete Composites*. 20(5):377–385. DOI: 10.1016/S0958-9465(98)00005-5.

Farag, G. 2008. Lateral spreading in basal reinforced embankments supported by pile-like elements. Ph. D. Thesis. Universität Kassel. Institut für Geotechnik und Geohydraulik. Kassel Univ. Press.

Fellenius, B.H. 1984. Negative Skin Friction and Settlement of Piles. In *Second International Seminar, Pile Foundations, Nanyang Technological Institute*. Singapore. 1–12.

Fellenius, B.H. 2006. Results from long-term measurement in piles of drag load and downdrag. *Canadian Geotechnical Journal*. 43(4):409–430. DOI: 10.1139/t06-009.

Fellenius, B.H. 2013. Pile Foundations. In *Foundation engineering handbook*. H.-Y. Fang, Ed. Springer Science & Business Media. 511–536.

Filz, G.M. & Navin, M.P. 2006. *Stability of column-supported embankments (Final contract report, VTRC 06-CR13)*. Virginia Center for Transportation Innovation and Research.

Fioravante, V. & Giretti, D. 2010. Contact versus noncontact piled raft foundations. *Canadian Geotechnical Journal*. 47(11):1271–1287. DOI: 10.1139/T10-021.

Fleming, K., Weltman, A., Randolph, M. & Elson, K. 2009. *Piling engineering*. London; New York: Taylor & Francis.

Fok, N., Qiu, T., Vincent, P. & Kreminsky, M. 2012. A Case Study of Ground Improvement using Semi-Rigid Inclusions for Breakwater Road Bridge. In *Proceedings of the International Conference on Ground Improvement & Ground Control*. V. 45. 629–643. DOI: 10.3850/978-981-07-3559-3_02-0028.

German Geotechnical Society. 2012. Reinforced Earth Structures over Point or Linear Bearing Elements. In *Recommendations for Design and Analysis of Earth Structures using Geosynthetic Reinforcements - EBGEO*. Berlin, Germany: Ernst & Sohn Verlag für Architektur und technische Wissenschaften GmbH & Co. KG. 151–200. DOI: 10.1002/9783433600931.ch9.

Girout, R., Blanc, M., Dias, D. & Thorel, L. 2014. Numerical analysis of a geosynthetic-reinforced piled load transfer platform – Validation on centrifuge test. *Geotextiles and Geomembranes*. 42(5):525–539. DOI: 10.1016/j.geotexmem.2014.07.012.

Graham, J. 2006. The 2003 R.M. Hardy Lecture: Soil parameters for numerical analysis in clay. *Canadian Geotechnical Journal*. 43(2):187–209. DOI: 10.1139/t05-098.

Griffiths, D.V. V & Lane, P.A. 2001. Slope stability analysis by finite elements. *Géotechnique*. 51(7):653–654.

DOI: 10.1680/geot.51.7.653.51390.

Hamidi, B., Nikraz, H., Debats, J.. & Varaksin, S. 2013. Offshore ground improvement records. *Aust. Geomech. J. Australian Geomechanics Journal*. 48(4):111–122.

Han, J. 2015. *Principles and Practice of Ground Improvement*. John Wiley & Sons.

Han, J., Chai, J.-C., Leshchinsky, D. & Shen, S.-L. 2004. Evaluation of Deep-Seated Slope Stability of Embankments over Deep Mixed Foundations. In *GeoSupport 2004*. Reston, VA: American Society of Civil Engineers. 945–954. DOI: 10.1061/40713(2004)71.

Han, J., Parsons, R.J., Sheth, A.R. & Huang, J. 2005. Factors of safety against deep-seated failure of embankments over deep mixed columns. In *Proceedings of Deep Mixing 2005 Conference*. V. 1. 231–236.

Handy, R.L. 1987. Closure to " The Arch in Soil Arching " by Richard L. Handy (March, 1985, Vol. 111, No. 3). *Journal of Geotechnical Engineering*. 113(3):275–277. DOI: 10.1061/(ASCE)0733-9410(1987)113:3(275).

Head, K.H. 1992. *Manual of soil laboratory testing: Permeability, shear strength and compressibility tests*. V. 2. New York: Halsted Press.

Le Hello, B. & Villard, P. 2009. Embankments reinforced by piles and geosynthetics—Numerical and experimental studies dealing with the transfer of load on the soil embankment. *Engineering Geology*. 106(1–2):78–91. DOI: 10.1016/j.enggeo.2009.03.001.

Hewlett, W.J. & Randolph, M.F. 1988. Analysis of piled embankments. In *International Journal of Rock Mechanics and Mining Sciences and Geomechanics Abstracts*. V. 25. Elsevier Science. 297–298.

Hill, J.R. 2013. Ground improvement techniques allow flexibility for ports. *Port Technology International*. (60):29–30.

Horikoshi, K. & Randolph, M.F. 1996. Centrifuge modelling of piled raft foundations on clay. *Géotechnique*. 46(4):741–752. DOI: 10.1680/geot.1996.46.4.741.

Iglesia, G.R., Einstein, H.H. & Whitman, R. V. 2014. Investigation of Soil Arching with Centrifuge Tests. *Journal of Geotechnical and Geoenvironmental Engineering*. 140(2):4013005. DOI: 10.1061/(ASCE)GT.1943-5606.0000998.

Inagaki, M., Abe, T., Yamamoto, M., Nozu, M., Yanagawa, Y. & Li, L. 2002. Behavior of cement deep mixing columns under road embankment. In *Physical modelling in Geotechnics: ICPMG'02*. 967–972.

Jardine, R., Chow, F., Overy, R. & Standing, J. 2005. *ICP design methods for driven piles in sands and clays*. London: Thomas Telford.

Jenck, O., Dias, D. & Kastner, R. 2009. Discrete element modelling of a granular platform supported by piles in soft soil – Validation on a small scale model test and comparison to a numerical analysis in a continuum.

Computers and Geotechnics. 36(6):917–927. DOI: 10.1016/j.compgeo.2009.02.001.

Jewell, R.A. 1988. The mechanics of reinforcede bankments on soft soils. *Geotextiles and Geomembranes*. 7(4):237–273. DOI: 10.1016/0266-1144(88)90001-5.

Jones, G.A. & Davies, P. 1985. Soft clays : problem soils in South Africa - state of the art. *Civil Engineer in South Africa*. 27(7):355–265.

Kelesoglu, M.K. & Springman, S.M. 2011. Analytical and 3D numerical modelling of full-height bridge abutments constructed on pile foundations through soft soils. *Computers and Geotechnics*. 38(8):934–948. DOI: 10.1016/j.compgeo.2011.07.011.

Kempfert, H.-G. & Raithel, M. 2005. Soil improvement and foundation systems with encased columns and reinforced bearing layers. In *Ground improvement: Case histories*. Amsterdam: Elsevier. 923–947.

Kempfert, H.-G., Dieter, E.K. & Smoltczyk, U. 2003. Pile foundations. In *Geotechnical engineering handbook Volume 3*. Berlin: Ernst & Sohn Verlag. 82–227.

Kirstein, J., Wittorf, L. & Wittorf, N. 2012. Rigid inclusions in combination with fast wick drain consolidation as soil improvement method in very soft and fat northern German clay. In *Proceedings of the 18th International Conference on Soil Mechanics and Geotechnical Engineering*. V. 202. 469–479.

Kirstein, J.F., Ahner, C., Uhlemann, S. & Uhlich, P. 2013. Ground improvement methods for establishment of the federal road B 176 on a new elevated dump in the brown coal area of MIBRAG. In *Proceedings of the 18th International Conference on Soil Mechanics and Geotechnical Engineering*. 453–468.

Kitazume, M. 2005. *The sand compaction pile method*. Leiden; New York: A.A. Balkema Publishers.

Kitazume, M. 2008. *Stability of Group Column Type DM under Embankment Loading Behavior of Sheet Pile Quay Wall. Report of The Port and Harbour Research Institute Japan*. V. 47.

Kitazume, M. & Terashi, M. 2013a. *The deep mixing method*. 1st ed. Boca Raton : CRC Press, Taylor & Francis Group.

Kitazume, M. & Terashi, M. 2013b. Design of improved ground by the deep mixing method. In *The Deep Mixing Method*. CRC Press. 263–367. DOI: 10.1201/b13873-7.

Kitazume, M., Ikeda, T., Miyajima, S. & Karastanev, D. 1996. Bearing capacity of improved ground with column type DMM. In *Grouting and deep mixing : proceedings of IS-Tokyo'96, the Second International Conference on Ground Improvement Geosystems, Tokyo 14-17 May 1996*. R. Yonekura, M. Terashi, & M. Shibazaki, Eds. A.A. Balkema. 503–508.

Kitazume, M., Okano, K. & Miyajima, S. 2000. Centrifuge Model Tests on Failure Envelope of Column Type Deep Mixing Method Improved Ground. *Soils and foundations*. 40(4):43–55.

Kivelö, M. 1998. Stabilization of embankments on soft soil with lime/cement columns. Royal Institute of Technology, Sweden.

Lade, P. V. 2005. Overview of Constitutive Models For Soils. In *Calibration of Constitutive Models*. Reston, VA: American Society of Civil Engineers. 1–34. DOI: 10.1061/40786(165)1.

Lees, A. 2012. *Obtaining geotechnical parameters for numerical analysis*. NAFEMS.

Lees, A. 2016. *Geotechnical finite element analysis : a practical guide*. London: ICE Publishing.

Leung, C.F. & Shen, R.F. 2008. Performance of gravity caisson on sand compaction piles. *Canadian Geotechnical Journal*. 45(3):393–407. DOI: 10.1139/T07-093.

Mayne, P.W. & Kulhawy, F.H. 1982. Ko- OCR Relationships in Soil. *Journal of the Soil Mechanics and Foundations Division*. 108(6):851–872.

McGuire, M., Sloan, J., Collin, J. & Filz, G. 2012. Critical Height of Column-Supported Embankments from Bench-Scale and Field-Scale Tests. In *Proceedings of the 18th International Conference on Soil Mechanics and Geotechnical Engineering*. 481–490.

Menard. 2016a. *Applicable soils for various ground improvement techniques*. Available: http://www.menardgroupusa.com/solutions/controlled-modulus-column-rigid-inclusions-for-ground-improvement [2016, November 16].

Menard. 2016b. *Menard Vibro Concrete Columns (VCC) Technical Datasheet*. Menard. Available: http://www.vibromenard.co.uk/wp-content/uploads/2011/09/VCC.pdf.

Miao, L.F., Goh, A.T.C., Wong, K.S. & Teh, C.I. 2006. Three-dimensional finite element analyses of passive pile behaviour. *International Journal for Numerical and Analytical Methods in Geomechanics*. 30(7):599–613. DOI: 10.1002/nag.493.

Naughton, P.J. 2007. The Significance of Critical Height in the Design of Piled Embankments. In *Soil improvement (GSP 172)*. Reston, VA: American Society of Civil Engineers. 1–10. DOI: 10.1061/40916(235)3.

Navin, M.P. 2005. Stability of embankments founded on soft soil improved with deep-mixing-method columns. Ph.D. Thesis. Virginia Polytechnic Institute and State University.

Nicks, J. & Adams, M. 2013. *Friction Angles of Open-Graded Aggregates From Large-Scale Direct Shear Testing. (N0. FHWA-HRT-13-068)*.

Okyay, U.S., Dias, D., Thorel, L. & Rault, G. 2014. Centrifuge Modeling of a Pile-Supported Granular Earth-Platform. *Journal of Geotechnical and Geoenvironmental Engineering*. 140(2):4013015. DOI: 10.1061/(ASCE)GT.1943-5606.0001004.

Oteo, C.S. 1977. Horizontally loaded piles-deformation influence. In *Proc. of 9th ICSMFE, Specialty session*. V.

10. 101–106.

Peet, T. Van Der. 2014. Arching in basal reinforced piled embankments. MSc. Thesis. Delft University of Technology.

Potts, D. 2002. *Guidelines for the use of advanced numerical analysis*. London: Thomas Telford.

Potts, D.M. & Zdravkovic, L. 1999. *Finite Element Analysis in Geotechnical Engineering: Volume One - Theory*. V. 1. Thomas Telford Ltd. DOI: 10.1680/feaiget.27534.

Poulos, H.G. 1995. Design of reinforcing piles to increase slope stability. *Canadian Geotechnical Journal*. 32(5):808–818. DOI: 10.1139/t95-078.

Poulos, H.G. 1997. Piles subjected to negative friction: a procedure for design. *Geotechnical Engineering*. 28(1).

Poulos, H.G. 2001. Piled raft foundations: design and applications. *Géotechnique*. 51(2):95–113. DOI: 10.1680/geot.2001.51.2.95.

Poulos, H.G. 2009. Discussion: A practical design approach for piles with negative friction. *Proceedings of the Institution of Civil Engineers - Geotechnical Engineering*. 162(3):187–188. DOI: 10.1680/geng.2009.162.3.187.

Poulos, H.G. & Davis, E.H. 1980. *Pile foundation analysis and design*. New York: John Wiley & Sons.

Prandtl, L. 1921. Hauptaufsätze: Über die eindringungsfestigkeit (härte) plastischer baustoffe und die festigkeit von schneiden. *ZAMM-Journal of Applied Mathematics and Mechanics/Zeitschrift für Angewandte Mathematik und Mechanik*. 1(1):15–20.

Randolph, M.F. 2003. Science and empiricism in pile foundation design. *Géotechnique*. 53(10):847–875. DOI: 10.1680/geot.2003.53.10.847.

Reid, W.M. & Buchanan, N.W. 1984. PAPER 21 Bridge approach support piling. In *Piling and ground treatment*. Thomas Telford Publishing. 267–274. DOI: 10.1680/pagt.01855.0028.

Roscoe, K. & Burland, J.B. 1968. On the generalized stress-strain behaviour of wet clay. In *Engineering Plasticity*. Cambridge. Cambridge Univeristy Press. 535–609.

Satibi, S. 2009. Numerical analysis and design criteria of embankments on floating piles. Ph.D. Thesis. Univiverity Stuttgart. Inst. f. Geotechnik.

Schanz, T., Vermeer, A. & Bonnier, P. 1999. The hardening soil model: formulation and verification. In *International Symposium: Beyond 2000 in Computational Geotechnics*. Amsterdam: Balkema, Rotterdam. 281.

Seaman, J.W. 1994. *A guide to accomodating or avoiding soil-induced lateral loading of piled foundations for highway bridges*. Project report- Transport Research Laboratory (TRL Limited).

Simon, B. 2012. General Report - Session 5 - Rigid Inclusions and Stone Columns. In *Proceedings of the 18th International Conference on Soil Mechanics and Geotechnical Engineering*. Brussels, Belgium.

Simon, B. & Schlosser, F. 2006. Soil reinforcement by vertical stiff inclusions in France. In *Symposium Rigid Inclusions in difficult subsoil conditions, ISSMGE TC36, Sociedad Mexicana de Mecanica de Suelos*. Mexico.

Stewart, D.P. 1992. Lateral loading of piled bridge abutments due to embankment construction. Ph.D. Thesis. University of Western Australia.

Stewart, D.P., Jewell, R.J. & Randolph, M.F. 1991. Embankment loading of piled bridge abutments on soft clay. In *Proc International Conference on Geotechnical Engineering for Coastal Development*. V. 1. Yokahama: Coastal Development Institute of Technology. 741–746.

Stewart, D.P., Jewell, R.J. & Randolph, M.F. 1994. Design of piled bridge abutments on soft clay for loading from lateral soil movements. *Géotechnique*. 44(2):277–296. DOI: 10.1680/geot.1994.44.2.277.

Stolle, D.F.E., Bonnier, P.G. & Vermeer, P.A. 1997. A soft soil model and experiences with two integration schemes. In *Numerical Models in Geomechanics*. V. 1. Montreal: AA Balkema. 123–128.

Surarak, C., Likitlersuang, S., Wanatowski, D., Balasubramaniam, A., Oh, E. & Guan, H. 2012a. Stiffness and strength parameters for hardening soil model of soft and stiff Bangkok clays. *Soils and Foundations*. 52(4):682–697. DOI: 10.1016/j.sandf.2012.07.009.

Surarak, C., Likitlersuang, S., Wanatowski, D., Balasubramaniam, A., Oh, E. & Guan, H. 2012b. Stiffness and strength parameters for hardening soil model of soft and stiff Bangkok clays. *Soils and Foundations*. 52(4):682–697. DOI: 10.1016/j.sandf.2012.07.009.

Terzaghi, K., Peck, R.B. & Mesri, G. 1996. *Soil mechanics in engineering practice*. John Wiley & Sons.

Tschuchnigg, F., Schweiger, H.F., Sloan, S.W., Lyamin, A.V. & Raissakis, I. 2015. Comparison of finite-element limit analysis and strength reduction techniques. *Géotechnique*. 65(4):249–257. DOI: 10.1680/geot.14.P.022.

Vermeer, P.A. & Neher, H.P. 1999. A soft soil model that accounts for creep. In *International Symposium: Beyond 2000 in Computational Geotechnics*. 249–261.

Villard, P., Chevalier, B., Le Hello, B. & Combe, G. 2009. Coupling between finite and discrete element methods for the modelling of earth structures reinforced by geosynthetic. *Computers and Geotechnics*. 36(5):709–717. DOI: 10.1016/j.compgeo.2008.11.005.

White, D.J. 2005. A general framework for shaft resistance on displacement piles in sand. In *Proceedings of the 1st International Symposium on Frontiers in Offshore Geotechnics, ISFOG 2005*. Taylor and Francis. 697–704.

Wood, D.M. 2003. *Geotechnical modelling*. V. 1. CRC Press.

Woodward, J. 2005. *An introduction to geotechnical processes*. CRC Press.

Wroth, C.P. 1984. The interpretation of in situ soil tests. *Geotechnique*. 34(4):449–489.

WSC. 2015. Some Observations on Port Congestion, Vessel Size and Vessel Sharing Agreements. *World Shipping Council*.

ZAA. 2015. *Internal report*. ZAA Engineering Projects and Naval Architecture (Pty) Ltd.

Zienkiewicz, O.C. & Taylor, R.L. 1977. *The finite element method*. V. 3. McGraw-hill London.

Appendix A Analytical Calculations

A.1 Undrained bearing capacity of a foundation subjected to an inclined eccentric load

The geometrical details of the problem are discussed in section 3.2 and shown in Figure 3.4b. The bearing capacity calculation is carried out at the base of the LTP which is 3 m thick. The forces acting on the caisson during construction are summarised in Table 6.1.

The lever arm of the base resultant is given by:

$$\frac{\sum M}{V} = \frac{51024.7}{5277.9} = 9.66\ m\ ;\ \frac{B}{6} = 3.33\ m\ (acts\ within\ the\ middle\ third)$$

The eccentricity of the base reaction, $e = 10 - 9.68 = 0.33\ m$

The maximum and minimum base pressure are given by:

$$p = \frac{5519.2}{20}\left(1 \pm \frac{6 \times 0.32}{20}\right) = 290\ kPa\ at\ the\ toe\ and\ 237\ kPa\ at\ the\ heel$$

The effective width, $B' = B - 2e = 20 - 2(1.03) = 19.34\ m$

For a foundation loaded eccentrically on cohesive soil the short-term ultimate bearing capacity is given by:

$$q_{ult} = N_c \cdot S_u \cdot f_{ci}$$

Where q_{ult} is the ultimate bearing capacity; N_c is Skempton's bearing capacity factor; S_u is the average undrained shear strength of the foundation soil; f_{ci} is a factor to take account of eccentric and inclined loading. According to Vesic (1975):

$$f_{ci} = 1 - \frac{2 \cdot R_h}{B' \cdot S_u \cdot N_c} = 1 - \frac{2 \cdot 1083}{19.36 \cdot 30 \cdot 5.14} = 0.73$$

Where R_h is the horizontal component of loading. $N_c = 5.14$ for small ratios of D/B. Now:

$$q_{ult;\,vert} = N_c \cdot S_u = 5.14 \cdot 33 = 169\ kPa$$

$$q_{ult;\,eccn} = N_c \cdot S_u \cdot f_{ci} = 5.14 \cdot 33 \cdot 0.73 = 123\ kPa$$

The reduction in the ultimate bearing capacity due to the inclined eccentric load is 27 %.

Table 6.1 – Calculation of forces and moments

Reference		Pressure	Force	Lever Arm	Moment
(per meter)	Stabilising / destabilising	kN/m^2	kN	m	KN.m
(1) Lateral earth pressure (above wt)	Horizontal destabilising	14.4	17.1	20	342
(2) Lateral earth pressure (below wt)	Horizontal destabilising	58.9	602.2	6.38	3842.0
(3) Lateral earth pressure (below wt)	Horizontal destabilising	14.4	294.5	9.58	2821.3
(4) Hydrostatic pressure (Tidal lag)	Horizontal destabilising	175	1531.3	5.83	8927.5
(5) Hydrostatic pressure (Basin)	Horizontal stabilising	-165	-1362.3	5.5	-7487.2
			1083.8	**∑MH =**	**8445.7**
(6) Base	Vertical stabilising		364	10	3640
(7) Caisson box (above wt.)	Vertical stabilising		819	10	8190
(8) Caisson box (Below wt.)	Vertical stabilising		3313	10	33129.6
(9) Soil above caisson heel (above wt)	Vertical stabilising		90.1	19	1711.9
(10) Soil above caisson heel (Below wt)	Vertical stabilising		344.7	19	6549.3
(11) Vertical force due to self-weight of backfill	Vertical stabilising		347.2	18	6249.6
			5277.9	**∑MV =**	**59470.4**
				∑M =	**51024.7**

A.2 Estimation of ground movements due to embankment loading

Bourges & Mieussens (1979) have evaluated the results of a number of field observations of ground movements near the toe of embankments. An empirical model was developed to estimate horizontal ground movements as a function of:

- The undrained shear strength of the clay (s_u),
- The embankment load $(h \times \gamma)$,
- The ratio of the distance from the crest (X) to the horizontal length of the slope (L),
- The ratio of the thickness of the clay layer (D), to embankment width (B).

The magnitude of the maximum immediate horizontal displacement is related to the position of the point in question (X/L) and the stability number F, where:

$$F = (\pi + 2) \times S_u / h \times \gamma \tag{6.1}$$

Where h is the height of the embankment and γ is the unit weight of the embankment fill. Figure 6.1 plots the dimensionless immediate horizontal displacement λ against F. Alternatively the magnitude of the maximum immediate horizontal displacement is related to the ratio of the thickness of the clay layer to embankment width (D/B) and the stability number F. The horizontal displacement is relatively large at failure where F=1.

For the problem of a caisson quay wall retaining backfill to 2.65 m CD, the toe of the slope is taken as the toe of the caisson. For this case the parameters for estimating maximum immediate horizontal displacement are:

- $S_{u;mean} = 33\ kPa$
- $h \times \gamma = 19.5 \times 10.5 = 205\ kPa$
- $X/L = 20/20 = 1$
- $D/B = 9/30 = 0.3$
- $F = (\pi + 2) \times 33/205 = 0.82; taken\ as\ 1\ which\ represents\ failure$
- $\lambda = 3.7\ \%$

Now the maximum immediate horizontal displacement is given by:

$$\lambda = \frac{\gamma_{max}}{D} \tag{6.2}$$

$$\gamma_{max} = \lambda \times D = 3.7\ \% \times 9\ m = 333\ mm$$

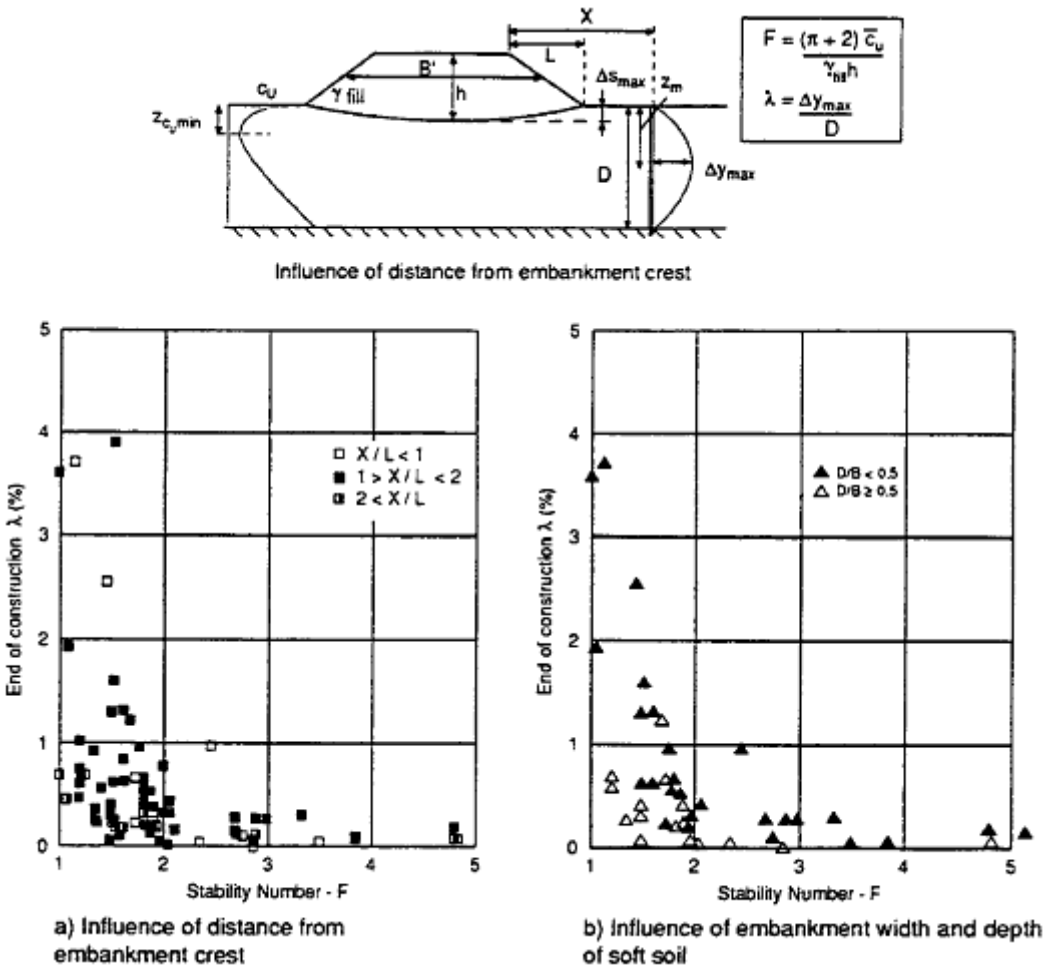

Figure 6.1 – Relationship between embankment stability and maximum ground movement based on data from Bourges & Mieussens (1979) and other sources (Seaman, 1994)

A.3 Estimation of maximum inclusion bending moment and inclusion head deflection

On the basis of two independent sets of centrifuge test data and limited field data, Stewart et al. (1994) presented empirical design charts to assess pile group response to embankment type loading. These charts enable simple estimates of maximum pile bending moment and pile head deflection as a function of the embankment load level and soil-pile stiffness. Stewart et al. (1994) plotted non-dimensional change in maximum pile bending moment M_q and pile head deflection y_q against relative soil-pile stiffness K_R :

$$M_q = \Delta M_{max}/\Delta q\ d\ \left(L_{eq}\right)^2 \tag{6.3}$$

$$y_q = \Delta y\ E_p\ I_p/\Delta q\ d\ \left(L_{eq}\right)^4 \tag{6.4}$$

$$K_R = E_p\ I_p/E_s(h_s)^4 \tag{6.5}$$

Where q is the embankment load, d is the pile diameter, L_{eq} is the equivalent length of the piles between points of fixity, E_p is the young's modulus of the pile, I_p is the moment of inertia of the pile, E_s is the representative stiffness of the clay layer and h_s is the thickness of the clay layer. The graphs identifies pre-threshold load levels where $q < 3\ S_u$ and post threshold load levels where $q > 3\ S_u$. The pile configurations for the data include piles pinned at the head, free headed and groups connected by a rigid cap. To account for this an equivalent length is defined where L is the length of the piles from the head to the base of the clay stratum:

$$L_{eq} = L\ ; rotation\ prevented \tag{6.6}$$

$$L_{eq} = 0.6\ L\ ; pinned \tag{6.7}$$

$$L_{eq} = 1.3\ L\ ; free \tag{6.8}$$

For the problem of a caisson quay wall retaining backfill presented in Figure 3.4b, the parameters for estimating the maximum inclusion bending moment and inclusion head deflection are:

- $d = 0.75\ m$
- $L_{eq} = 1.3 \times 9 = 11.7\ m$
- $\Delta q = 205\ kPa$
- $E_p = 22300$ MPa

- $I_p = \pi \times r^4/4 = 0.01553$
- $E_s = 5000\ kPa$
- $h_s = 9\ m$

Now,

$$K_R = 22300000 \times\ 0.01553/5000 \times (9)^4 = 1.06 \times 10^{-2}$$

$$M_q; y_q = 0.1\ on\ post\ threshold\ curve$$

$$\Delta M_{max} = 0.1 \times 205 \times\ 0.75\ (11.7)^2 = 2104\ kN.m$$

$$\Delta y = 0.1 \times 205 \times 0.75\ (9)^4\ /22300000 \times\ 0.01553 = 291\ mm$$

For a reduced embankment load of 99 kPa at threshold the maximum moment reduces to $406\ kN.m$ and the maximum inclusion head deflection to 32 mm.

Appendix B Numerical Modelling

B.1 Material constitutive model parameters

Table 6.2 – LE model parameters for RIs C35/45

Parameter	Unit	Value	Comment
γ_{unsat}	kN/m^3	24	-
γ_{sat}	kN/m^3	-	Non-porous
E	kPa	22300000	Refer to section 4.1.1.2 and to Table 3.4
v	-	0.2	-

Table 6.3 – MC model parameters for RIs C35/45

Parameter	Unit	Value	Comment
γ_{unsat}	kN/m^3	24	-
γ_{sat}	kN/m^3	-	Non-porous
E'	kPa	22300000	Refer to section 4.1.1.2 and to Table 3.4
v'	-	0.2	-
φ'	°	35	Refer to section 4.1.1.2 and to Table 3.4
c'	kPa	585	Refer to section 4.1.1.2 and to Table 3.4
ψ	°	0	-
$Tensile\ strength$	kPa	2200	Refer to section 4.1.1.2 and to Table 3.4

Table 6.4 – HS-Small model parameters for firm clay

Parameter	Unit	Value	Comment
γ_{unsat}	kN/m^3	16	-
γ_{sat}	kN/m^3	17.5	
e_{imt}	-	1.5	Initial void ratio
$k_{x,y}$	m/day	0.039×10^{-3}	-
φ'	°	29	S_u is a model output; S_u increases linearly with depth from 30 kPa to 50 kPa
c'	kPa	0	$c' = 0\ for\ NC$
R_f	-	0.9	Failure ratios for various soils range from 0.75 to 1.0
ψ	°	0	-
E_{50}^{ref}	kPa	5000	Typical range 3333 to 10000 after Carter
E_{oed}^{ref}	kPa	5000	$E_{50}^{ref} \approx E_{oed}^{ref}$
E_{ur}^{ref}	kPa	15000	$E_{ur}^{ref} / E_{50}^{ref} \approx 3$
m	-	1	Exponential power (m) is close to unity for soft to firm clay
v_{ur}	-	0.2	0.2 for clays
P_{ref}	kPa	100	Minor reference principal stress
K_0^{nc}	-	0.51	$K_0^{nc} = 1 - \sin\varphi'$
POP	kPa	100	Pre-overburden pressure equivalent to paleo seabed at -2 mCD
G_0^{ref}	kPa	46000	-
$\gamma_{0.7}$	-	0.00024	-

Table 6.5 – HS-Small model parameters for uncompacted loose sand

Parameter	Unit	Value	Comment
γ_{unsat}	kN/m^3	16.0	-
γ_{sat}	kN/m^3	19.4	-
e_{imt}	-	0.85	Initial void ratio
$k_{x,y}$	m/day	7.12	-
φ'	°	31	-
c'	kPa	0	-
R_f	-	0.9	Failure ratios for various soils range from 0.75 to 1.0
ψ	°	1	-
E_{50}^{ref}	kPa	15000	-
E_{oed}^{ref}	kPa	15000	$E_{50}^{ref} \approx E_{oed}^{ref}$
E_{ur}^{ref}	kPa	45000	$E_{ur}^{ref} / E_{50}^{ref} \approx 3$
m	-	0.5	Exponential power (m) is approximately 0.5 for sands
v_{ur}	-	0.25	Approximately 0.25 for loose sands
P_{ref}	kPa	100	Minor reference principal stress
K_0^{nc}	-	0.48	$K_0^{nc} = 1 - \sin\varphi'$
POP	kPa	0	-
G_0^{ref}	kPa	77000	-
$\gamma_{0.7}$	-	0.00018	-

Table 6.6 – HS-Small model parameters for dense sand

Parameter	Unit	Value	Comment
γ_{unsat}	kN/m^3	19	-
γ_{sat}	kN/m^3	20	-
e_{imt}	-	0.62	Initial void ratio
$k_{x,y}$	m/day	7.12	-
φ'	°	34	-
c'	kPa	0	-
R_f	-	0.9	Failure ratios for various soils range from 0.75 to 1.0
ψ	°	4	-
E_{50}^{ref}	kPa	50000	-
E_{oed}^{ref}	kPa	50000	$E_{50}^{ref} \approx E_{oed}^{ref}$
E_{ur}^{ref}	kPa	150000	$E_{ur}^{ref} / E_{50}^{ref} \approx 3$
m	-	0.5	Exponential power (m) is approximately 0.5 for sands
v_{ur}	-	0.2	Approximately 0.2 for dense sands
P_{ref}	kPa	100	Minor reference principal stress
K_0^{nc}	-	0.44	$K_0^{nc} = 1 - \sin\varphi'$
POP	kPa	0	-
G_0^{ref}	kPa	114400	-
$\gamma_{0.7}$	-	0.00012	-

Table 6.7 – HS-Small model parameters for very dense compacted sand

Parameter	Unit	Value	Comment
γ_{unsat}	kN/m^3	19.5	-
γ_{sat}	kN/m^3	20.5	-
e_{imt}	-	0.57	Initial void ratio
$k_{x,y}$	m/day	7.12	-
φ'	°	40	-
c'	kPa	0	-
R_f	-	0.9	Failure ratios for various soils range from 0.75 to 1.0
ψ	°	10	-
E_{50}^{ref}	kPa	100000	-
E_{oed}^{ref}	kPa	100000	$E_{50}^{ref} \approx E_{oed}^{ref}$
E_{ur}^{ref}	kPa	300000	$E_{ur}^{ref} / E_{50}^{ref} \approx 3$
m	-	0.5	Exponential power (m) is approximately 0.5 for sands
v_{ur}	-	0.2	Approximately 0.2 for dense sands
P_{ref}	kPa	100	Minor reference principal stress
K_0^{nc}	-	0.36	$K_0^{nc} = 1 - \sin\varphi'$
POP	kPa	0	-
G_0^{ref}	kPa	200000	-
$\gamma_{0.7}$	-	0.00010	-

Table 6.8 – HS-Small model parameters for very dense crushed stone

Parameter	Unit	Value	Comment
γ_{unsat}	kN/m^3	20	-
γ_{sat}	kN/m^3	21	-
e_{imt}	-	0.57	Initial void ratio
$k_{x,y}$	m/day	7.12	-
φ'	°	42	-
c'	kPa	0	-
R_f	-	0.9	Failure ratios for various soils range from 0.75 to 1.0
ψ	°	15	-
E_{50}^{ref}	kPa	100000	-
E_{oed}^{ref}	kPa	100000	$E_{50}^{ref} \approx E_{oed}^{ref}$
E_{ur}^{ref}	kPa	300000	$E_{ur}^{ref} / E_{50}^{ref} \approx 3$
m	-	0.5	Exponential power (m) is approximately 0.5 for sands
v_{ur}	-	0.2	Approximately 0.2 for dense sands
P_{ref}	kPa	100	Minor reference principal stress
K_0^{nc}	-	0.30	$K_0^{nc} = 1 - \sin\varphi'$
POP	kPa	0	-
G_0^{ref}	kPa	200000	-
$\gamma_{0.7}$	-	0.00010	-

Table 6.9 – HS-Small model parameters for dense scour rock

Parameter	Unit	Value	Comment
γ_{unsat}	kN/m^3	20	-
γ_{sat}	kN/m^3	21	-
e_{imt}	-	0.57	Initial void ratio
$k_{x,y}$	m/day	7.12	-
φ'	°	45	-
c'	kPa	0	-
R_f	-	0.9	Failure ratios for various soils range from 0.75 to 1.0
ψ	°	15	-
E_{50}^{ref}	kPa	48000	-
E_{oed}^{ref}	kPa	48000	$E_{50}^{ref} \approx E_{oed}^{ref}$
E_{ur}^{ref}	kPa	144000	$E_{ur}^{ref} / E_{50}^{ref} \approx 3$
m	-	0.5	Exponential power (m) is approximately 0.5 for sands
v_{ur}	-	0.2	Approximately 0.2 for dense sands
P_{ref}	kPa	100	Minor reference principal stress
K_0^{nc}	-	0.30	$K_0^{nc} = 1 - \sin\varphi'$
POP	kPa	0	-
G_0^{ref}	kPa	200000	-
$\gamma_{0.7}$	-	0.00010	-

Table 6.10 – Model parameters for elastic geogrid element

Parameter	Unit	Value	Comment
Isotropic	-	-	Biaxial geogrid
EA_1	kN/m	2000	-
EA_2	kN/m	2000	-
GA	kN/m	1000	-

B.2 Model calculation phases

Basis for construction durations:

- Berth length of 400 m: Approximate length of Post Panamax sized vessel (EAU, 2015)
- Caisson floating, positioning, sinking, levelling: 2 days / caisson (ZAA, 2015)
- Caisson filling: 1 day; dredger hopper size of 2700 m^3; discharge rate of 320 m^3/hour (ZAA, 2015)
- Install grout socks and geofabric before backfilling: 1 day / caisson (ZAA, 2015)
- Reclamation: 80 days; dredger hopper size of 2700 m^3; discharge rate of 320 m^3/hour (ZAA, 2015)
- Vibrocompaction: 60 days; 30m to 90m of treatment per hour (Woodward, 2005); 4m treatment grid
- Construct capping beam: 50 days (ZAA, 2015)
- Construct piled rear crane beam and concrete pavement etc: 120 days (ZAA, 2015)

Phase 0: Initial conditions:

- K_0 procedure.

Phase 1: Dredge to foundation trench elevation:

- Deactivate dredge material in a plastic undrained calculation where the undrained behaviour is ignored (i.e. no beneficial effects of suction included).

Phase 2: Installation of rigid inclusions system:

- Activate RIs, LTP and geogrid in a consolidation calculation over a nominal 10 days with updated mesh.
- The RI installation effects are not modelled.

Phase 3 to 5: Caisson placement and filling with sand:

- Activate sand filled caisson in a consolidation calculation over 40 days with updated mesh.
- The most conservative duration for consolidation is estimated based on the duration for activities such as floating and sinking the final caisson, filling and compacting inside the caissons, placing grout socks between caissons, placing filter fabric behind caisson etc.

Phase 6 to 13: Hydraulically place sand behind caisson:

- Activate uncompacted backfill behind caissons to 2.65 m CD in a consolidation calculation over 40 days with updated mesh.
- Divided into eight lifts each taking ten days

Phase 14: Tidal lag:

- Activate one meter tidal lag.

Phase 15: Vibro-compact backfill:

- Activate very dense vibro-compacted backfill in a consolidation calculation over 60 days with updated mesh.

Phase 16: Construct capping beam

- Activate capping beam in a consolidation calculation over 50 days with updated mesh.

Phase 17: Construct piled rear crane beam and concrete pavement:

- Activate piled rear crane beam and very dense backfill behind capping beam to 5 m CD in a consolidation calculation over 120 days with updated mesh.

Phase 18: Unload tidal lag:

- Deactivate tidal lag.

Phase 19: Plastic nil step:

- Plastic undrained calculation with updated mesh.

Phase 20to 21: Activate and then deactivate transient crane load:

- Plastic undrained calculation with updated mesh.

Phase 22 to 23: Activate and deactivate transient bollard load:

- Plastic undrained calculation with updated mesh.

Phase 24 to 25: Activate and deactivate surcharge:

- Plastic undrained calculation with updated mesh.

Phase 26: Activate transient crane load, transient bollard load, surcharge and tidal lag:

- Plastic undrained calculation with updated mesh.

Phase 27 to 28: Reduce to sustained crane load, surcharge and tidal lag:

- Consolidation calculation with updated mesh.
- Dissipation of excess pore pressure to 100 % consolidation.

B.3 Model validation results

The following subsections present the validation results for the HS-Small constitutive model used for the clay subsoil, initial model ground conditions and global load-deflection behaviour of the rigid inclusions under vertical loading.

B.3.1 Validation of the HS-Small model for clay

Undrained triaxial tests (CIUC) on soft and stiff clay have been simulated using the soil test feature in Plaxis 3D. The constitutive model parameters used in the simulations are presented in Table 6.11. The CIUC test simulation results and real CIUC test results for Bangkok clays are presented in Figure 6.2 below and Figure 6.3 in annexure B.3. The results for soft clay show a good fit between the simulated test data and the real test data, whereas the results for stiff clays show a poor fit. The HS-Small Model cannot accurately predict the drop in excess pore pressure and deviator stress due to the dilatant behaviour typical of heavily OC clay. It is concluded from these results that the HS-Small Model best describes clay behaviour in the normally consolidated to lightly over-consolidated range. HS-Small Model parameters for firm clay have been derived and represent the average condition between soft and stiff clay. The soft and firm clay parameters in Table 6.11 are considered to be within the plausible range for normally consolidated to lightly over-consolidated clays.

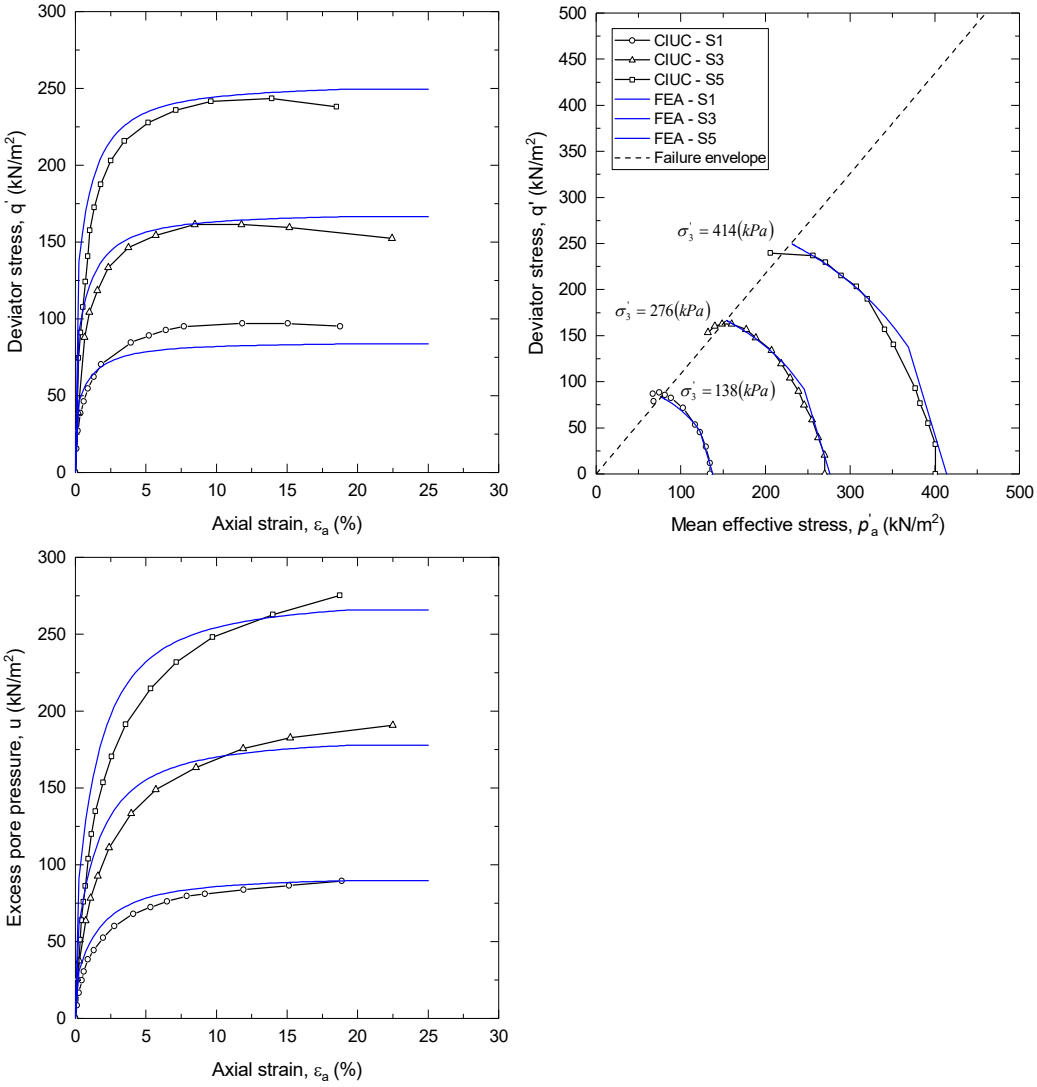

Figure 6.2 – Bangkok soft clay CIUC testing results and their prediction by simulation using the HS-Small Model

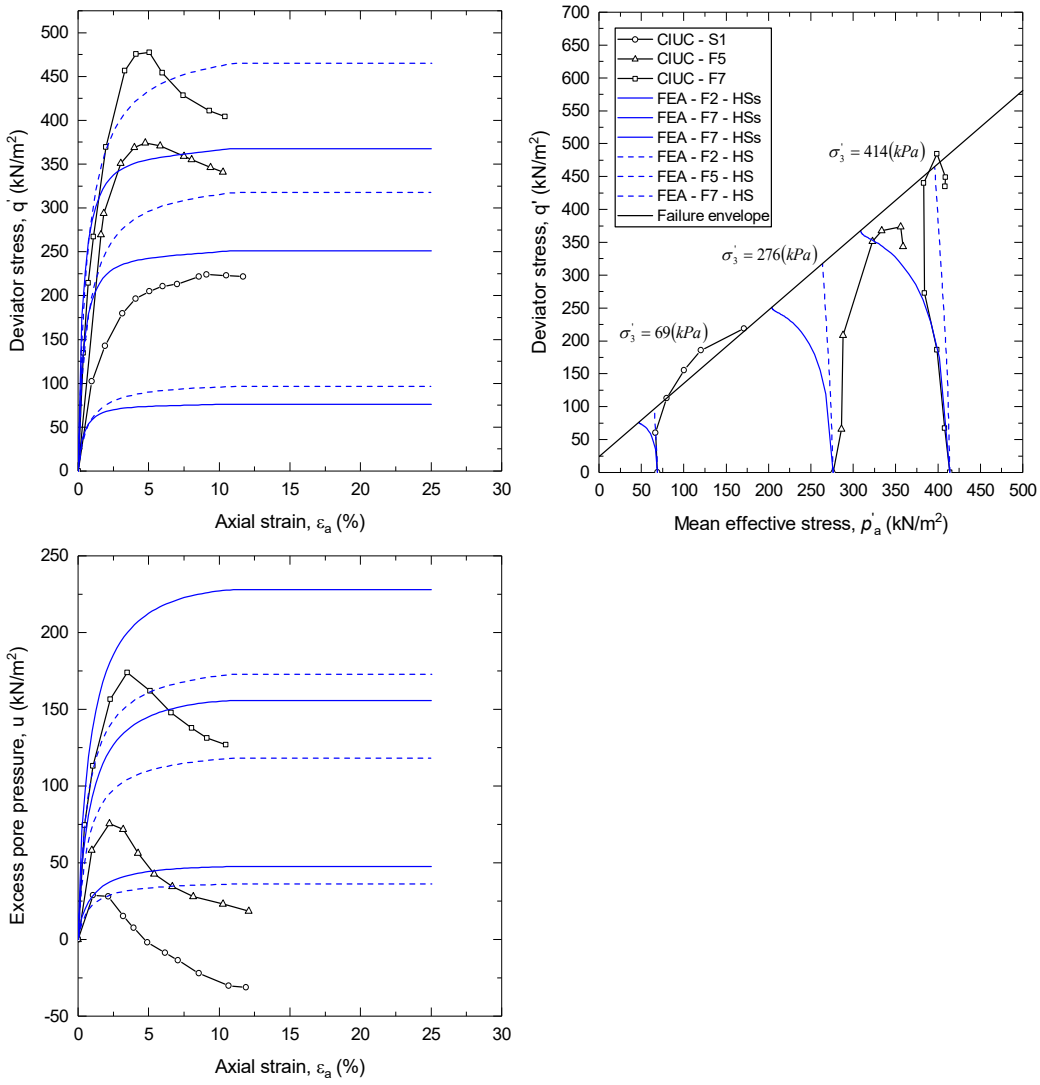

Figure 6.3 – Bangkok stiff clay CIUC testing results and their prediction by simulation using the HS-Small Model and HS Model

Table 6.11 – Validated HS-Small Model parameters for clay

φ' (deg)	ψ (deg)	c' (kPa)	E_{50}^{ref} (kPa)	E_{oed}^{ref} (kPa)	E_{ur}^{ref} (kPa)	R_f	m	K_0^{nc}	v_{ur}	G_0^{ref} (MPa)	$\gamma_{0.7}$
Hardening soil model										*Small strain overlay*	
Soft clay (Validated by Surarak et al., 2012*)*										*Estimated*	
27	0	1	800	850	8000	0.9	1	0.74	0.2	46	0.00024
Stiff clay (Validated by Surarak et al., 2012*)*										*Estimated*	
28	0	11.5	9500	12000	30000	0.9	1	0.5	0.2	46	0.00024
Firm clay (Hypothetical condition between soft and stiff)										*Estimated*	
28	0	1	5000	5000	15000	0.9	1	0.53	0.2	46	0.00024

B.3.2 Validation of initial conditions

The initial model conditions for the clay subsoil are presented in Figure 6.4. The initial horizontal stress state is defined by K_0 conditions which range from 0.75 to 1.0. The model predictions compare well with simple empirical predictions after Mayne & Kulhawy (1982). The stress history is defined by a pre-overburden pressure of 100 kPa which results in the clay subsoil OCR varying with depth from 1.9 to 2.6. The initial model stress state defined by K_0 and OCR is typical for NC to lightly OC clay. The undrained shear strength profile obtained using "Method A" varies linearly with depth from 30 kPa to 60 kPa which is typical for soft to firm clay. The model predictions of S_u compare well with empirical predictions after Wroth (1984).

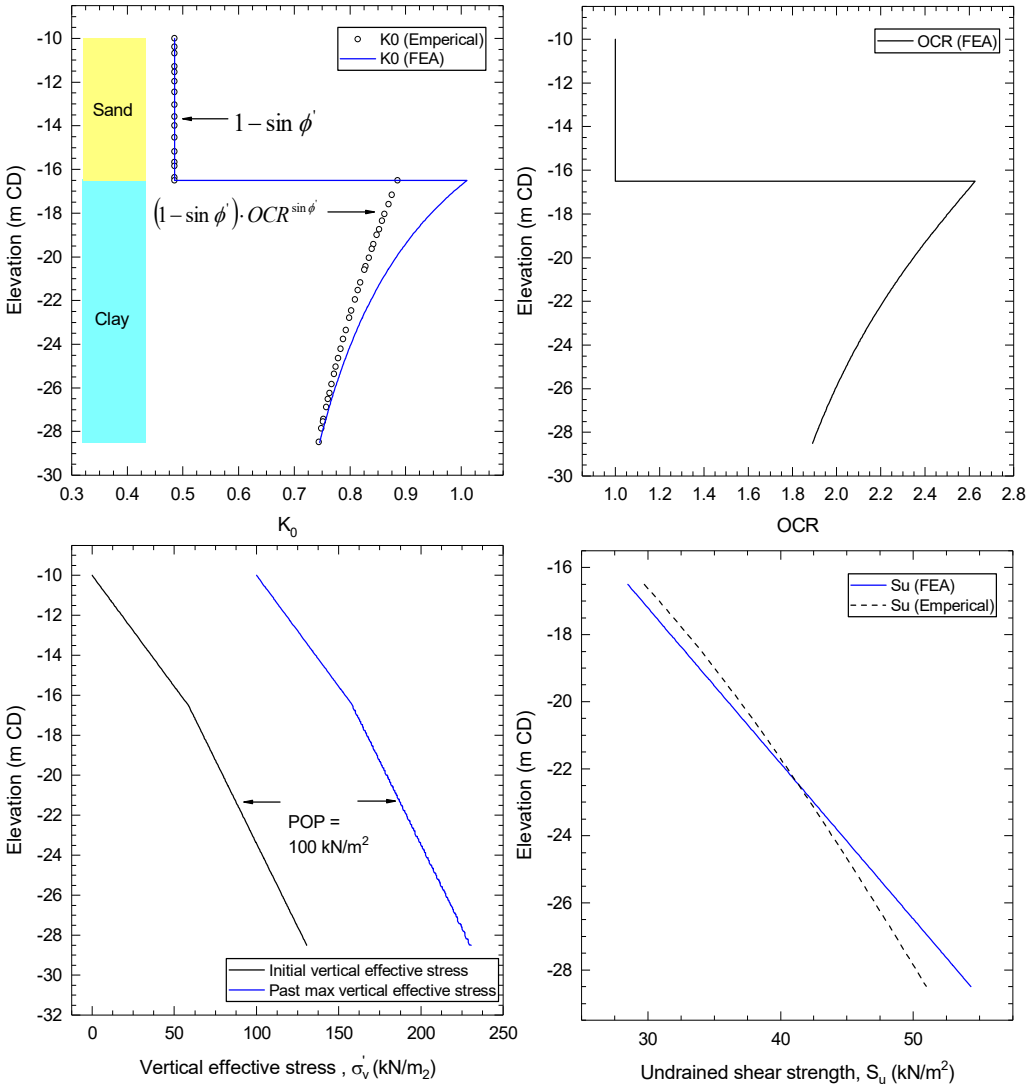

Figure 6.4 – Validation of initial model conditions

B.3.3 Validation of the global load deflection behaviour of RIs

The load deflection behaviour of an RI under the centre of the caisson (position “k” in Figure 3.1) subjected to rigid vertical loading during caisson placement and filling is presented in Figure 6.5. The vertical load during caisson placement (water filled) is ≈ 110 kPa which increases to 200 kPa when the caisson is filled with sand. Figure 6.5 shows the vertical settlement profile at the position of the inclusion and between the inclusions in the subsoil. Additionally the axial stress in the inclusion with depth is shown. Analytical predictions using FOXTA V3 for the same ground profile, loading and boundary conditions are plotted with the FE predictions.

The FE model predicts a vertical settlement at founding level of 19 mm during caisson placement, which increases to 32 mm when the caisson is filled with sand. The corresponding analytical prediction is 16 mm increasing to 33 mm. There is good agreement between the FE model and analytical model predictions of settlement. The FE model predicts that 82% of the total load is directed to the inclusion heads during caisson placement, which increases to 88% during caisson filling. The corresponding analytical prediction is 71% increasing to 76%. There is good agreement between the FE model and analytical model predictions of load efficiency. The most significant difference between the models is the magnitude of drag load due to negative skin friction; and the difference in length of approximately 4 m over which the negative skin friction acts (depth to neutral plane). Although partly due to the difference in load efficiency at the inclusion head it is proposed that an additional reason for this difference is the ability of the 3D model to shed load at the vertical model boundaries. The analytical unit cell model assumes zero shear along the vertical model boundaries.

The model results presented in Figure 6.5 demonstrate that the fundamental load transfer mechanisms such as arching above the inclusion head and negative skin friction along the inclusion shaft have been captured in the 3D model.

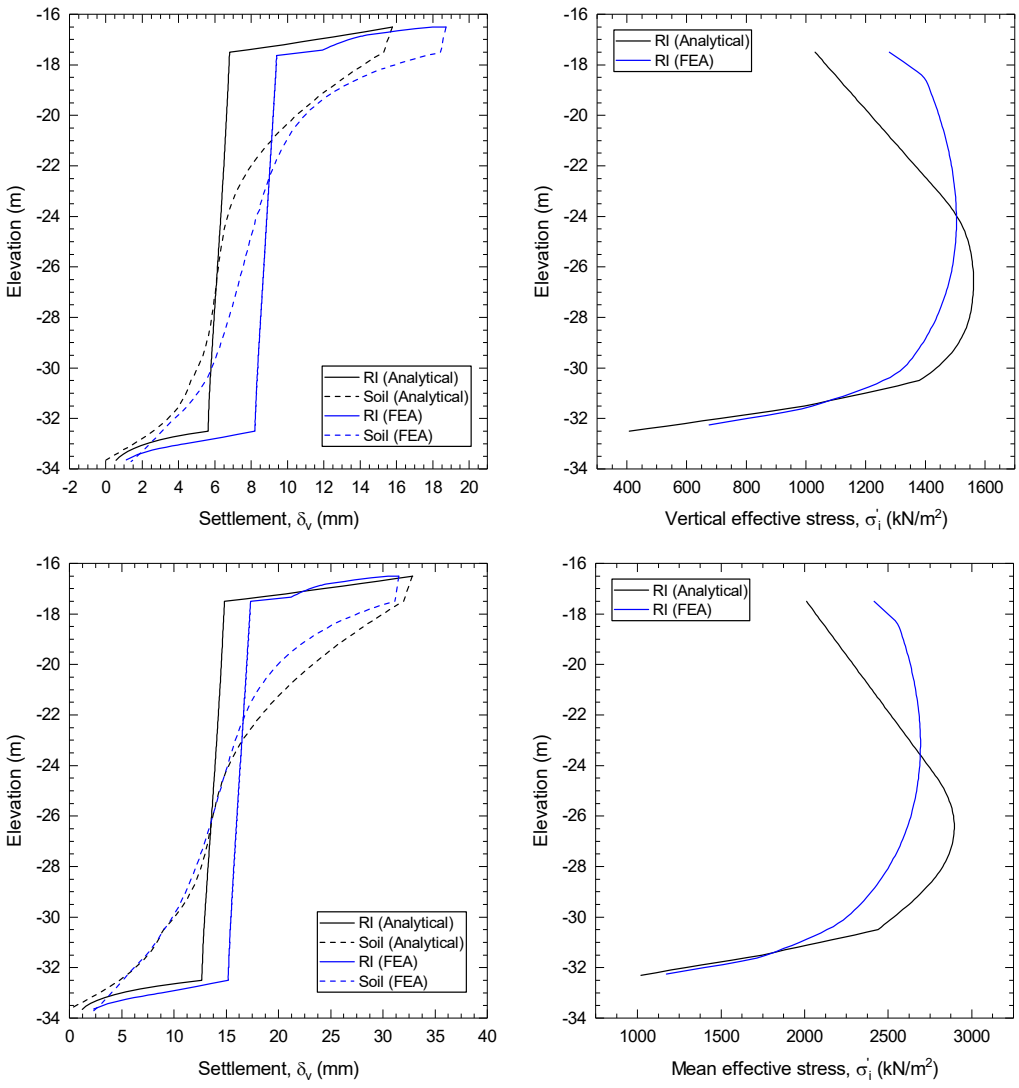

Figure 6.5 – Validation of the load-deflection behaviour of RIs subjected to vertical rigid loading